JULY-SEPTEMBER 2018 VOL. 10 № 3 (38)

ISSN 2075-8251

ActaNaturae

B Cell Regulation in Autoimmune Diseases

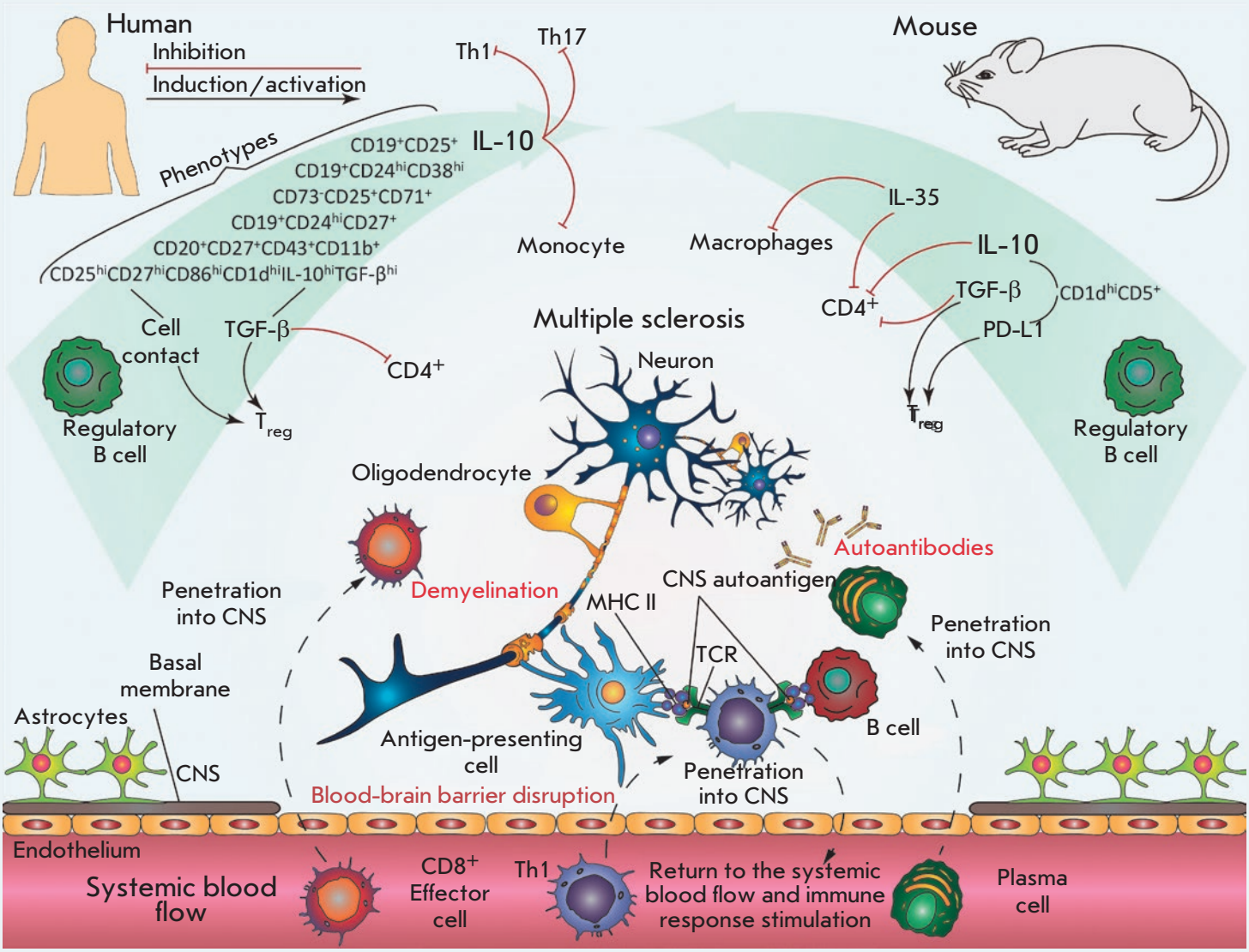

MERCK

Comprehensive solutions for cell analysis

- Cell lines and primary cells
- Traditional and specialized culture media
- Sterilizing filtration
- Biochemical reagents
- Water purification systems
- Cell counting and analysis
- Cryopreservation

An extensive range and top quality of cell lines from our partner, the European Collection of Authenticated Cell Cultures (ECACC):

- 4000 animal and human cell lines;
- Cells of 45 animal species and 50 tissue types;
- 370 B-lymphoblastoid cell lines for which human leukocyte antigen (HLA) typing data are available;
- 480 hybridoma cell lines secreting monoclonal antibodies;
- DNA, RNA, and cDNA extracted from the cell lines from our collection;

SIGMAaldrich.com/ECACC

LLC Merck
Valovaya Str., 35, Moscow, 115054, Russia;
Tel. +7 (495) 937-33-04
E-mail: mm.russia@merckgroup.com, ruorder@sial.com

SIGMAaldrich.com/cellculture
MERCKmillipore.com/cellculture

SIGMA-ALDRICH® is now MERCK

Possibilities for Using Pluripotent Stem Cells for Restoring Damaged Eye Retinal Pigment Epithelium

A. E. Kharitonov, A. V. Surdina, O. S. Lebedeva, A. N. Bogomazova, M. A. Lagarkova

Pluripotent stem cells can be differentiated with high efficiency into the pigment epithelium of the retina, which opens up possibilities for cellular therapy in macular degeneration and can slow down the development of pathology and, perhaps, restore a patient's vision. This review summarizes the current state of preclinical and clinical studies in the field of retinal pigment epithelial transplantation therapy. Authors also discuss different differentiation protocols based on data in the literature and our own data, and the problems holding back the widespread therapeutic application of retinal pigment epithelium differentiated from pluripotent stem cells.

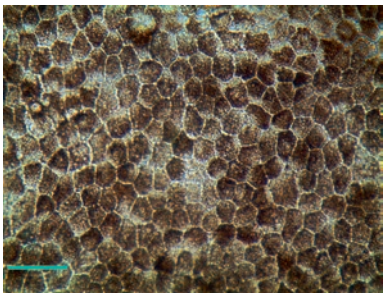

Retinal pigment epithelium cells differentiated from the induced pluripotent stem cells of a healthy donor

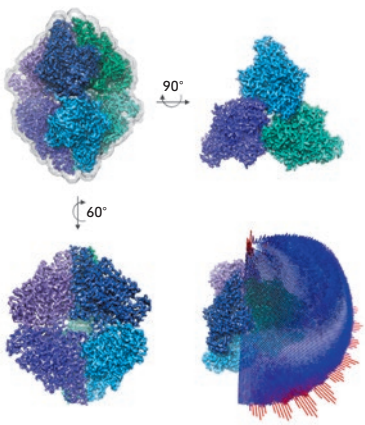

Final density map with the best resolution of 2.56 Å

Three-Dimensional Structure of Cytochrome *c* Nitrite Reductase As Determined by Cryo-Electron Microscopy

T. N. Baymukhametov, Y. M. Chesnokov, E. B. Pichkur, K. M. Boyko, T. V. Tikhonova, A. G. Myasnikov, A. L. Vasiliev, A. V. Lipkin, V. O. Popov, M. V. Kovalchuk

The structure of cytochrome c nitrite reductase from the bacterium *Thioalkalivibrio nitratireducens* was determined by cryo-electron microscopy (cryo-EM) at a 2.56 Å resolution. Possible structural heterogeneity of the enzyme was assessed. The backbone and side-chain orientations in the cryo-EM-based model are, in general, similar to those in the high-resolution X-ray diffraction structure of this enzyme.

Expression and Intracellular Localization of Paraoxonase 2 in Different Types of Malignancies

M. I. Shakhparonov, N. V. Antipova, V. O. Shender, P. V. Shnaider, G. P. Arapidi, N. B. Pestov, M. S. Pavlyukov

In the current study, authors performed a bioinformatic analysis of RNA and DNA sequencing data extracted from tumor samples taken from more than 10,000 patients with 31 different types of cancer and determined expression levels and mutations in the PON2 gene. Author's data indicate that a high PON2 expression level correlates with a worse prognosis for patients with multiple types of solid tumors and suggest that PON2, when localized on the nuclear envelope and endoplasmic reticulum, may protect cancer cells against unfavorable environmental conditions and chemotherapy.

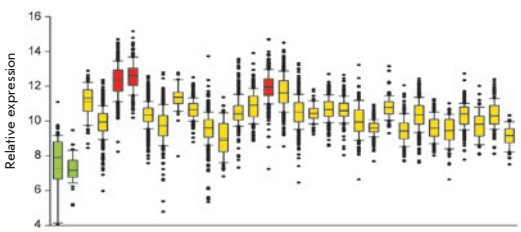

Relative expression level of the PON2 gene in tumors from patients with different types of cancer

ActaNaturae
JULY–SEPTEMBER 2018 VOL. 10 № 3 (38)

Founders
Ministry of Education and
Science of the Russian Federation,
Lomonosov Moscow State University,
Park Media Ltd

Phone/Fax: +7 (495) 727 38 60
E-mail: vera.knorre@gmail.com, actanaturae@gmail.com

Номер подписан в печать 27 сентября 2018 г.
Тираж 200 экз. Цена свободная.
Отпечатано в типографии «МИГ ПРИНТ»

Indexed in Pubmed, Web of Science, Scopus, and RISC

CONTENTS

REVIEWS

RESEARCH ARTICLES

SHORT REPORTS

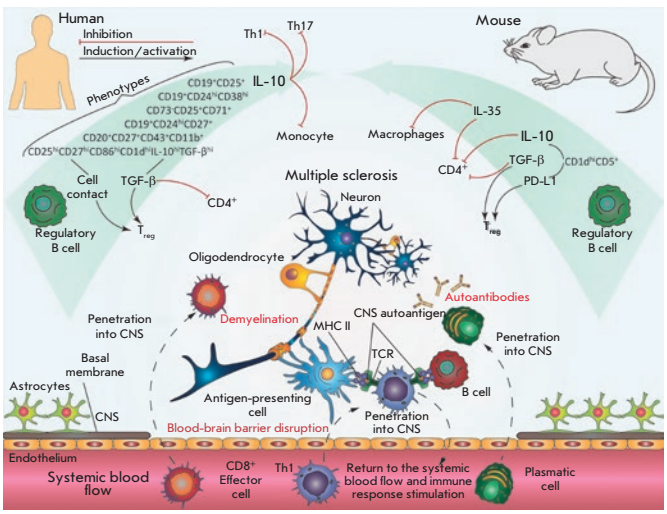

IMAGE ON THE COVER PAGE
(see the article by Sokolov *et al.*)

Experimental Models of Spinal Cord Injury in Laboratory Rats

A. N. Minakov[1], A. S. Chernov[1], D. S. Asutin[2], N. A. Konovalov[2], G. B. Telegin[1*]
[1]Branch of Shemyakin and Ovchinnikov institute of bioorganic chemistry Russian academy of sciences, Prospekt Nauki, 6, Moscow region, Pushchino, 142290, Russia
[2]Federal State Autonomous Institution «N .N. Burdenko National Scientific and Practical Center for Neurosurgery» of the Ministry of Healthcare of the Russian Federation, 4th Tverskaya-Yamskaya Str., 16, Moscow, 125047, Russia
*E-mail: telegin@bibch.ru
Received November 08, 2017; in final form June 25, 2018

ABSTRACT **Pathologies associated with spinal cord injury are some of the leading diseases in the world. The search for new therapeutic agents and 3D biodegradable materials for the recovery of spinal cord functions is a topical issue. In this review, we have summarized the literature data on the most common experimental models of spinal cord injury in laboratory rats and analyzed the experience of using 3D biodegradable materials (scaffolds) in experimental studies of spinal trauma. The advantages and disadvantages of the described models are systematically analyzed in this review.**
KEYWORDS **spinal cord injury, laboratory rat, biomodeling, scaffolds.**
ABBREVIATIONS **SCI – spinal cord injury, C – cervical spine, T – thoracic spine, L – lumbar spine.**

INTRODUCTION

One of the most topical and socially significant issues of modern regenerative medicine is the recovery of spinal cord functions in structural defects of various genesis, most of which are caused by injury [1]. Spinal cord injury (SCI) is recognized as one of the main causes of disability [2]. According to the WHO, up to 500,000 people suffer spinal cord injuries annually [3]. The main causes of SCI are road traffic accidents (38%), falls (22.2%), and sports injuries and accidents (22.5%) [4]. The clinical picture of SCI is characterized by a motor activity deficit, impaired sensory and autonomic functions, and neuropathic pain. The pathogenesis of spinal trauma is usually burdened with a poor prognosis associated with the development of paralysis. In addition, some diseases may cause or increase the risk of spinal cord injury [5]. Along with the direct SCIconsequences associated with a loss of motor, sensory, and autonomic functions, there is a risk of secondary processes that may aggravate injury and lead to muscle atrophy, chronic pain, urinary tract infection, and pressure ulcers [6, 7].

Our modern understanding of nerve growth stimulation and immunological, inflammatory, and cicatricial reactions arising in response to SCI has led to the development of several pharmacological treatments. These treatments, in combination with various cellular and additive techniques, bring hope that most spinal cord injuries will be curable in the near future [8–11].

Testing of new materials and techniques that promote regeneration of the spinal cord in animal models is a necessary and important stage in the preclinical development of a strategy for treating spinal cord injuries. One of the key objects used for biomodeling of spinal trauma is the rat. Spinal cord injuries in rats have become the main model used to evaluate the strategy of experimental treatment of SCI [4, 12]. In this review, we describe recent advances in the use of 3D biodegradable materials (scaffolds) designed to provide regenerative growth of axons over the entire injury area of the spinal cord, thereby creating the environment for its endogenous recovery.

EXPERIMENTAL MODELS OF SPINAL CORD INJURY IN LABORATORY RATS

When choosing the optimal animal model for solving specific research problems, it is necessary to take into account many factors: the type, age, size, and gender of animals and the possibility of using visualization techniques and a functional assessment of their condition. Since the second half of the last century, techniques for the prevention of consequences arising from spinal cord injury have been the subject of systematic studies in various animals, including rats, mice, cats, dogs, and minipigs [13–15]. Experimental models differ in the types of spinal cord injury: contusion, compression, distraction, dislocation, chemical, ischemic, and reperfusion injury, as well as various types of laceration. Of

the numerous SCI models developed on rats, the most extensively used models are those relevant to the clinical practice of closed injuries: compression-simulating impaction and contusion-simulating bruise [16–18]. The mean experiment duration in most studies is about 2 months. The main criterion for assessing the adequacy of a model is the detection of morphological changes (axonal regeneration, myelination, vascularization, glial scar density, inflammatory reaction) using histological techniques (usually, transverse and sagittal sections in the injury area and in adjacent (proximal and distal) areas are studied). Auxiliary criteria include MRI diagnostics and electromyography-based functional evaluation. Clinical evaluation is based on the Basso, Beattie, and Bresnahan rating scales (BBB test), with a rat moving inside a plexiglass cage equipped with digital cameras and somatosensory potential registration [19–21], dynamic weight bearing (DVN) test [22], and behavioral tests.

The disadvantages of most experimental rat SCI models are poor control of the impact extent, as well as deep destructive changes in the gray and white matter of the spinal cord, including pathological shifts, death of neurons and glial cells, degeneration of nerve fibers, demyelination, and activation of microglia and macrophages [23]. All these impairments lead to the development of a stable functional deficit. Models of contusion, compression, traction, photochemical, inflammatory, ischemic, and reperfusion injuries have been primarily used for the investigation of the SCI pathophysiology, because they reproduce the potential mechanisms of trauma and spinal cord injury [15]. The presented modeling methods might adequately reflect clinical and morphological shifts in SCI in humans, but most of the models are difficult to reproduce, and they cannot be used to study spinal cord regeneration in structural injuries.

Functional deficit of the spinal cord in rats has been proven to be mainly associated with failure of the conductive white matter tracts [24]. Therefore, the pathophysiological processes of spinal cord injury should be considered analogously to the processes associated with injury to the peripheral nervous system. The dependence of the peripheral nerve ability to restore innervation on the injury extent was established and quantified (as three- and five-point scales) as early as the middle of the last century [25–28].

In the case of mild injury (neuropraxia) to peripheral nerves, axonal regeneration has been experimentally proven and confirmed in clinical practice. There are numerous examples of restoration of effector site innervation in mammals both surgically and spontaneously. Cell-signaling factors were found to arise among neurons, Schwann cells, macrophages, and the environment, which contributes to remyelination, growth, and, which is noteworthy, self-guidance of the regenerating axon [29–32]. Restoration of conduction occurs in several stages, including myelination, axonal growth, formation of synaptic contacts, and, finally, recovery of effector functions [33]. Axonal regeneration has been proven to occur in the rostrocaudal direction, along the former fiber course, with a mean rate of about 1 to 2 mm per day [34–38].

In moderate injuries, the injury site is characterized by axonal demyelination and anterograde (extending from the injury site to the peripheral segment) Wallerian degeneration of the distal nerve coming to the effector, while the proximal nerve and neuronal body remain unaffected, causing, e.g., phantom pain after limb amputation [39].

In severe cases, neuroma and glial scars may develop. Ipsilateral cysts (syringomyelia, cystic degeneration), mainly in the lateral funiculi of the spinal cord white matter, develop in 30% of the total number of clinical cases [40]. At the stage of cicatricial degeneration, glia has been found to perform the barrier function, preventing the spread of histolysis products and inflammatory mediators (mainly macrophages), and also to support the architectonics of central nervous system organs. However, the tissue structure of these defects tightens in the course its formation and prevents regenerative growth of axons, resulting in the fact that the central nervous system axons of adult mammals cannot regenerate spontaneously after an injury associated with demyelination [40–42].

One of the surgical treatment options for the most common form of chronic SCI (at the stage of formed structural defects) requiring surgery is to create favorable conditions for axonal growth by providing "free" space in the structural defect area via the removal of mechanical barriers (scars) by their excision to healthy tissue. This idea has served as the basis for a number of studies on the surgical creation of a structural defect of the spinal cord in rats by complete transection of the cord with a scalpel [43–52] and partial resection with microsurgical scissors [41, 53–57].

Partial transection of the spinal cord (hemisection) enables a comparison of damaged and healthy fibers in the same animal. For example, hemisection may be used to study the locomotor function and its recovery at different levels of the spinal cord, as well as to compare neurological deficits in contra- and ipsilateral lesions. In addition, partial transection of the spinal cord results in a less severe injury compared to complete transection, which largely facilitates postoperative care of animals [58]. Many studies have shown that recovery of the spinal cord function in rats occurs within the first 3 weeks after injury [13, 59], which cannot be attributed solely to the compensatory abilities and regeneration of dam-

aged axons. This also indicates that a unilateral spinal cord injury leads to reversible dysfunction of the spinal cord, because posttraumatic changes in the tissue do not involve the spinal cord areas contralateral to the injury site [60]. It should also be remembered that assessment of the extent of the injury is not always possible. In these cases, researchers have to use somatosensory-evoked potentials to improve the accuracy of their experiments [61].

The complete spinal cord transection model is a dissociation between the caudal and rostral segments of the spinal cord and is easily reproducible. Spinal cord transection is followed by a cascade of complex pathophysiological processes that inhibit potential regeneration of axons and form a glial scar. This model is described in various animals, including rats, mice, cats, dogs, and primates [62]. Thus, the complete spinal cord transection model is most convenient in terms of tissue engineering opportunities [63]. A complex approach to the treatment of SCI using scaffolds that are also able to deliver both target molecules and cells to an injured site of the spinal cord can use only models of partial structural injury of the spinal cord: they are helpful both for the assessment of axonal regeneration and for the subsequent functional recovery.

In most studies, an experimental spinal cord injury is modeled at the thoracic spine level [37, 47, 50–54, 57, 64, 65]. In humans, SCI usually occurs at the cervical level; in particular sports injuries or road accident injuries [48, 49, 55, 56]. In this regard, recent studies have mainly focused on cervical-level-injury models. In these models, compared to thoracic-spinal-cord-injury models, a pronounced neurological deficit develops, complicating the care and observation of animals in the postoperative period and dramatically increasing lethality [66]. Lumbar-level SCI models have been described, but less frequently [67]. However, the neurological deficit caused by a lumbar-spinal-cord injury largely results from damage to the gray matter (most developed in the lumbar enlargement region) rather than from damage to the white matter. Observations demonstrate that gray matter injury may lead to significant functional deficit, including paraplegia, without interruption of the main descent pathways.

THE USE OF SCAFFOLDS FOR STIMULATION OF REGENERATION AND FUNCTIONAL RECOVERY OF THE SPINAL CORD

The active development of additive technologies of stereolithography and tissue engineering has provided a powerful impetus for the creation of new biocompatible biodegradable three-dimensional scaffold materials capable of stimulating the regeneration of axons and their functional recovery. Most studies in the SCI field are aimed at reducing secondary injuries and promoting tissue regeneration [7]. The most common approach to the treatment of SCI is the combined one that involves scaffolds, cell transplantation, and the delivery of bioactive substances [33, 68].

The main requirement for scaffolds is biocompatibility, which should create an environment that promotes growth and vascularization of tissue and enables axons to regenerate through a graft. A number of research teams have studied biodegradable 3D scaffold materials [7, 49, 65, 69–78]. Honeycomb [47], nanofiber [49], and sponge [50] scaffolds were studied. In this case, many questions related to material biocompatibility arose. Recent studies have quantitatively proven that implantation of scaffolds into the area of a structural defect of the spinal cord contributes to axonal regeneration. For example, in one study, the motor function was recovered one month after microfilament scaffold implantation, and remyelinated nerve fibers were reliably detected in the scaffold structure two months after the completion of the experiment. The fibers amounted to 10–25% of the total amount of conductive pathways [33].

Another direction in the development of scaffolds is the creation of carcasses (hydrogels) with physical properties close to those of tissues [54, 57]. The similarity of the physical properties of an implant and a substrate revealed a 3- to 4-fold increase in the intensity of regenerative axonal growth in hydrogels compared to rigid mechanical scaffolds [37]. Capillary and porous hydrogels were studied *in vivo*. A characteristic feature of hydrogels noted by the authors was the loss of channel linearity in implants in a chronic experiment [22]. One of the advanced technologies for the production of hydrogel implants is two-photon polymerization. According to the authors, scaffolds produced using this innovative technique minimize injury to the surrounding tissues and provide architectural support to the surrounding tissues during the post-traumatic period, which prevents the destruction of neural networks in the defect area [79, 80].

Along with providing mechanical support and identifying the direction of axonal growth, there are studies that focus on the stimulation of regenerative processes by the bioactive compounds present in scaffold channels. Synergism of the microenvironment with neurotrophic factors has been proven to promote more efficient regenerative processes during the rehabilitation period in a structural injury of the spinal cord [81]. These growth factors include stem cells [7, 42, 44, 82–85], nerve cell growth factors [86–89], and even locally delivered magnetic nanoparticles [90]. Polylactide-co-glycolide multichannel scaffolds containing Schwann cells derived from newborn rats were

Generalized information on experimental models of SCI in rats

No.	Approach level	Injury	Complexity degree*	Invasiveness degree*	Application	References
1	C2	Left hemisection	+++	+++	Assessment of functional recovery	[20]
2	C4	Resection	+++	+++	Investigation of regenerative processes in the conductive pathways upon scaffold implantation and under the influence of a neurotrophic growth factor	[48, 58]
3	C5	Contusion	++	+++	Study of electro- and pathophysiology of injury	[13, 66]
4	C5	Transverse resection of a spinal cord segment	+++	+++	Investigation of axonal regeneration within the scaffold structure	[37, 65]
5	T3, T3–6	Transverse resection of the spinal cord	+++	+++	Study of motor axon regeneration in fibrin gel under action of neuronal stem cells and growth factor (NGF) within the scaffold structure	[9, 46, 47]
6	T5–7	Compression	+++	++	Assessment of clinical consequences, depending on the time of experimental compression of the spinal cord	[16, 18]
7	T6–7	Transverse resection of the spinal cord	+++	+++	Implantation of scaffolds; investigation of regeneration of injured axons	[83]
8	T6–10	Chemical injury	++	+++	Investigation of nerve fiber remyelination	[32]
9	T7–9, T7–10	Transverse resection of a spinal cord segment	++	+++	Implantation of scaffold; study of the axon ability to grow through the scaffold	[53, 63]
10	T7–12	Complete spinal cord transection	+++	+++	Study of spontaneous recovery of hindlimb mobility after injury	[60]
11	T8	Transverse resection of a spinal cord segment	++	+++	Implantation of scaffolds of different structure	[67, 69, 70, 78]
12	T8–9, T9	Transverse resection of a spinal cord segment	++	+++	Investigation of axonal remyelination within fibrillar collagen scaffolds and the possibility of spontaneous functional recovery	[33, 50. 52, 59]
13	T9	Contusion	++	+++	Assessment of contusion severity by locomotor tests and investigation of the influence of mesenchymal stem cells on regenerative processes	[21, 64]
14	T9	Contusion followed by resection of a glial scar	+++	+++	Replacement of a glial scar with collagen scaffolds with mesenchymal stem cells	[84]
15	T9–10	Hemilaminectomy	++	++	Scaffold implantation	[61]
16	T9–12	Transverse resection of a spinal cord segment	++	+++	Investigation of the effect of autologous olfactory ensheathing cells on spinal cord regeneration	[11]
17	T10	Contusion	++	+++	Investigation of contusion injury	[23]
18	T10	Transverse resection of a spinal cord segment	++	+++	Investigation of myelination of injured nerve fibers and formation of a glial scar; study of functional recovery using neuronal stem cells	[41, 44]
19	T10–11	Chemical injury	++	+++	Investigation of magnetic field-driven migration of astrocytes to the injury site	[42]
20	T11	Contusion	++	+	Simulation of contusion injury	[40]
21	T11	Electrostimulation	+++	++	Comparison of compensatory abilities in primates and rats in spinal cord injury	[1]
22	T11–12	Complete transection	+++	+++	Implantation of scaffolds; investigation of the effect of neuronal factor on axonal regeneration	[74]
23	L1–5	Transverse resection of a spinal cord segment	++	+++	Investigation of regeneration of motor neuron axons	[43]

*Severity: + – mild, ++ – moderate; +++ – pronounced.

proposed for directed axonal growth [76]. Placement of these structures in the spinal cord wound of adult rats led to the regeneration of injured axons a month after implantation. Later, replacement of Schwann cells in the scaffold channels with mesenchymal stem cells of the bone marrow led to a similar effect of injured axon regeneration in rats with SCI [83].

The issue of an adequate choice of the channel diameter is of particular importance in the development of multichannel biodegradable scaffolds [48, 56]. In rats, the diameter of axons is known to range from 1 to 8 μm, with a cross section of 2–4 μm being predominant [91, 92]. When creating the structure of internal scaffold channels, it is necessary to take into account the fact that, during regeneration, a new myelin sheath is first formed, through which the axon grows subsequently [93, 94]. For example, an increase in the channel diameters of alginate scaffolds by 50% (from 41 to 64 μm) stimulated the regenerative activity of axons by more than two fold [37].

CONCLUSION

This review has described the main approaches to and features of SCI modeling in laboratory rats and demonstrated the use of biodegradable 3D scaffolds for restoring the functions of an injured spinal cord. However, each SCI model should be improved and adapted to the type and form of a new tested scaffold. The relationship between a quantitative recovery of axons and maintenance of the motor function after injury depends on the model type, material, and shape of the scaffold. Generalized data on the main experimental models of SCI in rats are presented in the *Table*.

The presented data, unfortunately, do not reflect the entire range of SCI models developed to date. Their number continues to increase. The advantages and disadvantages of each model should be considered in the context of its etiological and pathogenetic conformity to a human disease. Model adequacy is a key criterion for evaluating the possibility of extrapolating the findings to clinical practice. The question of to which extent the results obtained in rat biomodels can be extrapolated to humans is both of utmost importance and complexity in experimental animal modeling [95, 96]. The question of the adequacy of a given experimental biomodel to processes occurring in the human body remains open for most animal models. ●

REFERENCES

1. Friedli L., Rosenzweig E.S., Barraud Q., Schubert M., Dominici N., Awai L., Nielson J.L., Musienko P., Nout-Lomas Y., Zhong H., et al. // Sci. Transl. Med. 2015. V. 7. № 302. P. 134.
2. La Placa M.C., Simon C.M., Prado G.R., Cullen D.K. // Prog. Brain. Res. 2007. V. 161. P. 13–26.
3. Information Bulletin № 384, November 2013, WHO.
4. Gomes-Osman J., Cortes M., Guest J., Pascual-Leone A. // J. Neurotrauma. 2016. V. 33. P. 425–438.
5. National Spinal Cord Injury Statistical Center // J. Spinal Cord Med. 2016. V. 39. P. 370–371.
6. Abrams G.M., Ganguly K. // Neurol. 2015. V. 21. P. 188–200.
7. Sakiyama-Elbert S., Johnson P.J., Hodgetts S.I., Plant G.W., Harvey A.R. // Handb. Clin. Neurol. 2012. V. 109. P. 575–594.
8. Silver J., Schwab M.E., Popovich P.G. // Cold Spring Harb. Perspect. Biol. 2014. V. 7. a020602.
9. Olson L. // Exp. Neurol. 2013. V. 248. P. 309–315.
10. Ahuja C.S., Fehlings M. // Stem Cells Transl. Med. 2016. V. 5. P. 914–924.
11. Watzlawick R., Rind J., Sena E.S., Brommer B., Zhang T., Kopp M.A., Dirnagl U., Macleod M.R., Howells D.W., Schwab J.M. // PLoS Biol. 2016. V. 14. P. e1002468.
12. Reier. P.J., Lane M.A., Hall E.D., Teng Y.D., Howland D.R. // Handb. Clin. Neurol. 2012. V. 109. P. 411–433.
13. Onifer S.M., Nunn C.D., Decker J.A., Payne B.N., Wagoner M.R., Puckett A.H., Massey J.M., Armstrong J., Kaddumi E.G., Fentress K.G., et al. // Exp. Neurol. 2007. V. 207. P. 238–247.
14. Cheriyan T., Ryan D.J., Weinreb J.H., Cheriyan J., Paul J.C., Lafage V., Kirsch T., Errico T.J. // Spinal Cord. 2014. V. 52. № 8. P. 588–595.
15. Zhang N., Fang M., Chen H., Gou F., Ding M. // Neural. Regen. Res. 2014. V. 9. № 22. P. 2008–2012.
16. Rivlin A.S., Tator C.H. // Surg. Neurol. 1978. V. 10. P. 38–43.
17. von Euler M., Seiger A., Sundström E. // Exp. Neurol. 1997. V. 145. P. 502–510.
18. Gruner J.A., Yee A.K., Blight A.R. // Brain Res. 1996. V. 729. P. 90–101.
19. Basso D.M., Beattie M.S., Bresnahan J.C. // Exp. Neurol. 1996. V. 139. P. 244–256.
20. Fujiki M., Kobayashi H., Inoue R., Ishii K. // Exp. Neurol. 2004. V. 187. P. 468–477.
21. Cao Q., Zhang Y.P., Iannotti C., DeVries W.H., Xu X.M., Shields C.B., Whittemore S.R. // Exp. Neurol. 2005. V. 191. P. 3–16.
22. Pertici V., Trimaille T., Laurin J., Felix M.S., Marqueste T., Pettmann B., Chauvin J.P., Gigmes D., Decherchi P. // Biomaterials. 2014. V. 35. № 24. P. 6248–6258.
23. Mills C.D., Grady J.J., Hulsebosch C.E. // J. Neurotrauma. 2001. V. 18. P. 1091–1105.
24. Fehlings M.G., Tator C.H. // Exp. Neurol. 1995. V. 132. P. 220–228.
25. Seddon H. // Brain. 1943. V. 66. № 4. P. 237–288.
26. Sunderland S. // Brain. 1951. V. 74. № 4. P. 491–516.
27. Zhou L., Kambin P., Casey K.F., Bonner F.J., O'Brien E., Shao Z., Ou S. // Neurol. Res. 1995. V. 17. № 4. P. 307–311.
28. Alant J.D., Kemp S.W., Khu K.J., Kumar R., Webb A.A., Midha R. // J. Neurotrauma. 2012. V. 29. № 8. P. 1691–1703.
29. Geuna S., Raimondo S., Ronchi G., Di Scipio F., Tos P., Czaja K., Fornaro M. // Int. Rev. Neurobiol. 2009. V. 87. P. 27–46.
30. Belkas J.S., Shoichet M.S., Midha R. // Neurol. Res. 2004. V. 26. № 2. P. 151–160.
31. Hilliard M.A. // J. Neurochem. 2009. V. 108. № 1. P. 23–32.
32. Taveggia C., Feltri M.L., Wrabetz L. // Nat. Rev. Neurol. 2010. V. 6. № 5. P. 276–287.

33. Suzuki H., Kanchiku T., Imajo Y., Yoshida Y., Nishida N., Gondo T., Yoshii S., Taguchi T. // Med. Mol. Morphol. 2015. V. 48. № 4. P. 214–224.
34. Lundy-Ekman L. Neuroscience: Fundamentals for Reh abilitation. 3rd ed. St. Louis, Missouri: Elsevier Saunders, 2007.
35. Campos N.A., Chiles J.H., Plunkett A.R. // Pain Physician. 2009. V. 12. № 6. P. 997–1000.
36. Willenbring S., DeLeo J.A., Coombs D.W. // Anesth. Analg. 1995. V. 81. № 3. P. 549–554.
37. Günther M.I., Weidner N., Müller R., Blesch A. // Acta Biomater. 2015. V. 27. P. 140–150.
38. Ilfeld B.M., Preciado J., Trescot A.M. // Expert. Rev. Med. Devices. 2016. V. 13. № 8. P. 713–725.
39. Gruber H., Glodny B., Kopf H., Bendix N., Galiano K., Strasak A., Peer S.A. // J. Roentgenol. 2008. V. 190. № 5. P. 1263–1269.
40. Marcol W., Slusarczyk W., Gzik M., Larysz-Brysz M., Bobrowski M., Grynkiewicz-Bylina B., Rosicka P., Kalita K., Węglarz W., Barski J.J., et al. // J. Reconstr. Microsurg. 2012. V. 28. № 8. P. 561–568.
41. Cui Z.S., Zhao P., Jia C.X., Liu H.J., Qi R., Cui J.W., Cui J.H., Peng Q., Lin B., Rao Y.J. // Genet. Mol. Res. 2015. V. 14. № 3. P. 9109–9117.
42. Li Z., Fang Z.Y., Xiong L., Huang X.L. // Indian J. Biochem. Biophys. 2010. V. 47. P. 359–363.
43. Kjell J., Olson L. // Dis. Model Mech. 2016. V. 9. № 10. P. 125–1137.
44. Liao Y., Zhong D., Kang M., Yao S., Zhang Y., Yu Y. // Zhongguo Xiu Fu Chong Jian Wai Ke Za Zhi. 2015. V. 29. № 8. P. 1009–1015.
45. Schrimsher G.W., Reier P.J. // Exp. Neurol. 1993. V. 120. P. 264–276.
46. Cameron A.A., Smith G.M., Randal D.C., Brown D.R., Rabchevsky A.G. // J. Neurosci. 2006. V. 26. P. 2923–2932.
47. Gao M., Lu P., Bednark B., Lynam D., Conner J.M., Sakamoto J., Tuszynski M.H. // Biomaterials. 2013. V. 34. P. 1529–1536.
48. Gros T., Sakamoto J.S., Blesch A., Havton L.A., Tuszynski M.H. // Biomaterials. 2010. V. 31. P. 6719–6729.
49. Huang Y.C., Huang Y.Y. // Artif. Organs. 2006. V. 30. P. 514–522.
50. Patist C.M., Mulder M.B., Gautier S.E., Maquet V., Jérôme R., Oudega M. // Biomaterials. 2004. V. 25. P. 1569–1582.
51. Spilker M.H., Yannas I.V., Kostyk S.K., Norregaard T.V., Hsu H.P., Spector M. // Restor. Neurol. Neurosci. 2001. V. 18. P. 23–28.
52. Taylor S.J., Sakiyama-Elbert S.E. // J. Control. Release. 2006. V. 116. P. 204–210.
53. King V., Phillips J., Hunt-Grubbe H., Brown R., Priestley J. // Biomaterials. 2006. V. 27. P. 485–496.
54. King V.R., Alovskaya A., Wei D.Y., Brown R.A., Priestley J.V. // Biomaterials. 2010. V. 31. P. 4447–4456.
55. Mothe A.J., Tam R.Y., Zahir T., Tator C.H., Shoichet M.S. // Biomaterials. 2013. V. 34. P. 3775–3783.
56. Stokols S., Tuszynski M.H. // Biomaterials. 2006. V. 27. P. 443–451.
57. Wei Y., He Y., Xu C., Wang Y., Liu B., Wang X., Sun X.D., Cui F.Z., Xu Q.Y. // J. Biomed. Mater. Res. B. Appl. Biomater. 2010. V. 95. P. 110–117.
58. Kwon B.K., Liu J., Messerer C., Kobayashi N.R., McGraw J., Oschipok L., Tetzlaff W. // Proc. Natl. Acad. Sci. USA. 2002. V. 99. № 5. P. 3246–3251.
59. You S.W., Chen B.Y., Liu H.L., Lang B., Xia J.L., Jiao X.Y., Ju G. // Restor. Neurol. Neurosci. 2003. V. 21. № 1–2. P. 39–45.
60. Li L.-S., Yu H., Raynald R., Wang X.-D., Dai G.-H., Cheng H.-B., Liu X.-B., An Y.-H. // Peer. J. 2017. V. 5. e2865.
61. Cloud B.A., Ball B.G., Chen B.K., Knight A.M., Hakim J.S., Ortiz A.M., Windebank A.J. // J. Neurosci. Meth. 2012. V. 211. P. 179–184.
62. Heimburger R.F. // Spinal Cord. 2005. V. 43. P. 438–440.
63. Lukovic D., Moreno-Manzano V., Lopez-Mocholi E., Javier Rodriguez-Jiménez F., Jendelova P., Sykova E., Oria M., Stojkovic M., Erceg S. // Sci. Repts. 2015. V. 5. № 9640.
64. Cho S., Kim Y.R., Kang H., Yim S.H., Park C., Min Y.H., Lee B.H., Shin J.C., Lim J.B. // Cell Transplant. 2009. V. 18. P. 1359–1368.
65. Novikova L.N., Pettersson J., Brohlin M., Wiberg M. // Biomaterials. 2008. V. 29. P. 1198–1206.
66. Dunham K.A., Siriphorn A., Chompoopong S., Floyd C.L. // J. Neurotrauma. 2010. V. 27. P. 2091–2106.
67. Zhao Z., Alam S., Oppenheim R.W., Prevette D.M. // Exp. Neurol. 2004. V. 190. P. 356–372.
68. Straley K.S., Foo C.W., Heilshorn S.C. // J. Neurotrauma. 2010. V. 27. № 1. P. 1–19.
69. Yara T., Kato Y., Kataoka H., Kanchiku T., Suzuki H., Gondo T., Yoshii S., Taguchi T. // Med. Mol. Morphol. 2009. V. 42. P. 150–154.
70. Yoshii S., Oka M., Shima M., Akagi M., Taniguchi A. // Spine. 2003. V. 28. P. 2346–2351.
71. Yoshii S., Oka M., Shima M., Taniguchi A., Taki Y., Akagi M. // J. Biomed. Mater. Res. 2004. V. 70. P. 569–575.
72. Guo S.Z., Ren X.J., Wu B., Jiang T. // Spinal Cord. 2010. V. 48. P. 576–581.
73. Geller M., Fawcett J.W. // Exp. Neurol. 2002. V. 174. P. 125–136.
74. Jain A., Kim Y.T., McKeon R.J., Bellamkonda R.V. // Biomaterials. 2006. V. 27. P. 497–504.
75. Hurtado A., Moon L.D., Maquet V., Blits B., Jérôme R., Oudega M. // Biomaterials. 2006. V. 27. P. 430–442.
76. Moore M.J., Friedman J.A., Lewellyn E.B., Mantila S.M., Krych A.J., Ameenuddin S., Knight A.M., Lu L., Currier B.L., Spinner R.J., Marsh R.W., Windebank A.J., Yaszemski M.J. // Biomaterials. 2006. V. 27. P. 419–429.
77. Novikova L.N., Novikov L.N., Kellerth J.O. // Curr. Opin. Neurol. 2003. V. 16. P. 711–715.
78. Tsai E.C., Dalton P.D., Shoichet M.S., Tator C.H. // Biomaterials. 2006. V. 27. P. 519–533.
79. Balyabin A.V., Tikhobrazova O.P., Muravyeva M.S., Klyuev E.A., Ponyatovskaya A.V., Shirokova O.M., Bardakova K.N., Minaev N.V., Koroleva A.V., Mitaeva Y.I., et al. // Neurosci. Res. 2016. V. 8. № 4. P. 198–211.
80. Timashev P.S., Vedunova M.V., Guseva D., Ponimaskin E., Deiwick A., Mishchenko T.A., Mitroshina E.V., Koroleva A.V., Pimashkin A.S., PanchenkoV.Ya., et al. // Biomed. Phys. Eng. Express. 2016. V. 2. № 3. P. 035001.
81. Jerani T.S., Pettikiriarachchi C., Parish L., Shoichet M.S., Forsythe J.S., Nisbet D.R. // Aust. J. Chem. 2010. V. 63. P. 1143–1154.
82. Ragnarsson K.T. // Spinal Cord. 2008. V. 46. P. 255–274.
83. Yang E.-Z., Zhang G.-W., Xu J.-G., Chen S., Wang H., Cao L.-L., Liang B., Lian X.-F. // Acta Pharmacol. Sinica. 2017. V. 38. P. 623–637.
84. Wang N., Xiao Z., Zhao Y., Wang B., Li X., Li J., Dai J. // J. Tissue. Eng. Regen. Med. 2017. doi: 10.1002/term.2450.
85. Zhao Y., Xiao Z., Chen B., Dai J. // Organogenesis. 2017. V. 10. P. 1–8.
86. Shi Q., Gao W., Han X., Zhu X.S., Sun J., Xie F., Hou X.L., Yang H.L., Dai J.W., Chen L. // Stem Cells Reg Med. China. 2014. V. 57. № 2. P. 232–240.

87. Jiao G., Pan Y., Wang C., Li Z., Li Z., Guo R. // Mater. Sci. Eng. C. Mater. Biol. Appl. 2017a. V. 76. P. 81–87.
88. Jiao G., Lou G., Mo Y., Pan Y., Zhang Z., Guo R., Li Z. // Mater. Sci. Eng. C. Mater. Biol. Appl. 2017b. V. 74. P. 230–237.
89. Xu Z.X., Zhang L.Q., Wang C.S., Chen R.S., Li G.S., Guo Y., Xu W.H. // Curr. Neurovasc. Res. 2017. doi: 10.2174/1567202614666170718093508.
90. Zhang C., Morozova A.Y., Abakumov M.A., Gubsky I.L., Douglas P., Feng S., Bryukhovetskiy A.S., Chekhonin V.P. // Med. Sci. Monit. 2015. V. 21. P. 3179–3185.
91. Kato N., Nemoto K., Nakanishi K., Morishita R., Kaneda Y., Uenoyama M., Ikeda T., Fujikawa K. // Diabetes. 2005. V. 54. № 3. P. 846–854.
92. Boehmerle W., Huehnchen P., Peruzzaro S., Balkaya M., Endres M. // Sci. Rep. 2014. V. 18. № 4. P. 63–70.
93. Abdullah M., O'Daly A., Vyas A., Rohde C., Brushart T.M. // Exp. Neurol. 2013. V. 249. P. 1–7.
94. Muheremu A., Wang Y., Peng J. // Can. J. Neurol. Sci. 2013. V. 40. P. 292–298.
95. Roep B.O., Atkinson M. // Diabetologia. 2004. V. 47. № 10. P. 1650–1656.
96. Mestas J., Hughes C.C. // J. Immunol. 2004. V. 172. № 5. P. 2731–2738.

B Cell Regulation in Autoimmune Diseases

A. V. Sokolov[1], A. A. Shmidt[1], Y. A. Lomakin[1,2*]
[1]Shemyakin-Ovchinnikov Institute of Bioorganic Chemistry RAS, Miklukho-Maklaya Str., 16/10, Moscow, 117997, Russia
[2]Institute of Fundamental Medicine and Biology, Kazan Federal University, Kremlevskay Str., 18, Kazan, 420008, Russia
*E-mail: yasha.l@bk.ru
Received December 12, 2017; in final form June 21, 2018

ABSTRACT **Antibody-independent B cell effector functions play an important role in the development and suppression of the immune response. An extensive body of data on cytokine regulation of the immune response by B lymphocytes has been accumulated over the past fifteen years. In this review, we focused on the mechanisms of inflammatory response suppression by subpopulations of regulatory B cells in health and autoimmune pathologies.**
KEYWORDS **Multiple sclerosis, systemic lupus erythematosus, rheumatoid arthritis, experimental autoimmune encephalomyelitis, Breg, regulatory B cells, IL-10, IL-35, CD19+CD24(hi)CD38(hi).**
ABBREVIATIONS **EAE – experimental autoimmune encephalomyelitis, APC – antigen-presenting cells, MHC – major histocompatibility complex, IL – interleukin, MS – multiple sclerosis, RA – rheumatoid arthritis, Breg – regulatory B cell, Treg – regulatory T cell, SLE – systemic lupus erythematosus, CNS – central nervous system**

INTRODUCTION

B cells are one of the central elements of humoral immunity. Traditionally, it had been believed that the main role of B cells lay in the production of antibodies, until their direct participation in cellular immunity was discovered later. B-lymphocytes are involved in T cell activation by antigen presentation, co-stimulation, and cytokine production; they affect antimicrobial protective mechanisms and inflammatory processes in the tissues of the body; they also act as regulatory cells that control both the cellular and humoral immune responses.

The existence of B cells capable of suppressing the immune response was first suggested as early as in the 1970s. Professor James Turk's team found that removal of B cells from a pool of guinea pig splenocytes disabled the inhibition of delayed-type hypersensitivity (DTH) [1]. However, as it was not possible to characterize this observation from the molecular or biochemical point of view at that time, the studies were suspended. The regulatory properties of B cells were for the first time reliably described for experimental autoimmune encephalomyelitis (EAE), the animal model of multiple sclerosis, only 20 years later. Immunization of genetically modified mice with deletion of B lymphocytes (B10.PLμMT line) with a myelin basic protein (MBP) peptide led to the development of an acute and more severe form of EAE. The pathological process was uncontrollable, and there was no spontaneous remission characteristic of B10.PL mice producing mature B cells [2]. Over the past 10 years, much progress has been made in the study of immunosuppressive B cells. It has been found that regulatory B cells (Breg) can influence T cell differentiation, shifting it towards the regulatory phenotype [3]. Since then, the regulatory function of B-lymphocytes has been demonstrated in animal models of autoimmune colitis, rheumatoid arthritis, autoimmune diabetes, and systemic lupus erythematosus (SLE) [4–6].

MECHANISMS OF REGULATORY B CELL FUNCTIONING

The very concept of regulatory B cells was first formulated by S. Fillatreau quite recently [4], when he described B cells (B10 cells) that produce interleukin-10 (IL-10), which can reduce clinical manifestations of EAE. IL-10 is one of the anti-inflammatory cytokines which regulate immune response and affect mainly antigen-presenting cells, reducing the expression of pro-inflammatory cytokines and the molecules involved in antigen presentation (MHC I, MHC II, adhesion molecules, etc.), and also inhibit the proliferation of $CD4^+$ T lymphocytes [5]. Subsequent experimental removal of the population of B10 lymphocytes in mice also revealed a correlation with a decrease in the amount of Tregs, which was also associated with excessive proliferation of pro-inflammatory T cells after induction of the autoimmune response [6]. Bregs produce IL-10, and therethrough inhibit the differentiation of T helper type 1 (Th1) and T helper type 17 cells (Th17), decreasing the production of inflammatory cytokines

by dendritic cells [7]. For this reason, production of IL-10 is the most extensively studied B cell regulatory mechanism and it is often applied to identify new Breg subpopulations. Nevertheless, other mechanisms could be used by Breg to control the development of an immune response, such as production of TGF-β (transforming growth factor-β), IL-35, IgM, IgG4, action on T lymphocytes through direct cell-to-cell contact, etc. (*Table*). At the same time, the regulation of immune processes using several simultaneous mechanisms is often observed, for example, by the production of IL-10 and TGF-β, both of which essentially inhibit the T cell response [8]. It was shown that lipopolysaccharide-activated B cells facilitate the apoptosis of $CD4^+$ and inactivation of $CD8^+$ effector T cells through the production of TGF-β despite an increased level of IL-10 expression [9, 10]. Particular attention should be paid to IL-35, another recently described key immunoregulatory cytokine produced by Bregs. Genetically modified mice, whose B cells do not express IL-35 subunits, developed acute EAE. In the case of inflammation caused by *Salmonella typhimurium*, the lack of IL-35 expression by B cells led to an increase in Th1 proliferation and increase in the amount of macrophages in the spleen [11]. Another independent study showed that IL-35-stimulated B cells-produced IL-35 and inhibited experimental uveitis under conditions of adoptive transfer [12]. An important role of Bregs in maintaining the equilibrium and functions of the type 1 natural killer cells (invariant natural killers, iNKT) required to maintain tolerance to autoantigens in autoimmune diseases has been proven [13].

As shown in *Table*, the aforementioned mechanisms primarily act on T lymphocyte subpopulations with

The functioning mechanisms of B regulatory cells

Regulatory mechanism	Effect	Experimentally validated in B cells of	
		Mouse	Human
IL-10 production	Inhibition of $CD4^+$ T cell proliferation	✔ [15]	✔ [3]
	Inhibition of Th1 and Th17 differentiation	✔ [4, 16]	✔ [3, 17]
	Induction of regulatory T cell proliferation	✔ [18–21]	✔
	Inhibition of TNF-α[1] production by monocytes		✔ [22]
	Inhibition of cytotoxic activity of T lymphocytes		✔ [23]
	Inhibition of T follicular helper (T_{FH}) and B cell differentiation		✔ [24]
TGF-β production	Inhibition of Th1 and APC differentiation	✔ [9, 11]	
	Induction of regulatory T cell proliferation	✔ [24, 25]	✔ [26]
	Regulation of macrophage activity	✔ [27]	
	Inhibition of T follicular helper (T_{FH}) and B cell differentiation		✔ [24]
IL-35 production	Inhibition of activation of macrophages and pro-inflammatory T-lymphocytes	✔ [11]	
IgM production	Induction of apoptotic bodies elimination	✔ [28]	
	Suppression of allergic response of Th2	✔ [29]	
Cell-to-cell contact	Inhibition of $CD4^+$ T cell proliferation	✔ [30, 31]	✔ [32]
GITRL[2]	Induction of regulatory T cell proliferation	✔ [33]	
IgG4 production	Attenuation of complement system activation		✔ [34]
BTLA expression[3]	Induction of regulatory T cell proliferation and activation	✔ [35]	
	BTLA/HVEM[4] interaction? Inhibition of T cell activation? Inhibition of B cell proliferation?		✔ [36]
PD-L1 expression[5]	Suppression of inflammatory response by inhibiting T follicular helpers (T_{FH}) and reducing antibody production	✔ [37]	
	Induction of regulatory T cell proliferation?		✔ [38]
	Inhibition of $CD8^+$? Inhibition of $CD4^+$? Inhibition of APC?		✔ [23, 39]

[1] – TNF-α, tumor necrosis factor α;
[2] – GITRL, glucocorticoid-induced tumor necrosis factor receptor-related ligand;
[3] – BTLA, B and T lymphocyte attenuator;
[4] – HVEM – herpes virus entry mediator;
[5] – PD-L1 – programmed death-1-ligand.

proinflammatory properties by inhibiting their differentiation and development. However, other effects of Breg are also observed (e.g., attenuation of complementary system activation and elimination of apoptotic cells) that eventually also lead to a decrease in the intensity of the immune response [14].

Breg functioning involves CD40, TLR, B cell receptor, CD19, CD1d, etc. [14]. The membrane receptor CD40 activated by the corresponding ligand (CD40L present on the effector T cell membrane) can stimulate cascade reactions. Therefore, CD40 is involved in the development of memory B cells, the switching of immunoglobulin classes, and formation of germinal centers. Its participation in the functioning of regulatory B cells was shown in murine and human B lymphocytes. Activation of B cells in the presence of the ligand or activated T cells initiated the production of IL-10 and triggered a regeneration process in the case of EAE and, vice versa, suppression or elimination of the receptor ($CD40^{-/-}$) disabled IL-10 synthesis.

It is known that Toll-like receptors (TLRs) recognize a wide variety of molecular epitopes and play an important role in the signal transfer in innate and adoptive immunity. Stimulation of TLR with appropriate antigens increases the survival rate of mice in SLE and EAE models, as compared to a control group that did not receive the stimulating agent; this also results in a decrease in T cell proliferation and secretion of proinflammatory cytokines by these cells [40]. In *in vitro* studies on human splenic B cells and peripheral blood cells, stimulation with TLR antigens induced IL-10 production and the highest impact involved stimulation with lipopolysaccharide and CpG (ligands TLR4 and TLR9, respectively) [22]. The role of BCR, CD19, and other surface B cell markers in the induction of a regulatory phenotype was also studied. It was shown that activation of receptors leads to IL-10 production, and to a decrease in the intensity of clinical manifestations of the investigated diseases in animal models. The absence of these molecules significantly reduces the ability of B cells to regulate immune responses [14]. Elevated levels of expression of B and T lymphocyte attenuators (BTLA) or the ligand of the programmable death receptor (PD-L1) in certain populations of regulatory B cells can lead to a decrease in the inflammatory response, due to the inhibition of effector T and B cells through an interaction with the HVEM or PD receptor, respectively [23, 35, 41]. The examples above demonstrate our improved understanding of the multiple roles of B regulatory cells, provided that Bregs can interact with many immune cells to suppress the immune response (*Fig. 1*). Abnormal functions and the amount of regulatory B cells are most often associated with autoimmune diseases. It is clear that how this subpopulation of lymphocytes functions must be strictly controlled by the body, starting from the recognition of proinflammatory signals by these cells in their microenvironment and ending with a strict control of their differentiation and development. Nevertheless, it remains unclear whether a Breg subpopulation is always present in the body or whether its development is induced by external signals. Although it is obvious that B lymphocytes perform many functions in both healthy and impaired immune systems, they play both pathological and protective roles in autoimmune processes, infections, and allergies [42].

PHENOTYPE AND ORIGIN OF REGULATORY B CELLS

When investigating B regulatory cells, it is also important to determine their phenotype. To date, many different subpopulations of Breg have been described, most of which are similar in both phenotype and functions. It is still unclear whether the differences observed between these subpopulations are due to the influence of the immunological environment or whether there are lines of B regulatory cells of different origins. In mice, the populations of regulatory B cells account for up to 5% of the total pool of B cells in the spleen and lymph nodes and their amount significantly increases with the development of inflammatory responses (e.g., EAE [43], collagen-induced arthritis [21], or helminthiasis [44]). There are three main subpopulations of regulatory B cells in mice: T2-MZP (transitional 2 marginal-zone precursor) $CD19^{+}CD21^{high}CD23^{high}IgM^{high}$ [31], $CD19^{+}CD5^{+}CD1d^{high}$ [45], and Tim-1^{+} B cells [46]. In humans, B10 cells account for less than 1—2% of the total amount of B cells in the blood. Human Bregs include $CD19^{+}CD24^{hi}CD38^{hi}CD1d^{hi}$ and $CD19^{+}CD24^{hi}CD27^{+}$ [22]. The relationship between the development and differentiation of these subpopulations is unknown. Although identification of IL-10 production was a good approach toward determining suppressor B cells, many of the surface marker molecules required for a more accurate characterization of the subpopulation can be differently expressed under conditions of immune response activation, making it difficult to study Bregs under various experimental conditions, which often alter the phenotype of Breg subtypes. This problem can be solved by means of identification of a Breg-specific transcription factor, which can be used to answer the question of whether these cells belong to the same developmental line. Currently, two models of Breg development can be suggested. According to the first one, regulatory B cells, like Treg, represent a separate B cell line with a specific set of factors of gene expression control responsible for their capability to suppress the immune response. The second theory is that B lymphocytes undergo phe-

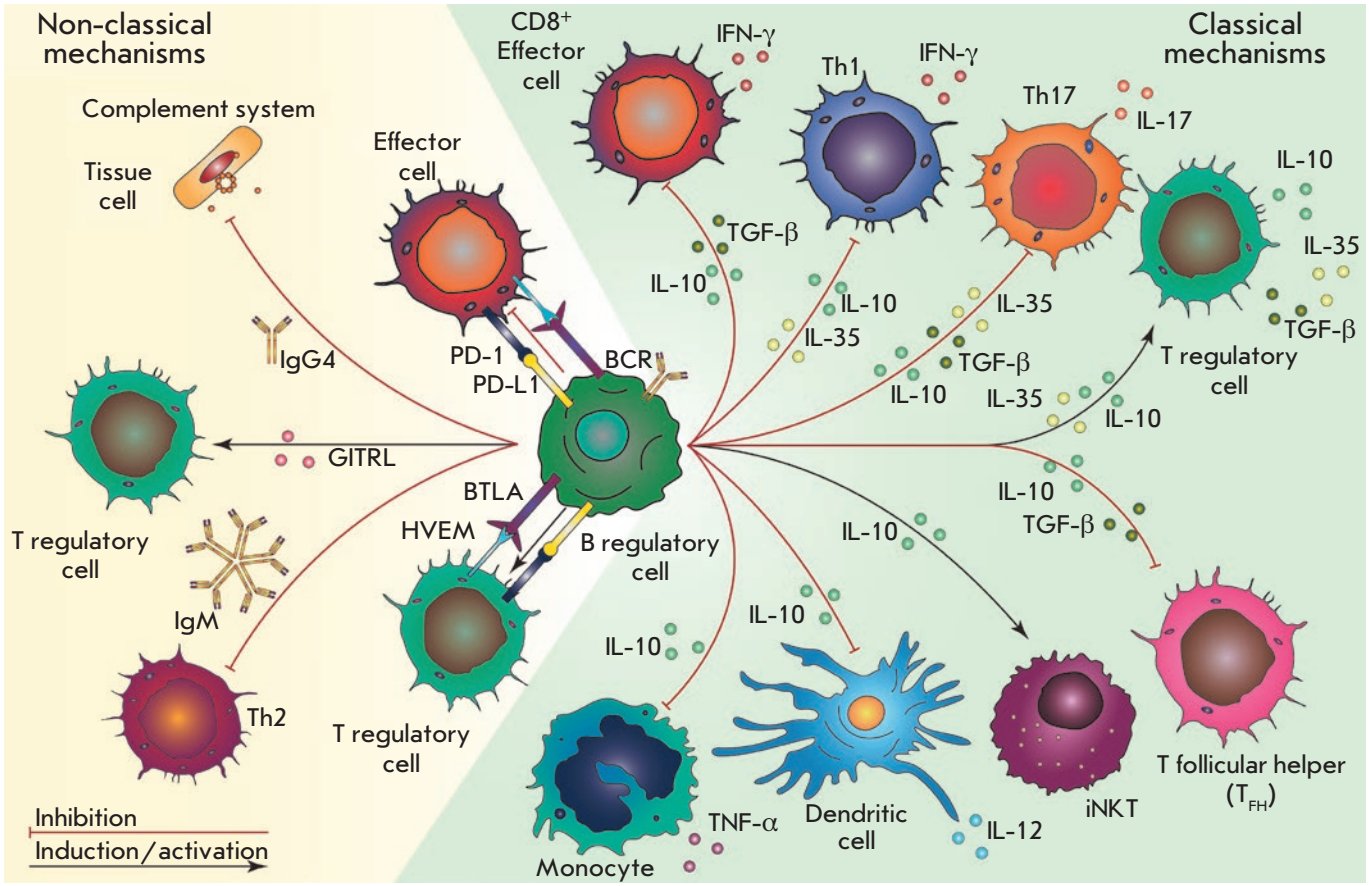

Fig. 1. Mechanisms of regulatory B cell functioning and their impact on immune cells. Regulatory B cells produce anti-inflammatory cytokines that induce the formation of regulatory T cells and support invariant natural killers (iNKT), shown by black arrows. Breg-produced interleukins inhibit the differentiation of T follicular helpers, T helpers 1 and 17, inhibit the cytotoxic activity of T-lymphocytes ($CD8^+$), and inhibit the production of pro-inflammatory cytokines by monocytes and dendritic cells (red arrows). Additionally, regulatory B cells reduce inflammation through direct cell contact, expression of B and T lymphocyte attenuators (BTLA), programmable death receptor ligands (PD-L1), production of IgM, IgG4, etc.

notypic reconstructions in response to certain stimuli to suppress a local inflammation. Despite the studies in mice and humans, it has not yet been possible to identify a specific transcription factor. The inability to identify these markers, as well as the heterogeneity of Breg phenotypes, indicates that suppressor B cells are not a distinct developmental line: i.e., any B cell can be potentially differentiated into a regulatory one under the influence of external factors [8]. It was also shown that, along with previously described Breg subpopulations, plasmablasts can also suppress inflammatory responses. Mice lacking plasmablasts due to a genetic removal of the Irf4 and Prdm1 (Blimp1) transcription factors required for plasma cell differentiation developed acute EAE [7]. This is not the first case when B cells-producing antibodies also perform a regulatory function: $CD138^+$ plasma cells, producing IL-10 and IL-35, suppressed pro-inflammatory responses in the case of EAE and a *Salmonella enterica* infection [11]. Moreover, splenic B10 cells that were differentiated into antibody-producing plasmablasts after stimulation both *in vivo* and *in vitro* have been described [47]. A relationship between $CD19^+CD24^{hi}CD38^{hi}$ B cells performing regulatory functions and IL-10-secreting plasmablasts in humans has been suggested. This assumption suggests a similar differentiation vector, i.e. development into plasma cells, of Bregs in mice and humans. The idea that antibody-producing cells also regulate immune responses conflicts with the modern concept that plasma cells cause an inflammatory re-

sponse, producing antibodies that are often pathogenic in the context of autoimmune diseases or allergies. Therefore, it is possible that a certain subpopulation of plasmablasts produces antibodies and, thus, supports the possibility of inflammatory response regulation. This assumption is supported by evidence that deficiency in Bcl6, the transcription factor required for B cell proliferation in germinal centers, does not affect the development of regulatory plasmablasts [7].

According to recent studies, immature B cells, mature B cells, and plasmablasts are able to differentiate into IL-10-producing Bregs in the body of mice and humans. This confirms the assumption that the B lymphocyte environment, rather than a specific transcription factor, is required for the differentiation of regulatory B cells. Thus, the search for the stimuli required for B cells to acquire regulatory functions becomes important in order to assess the origin of Bregs. However, it has recently been shown that differentiation of IL-10-producing regulatory B cells can be also induced by pro-inflammatory cytokines [8].

THE ROLE OF REGULATORY B CELLS IN THE DEVELOPMENT OF AN INFLAMMATORY RESPONSE

There is strong evidence that inflammation leads to an increase in the amount of Bregs and their ability to suppress the immune response. It is known that they are present in naïve mice, but their amount increases with the development of some autoimmune diseases [31, 48]. Moreover, it was found that Bregs are involved in the suppression of inflammation in autoimmune pathologies. For example, the absence of Bregs in an animal model of MS results in the development of more severe and acute forms of EAE [4, 6]. Recently, it has been shown that the amount of regulatory B cells increases in response to the secretion of the proinflammatory cytokines IL-1β and IL-6 after induction of arthritis [49]. Secretion of these cytokines in mice with arthritis is controlled by bacteria in the intestine. Previously, the role of the microbiota had already been shown in the differentiation of pro-arthritogenic Th17 [50]. Mice grown in nonsterile conditions, whose B cells do not express IL-1R1 or IL-6R, develop acute arthritis [49]. Therefore, it can be assumed that Breg proliferation increases in response to IL-1β and IL-6 in order to prevent uncontrolled amplification of pro-inflammatory lymphocytes, such as Th17. Other inflammatory cytokines required for the differentiation of a Th17 phenotype, the IL-21 and granulocyte macrophage colony-stimulating factor (GM-CSF), together with IL-15, also play an important role in the development of Bregs [51, 52]. Various sources of cytokines that can enhance the production of IL-10 B cells have been identified. Myeloid cells of lymphatic vessels and spleen producing IL-6 and IL-1β are responsible for an increase in the amount of Bregs associated with arthritis, while $CD4^+$ splenic T cells producing IL-21 activate Bregs in experimental arthritis models [49, 52]. On the other hand, administration of the anti-inflammatory cytokine IL-35 to mice increased the population of B cells expressing IL-10 and IL-35 and thereby suppressed the development of uveitis [53]. However, it should be taken into account that IL-35 is not expressed permanently, but is rather induced in response to inflammation [54].

Although these cytokines evidently play an important role in the proliferation of Bregs, it should be kept in mind that, during immune response development, B cell receptors (BCR) are also required for Breg induction. MD4 mice, whose BCR is specific to hen egg lysozyme (HEL), demonstrate impaired activation of Bregs during the development of EAE. It has been shown that chimeric animals with MD4 B cells incapable of IL-10 production develop a more severe form of EAE and are not capable of recovery [4]. Furthermore, MD4 B cells secrete less IL-10 and the amount of B10 cells themselves is lower than that in wild-type mice [45, 55]. The importance of correct recognition of BCR in Bregs is evidenced by the results obtained using mice with a specific deletion of the stromal interaction molecule 1 (STIM-1) and STIM-2 in B cells. These molecules are required for the regulation of the calcium inflow into the cytosol of B cells after BCR interaction with an antigen. Mice whose B lymphocytes lack STIM-1 and STIM-2 demonstrate a decrease in IL-10 production after stimulation with MOG (myelin oligodendrocyte glycoprotein) autoantigen [56]. These data show that antigen-specific recognition of the B cell receptor is important for the functioning and proliferation of Bregs. B cells can differentiate into regulatory or antibody-producing cells in response to B cell receptor recognition during the development of the immune response.

The significance of the inflammatory response in Breg differentiation raises the question of the place of their maturation. To date, most studies have investigated B cell populations in the spleen. However, in the case of colitis and EAE, Breg cells were also found in lymphatic vessels close to the inflammation site [7, 48]. Moreover, regulatory B cells can develop and gain the ability to suppress the immune response outside the spleen; namely, in the lymphatic vessels (in this instance, spleen removal does not affect their production) [7]. All these data support the theory that Breg induction is influenced by the inflammatory environment, which contradicts previously published results characterizing the spleen as the major regulatory B cell development site.

B CELL REGULATION IN THE DEVELOPMENT OF AUTOIMMUNE PATHOLOGIES

Multiple sclerosis (MS)

The population of regulatory B cells also participates in the pathogenesis of MS, which holds a special place in the list of autoimmune pathologies and is one of the most socially and economically significant neurological diseases of our time. MS occurs mainly in middle-aged people and leads to an almost complete loss of working ability or, in the case of insufficiently effective and timely treatment, even death within 10–15 years. For a long time, the leading role in MS development was attributed to Tcell-mediated immunity. However, there is now extensive evidence of the important role of B cells in the pathogenesis of MS [57, 58]. Catalytic antibodies, hydrolyzing the myelin basic protein, one of the characteristic autoantigens in MS, were found in these patients [59, 60]. Although the etiology of MS is still not fully understood, special attention is paid to bacterial and viral infections, along with genetic predisposition, hormonal status, and climatic conditions as the factors associated with its development. It is believed that molecular mimicry and cross-reactivity can underlie the mechanisms of viral induction of the disease. In 2003, cross-reactive recognition of the nuclear antigen of the Epstein-Barr virus (EBNA) and the autoantigen peptide of the myelin basic protein (MBP) by the monoclonal T cell receptor was demonstrated [61]. Later on, cross-reactivity was also detected and validated in autoantibodies to the LMP1 protein of the Epstein-Barr virus and MBP [62, 63]. In the case of EAE, Bregs can inhibit autoimmune T cell responses by slowing the differentiation of the pro-inflammatory T helpers 1 specific to CNS autoantigens [57]. The absence of Bregs leads to an exacerbation of immune responses. As mentioned earlier, mice with EAE devoid of B10 cells develop an acute form of the disease without remission [4]. The regulatory functions of IL-10-producing B cells were confirmed by the results of the study, where adaptive transfer of wild-type B cells reduced the severity of EAE manifestations in contrast to a transfer of IL-$10^{-/-}$ B lymphocytes from μMT mice. In that experiment, B cells from the first group of mice produced IL-10. Recently, the relationship between B and T regulatory cells in the development of EAE pathology has been characterized [43]. Indeed, adoptively transferred B10-cells directly affected the pathogenesis of EAE, as in the study by M. Yang [64], and their amount increased in the spleen, but not in the central nervous system, which is in agreement with the idea that they possess regulatory functions. Moreover, the transfer of antigen-activated B10 cells into wild-type mice strongly inhibited EAE induction, but B10 lymphocytes could not inhibit further EAE progression. At the same time, the amount of regulatory T cells in the central nervous system significantly increased with the development of the disease and this process influenced the course of EAE at the late stages. These data suggest that Bregs play a key role at the early stages of the disease, while Tregs perform regulatory functions in further development of the disease.

The EAE model showed that regulatory B cells are involved in the development of the pathological process. The levels of IL-10 production by peripheral blood B lymphocytes in MS patients were first determined in 2007 [65]. A significantly lower level of IL-10 production by B cells stimulated in the presence of the CD40 ligand was found in groups with relapsing-remitting and secondary-progressive MS compared to healthy donors. A similar effect was observed in the case of B cell stimulation with CpG [66]. Therefore, impaired IL-10 production and the functions of regulatory B cells from the peripheral blood of MS patients have been established. Apart from IL-10 production, regulatory B cells are involved in the development of MS by the production of IL-35 and TGF-β, and they can also enhance Foxp3 and CTLA-4 expression in regulatory T cells, as a result of direct cell contact [11, 32].

Thus, B cells can perform dual functions in the development of the demyelination process (possibly both positive and negative effects on immune responses), but their role in the pathogenesis of MS is well-traceable (*Fig. 2*).

Systemic lupus erythematosus (SLE)

Systemic lupus erythematosus is a chronic autoimmune disease of connective tissue characterized by a wide range of clinical manifestations. The danger of SLE is associated with the possibility of simultaneous involvement of many vital organs, which leads either to death or chronic health deterioration [67]. Increase in the titer of autoreactive antibodies, such as anti-DNA, anti-nuclear, anti-Ro, anti-La, anti-Sm, anti-RNP, and anti-phospholipid antibodies, is observed at different stages of the disease, often before the onset of clinical symptoms [68, 69]. In this case, detection of autoreactive antibodies is not considered as a sufficient criterion of disease onset, and, therefore, other factors, genetic and exogenous ones, may play an important role [67]. The causes of SLE are still unknown, although the current view that apoptosis largely contributes to the pathogenesis explains why the immune system reacts primarily to internal antigens. Autoantigens are released by cells that have undergone apoptosis and necrosis. The disorders in the elimination of apoptotic cells described in patients with this disease can lead to their abnormal ingestion by macrophages, which, in turn,

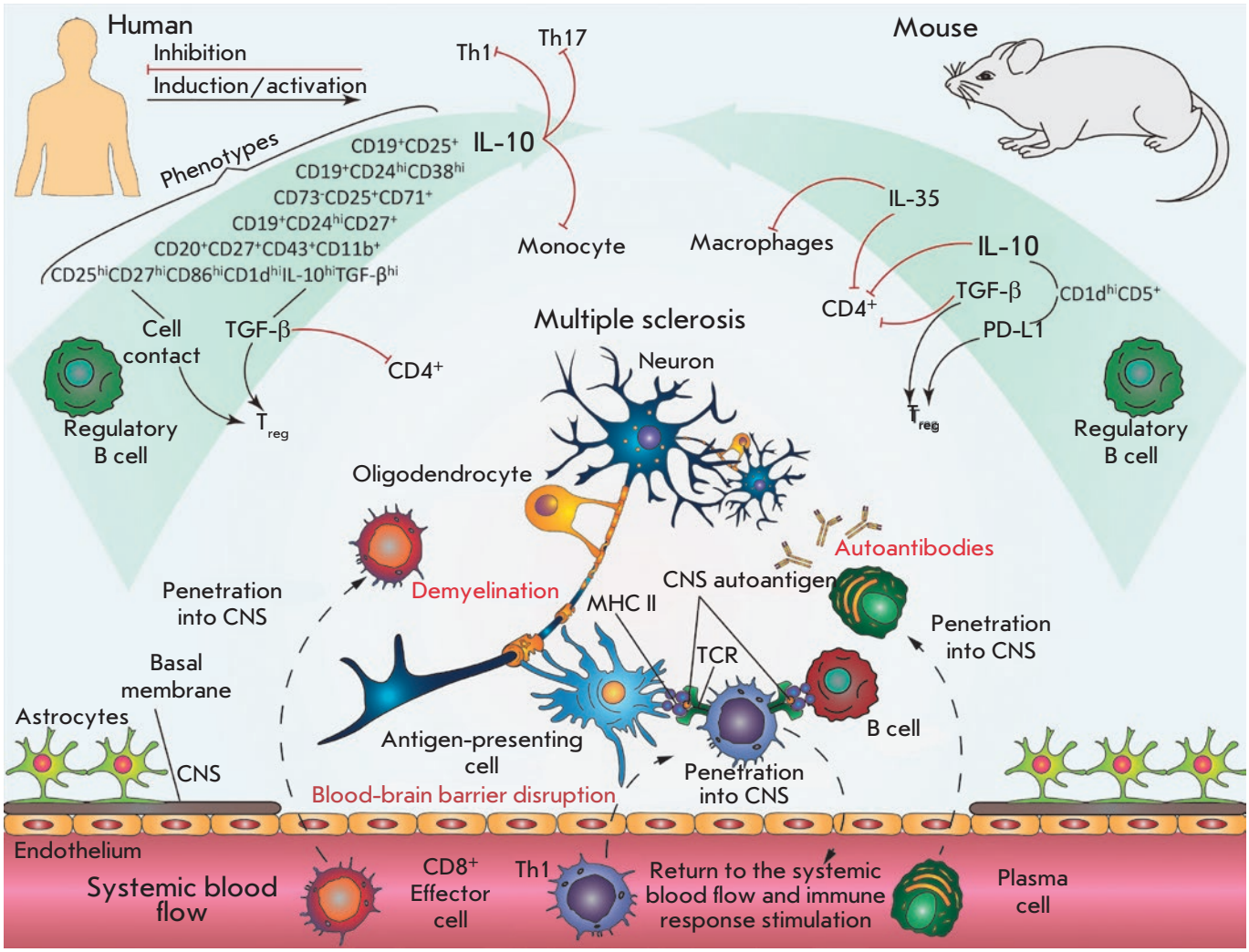

Fig. 2. Participation of regulatory B cells in the pathogenesis of multiple sclerosis. During the disease, Bregs can suppress the development of the autoimmune reaction, along with production of autoantibodies, autoantigen presentation, and activation of the T cell response. Various subpopulations of regulatory B cells with corresponding surface markers were identified in murine models and MS patients. In most cases, the immunosuppressive function of Breg is performed by the production of IL-10, IL-35, TGF-β, and direct cell-cell interactions

provide intracellular antigens to T and B cells, thereby triggering an autoimmune process [70]. The cytokine status of the organism also affects the development of the disease. Most patients with an active form of SLE demonstrate increased expression of interferon-alpha (IFN-α), which can enhance the function of antigen-presenting cells and activation of T cells [71].

It is known that regulatory B cells are important for SLE suppression (*Fig. 3*). It was shown in murine models that two independent populations of regulatory B cells, $CD1d^{hi}CD5^{+}$ and $CD21^{hi}CD23^{hi}$ T2 MZP, play a protective role in the development of the disease, and that their activation contributes to the survival of animals [20, 72]. At the same time, the question of the participation of regulatory B cells in the pathogenesis of SLE in humans remains open. It was shown that the amount of regulatory B cells increases with the development of the pathology [22] and even correlates with the severity of the disease [73]. However, the anti-inflammatory function of the $CD19^{+}CD24^{hi}CD38^{hi}$ population worsens as the disease progresses [17].

Rheumatoid arthritis (RA)

Rheumatoid arthritis is a disease with unknown etiology that manifests itself in connective tissue and joint impairment resulting from an autoimmune inflamma-

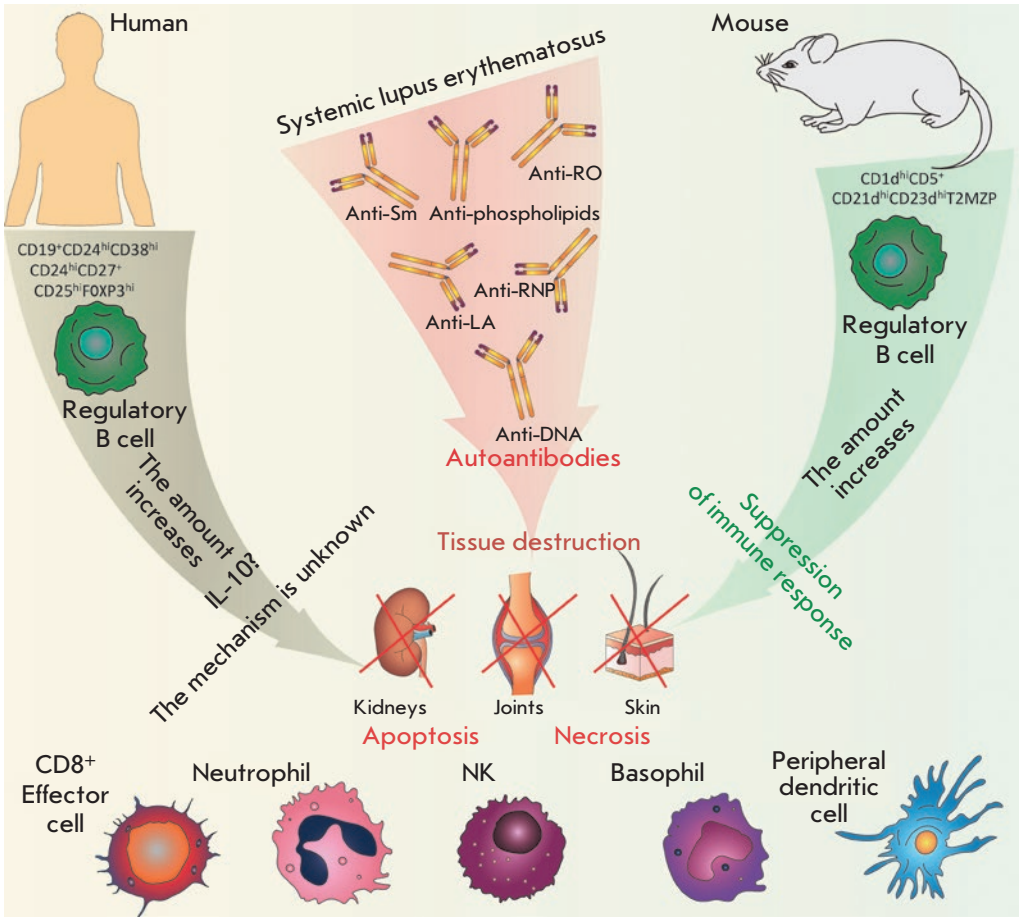

Fig. 3. Participation of regulatory B cells in the development of systemic lupus erythematosus. During the disease, B cells participate in the regulation of the autoimmune inflammation, along with the production of autoantibodies to nuclear autoantigens. Various subpopulations of regulatory B cells with corresponding surface markers were identified in murine models and patients with SLE, whose number increases with the course of the disease. An apparent protective role of Bregs was shown in animal models. In patients with SLE, the mechanism is not fully understood at the moment

tory response. The pathogenesis of rheumatoid arthritis involves a lot of immune cells, as well as various cytokines and arachidonic acid metabolites. The role of B cells in this disease is associated primarily with the production of autoantibodies to the Fc-domain of IgG (rheumatoid factors), as well as autoantibodies to the cyclic citrulline peptide, carbamylated proteins, etc. [74, 75]. For a long time, the role of regulatory B cells remained insufficiently studied.

IL-10, IL-35, and TGF-β are the main effector molecules of regulatory B cells in the development of RA. IL-10 is a typical anti-inflammatory cytokine: its influence on the course of rheumatoid arthritis is considered as favorable, since it inhibits the action of autoimmune Th17 and reduces IL-17 production by immune cells, preventing joint destruction [76–79]. IL-35 is another immunosuppressive cytokine. However, there are controversial data on its impact on the course of rheumatoid arthritis. Some studies have demonstrated a protective effect of IL-35 on the development of RA due to a decrease in IL-17 and IFN-γ production, as well as inhibition of VEGF [80, 81]. Other studies suggest that IL-35 has a pro-inflammatory effect and is directly involved in the pathogenesis of this disease. Furthermore, its plasma level decreases during treatment [82, 83]. The effect of TGF-β cannot be referred to as totally immunosuppressive and favorable to RA, although this cytokine is characteristic, for example, of regulatory T cells and enhances the expression of their main regulator, the FOXP3 transcription factor [84]. A significant increase in the level of TGF-β was found in animal models of RA (collagen-induced arthritis in mice and rats immunized with type 2 collagen, as well as TNF-α transgenic mice) compared to non-immunized control animals. Moreover, the increase in the level of this cytokine was accompanied by the involvement and incorrect differentiation of mesenchymal stem cells and pre-osteoblasts in the subchondral area of the bone marrow, which contributed to joint degeneration. At the same time, inhibition of TGF-β reduced the amount of these cells in this area, reduced chondrocyte hypertrophy, and slowed down joint degeneration [85]. However, in a similar study, inhibition of TGF-β in a mouse model of RA (collagen-induced arthritis) had virtually no effect. In this case, increased activity of this cytokine was observed in the lymphoid cells of tissue samples

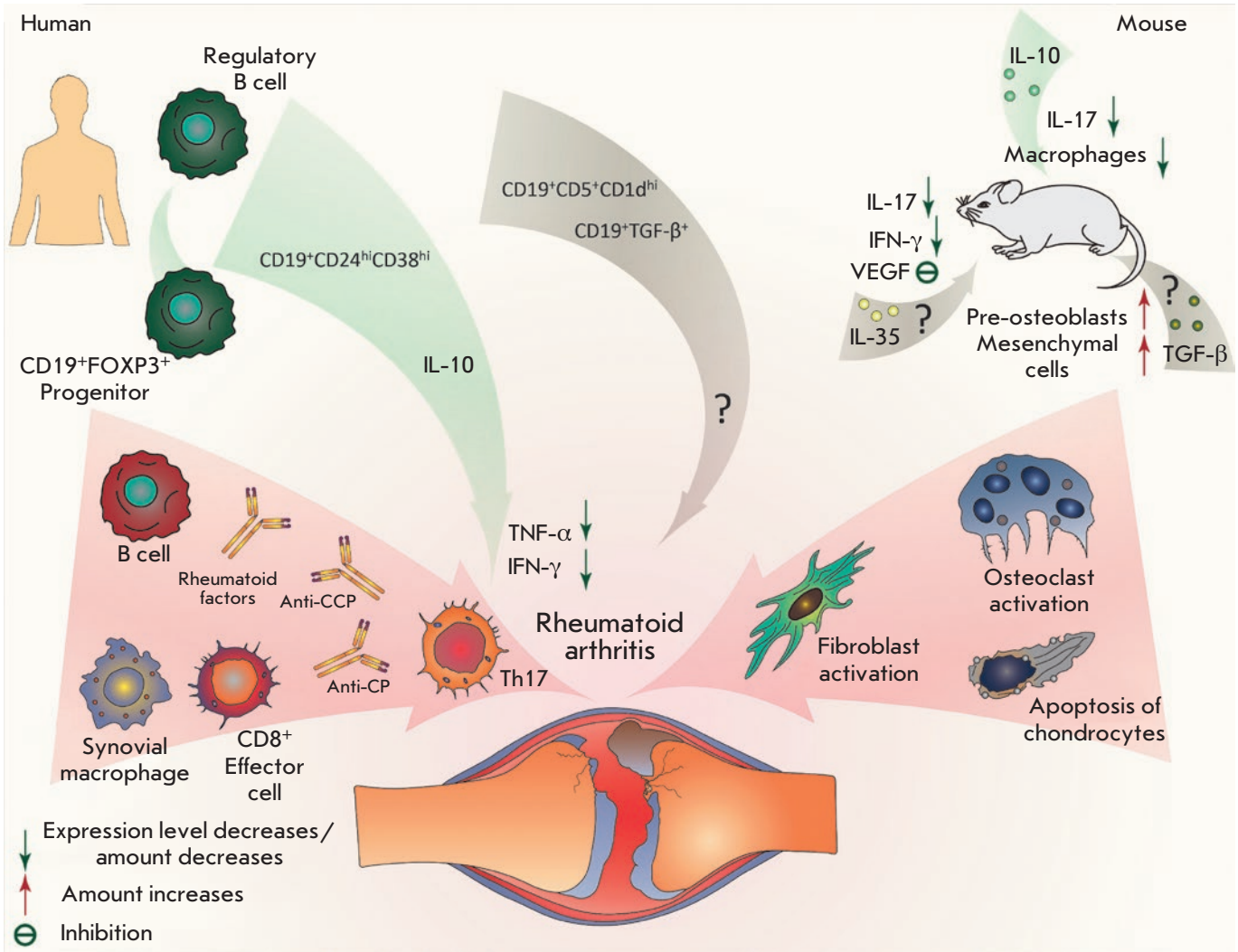

Fig. 4. Participation of regulatory B cells in the development of rheumatoid arthritis. During the disease, B cells participate in the regulation of the autoimmune inflammation, along with the production of autoantibodies. Three main subpopulations of regulatory B cells were discovered in RA patients. $CD19^+CD24^{hi}CD38^{hi}$ demonstrated a suppression of the inflammatory response by inhibiting Th17 activity and reducing the level of IFN-γ and TNF-α in a IL-10-dependent manner. The mechanism and role of the $CD19^+CD5^+CD1d^{hi}$ and $CD19^+TGF\text{-}\beta^+$ subpopulations in the development of RA has not yet been clearly identified. An apparent protective role of IL-10 was shown in animal models. Participation of IL-35 and TGF-β is in question

from RA patients [86]. Parallel studies showed that RA patients have a lower level of CD19(+)TGFβ(+) Bregs than healthy donors [87].

Evaluation of a direct impact of regulatory B cells on the course of rheumatoid arthritis development is challenging, since RA, like other autoimmune diseases, is characterized by the existence of Breg populations that differ in surface markers. In this case, it seems that phenotypically different Bregs can perform different functions in the pathogenesis of RA (*Fig. 4*). It was shown that the level of $CD19^+CD5^+CD1d^{hi}$ decreases in RA patients. In this case, the granzyme-producing B cells $CD19^+CD5^+GzmB^+$ may be involved in the pathogenesis of this disease [88]. It was found that the level of $IL\text{-}10^+$ B cells in patients with rheumatoid arthritis remains the same as in healthy donors. However, induction of these cells from $CD19^+$ B-lymphocytes sampled from patients using CpG deoxyoligonucleotide and CD40L was easier than in healthy donors. A negative correlation was found between the amount of induced $IL\text{-}10^+$ B cells and the severity of the disease according to the DAS28 index (disease activity score

in 28 joints) [89]. An analysis of the potential precursors of IL-10$^+$ B cells (CD19$^+$TGF-β$^+$ and CD19$^+$FOXP3$^+$ populations) showed a decrease in the number of both populations in patients with rheumatoid arthritis. However, only the FOXP3$^+$ population showed a negative correlation with the severity of the disease [87]. It was also shown that IL-10$^+$ B cells cannot be considered as a separate population and that the number of these cells inversely correlates with the severity of the disease, especially during the first 5 years after diagnosis [90]. CD19$^+$CD24^{hi}CD38^{hi} B cells were found to inhibit the production of IFN-γ and TNF-α CD4$^+$ T cells. Moreover, CD19$^+$CD24^{hi}CD38^{hi} hampers the differentiation of CD4$^+$ T cells into the Th1 and Th17 associated with rheumatoid arthritis. The number of regulatory B cells of this phenotype is reduced in the active phase of the disease [3]. The study of CD19$^+$CD24^{hi}CD38^{hi} B cells provided conflicting results. The level of these cells is high in patients with rheumatoid arthritis, which, again, is indicative of a variety of regulatory B cells and their various functions [91]. Note that increasing concentration of cells cannot be unambiguously regarded as a signal that they contribute to the progression of the disease, since this can be interpreted as a compensatory reaction by the organism. It is assumed that IL-10$^+$ B cells are part of the population of CD19$^+$CD24^{hi}CD38^{hi} B cells, and these data agree with earlier results [17, 91]. When comparing the population of CD19$^+$CD24^{hi}CD38^{hi} with all CD19$^+$ B cells, the number of IL-10-producing cells is higher in this population [17, 91]. No correlation between the level of IL-10$^+$ B cells and the concentration of proinflammatory cytokines in the serum of patients with rheumatoid arthritis was found, but the number of these cells is inversely proportional to the duration of the symptoms and the number of affected (swollen) joints. Note that heterogeneity of IL-10$^+$ B cells was detected, some of which were characterized by a lower production of IL-10 and weaker inhibition of CD3$^+$ lymphocyte proliferation [91].

The general picture that emerged during the studies of regulatory B cells in RA patients is rather indicative of their immunosuppressive role. However, taking into account the results of those aforementioned studies, it can be concluded that regulatory B cells are highly heterogeneous (even within the same population) and do not always identically influence the course of rheumatoid arthritis. Additional studies will provide accurate information about the functions of regulatory B cells in the pathogenesis of rheumatoid arthritis. Note that the evaluation of the impact of these cells is hampered not only by their heterogeneity, but also by their small amount and the complex action of their effector molecules.

CONCLUSION

Over the past decade, the key role of B cell regulatory elements in maintaining immunotolerance, controlling, and suppressing the inflammatory response has been confirmed in numerous independent studies. Some disparity in the data and the absence of an unambiguous phenotypic portrait of these cells are largely due to the great heterogeneity of their subpopulations. Despite many questions about the exact regulation mechanism, it is obvious that abnormal amounts and functioning of Breg can lead to a number of immunological pathologies: in particular cancer, autoimmune, and chronic infectious diseases. Therefore, further investigation of the role of the B cell regulation of the inflammatory response will further not only our understanding of the etiology of autoimmune pathologies, but also the development of approaches to the therapeutic use of regulatory B cells. ●

This work was supported by the grant of the Russian Science Foundation No. 17-74-30019 "Structural and kinetic features of antigen presentation as a key to understanding the mechanisms of induction of autoimmune pathologies and lymphomagenesis".

REFERENCES

1. Katz S.I., Parker D.,Turk J.L. // Nature. 1974. V. 251. № 5475. P. 550–551.
2. Wolf S.D., Dittel B.N., Hardardottir F., Janeway C.A. // J. Exp. Med. 1996. V. 184. № 6. P. 2271–2278.
3. Flores-Borja F., Bosma A., Ng D., Reddy V., Ehrenstein M.R., Isenberg D.A., Mauri C. // Sci. Transl. Med. 2013. V. 5. № 173. P. 173ra123.
4. Fillatreau S., Sweenie C.H., McGeachy M.J., Gray D., Anderton S.M. // Nat. Immunol. 2002. V. 3. № 10. P. 944–950.
5. Couper K.N., Blount D.G., Riley E.M. // J. Immunol. 2008. V. 180. № 9. P. 5771–5777.
6. Carter N.A., Vasconcellos R., Rosser E.C., Tulone C., Muñoz-Suano A., Kamanaka M., Ehrenstein M.R., Flavell R.A., Mauri C. // J. Immunol. 2011. V. 186. № 10. P. 5569–5579.
7. Matsumoto M., Baba A., Yokota T., Nishikawa H., Ohkawa Y., Kayama H., Kallies A., Nutt S.L., Sakaguchi S., Takeda K., et al. // Immunity. 2014. V. 41. № 6. P. 1040–1051.
8. Rosser E.C., Mauri C. // Immunity. 2015. V. 42. № 4. P. 607–612.
9. Tian J., Zekzer D., Hanssen L., Lu Y., Olcott A., Kaufman D.L. // J. Immunol. 2001. V. 167. № 2. P. 1081–1089.
10. Parekh V.V., Prasad D.V., Banerjee P.P., Joshi B.N., Kumar A., Mishra G.C. // J. Immunol. 2003. V. 170. № 12. P. 5897–5911.
11. Shen P., Roch T., Lampropoulou V., O'Connor R.A., Stervbo U., Hilgenberg E., Ries S., Dang V.D., Jaimes Y., Daridon C., et al. // Nature. 2014. V. 507. № 7492. P. 366–370.
12. Wang R.X., Yu C.R., Dambuza I.M., Mahdi R.M., Dolinska M.B., Sergeev Y.V., Wingfield P.T., Kim S.H., Egwuagu C.E. // Nat. Med. 2014. V. 20. № 6. P. 633–641.

13. Bosma A., Abdel-Gadir A., Isenberg D.A., Jury E.C., Mauri C. // Immunity. 2012. V. 36. № 3. P. 477–490.
14. Rincón-Arévalo H., Sanchez-Parra C.C., Castaño D., Yassin L., Vásquez G. // Int. Rev. Immunol. 2016. V. 35. № 2. P. 156–176.
15. Wei B., Velazquez P., Turovskaya O., Spricher K., Aranda R., Kronenberg M., Birnbaumer L., Braun J. // Proc. Natl. Acad. Sci. USA. 2005. V. 102. № 6. P. 2010–2015.
16. Lampropoulou V., Hoehlig K., Roch T., Neves P., Calderón Gómez E., Sweenie C.H., Hao Y., Freitas A.A., Steinhoff U., Anderton S.M., et al. // J. Immunol. 2008. V. 180. № 7. P. 4763–4773.
17. Blair P.A., Noreña L.Y., Flores-Borja F., Rawlings D.J., Isenberg D.A., Ehrenstein M.R., Mauri C. // Immunity. 2010. V. 32. № 1. P. 129–140.
18. Mann M.K., Maresz K., Shriver L.P., Tan Y., Dittel B.N. // J. Immunol. 2007. V. 178. № 6. P. 3447–3456.
19. Wei B., McPherson M., Turovskaya O., Velazquez P., Fujiwara D., Brewer S., Braun J. // Clin. Immunol. 2008. V. 127. № 3. P. 303–312.
20. Watanabe R., Ishiura N., Nakashima H., Kuwano Y., Okochi H., Tamaki K., Sato S., Tedder T.F., Fujimoto M. // J. Immunol. 2010. V. 184. № 9. P. 4801–4809.
21. Mauri C., Gray D., Mushtaq N., Londei M. // J. Exp. Med. 2003. V. 197. № 4. P. 489–501.
22. Iwata Y., Matsushita T., Horikawa M., Dilillo D.J., Yanaba K., Venturi G.M., Szabolcs P.M., Bernstein S.H., Magro C.M., Williams A.D., et al. // Blood. 2011. V. 117. № 2. P. 530–541.
23. Siewe B., Wallace J., Rygielski S., Stapleton J.T., Martin J., Deeks S.G., Landay A. // PLoS One. 2014. V. 9. № 4. P. e92934.
24. Huang X., Moore D.J., Mohiuddin M., Lian M.M., Kim J.I., Sonawane S., Wang J., Gu Y., Yeh H., Markmann J.F., et al. // Transplantation. 2008. V. 85. № 5. P. 675–680.
25. Lee K.M., Stott R.T., Zhao G., SooHoo J., Xiong W., Lian M.M., Fitzgerald L., Shi S., Akrawi E., Lei J., et al. // Eur. J. Immunol. 2014. V. 44. № 6. P. 1728–1736.
26. Nouël A., Pochard P., Simon Q., Ségalen I., Le Meur Y., Pers J.O., Hillion S. // J. Autoimmun. 2015. V. 59. P. 53–60.
27. Reyes J.L., Wang A., Fernando M.R., Graepel R., Leung G., van Rooijen N., Sigvardsson M., McKay D.M. // J. Immunol. 2015. V. 194. № 1. P. 364–378.
28. Mizoguchi A., Mizoguchi E., Smith R.N., Preffer F.I., Bhan A.K. // J. Exp. Med. 1997. V. 186. № 10. P. 1749–1756.
29. Shimomura Y., Mizoguchi E., Sugimoto K., Kibe R., Benno Y., Mizoguchi A., Bhan A.K. // Int. Immunol. 2008. V. 20. № 6. P. 729–737.
30. Yanaba K., Bouaziz J.D., Haas K.M., Poe J.C., Fujimoto M.,Tedder T.F. // Immunity. 2008. V. 28. № 5. P. 639–650.
31. Evans J.G., Chavez-Rueda K.A., Eddaoudi A., Meyer-Bahlburg A., Rawlings D.J., Ehrenstein M.R., Mauri C. // J. Immunol. 2007. V. 178. № 12. P. 7868–7878.
32. Kessel A., Haj T., Peri R., Snir A., Melamed D., Sabo E., Toubi E. // Autoimmun. Rev. 2012. V. 11. № 9. P. 670–677.
33. Ray A., Basu S., Williams C.B., Salzman N.H., Dittel B.N. // J. Immunol. 2012. V. 188. № 7. P. 3188–3198.
34. van de Veen W., Stanic B., Yaman G., Wawrzyniak M., Söllner S., Akdis D.G., Rückert B., Akdis C.A., Akdis M. // J. Allergy Clin. Immunol. 2013. V. 131. № 4. P. 1204–1212.
35. Huarte E., Jun S., Rynda-Apple A., Golden S., Jackiw L., Hoffman C., Maddaloni M., Pascual D.W. // J. Immunol. 2016. V. 196. № 12. P. 5036–5046.
36. Piancone F., Saresella M., Marventano I., La Rosa F., Zoppis M., Agostini S., Longhi R., Caputo D., Mendozzi L., Rovaris M., et al. // Sci. Rep. 2016. V. 6. P. 29699.
37. Khan A.R., Hams E., Floudas A., Sparwasser T., Weaver C.T., Fallon P.G. // Nat. Commun. 2015. V. 6. P. 5997.
38. Guan H., Wan Y., Lan J., Wang Q., Wang Z., Li Y., Zheng J., Zhang X., Shen Y., Xie F. // Sci. Rep. 2016. V. 6. P. 35651.
39. Siewe B., Stapleton J. T., Martinson J., Keshavarzian A., Kazmi N., Demarais P.M., French A.L., Landay A. // J. Leukoc. Biol. 2013. V. 93. № 5. P. 811–818.
40. Buenafe A.C., Bourdette D.N. // J. Neuroimmunol. 2007. V. 182. № 1–2. P. 32–40.
41. Xiao X., Lao X.M., Chen M.M., Liu R.X., Wei Y., Ouyang F.Z., Chen D.P., Zhao X.Y., Zhao Q., Li X. F., et al. // Cancer Discov. 2016. V. 6. № 5. P. 546–559.
42. Bao Y., Cao X. // J. Autoimmun. 2014. V. 55. P. 10–23.
43. Matsushita T., Horikawa M., Iwata Y.,Tedder T.F. // J. Immunol. 2010. V. 185. № 4. P. 2240–2252.
44. Mangan N.E., van Rooijen N., McKenzie A.N., Fallon P.G. // J. Immunol. 2006. V. 176. № 1. P. 138–147.
45. Yanaba K., Bouaziz J.D., Matsushita T., Tsubata T., Tedder T.F. // J. Immunol. 2009. V. 182. № 12. P. 7459–7472.
46. Ding Q., Yeung M., Camirand G., Zeng Q., Akiba H., Yagita H., Chalasani G., Sayegh M.H., Najafian N., Rothstein D.M. // J. Clin. Invest. 2011. V. 121. № 9. P. 3645–3656.
47. Maseda D., Smith S.H., DiLillo D.J., Bryant J.M., Candando K.M., Weaver C.T., Tedder T.F. // J. Immunol. 2012. V. 188. № 3. P. 1036–1048.
48. Mizoguchi A., Mizoguchi E., Takedatsu H., Blumberg R.S., Bhan A.K. // Immunity. 2002. V. 16. № 2. P. 219–230.
49. Rosser E.C., Oleinika K., Tonon S., Doyle R., Bosma A., Carter N.A., Harris K.A., Jones S.A., Klein N., Mauri C. // Nat. Med. 2014. V. 20. № 11. P. 1334–1339.
50. Wu H.J., Ivanov I.I., Darce J., Hattori K., Shima T., Umesaki Y., Littman D.R., Benoist C., Mathis D. // Immunity. 2010. V. 32. № 6. P. 815–827.
51. Rafei M., Hsieh J., Zehntner S., Li M., Forner K., Birman E., Boivin M.N., Young Y.K., Perreault C., Galipeau J. // Nat. Med. 2009. V. 15. № 9. P. 1038–1045.
52. Yoshizaki A., Miyagaki T., DiLillo D. J., Matsushita T., Horikawa M., Kountikov E.I., Spolski R., Poe J.C., Leonard W.J., Tedder T.F. // Nature. 2012. V. 491. № 7423. P. 264–268.
53. Wang B., Dai S., Dong Z., Sun Y., Song X., Guo C., Zhu F., Wang Q., Zhang L. // PLoS One. 2014. V. 9. № 1. P. e87787.
54. Li X., Mai J., Virtue A., Yin Y., Gong R., Sha X., Gutchigian S., Frisch A., Hodge I., Jiang X., et al. // PLoS One. 2012. V. 7. № 3. P. e33628.
55. Miles K., Heaney J., Sibinska Z., Salter D., Savill J., Gray D., Gray M. // Proc. Natl. Acad. Sci. USA. 2012. V. 109. № 3. P. 887–892.
56. Matsumoto M., Fujii Y., Baba A., Hikida M., Kurosaki T., Baba Y. // Immunity. 2011. V. 34. № 5. P. 703–714.
57. von Büdingen H.C., Palanichamy A., Lehmann-Horn K., Michel B.A., Zamvil S.S. // Eur. Neurol. 2015. V. 73. № 3–4. P. 238–246.
58. Blauth K., Owens G.P., Bennett J.L. // Front. Immunol. 2015. V. 6. P. 565.
59. Ponomarenko N.A., Durova O.M., Vorobiev I.I., Belogurov A.A., Kurkova I.N., Petrenko A.G., Telegin G.B., Suchkov S.V., Kiselev S.L., Lagarkova M.A., et al. // Proc. Natl. Acad. Sci. USA. 2006. V. 103. № 2. P. 281–286.
60. Belogurov A.A., Kurkova I.N., Friboulet A., Thomas D., Misikov V.K., Zakharova M., Suchkov S.V., Kotov S.V., Alehin A.I., Avalle B., et al. // J. Immunol. 2008. V. 180. № 2. P. 1258–1267.
61. Wekerle H., Hohlfeld R. // N. Engl. J. Med. 2003. V. 349. № 2. P. 185–186.
62. Lomakin Y., Arapidi G.P., Chernov A., Ziganshin R.,

Tcyganov E., Lyadova I., Butenko I.O., Osetrova M., Ponomarenko N., Telegin G., et al. // Front. Immunol. 2017. V. 8. P. 777.
63. Gabibov A.G., Belogurov A.A., Lomakin Y.A., Zakharova M.Y., Avakyan M.E., Dubrovskaya V.V., Smirnov I.V., Ivanov A.S., Molnar A.A., Gurtsevitch V.E., et al. // FASEB J. 2011. V. 25. № 12. P. 4211–4221.
64. Yang M., Deng J., Liu Y., Ko K. H., Wang X., Jiao Z., Wang S., Hua Z., Sun L., Srivastava G., et al. // Am. J. Pathol. 2012. V. 180. № 6. P. 2375–2385.
65. Duddy M., Niino M., Adatia F., Hebert S., Freedman M., Atkins H., Kim H.J., Bar-Or A. // J. Immunol. 2007. V. 178. № 10. P. 6092–6099.
66. Hirotani M., Niino M., Fukazawa T., Kikuchi S., Yabe I., Hamada S., Tajima Y., Sasaki H. // J. Neuroimmunol. 2010. V. 221. № 1–2. P. 95–100.
67. D'Cruz D.P., Khamashta M.A., Hughes G.R. // Lancet. 2007. V. 369. № 9561. P. 587–596.
68. Arbuckle M.R., McClain M.T., Rubertone M.V., Scofield R.H., Dennis G.J., James J.A., Harley J.B. // N. Engl. J. Med. 2003. V. 349. № 16. P. 1526–1533.
69. McClain M.T., Arbuckle M.R., Heinlen L.D., Dennis G.J., Roebuck J., Rubertone M.V., Harley J.B., James J.A. // Arthritis Rheum. 2004. V. 50. № 4. P. 1226–1232.
70. Munoz L.E., Gaipl U.S., Franz S., Sheriff A., Voll R.E., Kalden J.R., Herrmann M. // Rheumatology (Oxford). 2005. V. 44. № 9. P. 1101–1107.
71. Hua J., Kirou K., Lee C., Crow M.K. // Arthritis Rheum. 2006. V. 54. № 6. P. 1906–1916.
72. Blair P.A., Chavez-Rueda K.A., Evans J.G., Shlomchik M.J., Eddaoudi A., Isenberg D.A., Ehrenstein M.R., Mauri C. // J. Immunol. 2009. V. 182. № 6. P. 3492–3502.
73. Vadasz Z., Peri R., Eiza N., Slobodin G., Balbir-Gurman A., Toubi E. // J. Immunol. Res. 2015. V. 2015. Article ID 254245.
74. Burmester G.R., Feist E., Dörner T. // Nat. Rev. Rheumatol. 2014. V. 10. № 2. P. 77–88.
75. Verheul M.K., Fearon U., Trouw L.A., Veale D.J. // Clin. Immunol. 2015. V. 161. № 1. P. 2–10.
76. Ye L., Wen Z., Li Y., Chen B., Yu T., Liu L., Zhang J., Ma Y., Xiao S., Ding L., et al. // Arthritis Res. Ther. 2014. V. 16. № 2. P. R96.
77. Heo Y.J., Joo Y.B., Oh H.J., Park M.K., Heo Y.M., Cho M.L., Kwok S.K., Ju J.H., Park K.S., Cho S.G., et al. // Immunol. Lett. 2010. V. 127. № 2. P. 150–156.
78. Greenhill C.J., Jones G.W., Nowell M.A., Newton Z., Harvey A.K., Moideen A.N., Collins F.L., Bloom A.C., Coll R.C., Robertson A.A., et al. // Arthritis Res. Ther. 2014. V. 16. № 4. P. 419.
79. Verhoef C.M., van Roon J.A., Vianen M.E., Bijlsma J.W., Lafeber F.P. // J. Rheumatol. 2001. V. 28. № 9. P. 1960–1966.
80. Nakano S., Morimoto S., Suzuki S., Tsushima H., Yamanaka K., Sekigawa I., Takasaki Y. // Rheumatology (Oxford). 2015. V. 54. № 8. P. 1498–1506.
81. Wu S., Li Y., Yao L., Lin T., Jiang S., Shen H., Xia L., Lu J. // Int. Immunopharmacol. 2016. V. 34. P. 71–77.
82. Filková M., Vernerová Z., Hulejová H., Prajzlerová K., Veigl D., Pavelka K., Vencovský J., Šenolt L. // Cytokine. 2015. V. 73. № 1. P. 36–43.
83. Šenolt L., Šumová B., Jandová R., Hulejová H., Mann H., Pavelka K., Vencovský J., Filková M. // PLoS One. 2015. V. 10. № 7. P. e0132674.
84. Lu L., Barbi J., Pan F. // Nat. Rev. Immunol. 2017. V. 17. № 11. P. 703–717.
85. Xu X., Zheng L., Bian Q., Xie L., Liu W., Zhen G., Crane J.L., Zhou X., Cao X. // J. Bone Miner Res. 2015. V. 30. № 11. P. 2033–2043.
86. Gonzalo-Gil E., Criado G., Santiago B., Dotor J., Pablos J. L., Galindo M. // Clin. Exp. Immunol. 2013. V. 174. № 2. P. 245–255.
87. Guo Y., Zhang X., Qin M., Wang X. // J. Thorac. Dis. 2015. V. 7. № 3. P. 471–477.
88. Cui D., Zhang L., Chen J., Zhu M., Hou L., Chen B., Shen B. // Clin. Exp. Med. 2015. V. 15. № 3. P. 285–292.
89. Kim J., Lee H.J., Yoo I.S., Kang S.W., Lee J.H. // Yonsei Med. J. 2014. V. 55. № 5. P. 1354–1358.
90. Daien C.I., Gailhac S., Mura T., Audo R., Combe B., Hahne M., Morel J. // Arthritis Rheumatol. 2014. V. 66. № 8. P. 2037–2046.
91. Zheng Z., Li X., Ding J., Feng Y., Miao J., Luo X., Wu Z., Zhu P. // Mol. Med. Rep. 2015. V. 12. № 3. P. 4584–4591.

High-Throughput Screening of Biodiversity for Antibiotic Discovery

S. S. Terekhov[1*], I. A. Osterman[2,3], I. V. Smirnov[1,2,4]
[1]Shemyakin–Ovchinnikov Institute of Bioorganic Chemistry, Russian Academy of Sciences, Miklukho–Maklaya Str., 16/10, Moscow, 117997, Russia
[2]Department of Chemistry, Lomonosov Moscow State University, Leninskie Gory, 1, Moscow, 119991, Russia
[3]Skolkovo Institute of Science and Technology, Skolkovo, Moscow Region, 143026, Russia
[4]National Research University "Higher School of Economics", Myasnitskaya Str., 40, Moscow, 101000, Russia
[*]E-mail: sterekhoff@mail.ru
Received June 1, 2018; in final form, August 22, 2018

ABSTRACT **The increasing number of infections caused by antibiotic-resistant strains of pathogens challenges modern technologies of drug discovery. Combinatorial chemistry approaches are based on chemical libraries. They enable the creation of high-affinity low-molecular-weight ligands of the therapeutically significant molecular targets of human cells, thus opening an avenue toward a directed design of highly effective therapeutic agents. Nevertheless, these approaches face insurmountable difficulties in antibiotic discovery. Natural compounds that have evolved for such important characteristics as broad specificity and efficiency are a good alternative to chemical libraries. However, unrestricted use of natural antibiotics and their analogues leads to avalanche-like spread of resistance among bacteria. The search for new natural antibiotics, in its turn, is extremely complicated nowadays by the problem of antibiotic rediscovery. This calls for the application of alternative high-throughput platforms for antibiotic activity screening, cultivation of "unculturable" microorganisms, exploration of novel antibiotic biosynthetic gene clusters, as well as their activation and heterologous expression. Microfluidic technologies for the screening of antibiotic activity at the level of single cells are, therefore, of great interest, since they enable the use of a single platform to combine the technology of ultrahigh-throughput screening, next-generation sequencing, and genome mining, thus opening up unique opportunities for antibiotic discovery.**

KEYWORDS **high-throughput screening, antibiotic discovery, antibiotic resistance, microfluidics**

ABBREVIATIONS **MIC – minimal inhibitory concentration; ESKAPE –** *Enterococcus faecium*, *Staphylococcus aureus*, *Klebsiella pneumoniae*, *Acinetobacter baumannii*, *Pseudomonas aeruginosa* **and** *Enterobacter* **spp.; HPLC-MS – high-performance liquid chromatography coupled with mass spectrometry; HPLC-NMR – high-performance liquid chromatography coupled with nuclear magnetic resonance spectroscopy; BioMAP – antibiotic mode of action profile; FACS – fluorescence-activated cell sorting; GFP – green fluorescent protein; sCy5 – sulfo-Cyanine 5; NHS – N-hydroxysuccinimide; uHT – ultrahigh-throughput.**

INTRODUCTION

The discovery of antibiotics was one of the 20th century's greatest achievements: it increased the survival rate, life expectancy, and quality of life for millions of people. The period between the 1940s and 1960s, when most of the modern antibiotics and their derivatives were discovered, is commonly referred to as "the golden era of antibiotic discovery" [1]. Such impressive results were achieved thanks to the successful combination of an efficient, simple and inexpensive screening platform and the successful selection of the exploration object. This platform, later termed the Waksman platform [2], was based on the cultivation of soil-dwelling bacteria on agar plates. Antibiotic-producing bacteria were identified by covering these plates with an overlay agar layer seeded with the target bacteria, and the candidate clones were detected according to the formation of inhibition zones (*Fig. 1*) [3, 4]. Subsequent screening for the clones producing antibiotics in growth medium was carried out by using the serial dilution procedure and determining the minimum inhibitory concentrations (MICs). Eventually, the discovery of novel antibiotics using the Waksman platform was impeded by the antibiotic rediscovery problem. This platform could detect only culturable and rapidly growing soil bacteria (predominately *Streptomyces*),

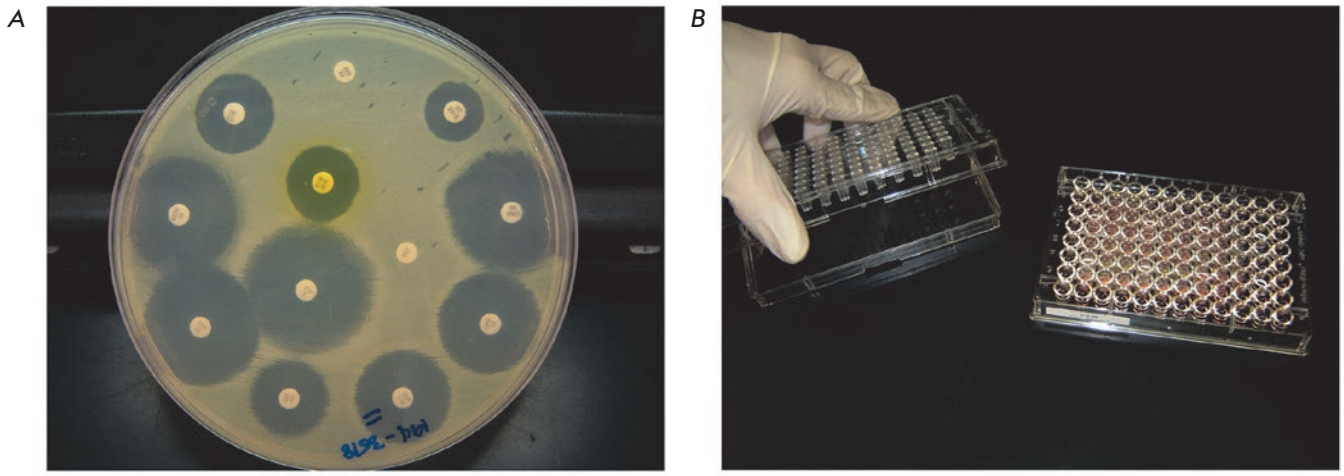

Fig. 1. The conventional methods used for antimicrobial activity screening: (*A*) searching for bacterial colonies yielding large zones of inhibition and (*B*) subsequent determination of MICs (adopted from [4])

which could constitutively produce large amounts of antibiotics. Meanwhile, this platform had also made inexpensive and highly efficient natural and semi-synthetic drugs easily available. Hence, the Waksman platform fully aligned with the goals and objectives of its time, since such a problem as the uncontrolled use of antibiotics did not exist during "the golden era of antibiotic discovery."

The role of antibiotics in nature consists in maintaining the biodiversity of microorganisms resulting from the counteraction of bacteria that produce and degrade antibiotics [5] via various mechanisms [6–8] which are fairly common in various ecological niches [8–11] and had evolved long before human civilizations appeared [12]. The uncontrolled use of large amounts of antibiotics has created unprecedented conditions for the selection and mobilization of resistance genes among bacterial populations and for their subsequent entrapment by the cells of pathogenic microorganisms. The resistance has been evolving via three main mechanisms [13]: primary capture of the resistance genes, mostly through mobilization and horizontal transfer from environmental sources; emergence of compensatory mutations that neutralize the negative effect of the entrapment of resistance genes [14]; and activation of the internal resistance mechanisms, such as active transport [15, 16]. All these factors give rise to the emergence of strains exhibiting multiple drug resistance [17], which is especially typical of the so-called ESKAPE pathogens (*Enterococcus faecium*, *Staphylococcus aureus*, *Klebsiella pneumoniae*, *Acinetobacter baumannii*, *Pseudomonas aeruginosa*, and *Enterobacter* spp.), which are health- and life-threatening [17].

LIMITATIONS IN USING THE COMBINATORIAL DIVERSITY OF CHEMICAL LIBRARIES IN ANTIBIOTIC DISCOVERY

Combinatorial chemistry and high-throughput screening of chemical libraries have proved efficient for creating drugs targeted at the regulation of various processes taking place in human cells. However, multiple attempts to use high-throughput combinatorial screening to design novel broad-spectrum antibiotics have failed, despite the substantial financial and material investments made and the fact that all the available technologies were used [18–20].

The key reasons for these failures were as follows: Firstly, xenobiotics are not particularly good at penetrating bacterial cells, especially Gram-negative bacteria. Secondly, antibiotics do not obey the Lipinski's "rule of five" [21]: the physicochemical properties of the combinatorial chemical libraries selected for most drugs are not optimal for antibiotics [22]. Thirdly, the chemical space of the existing libraries is noticeably limited [23]. Meanwhile, the use of chemical libraries enables one to identify various adjuvants, which significantly potentiate the antimicrobial properties of the known antibiotics [24–26], antimetabolites [27], and antivirulence drugs [28] and can also lead to the development of narrow-spectrum drugs specific to a certain target, as demonstrated for bedaquiline, a selective inhibitor of *Mycobacterium tuberculosis* ATP synthase [29]. The creation of specialized chemical libraries targeting an enhanced ability of xenobiotics to penetrate bacterial cells is of utmost importance for the combinatorial methods used to search for novel antibiotics. An alternative strategy is to search for ligands that inhibit the activity of bacterial xenobiotic transport systems.

SCREENING OF THE NATURAL BIODIVERSITY FOR THE SEARCH FOR NOVEL ANTIBIOTICS

Screening of natural products offers a significantly higher potential for discovering antimicrobial activity [30], probably due to the fact that natural products contain a broader range of stereoselective pharmacophores that have already undergone natural selection for various biological activities over the course of evolution [23]. Metabolomics, which underlies modern approaches for the screening of natural antibiotics [26], uses a combination of tandem separation and analysis techniques, such as high-performance liquid chromatography coupled with mass spectrometry or nuclear magnetic resonance spectroscopy (HLPC-MS or HLPC-NMR, respectively), and whole-genome sequencing methods [31]. Metabolomics makes it possible to proceed to functional genomics [32] and to identify novel ribosomal or nonribosomal peptides [33, 34], as well as secondary metabolites [35].

The range of natural products used to search for antibiotics is rather diverse and includes extracts from plants, fungi, lichens, endophytes, marine plants, seaweeds, corals, and other microorganisms [36]. Nevertheless, it is worth mention that many active substances from these sources have a nonspecific mechanism of membrane destabilization, which, in turn, impedes their application because of the high toxicity caused by a low therapeutic index. Hence, due to the diversity of bacteria and their evolutional propensity to produce antibiotics in order to conquer ecological niches, these organisms still remain one of the most attractive sources of antimicrobial activity. The problem of antibiotic rediscovery can be solved using various approaches.

STRATEGIES EMPLOYED TO SOLVE THE ANTIBIOTIC REDISCOVERY PROBLEM

The BioMAP platform, which enables the detection of known antibiotics and the discovery of novel ones according to their individual inhibition profiles, has shown that the growth-inhibiting activity of various microorganisms in the collection can be used as a characteristic "fingerprint" of the substance or extract [37]. Collections of bacterial strains of the same species can be used to discover the target of the active substance or, contrariwise, to search for compounds having a specific mechanism of action. A collection of 245 *S. aureus* strains with suppressed gene expression allowed to discover platensimycin, an antibiotic that belongs to a previously unknown class of inhibitors of the enzyme FabF/B that catalyze fatty acid biosynthesis [38].

The new insight into using soil bacteria as a source of novel antibiotics opens up new possibilities for the screening for antimicrobial activity. Whole-genome sequencing of actinomycetes has shown that they have a much higher ability to produce secondary metabolites upon cultivation. Complete genome sequencing of *Streptomyces coelicolor* has demonstrated that over 20 secondary metabolites can be produced in theory, whereas only three of them have been identified upon *in vitro* cultivation [39]. In its turn, activation of silent genes in antibiotic-producing bacteria opens up new sources of previously unknown antimicrobials [40], while the bioinformatic analysis and gene clustering methods enable *de novo* prediction of antibiotics [41]. Hence, genome mining strategies can be successfully employed to search for novel microbial secondary metabolites, including previously unknown antibiotics that show a high potential for drug design [42]. One of the approaches used to activate silent genes and produce novel antibiotics is to select a growth medium for culturing antibiotic-producing clones which have been pre-selected at the sequencing stage because of the presence of new genes [43]. Using quorum-sensing factors is another approach applied to activate silent genes [44]; however, their effect is difficult to predict, and, therefore, it is probably not always the optimal mechanism for activating silent genes. Meanwhile, recombinant expression is one of the most obvious strategies for activating silent genes [45, 46]. Application of new methods of cultivation of "unculturable" soil bacteria (*Fig. 2*) is another alternative approach that was used to search for novel antibiotics. The platform based on the cultivation of individual soil-dwelling bacteria in their natural environment using a semipermeable membrane has made it possible to discover the novel antibiotic teixobactin, which exhibits activity against resistant strains of Gram-positive bacteria, while resistance to this compound has not developed [47]. Furthermore, this platform allowed to identify the previously unknown genus *Entotheonella*, which is characterized by a unique combination of secondary metabolites and the pathways of their synthesis [48].

Screening of antibiotic-resistant bacteria can be used to reveal novel mechanisms of synergistic interactions, which opens up new prospects for the search for antibiotic adjuvants potentiating their effect [26]. Application of resistant strains has made it possible to discover acyldepsipeptides, a novel class of antibiotics that activate intracellular bacterial protease ClpP [49], which causes the death of bacteria, including persisters, and treats chronic infection [50]. Pre-screening of glycopeptide-resistant soil bacteria increased the probability of discovering clones that produce novel antibiotics belonging to that class by more than 1,000-fold and made it possible to identify pekiskomycin, a novel antibiotic with an unusual scaffold structure [51].

The strategy of designing bifunctional agents acting as 'Trojan horses' has also proved efficient. The conju-

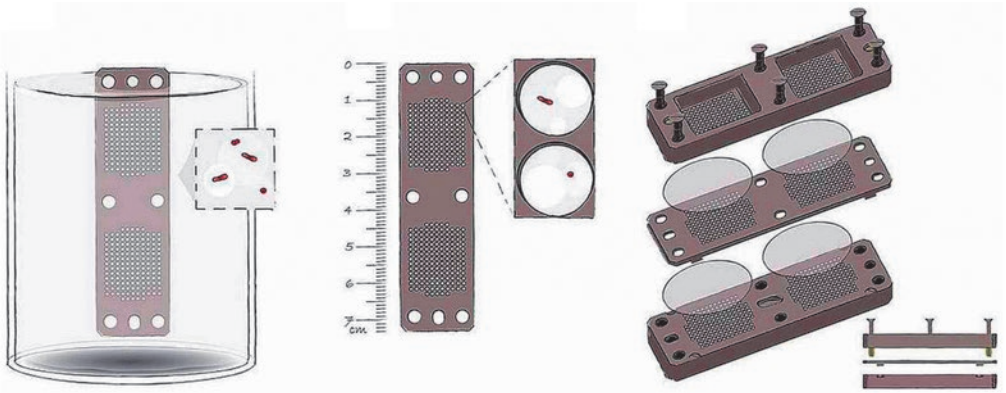

Fig. 2. A device for cultivation of "unculturable" soil bacteria (adopted from [47]). The device consists of two compartments separated by a semipermeable membrane. Individual cells of soil bacteria in the growth media are placed on one side of the membrane, while the other compartment contains soil with the required growth factors

gate of a rifampicin analogue connected to antibodies specific to *S. aureus* cell wall teichoic acids via a biodegradable linker proved efficient in eliminating not only suspension cells, but also the vancomycin-resistant intracellular reservoir of bacteria [52]. It was of crucial importance to select the antibody, linker, and antibiotic properly. Rational design of highly specific antibiotics proved efficient for siderophore–antibiotic conjugates [53].

Proceeding from *in vitro* inhibition to the direct assessment of the antimicrobial activity of an agent *in vivo* opens up new prospects for designing the most efficacious drugs. Screening of antimicrobial activity against *M. tuberculosis* using infected macrophages [54] enabled to make the *in vitro* model as similar to *in vivo* conditions as possible and to rule out compounds that exhibited nonspecific cytotoxicity and low ability to penetrate macrophage cells. Models of *in vivo* infection of the nematode *Caenorhabditis elegans* [55] and the zebrafish *Danio rerio* [56] allowed to select agents that cause the elimination of bacteria, including antibiotics acting via mechanisms that are different from those of the conventional antimicrobial activity.

A high sensitivity of the analytical signal is the fundamental parameter needed to enhance screening performance. Application of bacteria producing recombinant fluorescent reporter proteins as a biosensor of antimicrobial activity makes it possible to directly detect bacterial growth inhibition [57], to identify antibiotics that act via the given translation inhibition mechanism [58], and to screen antibiotic combinations using several fluorescent reporter proteins that have different excitation/emission spectra [59].

CONCLUSIONS

The search for novel antibiotics has become an urgent task because of the rapid development of antibiotic resistance. The success rate in the screening of chemical libraries is extremely low; this strategy can be efficient mainly when searching for adjuvants and narrow-spectrum antibiotics. Although the Waksman's platform traditionally used for screening for the antimicrobial activity of microorganisms has been effective in the past, its further application is associated with an extremely high risk of antibiotic rediscovery. It has been estimated that more than 10^7 different microorganisms need to be screened for every new antibiotic discovery [60]. This problem can be solved by using alternative platforms based on metabolomics, whole-genome sequencing, bioinformatic analysis, recombinant gene expression, and alternative approaches for the cultivation of "unculturable" microorganisms. The fact that physiologically important antibiotics can be discovered within the human microbiome [61] offers new sources for antimicrobial activity screening. The implementation of microfluidic platforms, which allows conversion from a conventional 2D plate-screening platform to emulsion-based 3D screening in isolated microcompartments, is of particular interest. Cultivation of individual cells in emulsion droplets can be used for screening for antibiotic-resistant bacteria [62] or bacteriolytic activity [63]. This alternative approach offers unique prospects for a high-throughput analysis of the activity of broad cell repertoires.

Encapsulation of individual cells into biocompatible double emulsion droplets (*Fig. 3*) enables the analysis of the activity of single cells and the coculturing of representatives of microbiota with target cells to identify antagonistic bacterial strains that produce antibiotics [64]. This method is based on the coencapsulation of individual microbiota species, together with the reporter strain of the target pathogen in droplets of a biocompatible double water-in-oil-in-water emulsion, their subsequent cocultivation in droplets, and FACS-based isolation of the target droplet population where pathogen growth is inhibited, while the effector cells stay viable. The principal advantage of this technology is the fact that the target population of bacterial effectors can be selected, resulting in ultrahigh-throughput (~30,000 cells per second) screening for antimicrobial activity for

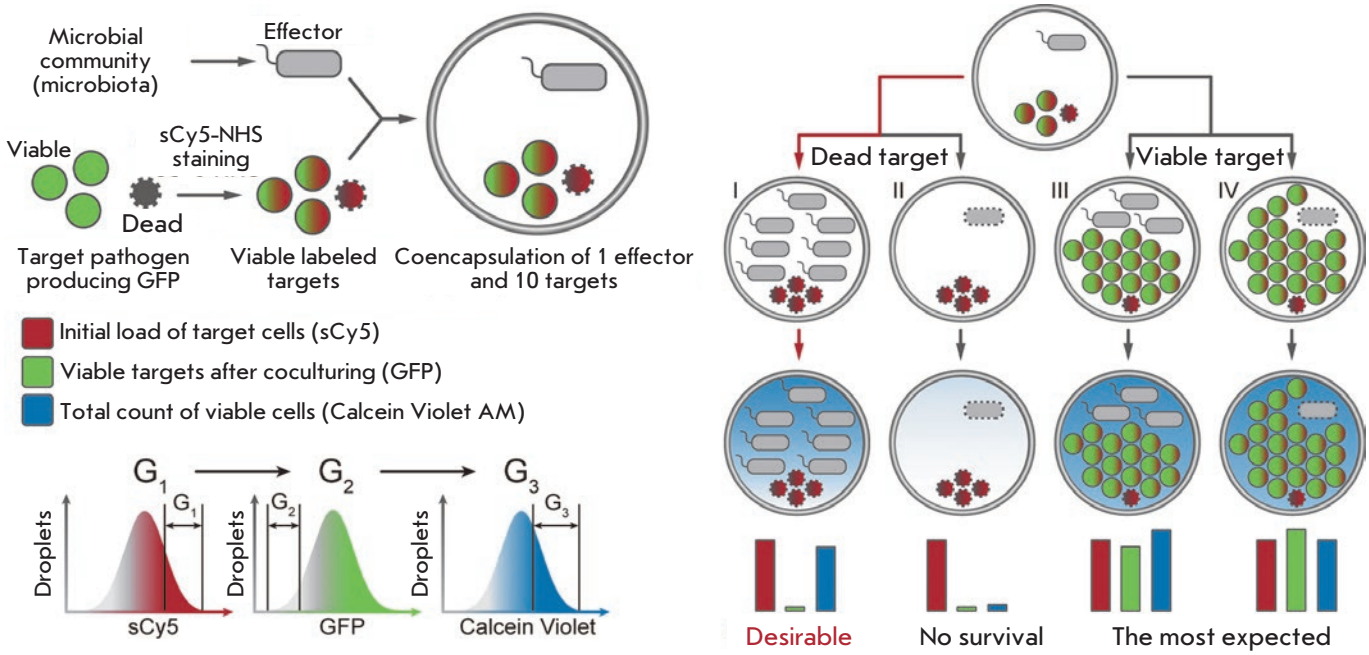

Fig. 3. Ultrahigh-throughput (uHT) screening of antimicrobial activity in biocompatible double emulsion droplets (adopted from [64]). Cultivation of single microbiota effector cells with the reporter strain of the target pathogen, followed by intravital staining to detect viable cells with subsequent selection of the target population of effector cells exhibiting antimicrobial activity using FACS

individual clones. Thus, the selected bacteria can represent a population of extremely rare, slow-growing, and "unculturable" microorganisms, which are, subsequently, identified using whole-genome sequencing, followed by a bioinformatic analysis. This platform was applied for intravital selection of particularly rare cell populations (representing ~0.005%) displaying antimicrobial activity using a single round of screening.

Further development of ultrahigh-throughput (uHT) methods for screening for antibiotic activity is of high interest, since bacterial biodiversity presents a multitude of challenges that require an integrated understanding of the interactions taking place both at the level of individual bacteria and at the level of an entire unique microbiome [65]. The combination of uHT screening and genome mining techniques offers great opportunities for the identification of rare clusters involved in the biosynthesis of microbial secondary metabolites that exhibit different spectra of antimicrobial activity. Such challenges as the analysis of the individual activity of each microbiota species with respect to the given target, as well as extensive assessment of the spectrum of antimicrobial activity against a given microbial community, are of great interest, as they enable one to untangle the interactions that take place within a microbiological community. We believe that advancements in microfluidic technologies, along with uHT screening, whole-genome sequencing, proteomics, and bioinformatics, will further our understanding of microbiological processes. The microfluidic technologies of uHT screening of the natural biodiversity of microorganisms or artificial libraries of antimicrobial compounds clearly has potential for the discovery of the next-generation antibiotics, as well as the selection of ligands that inhibit antibiotic resistance. The combination of these agents may play a crucial role in solving the problem of antibiotic resistance. ●

This work was supported by the Russian Science Foundation (grant no. 14-50-00131).

REFERENCES

1. Lewis K. // Nat. Rev. Drug Discov. 2013. V. 12. № 5. P. 371–387.
2. Lewis K. // Nature. 2012. V. 485. № 7399. P. 439–440.
3. Schatz A., Bugle E., Waksman S.A. // Exp. Biol. Medicine. 1944. V. 55. № 1. P. 66–69.
4. Reller L.B., Weinstein M., Jorgensen J.H., Ferraro M.J. // Clin. Infectious Dis. 2009. V. 49. № 11. P. 1749–1755.
5. Kelsic E.D., Zhao J., Vetsigian K., Kishony R. // Nature. 2015. V. 521. № 7553. P. 516–519.
6. Wright G.D. // Nat. Rev. Microbiol. 2007. V. 5. № 3. P. 175–186.
7. Perry J.A., Westman E.L., Wright G.D. // Curr. Opin. Microbiol. 2014. V. 21. P. 45–50.
8. Kommineni S., Bretl D.J., Lam V., Chakraborty R., Hayward M., Simpson P., Cao Y., Bousounis P., Kristich C.J.,

Salzman N.H. // Nature. 2015. V. 526. № 7575. P. 719–722.
9. Forsberg K.J., Reyes A., Wang B., Selleck E.M., Sommer M.O.A., Dantas G. // Science. 2012. V. 337. № 6098. P. 1107–1111.
10. Finley R.L., Collignon P., Larsson D.G.J., McEwen S.A., Li X.-Z., Gaze W.H., Reid-Smith R., Timinouni M., Graham D.W., Topp E. // Clin. Infectious Dis. 2013. V. 57. № 5. P. 704–710.
11. Forsberg K.J., Patel S., Gibson M.K., Lauber C.L., Knight R., Fierer N., Dantas G. // Nature. 2014. V. 509. № 7502. P. 612–616.
12. D'Costa V.M., King C.E., Kalan L., Morar M., Sung W.W.L., Schwarz C., Froese D., Zazula G., Calmels F., Debruyne R., et al. // Nature. 2011. V. 477. № 7365. P. 457–461.
13. Brown E.D., Wright G.D. // Nature. 2016. V. 529. № 7586. P. 336–343.
14. Andersson D.I., Hughes D. // FEMS Microbiol. Rev. 2011. V. 35. № 5. P. 901–911.
15. Cox G., Wright G.D. // Internat. J. Med. Microbiol. 2013. V. 303. № 6–7. P. 287–292.
16. Fajardo A., Martínez-Martín N., Mercadillo M., Galán J.C., Ghysels B., Matthijs S., Cornelis P., Wiehlmann L., Tümmler B., Baquero F., et al. // PLoS One. 2008. V. 3. № 2. P. e1619.
17. Davies J., Davies D. // Microbiol. Mol. Biol. Rev. 2010. V. 74. № 3. P. 417–433.
18. Payne D.J., Gwynn M.N., Holmes D.J., Pompliano D.L. // Nat. Rev. Drug Discov. 2007. V. 6. № 1. P. 29–40.
19. Silver L.L. // Clin. Microbiol. Rev. 2011. V. 24. № 1. P. 71–109.
20. Tommasi R., Brown D.G., Walkup G.K., Manchester J.I., Miller A.A. // Nat. Rev. Drug Discov. 2015. V. 14. № 8. P. 529–542.
21. Lipinski C.A., Lombardo F., Dominy B.W., Feeney P.J. // Advanced Drug Delivery Rev. 1997. V. 23. № 1. P. 3–25.
22. O'Shea R., Moser H.E. // J. Med. Chem. 2008. V. 51. № 10. P. 2871–2878.
23. Harvey A.L., Edrada-Ebel R., Quinn R.J. // Nat. Rev. Drug Discov. 2015. V. 14. № 2. P. 111–129.
24. Peterson E.J.R., Ma S., Sherman D.R., Baliga N.S. // Nat. Microbiol. 2016. V. 1. P. 16078.
25. Taylor P.L., Rossi L., De Pascale G., Wright G.D. // ACS Chem. Biol. 2012. V. 7. № 9. P. 1547–1555.
26. Roemer T., Boone C. // Nat. Chem. Biol. 2013. V. 9. № 4. P. 222–231.
27. Zlitni S., Ferruccio L.F., Brown E.D. // Nat. Chem. Biol. 2013. V. 9. № 12. P. 796–804.
28. Starkey M., Lepine F., Maura D., Bandyopadhaya A., Lesic B., He J., Kitao T., Righi V., Milot S., Tzika A., et al. // PLoS Pathog. 2014. V. 10. № 8. P. e1004321.
29. Koul A., Vranckx L., Dhar N., Göhlmann H.W.H., Özdemir E., Neefs J.-M., Schulz M., Lu P., Mørtz E., McKinney J.D., et al. // Nat. Commun. 2014. V. 5. P. 3369.
30. Sukuru S.C.K., Jenkins J.L., Beckwith R.E.J., Scheiber J., Bender A., Mikhailov D., Davies J.W., Glick M. // J. Biomol. Screening. 2009. V. 14. № 6. P. 690–699.
31. Glassbrook N., Beecher C., Ryals J. // Nat. Biotech. 2000. V. 18. № 11. P. 1142–1143.
32. Jewett M.C., Hofmann G., Nielsen J. // Curr. Opin. Biotechnol. 2006. V. 17. № 2. P. 191–197.
33. Kersten R.D., Yang Y.-L., Xu Y., Cimermancic P., Nam S.-J., Fenical W., Fischbach M.A., Moore B.S., Dorrestein P.C. // Nat. Chem. Biol. 2011. V. 7. № 11. P. 794–802.
34. Ibrahim A., Yang L., Johnston C., Liu X., Ma B., Magarvey N.A. // Proc. Natl. Acad. Sci. USA. 2012. V. 109. № 47. P. 19196–19201.
35. Kjer J., Debbab A., Aly A.H., Proksch P. // Nat. Protocols. 2010. V. 5. № 3. P. 479–490.
36. Moloney M.G. // Trends Pharmacol. Sci. 2016. V. 37. № 8. P. 689–701.
37. Wong W.R., Oliver A.G., Linington R.G. // Chem. Biol. 2012. V. 19. № 11. P. 1483–1495.
38. Wang J., Soisson S.M., Young K., Shoop W., Kodali S., Galgoci A., Painter R., Parthasarathy G., Tang Y.S., Cummings R., et al. // Nature. 2006. V. 441. № 7091. P. 358–361.
39. Bentley S.D., Chater K.F., Cerdeno-Tarraga A.M., Challis G.L., Thomson N.R., James K.D., Harris D.E., Quail M.A., Kieser H., Harper D., et al. // Nature. 2002. V. 417. № 6885. P. 141–147.
40. Peter J., Rutledge G.L.C. // Nat. Rev. Microbiol. 2015. V. 13. № 8. P. 509–523.
41. Marnix H., Medema M.A.F. // Nat. Chem. Biol. 2015. V. 11. № 9. P. 639–648.
42. Metelev M., Osterman I.A., Ghilarov D., Khabibullina N.F., Yakimov A., Shabalin K., Utkina I., Travin D.Y., Komarova E.S., Serebryakova M., et al. // Nat. Chem. Biol. 2017. V. 13. P. 1129.
43. Zazopoulos E., Huang K., Staffa A., Liu W., Bachmann B. O., Nonaka K., Ahlert J., Thorson J.S., Shen B., Farnet C.M. // Nat. Biotech. 2003. V. 21. № 2. P. 187–190.
44. Ohnishi Y., Kameyama S., Onaka H., Horinouchi S. // Mol. Microbiol. 1999. V. 34. № 1. P. 102–111.
45. Ikeda H., Ishikawa J., Hanamoto A., Shinose M., Kikuchi H., Shiba T., Sakaki Y., Hattori M., Omura S. // Nat. Biotech. 2003. V. 21. № 5. P. 526–531.
46. Komatsu M., Uchiyama T., Ōmura S., Cane D.E., Ikeda H. // Proc. Natl. Acad. Sci. USA. 2010. V. 107. № 6. P. 2646–2651.
47. Ling L.L., Schneider T., Peoples A.J., Spoering A.L., Engels I., Conlon B.P., Mueller A., Schaberle T.F., Hughes D.E., Epstein S., et al. // Nature. 2015. V. 517. № 7535. P. 455–459.
48. Wilson M.C., Mori T., Ruckert C., Uria A.R., Helf M.J., Takada K., Gernert C., Steffens U.A.E., Heycke N., Schmitt S., et al. // Nature. 2014. V. 506. № 7486. P. 58–62.
49. Brotz-Oesterhelt H., Beyer D., Kroll H.-P., Endermann R., Ladel C., Schroeder W., Hinzen B., Raddatz S., Paulsen H., Henninger K., et al. // Nat. Med. 2005. V. 11. № 10. P. 1082–1087.
50. Conlon B.P., Nakayasu E.S., Fleck L.E., LaFleur M.D., Isabella V.M., Coleman K., Leonard S.N., Smith R.D., Adkins J.N., Lewis K. // Nature. 2013. V. 503. № 7476. P. 365–370.
51. Thaker M.N., Wang W., Spanogiannopoulos P., Waglechner N., King A.M., Medina R., Wright G.D. // Nat. Biotech. 2013. V. 31. № 10. P. 922–927.
52. Lehar S.M., Pillow T., Xu M., Staben L., Kajihara K.K., Vandlen R., DePalatis L., Raab H., Hazenbos W.L., Hiroshi Morisaki J., et al. // Nature. 2015. V. 527. № 7578. P. 323–328.
53. Han S., Zaniewski R.P., Marr E.S., Lacey B.M., Tomaras A.P., Evdokimov A., Miller J.R., Shanmugasundaram V. // Proc. Natl. Acad. Sci. USA. 2010. V. 107. № 51. P. 22002–22007.
54. Pethe K., Bifani P., Jang J., Kang S., Park S., Ahn S., Jiricek J., Jung J., Jeon H.K., Cechetto J., et al. // Nat. Med. 2013. V. 19. № 9. P. 1157–1160.
55. Ewbank J.J., Zugasti O. // Disease Models Mechanisms. 2011. V. 4. № 3. P. 300–304.
56. Veneman W.J., Stockhammer O.W., de Boer L., Zaat S.A.J., Meijer A.H., Spaink H.P. // BMC Genomics. 2013. V. 14. № 1. P. 1–15.
57. Michels K., Heinke R., Schone P., Kuipers O.P., Arnold N., Wessjohann L.A. // J. Antibiot. 2015. V. 68. № 12. P. 734–740.

58. Osterman I.A., Komarova E.S., Shiryaev D.I., Korniltsev I.A., Khven I.M., Lukyanov D.A., Tashlitsky V.N., Serebryakova M.V., Efremenkova O.V., Ivanenkov Y.A., et al. // Antimicrob. Agents Chemotherapy. 2016. V. 60. № 12. P. 7481–7489.
59. FengTing Lv, LiBing Liu, Shu Wang // Sci. China Chem. 2014. V. 57. № 12. P. 1696–1702.
60. Baltz R.H. // SIM News. 2005. V. 55. P. 186–196.
61. Zipperer A., Konnerth M.C., Laux C., Berscheid A., Janek D., Weidenmaier C., Burian M., Schilling N.A., Slavetinsky C., Marschal M., et al. // Nature. 2016. V. 535. № 7613. P. 511–516.
62. Liu X., Painter R.E., Enesa K., Holmes D., Whyte G., Garlisi C.G., Monsma F.J., Rehak M., Craig F.F., Smith C.A. // Lab on a Chip. 2016. V. 16. № 9. P. 1636–1643.
63. Scanlon T.C., Dostal S.M., Griswold K.E. // Biotechnol. Bioengin. 2014. V. 111. № 2. P. 232–243.
64. Terekhov S.S., Smirnov I.V., Stepanova A.V., Bobik T.V., Mokrushina Y.A., Ponomarenko N.A., Belogurov A.A., Rubtsova M.P., Kartseva O.V., Gomzikova M.O., et al. // Proc. Natl. Acad. Sci. USA. 2017. V. 114. № 10. P. 2550–2555.
65. Terekhov S.S., Smirnov I.V., Malakhova M.V., Samoilov A.E., Manolov A.I., Nazarov A.S., Danilov D.V., Dubiley S.A., Osterman I.A., et al. // Proceedings of the National Academy of Sciences. 2018. in press.

Possibilities for Using Pluripotent Stem Cells for Restoring Damaged Eye Retinal Pigment Epithelium

A. E. Kharitonov, A. V. Surdina, O. S. Lebedeva, A. N. Bogomazova, M. A. Lagarkova*
Federal Research and Clinical Center of Physical-Chemical Medicine of Federal Medical Biological Agency, Malaya Pirogovskaya Str., 1a, Moscow, 119435, Russia
*E-mail: maryalag@yahoo.com
Received March 23, 2018; in final form July 02, 2018

ABSTRACT **The retinal pigment epithelium is a monolayer of pigmented, hexagonal cells connected by tight junctions. These cells compose part of the outer blood-retina barrier, protect the eye from excessive light, have important secretory functions, and support the function of photoreceptors, ensuring the coordination of a variety of regulatory mechanisms. It is the degeneration of the pigment epithelium that is the root cause of many retinal degenerative diseases. The search for reliable cell sources for the transplantation of retinal pigment epithelium is of extreme urgency. Pluripotent stem cells (embryonic stem or induced pluripotent) can be differentiated with high efficiency into the pigment epithelium of the retina, which opens up possibilities for cellular therapy in macular degeneration and can slow down the development of pathology and, perhaps, restore a patient's vision. Pioneering clinical trials on transplantation of retinal pigment epithelial cells differentiated from pluripotent stem cells in the United States and Japan confirmed the need for developing and optimizing such approaches to cell therapy. For effective use, pigment epithelial cells differentiated from pluripotent stem cells should have a set of functional properties characteristic of such cells *in vivo*. This review summarizes the current state of preclinical and clinical studies in the field of retinal pigment epithelial transplantation therapy. We also discuss different differentiation protocols based on data in the literature and our own data, and the problems holding back the widespread therapeutic application of retinal pigment epithelium differentiated from pluripotent stem cells.**
KEYWORDS **Retinal pigment epithelium, differentiation, embryonic stem cells, induced pluripotent stem cells, cell therapy, clinical trials.**
ABBREVIATIONS **AMD – age-related macular degeneration; IPSCs – induced pluripotent stem cells; BCVA – best-corrected visual acuity; MSCs – mesenchymal stem cells; PDR – pigmentary degeneration of the retina; PSCs – pluripotent stem cells; RPE – retinal pigment epithelium; ESCs – embryonic stem cells; ABCA4 – ATP-binding cassette, sub-family A (ABC1) member 4; BEST-1 – Bestrophin 1; CNV – copy number variations; NIC – nicotinamide; NK – natural killers; PEDF – pigment epithelium-derived factor, bFGF-basic fibroblast growth factor; VEGF – vascular endothelial growth factor.**

INTRODUCTION

Retinal pigment epithelium (RPE) is formed by a monolayer of hexagonal epithelial cells with a large number of melanosomes containing a pigment's melanin (*Fig. 1*). The inner layer of the five-layer Bruch's membrane serves as the basal membrane for pigment epithelium. The nuclei of RPE cells are located closer to the basal pole, which contains fewer melanosomes. The RPE apical pole contains many melanosomes and microvilli (cilia), which "envelop" the outer segments of the photoreceptor cells. There are long and short microvilli. Short microvilli are connected to the ends of the outer segments of the photoreceptors, whereas the long ones are located between the outer segments [1]. Each RPE cell is in contact with 20–55 photoreceptors [2] in the area of the macula. The space between the RPE microvilli and the outer segments of the photoreceptors is filled with matrix, which, together with the microvilli, ensures close fitting of the retina to the RPE.

Functions of the RPE:

Absorption of light. The RPE melanosomes absorb most of the light uncaptured by photoreceptors. It prevents reflection and diffusion of light across the retina, which allows for maintaining contrast and clarity of an image. Under the influence of light, melanosomes migrate to the apical side of cells, into the surroundings of the outer light-sensing segments of the photoreceptors microvilli. In the dark, melanosomes return back to

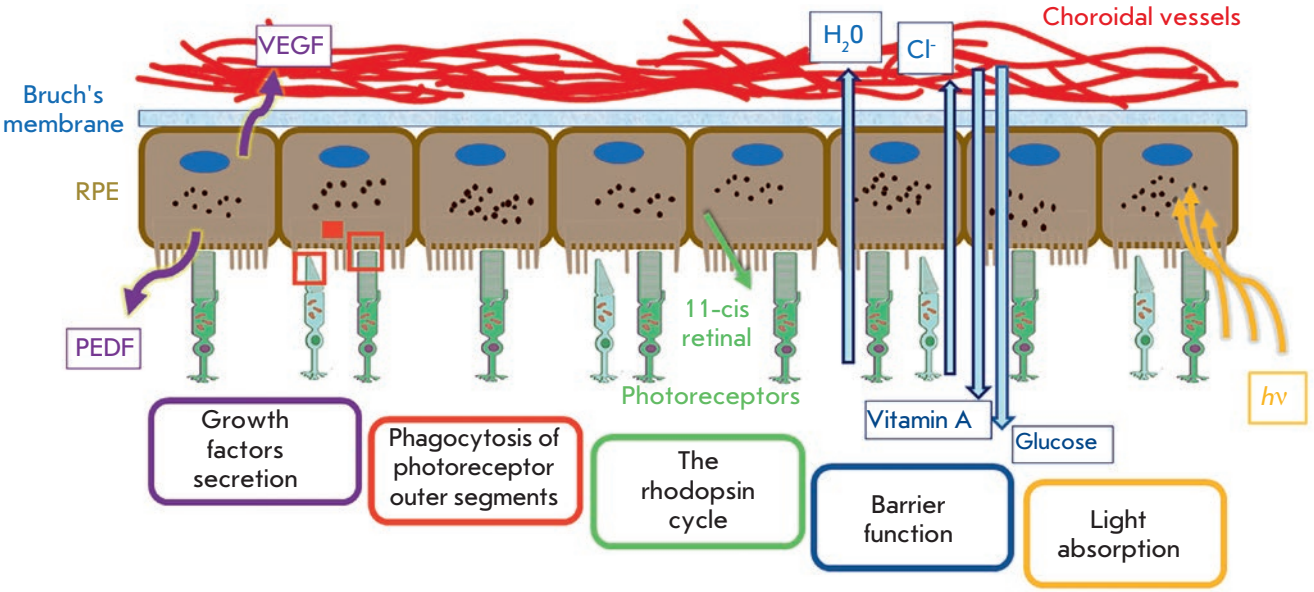

Fig. 1. Functions of retinal pigment epithelium (according to [4] with changes)

the central part of the cell with the assistance of microfilaments and a hormone known as melanotropin. The light-absorbing function is provided mainly by long microvilli [3]. In addition, the RPE helps dissipate heat in the retina, which is released as a result of lightcapture and the process of visual phototransduction [2].

Phagocytosis. The RPE cells carry out phagocytosis of used photoreceptor discs [5]. Each RPE cell daily phagocytizes 2–4 thousand used disks [6].

Implementation of the visual cycle. The disks of the outer segments of the photoreceptors contain large opsine proteins and are responsible for the absorption of light. It is synthesized in the inner segments and transported to the outer segments. Rhodopsin is necessary for the visual cycle and consists of opsin bound to 11-*cis*-retinal. When light has been captured, retinal isomerizes from 11-*cis*-retinal into *trans*-retinal and then converts to *trans*-retinol. During the visual cycle, photoreceptors find themselves unable to convert *trans*-retinol back to 11-*cis*-retinal; therefore, it is transported to the RPE for re-isomerization and subsequently returns to the photoreceptors [1].

Barrier function. Providing a selective supply of the necessary nutrients to the photoreceptors of the vascular membrane and removal of degradation products in the opposite direction. The RPE is the second part of the hematoretinal barrier, which prevents large molecules from entering the retina from the choriocapillaries. The first part of this barrier is the endothelium of retinal capillaries [3, 5, 6].

Secretion of hormones and growth factors. Polarized RPE cells secrete various cytokines and growth factors in different directions, which is very important for the functioning of choriocapillaries and retina. For example, secreted from the basal side of the RPE cells VEGF is vital for choriocapillaries, whereas PEDF and TGF-β, which are secreted mainly by the apical side of the RPE cells, are required in the subretinal space [1, 2].

There is no doubt that the RPE plays an important role in sustaining photoreceptors and that proper functioning of the photoreceptors is impossible without a healthy RPE.

DISEASES RELATED TO RPE DEGENERATION

The most common diseases involved in RPE degeneration are age-related macular degeneration (AMD) of the retina and pigment retinitis (PR) [6, 7]. These two diseases are the main causes of blindness in Western countries. To date, there are no satisfactory ways to treat them, since the retina and RPE do not regenerate, and only in the case of a "wet" form of AMD can the course of the disease be slowed down through anti-VEGF therapy [8].

AMD is a multifactorial disease that can develop under the influence of genetic factors, aging, and lifestyle (smoking, body mass index, diet) [1]. AMD has "dry" and "wet" forms. In the dry form of AMD, small amorphous deposits containing fats and proteins, known as druses, accumulate under the macula between the inner layer of the Bruch's membrane and the basal membrane of RPE [9]. This leads to local inflammation caused by oxidative stress [1]. Over time, the communication between RPE and photoreceptors is lost, which leads to the deterioration of central vision. This

form of AMD is the most common one and occurs in approximately 90% of people with this disease. In the case of the wet form of AMD, new blood vessels appear in parts of the macula where they should not be present. This causes the destruction of the macula structure and leads to a rapid loss of central vision. Although this type of AMD occurs in about 10% of people with this disease, it accounts for 90% of the AMD-related decline in vision.

Pigmented retinitis (PR) is the main cause of blindness among children and adolescents. The PR prevalence is 1 case per 3,500 people [8, 10]. This hereditary disease often leads to blindness and is characterized by progressing dysfunction and death of the rods. In some cases, PR is accompanied by damage to RPE. It was found that about 50 mutated genes are associated with PR. Among them, there are genes encoding proteins associated with the transmission of a light signal, retinoid cycle, cell adhesion, and cytoskeleton [10]. The most common type of PR is caused by mutations in the gene encoding opsin [11]. The early stages of PR involve degeneration of the rods, which results in patients losing night and peripheral vision. At the late stages of PR, patients develop the tunnel syndrome and cones also begin to die, leading to serious issues [1].

The Stargardt's and Best's diseases, forms of heritable juvenile macular degeneration, are less common than PR and AMD. Stargardt's macular dystrophy is caused by mutations in the *ABCA4* gene, which lead to the accumulation of di-retinoid-pyridinium ethanolamine (A2E) and its modification in RPE cells. These toxins demolish the pigment epithelium and follow the death of the photoreceptors of the retina's macula, accompanied by a loss of central vision [12, 13]. At the moment, there are no ways to stop the loss of vision caused by Stargardt's macular degeneration [14]. There is a whole series of so-called "Stargardt's-like diseases," caused by mutations in the genes *CNGB3*, *ELOVL4*, and *PROM1* [14, 15].

Best's disease is an autosomal-dominant hereditary disease caused by mutations in the *BEST1* gene that encodes transmembrane protein bestrophin-1. This protein is part of the basolateral plasma membrane of RPE, but its function has not been fully elucidated. It is known that Best's disease alters the transport of chloride ions and disrupts fluid transport through RPE and the accumulation of metabolites (for example, lipofuscin) and fluid between the Bruch's membrane and the RPE/photoreceptor complex. These processes cause the death of photoreceptors and loss of central vision [1, 12]. Best's disease was the first among retinal diseases whose cellular model was created with the help of patient-specific IPSCs. The model was used to demonstrate, at the molecular level, that processing in mutant RPE of the outer segments of photoreceptors is disrupted and that the rhodopsin transformation cycle is slowed down [16].

POTENTIAL OF CELLULAR THERAPY IN DISEASES OF THE EYE

There are various strategies for using autologous and allogeneic material for transplantation in patients with AMD [6] and other diseases associated with degenerative processes in the retina. Three main strategies are used for clinical trials with autologous material: translocation of the macula (e.g., [17]), autotransplantation of the RPE-choroid flap (e.g., [18]), and subretinal injection of a suspension of autologous RPE cells (e.g., [19]).

Meurs et al. described the experience of autotransplantation of peripheral RPE to seven patients with AMD. Postoperative follow-up lasting a year revealed no significant improvement in visual acuity, although three patients positively assessed their condition. Two patients reported a decline in vision, which, according to the authors, could have been associated with postoperative retinal detachment and proliferative vitreoretinopathy [20].

Falkner-Radler et al. compared the efficiency of autotransplantation of the RPE-choroid flap and subretinal injection of a RPE suspension in two groups of seven patients, each. Based on the results of a 24-month follow-up of the patients from both groups, no statistically significant differences were observed in the best corrected visual acuity test (BCVA). However, the individual results in the groups were ambiguous. For example, both improvement of visual function and deterioration of visual acuity were reported by individual patients in both the first and second groups [21].

In 2012, van Zeeburg et al. reported on the ability of a transplanted RPE-choroid flap to sustain the function of the macula over a long period of follow-up with a relatively low level of complications and relapses. The work was based on a 7-year postoperative follow-up period of 130 patients who underwent autologous transplantation of the RPE-choroid flap (a total of 133 eyes) in the period from 2001 to 2006 [22]. The study and its main findings were criticized in a review by Seiler and Aramant (2012), who pointed out the absence of a control group and the low number of eyes that were actually followed up after the surgery (only 9 eyes at year 7 of the follow-up) [23].

Therefore, the issue of the effectiveness and stability of results in an autotransplantation of RPE remains controversial. The undoubted advantage of the method is the lack of histocompatibility issues and absence of a need for immunosuppressive therapy. On the other hand, autotransplantation may lead to unpredictable results [24]. It cannot be excluded that cells transplant-

ed from a site unaffected by the degeneration already had hidden morphofunctional changes. In addition, the difficulty of obtaining material for autotransplantation from healthy areas limits the possibilities of treatment at late stages of the disease.

Donor tissue can be another source of cells for RPE transplantation in patients with macular degeneration, as long as there is donor-recipient histocompatibility. As a rule, fetal material is transplanted, although there are reports of transplantation of allogeneic tissue from adult donors.

Allogeneic fetal material was first used for RPE transplantation in 1999 in the treatment of 16 patients [25]. At the time, immunosuppressive therapy was not used in the postoperative period and 75% of the patients experienced slow rejection of the transplanted tissue. The first report on the transplantation of RPE from an adult donor was published in 2001 [26]. That surgery was performed on an 85-year-old patient who died 4 months after the procedure. The surgery itself did not lead to an improvement in visual indices. Therefore, the first clinical transplantations of RPE from allogenic donor tissues proved rather unsuccessful.

The first encouraging results of allogeneic transplantation were obtained by American surgeon Norman D. Radtke. In 2004, he published a report on the transplantation of the fetal neuroretina/RPE complex to a 64-year-old woman with pigmentary degeneration of the retina (PDR) [27]. The surgery led to an improvement in visual acuity in the patient during a 5-year follow-up period. Later, in 2008, the same surgery was performed by the same surgeon in 10 patients with PDG, and in seven of them it improved visual acuity. In one patient, visual acuity did not change in the postoperative period, while in two patients vision deteriorated [28].

In 2007, another group of ophthalmic surgeons performed transplantation of allogeneic RPE tissue from adults to 12 patients with exudative macular degeneration. The patients received a course of immunosuppressive therapy lasting up to 6 months. The postoperative follow-up during the first year showed improvement in visual acuity, reading, and other parameters of visual function, although statistical methods did not confirm the observed differences [24].

Thus, despite early promise, outcomes for the transplantation of autologous or donor tissue in AMD have been controversial. In the case of autotransplantation, there is a risk associated with a surgical intervention involving the gathering of healthy tissue in a degeneration-free area of the retina and further manipulations involving the introduction of an autograft into the macula area [29]. In addition, there is the possibility of continuing degradation of the autotransplanted healthy tissue. Allogeneic transplantation is inevitably accompanied by problems related to obtaining donor material, donor-recipient histocompatibility, and the need for immunosuppressive therapy, which in turn is associated with a variety of side effects.

Let us mention that descriptions of experiments with mesenchymal stem cell (MSC) transplantation for the treatment of eye diseases are beyond the scope of this review. We would only mention that it is already generally accepted that, in this case, MSCs can only have a paracrine effect, since these cells do not possess the ability to differentiate beyond the mesodermal germinal layer [30, 31].

At the end of the 20th century, cultures of mouse and human embryonic stem cells (ESC) were obtained from the internal cell mass of blastocysts [32, 33]. In 2006, induced pluripotent stem cells (IPSC), ESC analogues, were created by genetic reprogramming of differentiated cells [34]]. ESC and IPSC are pluripotent; i.e., they are capable of unlimited growth and self-renewal, as well as differentiation into cells of any type. Pluripotent stem cells (PSC) can provide a solution to the problem of finding a source of cells for transplantation, which researchers have encountered in clinical trials of autologous and allogeneic RPE transplantation. In recent years, several protocols for directional differentiation of ESC and IPSC into RPE have been developed and some of them have been tested in clinical trials [5, 35-39]. It should be noted that the anatomical and morphological features of the eye (relatively small size, organ pairing, well-developed methods of diagnosis and instrumental monitoring, possible immune privilege and presence of the hematoretinal barrier) make it a convenient target for refining the technology of delivery of material in the case of cell therapy involving pluripotent cells derivatives [40].

DIRECTED DIFFERENTIATION OF PSCS INTO RPE

Directed differentiation of IPSCs into RPE and further use of the obtained material in clinical practice are of interest to many researchers (e.g., [11, 41]). We compare different differentiation protocols, their effectiveness, and time costs. Let's briefly consider some of the protocols that currently seem most effective to us.

Insignificant amounts of retinal pigment epithelial cells can be formed during spontaneous differentiation of human pluripotent stem cells [35]. If FGF2, which is necessary to maintain the pluripotent state in culture, is removed from the culture medium, human pluripotent stem cells cultured on a mouse embryonic fibroblast substrate, matrigel, polylysine, or laminin become capable of forming pigment epithelial cells [35, 42, 43]. After 10–12 weeks of spontaneous differentiation, small pigmented regions form, which are then

mechanically separated from the rest of the cell mass, yielding an almost pure cell culture of pigment epithelium (> 99% purity). Various modifications of culture medium composition and time of differentiation make it possible to increase the yield of pigment epithelial cells [44, 45]. However, effective directional differentiation protocols are required to obtain cultures that are enriched in retinal pigment epithelial cells without a labor-intensive mechanical selection of pigmented colonies. Recent studies have shown that it is possible to produce cells of retinal pigment epithelium from IPSCs and ESCs *in vitro* which are morphologically and functionally similar to such cells *in vivo*. For example, Leach et al. compared the effectiveness of spontaneous and directed differentiation protocols into RPE using five different IPSC lines obtained from different donors and different cell types. It has been shown that the source of donor cells, the method of reprogramming, and the protocol used can affect the possibility of effective differentiation [46], which once again underscores the need for a standardization of the procedure for obtaining RPE from PSCs for clinical use.

One of the first directional differentiations of PSC into RPE was performed by Hirami et al. [47]. Mouse and human IPSCs in a suspension culture were treated with Wnt and Nodal antagonists to promoted differentiation into pigment epithelium.

Since RPE cells differentiate from the neuroectoderm and share common characteristics with neuronal retina cells *in vivo*, a two-stage differentiation protocol was developed to produce pigment epithelial cells from neuroepithelial precursors [48–51]. The ESCs aggregates were initially cultured in a suspension in a medium for neuroepithelial differentiation. Then, neuroepithelial progenitors were expanded and differentiated into putative pigment epithelial cells by replacing FGF2 in the culture medium with B27 additive. The first cells, similar to retinal pigment epithelial cells, appeared after 4 weeks of differentiation, and after 8 weeks the number of cells suitable for subcultivation became significant. This two-step method is more effective than the method of spontaneous differentiation.

Based on the role of nicotinamide (NIC) in metabolism, survival, plasticity and cell differentiation, Idelson et al. investigated the effect of NIC on the differentiation of ESCs into pigment epithelial cells [5]. To induce a differentiation into RPE cells, ESC clusters obtained with collagenase were cultured in a suspension in a ESC medium supplemented with a serum substitute, NIC, and with or without activin A (a member of the TGF-β superfamily that directs the differentiation of the eyeball in embryogenesis) [52]. Pigmented areas appeared 4 weeks after the induction, and about half of the clusters were pigmented when cultured in media containing both NIC and activin A. It has been shown that NIC in the presence of activin A effectively induces and increases the efficiency of differentiation of ESCs into pigment epithelial cells.

The protocols described above assume a lengthy time of differentiation and produce a low-purity population, which requires additional laborious manipulations to purify the cells of the desired type. Buchholz et al. proposed a faster and more effective protocol. This method of directed differentiation of ESC into pigment epithelial cells is based on a combination of factors inducing retinal differentiation (IGF1, Noggin, Dkk1, bFGF), and other factors (NIC, activin A, SU5402 and vasoactive intestinal peptide (VIP)), and all factors are added at different, strictly defined time points [44]. Already 14 days after the initiation of the differentiation, about 80% of the cells in the culture were pigment epithelial cells. According to the authors, this protocol can be used to rapidly build up the large quantities of cells necessary for transplantation due to its high efficiency and speed (there are minor variations of this protocol proposed by other authors, e.g. Geng et al. [53]). A similar protocol was proposed by Foltz and Clegg, who used CHIR99021 instead of VIP [54].

To identify new compounds that contribute to the differentiation of IPSC into RPE, a quantitative PCR screening of RPE differentiation markers in a IPSC culture was performed by analyzing a chemical library [39]. As a result, chetomin, a substance that potentially activates differentiation, was identified. Then, using a reporter construct (GFP under the control of a RPE-specific tyrosinase enhancer), it was confirmed that chetomin, an inhibitor of the hypoxia-induced factor (HIF), significantly increased the differentiation of PSCs into RPE. The combination of chetomin with nicotinamide led to the differentiation of more than 50% of IPSCs into RPE. The molecular pathways by which chetomin promotes the differentiation into RPE are still unknown.

To obtain retinal cells, Zhu et al. also used inducers such as IWR1, SB431542, and IGF1, and they obtained functional photoreceptors and retinal pigment epithelium from IPSCs in compliance with GMP standards. It has been shown that the obtained derivatives can integrate the retina of immunodeficient mice [55].

In our laboratory, several methods of differentiating PSCs into RPE have been tested. A comparison of several differentiation protocols led us to the following conclusions:

1. In our experience, the protocol [39] with chetomin and nicotinamide is the best protocol, working reliably for all tested IPSC and ESC lines. In this case, the addition of activin to the medium is undesirable, since it reduces the survival rate of cells and the effectiveness of

the directed differentiation (unpublished data). Differentiation takes at least 30 days, but this "loss of time" is compensated for by a large number of pigmented cells obtained and their subsequent rapid proliferation.

2. Pigment epithelium cells are extremely sensitive to the extracellular matrix; their survival, maturation rate, and completeness of phenotypic and functional characteristics typical of this type of cells *in vivo* depend on the type and quality of the matrix [56, 57]. The natural substrate for the cells of retinal pigment epithelium is Bruch's membrane. According to our experimental data, matrigel is the most suitable substrate for a rapid growth of immature, rapidly dividing RPE cells in laboratory. Most likely, in order to achieve full hexagonal morphology and correct polarization of RPE, it is necessary for the liquid to wash the layer of the epithelial cells from both sides, apical and basal. In order to achieve that, the RPE cells are usually cultivated in chambers, transwells, where the medium is located above and under the membrane on which the cells grow. A representative photograph of RPE differentiated from IPSCs and having a characteristic morphology and pigmentation is shown in *Fig. 2*.

One of the most important functional characteristics of retinal pigment epithelial cells is the ability to secrete PEDF and VEGF, and also to form an extracellular matrix [4], interact with the outer segments of the photoreceptor, and phagocytize them [38]. Therefore, these physiological properties are usually tested to prove the functionality of the differentiated RPE. The expression of the genes that encode typical RPE proteins (e.g., RPE 65, BEST1, tyrosinase, MITF1, ZO-1, etc.) is also checked. Another very important characteristic of RPE is its transepithelial potential, which reflects the barrier properties of the epithelium. This potential can be measured with a conductometer.

The functionality of differentiated RPE *in vivo* is confirmed in animal models, primarily in rats of the RCS (Royal College of Surgeons) line with recessively inherited dystrophy of the retina [5, 38, 58] and in albino rabbits [59]. Numerous studies have shown that in animals after transplantation of the pigment epithelium, its histological and physiological features are preserved. Electroretinography was used to demonstrate the functionality of the transplanted RPE (review [60]).

CLINICAL TRIALS OF RPE DIFFERENTIATED FROM PSCS

The first clinical trials using RPE cells derived from pluripotent stem cells were performed by American specialists Schwartz et al. in 2011. ESC of a MA09 line were used to obtain RPE. This trial was registered in the ClinicalTrials.gov database under the IDs NCT01345006 (Stargardt's disease) and NCT01344993 (atrophic AMD). At the first stage, one patient with

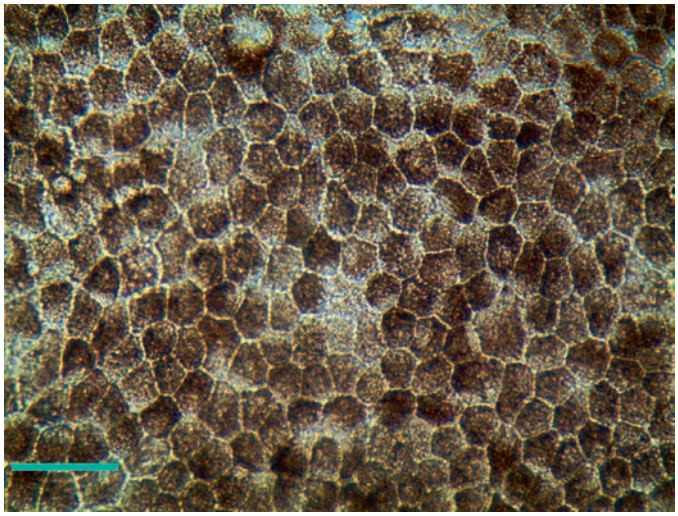

Fig. 2. RPE cells differentiated from the IPSC of a healthy donor. The cells were cultured for 3 months in a Transwell chamber. Phase contrast. The scale bar is 100 mM

Stargardt's disease and one patient with atrophic AMD received subretinal injections of 50,000 RPE cells. The results of the postoperative follow-up revealed no side effects over the course of 4 months, including hyperproliferation and oncogeneity. Visual acuity improved in both patients based on objective indicators [61]. At the next stage, a clinical cohort of 18 patients was given different doses of the transplantation material: 50×10^3, 100×10^3 and 150×10^3 cells. During a period of postoperative follow-up of 22 months, an increase in retinal pigmentation was noted in 13 patients; improvement of vision was noted in 10 patients [14].

The protocol by Schwartz et al. was used in 2012 by Korean ophthalmologists in the NCT01625559 clinical trial. Minor modifications of the protocol concerned screening for oncogenicity and a scheme of postoperative immunosuppressive therapy. Two patients with Stargardt's disease and two patients with AMD received a subretinal injection of 40×10^3 RPE cells differentiated from the ESC of a MA09 line. Based on the Early Treatment Diabetic Retinopathy Study and a BCVA test, visual improvement was registered in three patients. In one patient, immunosuppressive therapy was discontinued 4 weeks after the surgery due to the development of side effects, and the state of the retina returned to its preoperative level. In general, the feasibility and preliminary safety of cell therapy with RPE differentiated from ESC in macular degeneration of various etiologies have been confirmed. However, it has been noted that further observations, clinical trials, and studies are required [12].

In 2012, Pfizer launched a phase I clinical trial of a transplantation of ESC-derived RPE grown on a poly-

ester membrane (NCT01691261) at University College London. In that trial, the transplantation was performed in patients with the wet form of AMD with progressive loss of vision. Currently, patients who participated in the phase I are being recruited to the next clinical trial (NCT03102138), which will involve a 4-year follow-up and safety assessment of the earlier conducted transplantation.

In 2015, three different universities in China announced the start of phase I clinical trials of subretinal transplantation of RPE differentiated from ESCs (NCT02749734, NCT02755428, NCT03046407). In each trial, the surgery will be performed on 10–15 patients with various forms of retinal dystrophy. The studies will assess safety and the clinical effect of the transplantation.

Since 2015, the Federal University of São Paulo (Brazil) under the leadership of Professor Rubens Belfort has been conducting a two-stage clinical trial which examines the feasibility of transplantation of ESC-derived RPE (NCT02903576). The first stage will include transplantation of PRE in the form of a suspension; and the second stage, in the form of a monolayer on a polymer substrate. The purpose of the trial is to compare the efficacy of the two methods of transplantation, as well as to assess its safety and applicability in clinical practice.

Currently, Regenerative Patch Technologies, led by Jane Lebkowski, is recruiting patients in the United States to participate in the Phase I/II clinical trial of transplantation of ESC-derived RPE on a parylene membrane. The trial will include 20 patients, distributed into two groups based on the stage of "dry" AMD (NCT02590692).

A trial of the commercial cell productOpRegen®, a suspension of RPE cells derived from human ESCs, has been started by U.S. and Israeli medical teams. In this trial, 15 patients with atrophic AMD will undergo transplantation of the product into the subretinal space, followed by vitrectomy (NCT02286089).

An analysis of the ClinicalTrials.gov database shows that the main objects of clinical trials across the world are cells obtained from ESCs. The first – and so far only – published clinical trial of RPE differentiated from IPSCs has been carried out in Japan [62]. The bias in favor of ESCs can be attributed to greater reservations on the part of the biomedical community regarding IPSCs. The production of IPSCs requires a much higher number of manipulations per cell than the production of a ESC line. There are doubts regarding the stability of the IPSC genome, in the completeness of reprogramming and differentiation. IPSCs are also not quite as widely represented in clinical trials, since it is a relatively new type of cells; they were first obtained in 2006, whereas mouse and human ESC cells have been studied 25 and 8 years longer, respectively. In our opinion, one could expect an increase in the number of trials of IPSC products within the next three to four years, especially in Japan and China.

According to Federal Law of June 23, 2016, No. 180-FL, human ESCs and fetal cells are not allowed to be used as a source of cellular products. Regardless of the opinion of the authors about this prohibition, Russian researchers are faced with the fact that IPSCs remain essentially the only source of cells for producing RPE.

The first clinical trial of RPE differentiated from IPSCs was conducted in Japan [62]. The Japanese doctors transplanted a monolayer of RPE differentiated from IPSCs to a 70-year-old patient with neovascular age-related AMD. The patient underwent surgery which included the removal of the neovascular membrane and transplantation of the autologous RPE under the retina. A year after the surgery, the transplanted layer of RPE remained intact, visual acuity did not improve, but it did not worsen either, and cystoid macular edema was present. Autologous IPSCs were obtained using nonintegrating plasmid vectors and differentiated into RPE according to a previously published protocol that allows obtaining functional RPE [62]. The quality and safety of the IPSCs and the RPE cells obtained from them were carefully analyzed before the transplantation. In addition to the assessment of the morphology and expression of the relevant markers, the authors performed karyotyping with traditional GTG-banding and a full-genomic SNP-analysis, as well as full-genomic sequencing, and full-genome analysis of transcriptome and DNA methylation. The absence of RPE tumorigenicity was demonstrated by transplanting the RPE to immunodeficient NOG mice.

Pioneering transplantation of RPE differentiated from IPSCs certainly became a huge step in regenerative medicine. However, it also left many unresolved issues. It should be noted that, initially, the PRE transplantation should have been performed in two patients, but for one of them IPSCs did not pass quality control due to identified CNV that appeared during the reprogramming. In addition, 10 out of the 20 IPSC clones selected for further analysis contained plasmids integrated into the genome: i.e., the preparation of IPSCs using plasmids should not be recognized as the safest way of reprogramming [62]. Other means of production could be nonintegrable viruses, *in vitro* synthesized RNA, and reprogramming with small molecules [63–65].

So far, the international community has not developed unambiguous recommendations either on methods for obtaining or on the necessary and sufficient methods of characterization of cells derived from PSCs.

A prerequisite for the full-scale application of PSC-differentiated derivatives is the assessment of the effect of various protocols of their production and subsequent cultivation on the genetic and epigenetic stability of cells with sequencing and the methylation profiling of the whole genome, analyses of the expression, as well as elucidation of the molecular basis, of possible aberrations [66]. In addition, surgical transplantation and instruments are now being actively developed, which should make this procedure as safe as possible for patients [67].

Autologous transplantation of IPSC derivatives is a very expensive and long-term method. As mentioned above, allogeneic transplantation requires immunosuppression. It has seemed that the solution to this problem could be the development of IPSC banks from healthy donors with homozygous genes of the main histocompatibility complex HLA [68]. Each such homozygote will be compatible with any heterozygote in which there is one allele of the same haplotype. It is estimated that the 20 most common homozygous HLA haplotypes of the European population, identified after screening of 26,000 individuals, will be suitable for 50% of the population [68]. The creation of such a bank of IPSC lines began as a national initiative in Japan in 2012, and IPSCs with the most common "Japanese" haplotypes are already available for use at the IPSC Research and Application Center in Kyoto [69]. However, the work published last year [70] slightly dampened optimism regarding this approach. It turned out that when immune cells heterozygous for HLA interact with HLA-homozygous graft cells, the recipient's NK cells are able to cause the rejection of cells derived from homozygous IPSC by recognizing the "absence of one's own" [70]. This issue requires further study.

CONCLUSION

So far, there have been no proven methods for restoring or improving vision in patients with retinal degeneration. One such method can be the transplantation of retinal tissues, in particular pigment epithelium. The approach associated with the transplantation of RPE derived from human PSCs has already been used in several clinical trials. Retinal pigment epithelium could be obtained by directional differentiation of human ESCs and human IPSCs and selected based on morphological criteria and the accumulation of brown pigment granules. However, wide application of PRE differentiated from PSCs requireds addressing many different issues. In particular, methods for sorting the RPE, necessary and sufficient procedures for proving the equivalence of the differentiated cells to the RPE cells, methods and protocols of cell delivery, surgery technologies and criteria for selecting patients for RPE transplantation should be elaborated. For example, progression of the disease is associated with degeneration of both RPE and photoreceptors, and, therefore, it becomes necessary to transplant both RPE and the photoreceptors in order to achieve an effective clinical outcome. In addition, personalized therapy with autologous cells is unlikely to become a generally available medical procedure in the coming decades due to its labor-intensity and the high cost associated with obtaining and differentiating patient-specific IPSCs. The search for approaches to allogeneic transplantation of IPSC-derivatives would make it possible to reduce the cost and accelerate the production of RPE cells for transplantation in the degeneration of the retina. ●

This study was carried out with a grant from the Russian Science Foundation (No. 14-15-00930).

REFERENCES

1. Jones M.K., Lu B., Girman S., Wang S. // Prog. Retin. Eye Res. 2017. V. 57. P. 1–27.
2. Nazari H., Zhang L., Zhu D., Chader G.J., Falabella P., Stefanini F., Rowland T., Clegg D.O., Kashani A.H., Hinton D.R., et al. // Prog. Retin. Eye Res. 2015. V. 48. P. 1–39.
3. Diniz B., Thomas P., Thomas B., Ribeiro R., Hu Y., Brant R., Ahuja A., Zhu D., Liu L., Koss M., et al. // Invest. Ophthalmol. Vis. Sci. 2013. V. 54. № 7. P. 5087–5096.
4. Strauss O. // Physiol. Rev. 2005. V. 85. P. 845–881.
5. Idelson M., Alper R., Obolensky A., Ben-Shushan E., Hemo I., Yachimovich-Cohen N., Khaner H., Smith Y., Wiser O., Gropp M., et al. // Cell. Stem Cell. 2009. V. 5. № 4. P. 396–408.
6. Alexander P., Thomson H.A., Luff A.J., Lotery A.J. // Eye. 2015. V. 29. P. 992–1002.
7. Brandl C., Zimmermann S.J., Milenkovic V.M., Rosendahl S.M., Grassmann F., Milenkovic A., Hehr U., Federlin M., Wetzel C.H., Helbig H., et al. // Neuromolecular Med. 2014. V. 16. № 3. P. 551–564.
8. Tang Z., Zhang Y., Wang Y., Zhang D., Shen B., Luo M., Gu P. // J. Transl. Med. 2017. V. 15. № 1. P. 99–111.
9. Parameswaran S., Krishnakumar S. // Indian J. Ophthalmol. 2017. V. 65. № 3. P. 177–183.
10. Lukovic D., Artero Castro A., Delgado A.B., Bernal Mde L., Luna Pelaez N., Díez Lloret A., Perez Espejo R., Kamenarova K., Fernández Sánchez L., Cuenca N., et al. // Sci. Rep. 2015. V. 5. P. 12910.
11. Zhao C., Wang Q., Temple S. // Development. 2017. V. 144. № 8. P. 1368–1381.
12. Song W.K., Park K.-M., Kim H.-J., Lee J.H., Choi J., Chong S.Y., Shim S.H., Del Priore L.V., Lanza R. // Stem Cell Repts. 2015. V. 4. № 5. P. 860–872.
13. Allikmets R., Shroyer N.F., Singh N., Seddon J.M., Lewis R.A., Bernstein P.S., Peiffer A., Zabriskie N.A., Li Y., Hutchinson A., et al. // Science. 1997. V. 277. № 5333. P. 1805–1807.
14. Schwartz S.D., Regillo C.D., Lam B.L., Eliott D., Rosenfeld P.J., Gregori N.Z., Hubschman J.P., Davis J.L., Heilwell G., Spirn M., et al. // Lancet. 2015. V. 385. № 9967. P. 509–516.

15. Battu R., Verma A., Hariharan R., Krishna S., Kiran R., Jacob J., Ganapathy A., Ramprasad V.L., Kumaramanickavel G., Jeyabalan N., et al. // Biomed. Res. Int. 2015. V. 2015. Article ID 940864.
16. Li Y., Chan L., Nguyen H.V., Tsang S.H. // Adv. Exp. Med. Biol. 2016. V. 854. P. 549–555.
17. Oshima H., Iwase T., Ishikawa K., Yamamoto K., Terasaki H. // PLoS One. 2017. V. 12. № 5. e0177241.
18. Alpatov S.A., Shchuko A.G., Malyshev V.V. Autotransplantation of retinal pigment epithelium patch and choroidea in exudative age-related macular degeneration // RMJ "Clinical Ophthalmology". 2007. №1. P. 7
19. Binder S., Stolba U., Krebs I., Kellner L., Jahn C., Feichtinger H., Povelka M., Frohner U., Kruger A., Hilgers R.D., et al. // Am. J. Ophthalmol. 2002. V. 133. № 2. P. 215–225.
20. van Meurs J.C., ter Averst E., Hofland L.J., van Hagen P.M., Mooy C.M., Baarsma G.S., Kuijpers R.W., Boks T., Stalmans P. // British J. Ophthalmol. 2004. V. 88. № 1. P. 110–113.
21. Falkner-Radler C.I., Krebs I., Glittenberg C., Povazay B., Drexler W., Graf A., Binder S. // British J. Ophthalmol. 2011. V. 95. P. 370–375.
22. van Zeeburg E.J., Maaijwee K.J., Missotten T.O., Heimann H., van Meurs J.C. // Am. J. Ophthalmol. 2012. V. 153. P. 120–127.
23. Seiler M.J., Aramant R.B. // Prog. Retinal Eye Res. 2012. V. 31. № 6. P. 661–687.
24. Tezel T.H., Del Priore L.V., Berger A.S., Kaplan H.J. // Am. J. Ophthalmol. 2007. V. 143. № 4. P. 584–595.
25. lgvere P.V., Gouras P., Dafgard Kopp E. // Eur. J. Ophthalmol. 1999. V. 9. P. 217–230.
26. Del Priore L.V., Kaplan H.J., Tezel T.H., Hayashi N., Berger A.S., Green W.R. // Am. J. Ophthalmol. 2001. V. 131. P. 472–480.
27. Radtke N.D., Aramant R.B., Seiler M.J., Petry H.M., Pidwell D. // Arch. Ophthalmol. 2004. V. 122. P. 1159–1165.
28. Radtke N.D., Aramant R.B., Petry H.M., Green P.T., Pidwell D.J., Seiler M.J. // Am. J. Ophthalmol. 2008. V. 146. P. 172–182.
29. Binder S., Stanzel B.V., Krebs I., Glittenberg C. // Prog. Retin. Eye Res. 2007. V. 26. № 5. P. 516–554.
30. Meyer U., Meyer T., Handschel J., Wiesmann H.P. Fundamentals of Tissue Engineering and Regenerative Medicine. Berlin, Heidelberg, Leipzig, Germany: Springer–Verlag, 2009. P. 179 (total 1048).
31. Scuteri A., Miloso M., Foudah D., Orciani M., Cavaletti G., Tredici G. // Curr Stem Cell Res Ther. 2011. V. 6. № 2. P. 82–92.
32. Evans M.J., Kaufman M.H. // Nature. 1981. V. 292. P. 154–156.
33. Thomson J.A., Itskovitz-Eldor J., Shapiro S.S., Waknitz M.A., Swiergiel J.J., Marshall V.S., Jones J.M. // Science. 1998. V. 282. № 5391. P. 1145–1147.
34. Takahashi K., Yamanaka S. // Cell. 2006. № 126. P. 663–676.
35. Klimanskaya I., Hipp J., Rezai K.A., West M., Atala A., Lanza R. // Cloning Stem Cells. 2004. V. 6. P. 217–245.
36. Osakada F., Ikeda H., Mandai M., Wataya T., Watanabe K., Yoshimura N., Akaike A., Sasai Y., Takahashi M. // Nat. Biotechnol. 2008. V. 26. P. 215–224.
37. Lu B., Malcuit C., Wang S. // Stem Cells. 2009. V. 27. P. 2126–2135.
38. Kamao H., Mandai M., Okamoto S., Sakai N., Suga A., Sugita S., Kiryu J., Takahashi M. // Stem Cell Repts. 2014. V. 2. № 2. P. 205–218.
39. Maruotti J., Sripathi S.R., Bharti K., Fuller J., Wahlin K.J., Ranganathan V., Sluch V.M., Berlinicke C.A., Davis J., Kim C., et al. // Proc. Natl. Acad. Sci. USA. 2015. V. 112. P. 10950–10955.
40. Leach L.L., Clegg D.O. // Stem Cells. 2015. V. 33. P. 2363–2373.
41. Achberger K., Haderspeck J.C., Kleger A., Liebau S. // Adv. Drug Deliv. Rev. 2018. pii: S0169-409X(18)30108-X.
42. Rowland T.J., Blaschke A.J., Buchholz D.E., Hikita S.T., Johnson L.V., Clegg D.O. // J. Tissue Eng. Regen. Med. 2013. V. 7. № 8. P. 642–653.
43. Lagar'kova M.A., Shilov A.G., Gubanova N.I., Prokhorovich M.A., Kiselev S.L..// Bull Exp Biol Med. 2012. V. 152(4). P. 516-518.
44. Buchollz D.E., Pennington B.O., Croze R.H., Hinman C.R., Coffey P.J., Cleg D.O. // Stem Cells Transl. Med. 2013. V. 2. № 5. P. 384–393.
45. Shutova M.V., Surdina A.V., Ischenko D.S., Naumov V.A., Bogomazova A.N., Vassina E.M., Alekseev D.G., Lagarkova M.A., Kiselev S.L. // Cell Cycle. 2016. V. 15. № 7. P. 986–997.
46. Leach L.L., Croze R.H., Hu Q., Nadar V.P., Clevenger T.N., Pennington B.O., Gamm D.M., Clegg D.O. // J. Ocul. Pharmacol. Ther. 2016. V. 32. № 5. P. 317–330.
47. Hirami Y., Osakada F., Takahashi K., Okita K., Yamanaka S., Ikeda H., Yoshimura N., Takahashi M. // Neurosci. Lett. 2009. V. 458. № 3. P. 126–131.
48. Cho M.S., Kim S.J., Ku S.Y., Park J.H., Lee H., Yoo D.H., Park U.C., Song S.A., Choi Y.M., Yu H.G. // Stem Cell. Res. 2012. V. 9. № 2. P. 101–109.
49. Lamba D.A., McUsic A., Hirata R.K., Wang P.R., Russell D., Reh T.A. // PLoS One. 2010. V. 5. № 1. P. e8763.
50. Zhu D., Deng X., Spee C., Sonoda S., Hsieh C.L., Barron E., Pera M., Hinton D.R. // Invest. Ophthalmol. Vis. Sci. 2011. V. 52. № 3. P. 1573–1585.
51. Zhu Y., Carido M., Meinhardt A., Kurth T., Karl M.O., Ader M., Tanaka E.M. // PLoS One. 2013. V. 8. № 1. P. e54552.
52. Fuhrmann S., Levine E.M., Reh T.A. // Development. 2000. V. 127. № 21. P. 4599–4609.
53. Geng Z., Walsh P.J., Truong V., Hill C., Ebeling M., Kaphahn R.J., Dutton J.R. // PLoS ONE. 2017. V. 12. № 3. P. e0173575.
54. Foltz L.P., Clegg D.O. // J. Visual. Exp.: JoVE. 2017. № 128. P. 56274.
55. Zhu J., Reynolds J., Garcia T., Cifuentes H., Chew S., Zeng X., Lamba D.A. // Stem Cells Transl. Med. 2018. V. 7. № 2. P. 210–219.
56. Tezel T.H., Del Priore L.V. // Graefes Arch. Clin. Exp. Ophtalmol. 1997. V. 253. P. 41–47.
57. Feng W., Zheng J.J., Lutz D.A., McLaughlin B.J. // Graefes Arch. Clin. Exp. Ophtalmol. 2003. V. 241. P. 232–240.
58. Mullen R.J., Lavail M.M. // Science. 1976. V. 192. P. 799–801.
59. Reyes A.P., Petrus-Reurer S., Antonsson L., Stenfelt S., Bartuma H., Panula S., Mader T., Douagi I., André H., Hovatta Q. // Stem Cell Reports. 2016. V. 6. № 1. P. 9–17.
60. da Cruz L., Chen F.K., Ahmado A., Greenwood J., Coffey P. // Prog. Retin. Eye Res. 2007. V. 26. № 6. P. 598–635.
61. Schwartz S.D., Hubschman J.P., Heilwell G., Franco-Cardenas V., Pan C.K., Ostrick R.M., Mickunas E., Gay R., Klimanskaya I., Lanza R. // Lancet. 2012. V. 379. № 9817. P. 713–720.
62. Mandai M., Watanabe A., Kurimoto Y., Hirami Y., Morinaga C., Daimon T., Fujihara M., Akimaru H., Sakai N., Shibata Y., et al. // N. Engl. J. Med. 2017. V. 376. № 11. P. 1038–1046.

63. Fusaki N., Ban H., Nishiyama A., Saeki K., Hasegawa M. // Proc. Jpn. Acad. Ser. B Phys. Biol. Sci. 2009. V. 85. № 8. P. 348–362.
64. Warren L., Manos P. D., Ahfeldt T., Loh Y.H., Li H., Lau F., Ebina W., Mandal P.K., Smith Z.D., Meissner A., et al. // Cell Stem Cell. 2010. № 7. P. 1–13.
65. Hou P., Li Y., Zhang X., Liu C., Guan J., Li H., Zhao T., Ye J., Yang W., Liu K., et al. // Science. 2013. V. 341. № 6146. P. 651–654.
66. Luo M., Chen Y. // Int. J. Ophthalmol. 2018. V. 11. № 1. P. 150–159.
67. Kamao H., Mandai M., Ohashi W., Hirami Y., Kurimoto Y., Kiryu J., Takahashi M. // Invest. Ophthalmol. Vis. Sci. 2017. V. 58. № 1. P. 211–220.
68. Taylor C.J., Peacock S., Chaudhry A.N., Bradley J.A., Bolton E.M. // Cell Stem Cell. 2012. V. 3. № 11. P. 147–152.
69. Okita K., Matsumura Y., Sato Y., Okada A., Morizane A., Okamoto S., Hong H., Nakagawa M., Tanabe K., Tezuka K., et al. // Nat. Methods. 2011. V. 8. P. 409–412.
70. Ichise H., Nagano S., Maeda T., Miyazaki M., Miyazaki Y., Kojima H., Yawata N., Yawata M., Tanaka H., Saji H., et al. // Stem Cell Repts. 2017. V. 9. P. 853–867.

Production of Recombinant Proteins in the Milk of Transgenic Animals: Current State and Prospects

M. V. Shepelev*, S. V. Kalinichenko, A. V. Deykin, I. V. Korobko
Institute of Gene Biology, Russian Academy of Sciences, Vavilova Str., 34/5, Moscow, 119334, Russia
*E-mail: mshepelev@mail.ru
Received December 12, 2017; in final form August 16, 2018

ABSTRACT **The use of transgenic animals as bioreactors for the synthesis of the recombinant proteins secreted into milk is a current trend in the development of biotechnologies. Advances in genetic engineering, in particular the emergence of targeted genome editing technologies, have provided new opportunities and significantly improved efficiency in the generation of animals that produce recombinant proteins in milk, including economically important animals. Here, we present a retrospective review of technologies for generating transgenic animals, with emphasis on the creation of animals that produce recombinant proteins in milk. The current state and prospects for the development of this area of biotechnology are discussed in relation to the emergence of novel genome editing technologies. Experimental and practical techniques are briefly discussed.**
KEYWORDS **transgenic animal, recombinant protein, mammary gland, targeted genome editing, homologous recombination, site-specific recombination.**
ABBREVIATIONS **CRISPR – clustered regularly interspaced short palindromic repeat, HDR – homology-directed repair, MMEJ – microhomology-mediated end joining, NHEJ – non-homologous end joining, RMCE – recombinase-mediated cassette exchange, SCNT – somatic cell nuclear transfer, SSA – single strand annealing, TALE – transcription activator-like effector, TALEN – transcription activator-like effector nuclease, ZFN – zinc finger nuclease.**

INTRODUCTION

For many years, genetically modified laboratory animals have been an effective tool for studying the functional properties of genes, proteins, and other molecules, and their importance as human disease models in biomedical research can hardly be overestimated. Such animals can be used to study the pathogenesis and molecular features of diseases, for the identification and validation of new therapeutic targets, and for effective search and development of new drugs, including preclinical studies. At the same time, genetically modified animals are becoming increasingly attractive objects in fields such as livestock farming, where genome changes can be used to correct economically important animal traits. Finally, transgenic animals can serve as bioreactors for the synthesis of the recombinant proteins secreted into milk, which enables the production of recombinant proteins in substantially larger amounts and at much lower costs than the production of proteins in eukaryotic cell cultures [1]. According to a prognosis by the RAND Corporation, an analytical company, which was published in 2006, the use of the mammary gland as a bioreactor for the production of recombinant proteins will be one of the most important areas of biotechnology to the year 2020 [2]. The prognosis is evidenced not only by numerous experimental studies in this direction, but also by already commercially available drugs based on recombinant human proteins. For example, recombinant human antithrombin III (Atryn®) is produced from the milk of transgenic goats, and a recombinant human C1 esterase inhibitor (Ruconest®) is obtained from rabbit milk [3]. In the last decade, revolutionary changes have occurred in the field of genome modification, due to the opportunity afforded by highly effective targeted genome editing and the significant simplification of this technology after the discovery of the CRISPR/Cas9 system. This has enabled the development of new approaches to the generation of animals, including economically important species whose milk contains recombinant proteins. New approaches will dramatically simplify and improve efficiency in the creation of such animals. In this review, we consider technologies for the generation of transgenic animals, with an emphasis on animals that produce recombinant proteins in milk. We

outline today's landscape and prospects in this field in terms of the emergence of new genome editing technologies and briefly describe experimental and practical studies.

CLASSICAL TRANSGENESIS OF ANIMALS AND THE GENETIC ELEMENTS REQUIRED FOR THE PRODUCTION OF RECOMBINANT PROTEINS

The classical method for the generation of transgenic mammals, which was developed in the early 1980s and has been in wide use up to the present time, entails the microinjection of a transgene-containing DNA fragment into the pronucleus of a fertilized oocyte, followed by transplantation of the oocyte to competent (pseudo-pregnant) animals. In the scheme, the transgene-containing DNA fragment is randomly integrated into the recipient genome during natural processes of genomic DNA breakage and repair [4]. Transgene-containing linear DNA fragments, both intact and after nonspecific cleavage in the cell, can integrate into various sites of the genome. The number of transgene copies in the integration site also varies within a wide range [5]. In addition, the integration process can occur at various stages of embryo development, which leads to the mosaicism of primary transgenic animals: i.e., to the presence of a transgene not in all the cells of the organism. Obviously, generating a line of transgene-carrying animals requires the presence of a transgene in the genome of germ cells and inheritance of transgene-containing genomic DNA.

Therefore, during classical transgenesis, the transgene is randomly integrated into the recipient's genome; in this case, the number of integrated transgene copies, including incomplete transgene fragments, is uncontrolled. If production of a recombinant protein is required, the transgenic construct should include a full expression module that provides autonomous transcription of the transgene in target tissues of the organism and proper mRNA processing, because of random transgene integration. When using alternative methods of transgenesis and technologies of targeted genome editing (see below), this requirement is not mandatory.

The key determinant that provides tissue specificity in transgene expression is the promoter. A number of promoters of genes encoding milk proteins have been successfully used for the production of recombinant proteins in the mammary gland. Promoters that enable production of the target protein at a sufficiently high level in milk (up to tens of grams per liter of milk) include promoters of goat and cow β-casein, cow α-s1-casein, rabbit whey acidic protein (WAP), human α-lactalbumin, and sheep β-lactoglobulin genes. However, the level of protein production depends not only on the promoter, but also on a number of other factors. In this case, promoters of one animal species can provide effective transcription of the transgene in the mammary gland cells of another animal species due to conservatism of the transcription factors regulating the production of milk proteins in mammary cells [6–19].

As the experience of generating transgenic animals has demonstrated, effective production of a recombinant protein often requires, apart from a tissue-specific promoter that ensures a high level of transgene transcription, inclusion of introns into the transgene. Inclusion of introns into the transgene in some experimental systems enabled a 400-fold increase in the transgene transcription level, compared to that from intron-free cDNA, while the effect of intron inclusion is minimal in other systems [20, 21]. Different introns placed in the same region of a gene may have opposite effects on the transgene expression level [21], and the same intron at different positions in the transgene may have opposite effects on the expression level [20, 21]. Introns, along with the possible inclusion of enhancers promoting high tissue-specific transgene transcription, as in the case of the first intron of the mouse β-casein gene [22], may also have an effect on the transgene expression level which is not related to transcription enhancement. One of the potential mechanisms of expression enhancement is regular arrangement of nucleosomes in the gene and the promoter region due to the presence of introns in the DNA sequence. A disruption of the nucleosome arrangement is supposed to disrupt initiation or elongation of transcription, complicating access to transcription factors or movement of RNA polymerase in the case of too closely located nucleosomes [23]. Another mechanism of intron-dependent enhancement of transgene expression may be the association between splicing and transcript polyadenylation [24]. Therefore, inclusion of introns in a transgene is generally considered as a way of increasing the level of transgene expression [25]. This fact determines the design of the protein-coding sequence of transgene that can be represented by cDNA, a full-length gene copy containing endogenous introns, or a mini-gene that includes either minimized native gene introns or hybrid/artificial introns [25–28]. In some cases, the use of a mini gene increases the transgene expression level in comparison with the cDNA as a transgene, providing simultaneous reduction in the overall size of the genetic construct compared to a full-length gene copy, thus simplifying handling of the transgene. It should be noted that, despite a significant amount of data on transgene design, there is no unambiguous and universal recipe for constructing a transgene coding sequence. Ideally, the creation of an animal that secretes a recombinant protein into milk should be ac-

companied by a comparative analysis of protein production using genetic constructs for transgenesis that contain cDNA, a full-length gene, and a mini-gene. However, such studies are undoubtedly associated with considerable costs.

Even the optimal expression cassette design does not guarantee effective transgene expression, which is due to the random site of transgene integration into the recipient genome. The surrounding chromatin, depending on the transgene integration site, can have a negative effect on transgene transcription. In addition, widespread tandem integration of several transgene copies can lead to suppression of their transcription due to transcriptional interference by neighboring copies [29]. Therefore, to increase the transgene expression level in classical transgenesis, the genetic construct often includes *cis*-elements that are designed to protect the transcription of the transgene from the influence of its environment. One of the most commonly used *cis*-elements is the chicken β-globin locus HS4 insulator [30, 31]. Inclusion of two tandem copies of the chicken β-globin locus HS4 insulator to the 5'-end of a genetic construct for transgenesis improves transgene expression but does not provide expression independent of the genomic integration site and the number of transgene copies [31, 32].

Therefore, the classical transgenesis used since the early 1980s has a number of significant drawbacks that are primarily due to the high variability of transgene expression caused by the randomness of its genomic integration site. Thus, to select an animal line with satisfactory parameters of recombinant protein production, a sufficiently large number of primary transgenic animals should be available. This may be a significant technical problem when generating transgenic livestock that produce recombinant proteins in milk, which is due to the need for a large number of embryos to generate a line of transgenic animals with satisfactory parameters of target recombinant protein production.

In addition to these drawbacks of classical transgenesis, the randomness of transgene integration into the recipient genome and uncontrolled variability in the number of transgene copies create certain difficulties specific to transgenic animals intended for practical use in the real economy. Namely, registration of modified organisms requires mandatory identification of the transformation event (the exact integration site of the transgenic construct into the genome) unique to the line of transgenic animals. In the case of classical transgenesis, identification of the transformation event for each transgenic animal line is a separate experimental problem whose solution is complicated if multiple transgene copies are integrated into the genome.

ALTERNATIVES TO CLASSICAL TRANSGENESIS OF ANIMALS

The randomness of transgene integration into a recipient genome and uncontrolled variability in the number of transgene copies are significant drawbacks of the "classical" approach to the creation of transgenic animals. These drawbacks have stimulated the development of alternative technologies enabling transgene integration into a specific genomic site. Until recently, transgene integration into a specific genomic site using homologous recombination either in embryonic stem cells with a subsequent injection of genetically modified cells into blastocysts or in somatic cells, followed by somatic cell nuclear transfer (SCNT) into the oocyte, was the alternative to classical transgenesis. In both cases, genetic manipulations are performed with cells in culture, which enables a characterization of the accuracy of transgene integration before the generation of transgenic animals. In addition, a qualitative improvement of the classical transgenesis technology was a transgene integration into a pre-determined site of the genome, using homologous recombination through flanking of a transgenic expression cassette with genomic regions ("homology arms," usually several thousands of nucleotide base pairs in length). It should be noted that the genetic elements enabling the production of a recombinant protein in milk are identical for the described approaches and classical transgenesis. The drawbacks of these approaches include the need for selective markers for picking cell clones with a genome-integrated transgene and a laborious clonal selection process that requires the analysis of a large number of cell clones (several hundreds or more) even when negative selection is used, which is due to the low efficiency of homologous recombination. In this case, even upon subsequent removal of a selective marker from the expression cassette, e.g., by means of site-specific recombination when the marker is flanked with appropriate recombination sites, exogenous DNA sequences, along with the target transgene sequences, inevitably remain in the genome, which may be undesirable.

Embryonic stem cells can be used as recipient cells for genetic manipulations *in vitro*. In this case, to generate a genetically modified animal, stem cells carrying a genetic modification are injected into blastocysts, with their subsequent implantation and creation of transgenic mosaic animals [33]. The descendants of animals containing the transgene in germinal cells will be nonmosaic transgenic animals. The disadvantage of this technology is a potential loss of pluripotent properties by stem cells upon generation of genetically modified clones during cultivation. In addition, the capabilities of this approach are substantially limited by the avail-

ability of embryonic stem cells of the target animal species. Generation of modified animals using stem cells has been used extensively in laboratory animals only. Somatic cells are an alternative to embryonic stem cells, allowing one to exclude the dependence on the preservation of pluripotent properties and enabling genetic modifications of virtually any animal species. In this case, the SCNT technology is used to produce transgenic animals by replacing the oocyte nucleus with somatic cell nucleus carrying the genetic modification and inducing embryo development. Despite the fact that epigenetic differences between the zygote genome and the somatic cell genome in this case do not significantly affect the traits of the produced organisms, the SCNT efficiency remains low. Animals are often unviable and die prematurely, which is associated with the side effects of somatic cell nuclear transfer, in particular with defects in the development of extraembryonic tissues and epigenetic reprogramming [34–36]. However, this particular technological approach was successfully used to generate goats secreting recombinant human antithrombin III (the basis for the approved Atryn® drug [37]) into milk, as well as several other lines of transgenic animals suitable for industrial use [8, 38, 39].

SITE-SPECIFIC RECOMBINASES FOR TARGETED TRANSGENE INSERTION INTO THE GENOME

In addition to the methods based on homologous recombination of the transgene and on the use of cultured cells in combination with positive and negative selection for picking cell clones with homologous recombination, another alternative for targeted insertion of a transgene into a recipient genome is the use of site-specific recombinases. In general, the concept of usage of site-specific recombinases is based on the generation of a line of transgenic animals carrying recognition site(s) for recombinase in the genome. Such recognition sites can be integrated into a specific genomic site by means of homologous recombination or into a random genomic site by means of classical transgenesis. In the latter case, lines of transgenic animals with different variants of transgene localization in the genome are subjected to selection of a line with the transgene integrated into the genomic site that provides the required properties of transgene expression. This animal line is then used as a universal recipient for the insertion of different transgenes into a specific genomic site via site-specific recombination. For this purpose, a genetic construct containing a transgene flanked by recombination sites is microinjected into the fertilized egg of a transgenic animal containing the same recombination sites in the genome, together with a vector for the expression of recombinase or its mRNA [40, 41]. This results in site-specific recombination, and the transgene is inserted into the recipient genome. It is important to note that this can be done via microinjections directly into oocytes, in addition to the use of embryonic stem or somatic cell lines carrying recombinase recognition sites in their genome as recipients of the transgenic construct.

In practice, three recombination systems have been commonly used for site-specific transgenesis: phage P1 Cre recombinase, Flp recombinase of *Saccharomyces cerevisiae*, and phage φC31 integrase [42, 43]. In this case, the use of a native recombination site in a pair with its sequence-modified variant providing recombination only with a completely identical, but nonnative, recombination site enables insertion of the transgenic cassette in a predetermined direction – a recombinase-mediated cassette exchange (RMCE) technology [42, 44]. Integration of the cassette with recombination sites directly into the gene encoding the milk protein enables the expression of the target transgene, thus providing the production of the recombinant protein into the milk under the control of an endogenous promoter whose activity is specific to mammary cells [45]. The promoter of the β-casein encoding gene (gene for integration) [46–48] can be used for this purpose; lack of this gene does not affect normal lactation [49, 50].

An alternative approach to ensuring effective and stable transgene expression, in particular in mammary gland cells, using appropriate tissue-specific promoters is the use of so-called "safe harbors" as transgene integration sites. These harbors are genomic loci that are, on the one hand, insignificant for the development and functioning of the organism, which enables harmless transgene insertion into this locus and, on the other hand, provide a high level of transgene expression in the presence of appropriate regulatory elements in transgene. Examples of these genomic loci are the loci *ROSA26*, *Cd6*, *Hipp11*, and some others [33, 40, 51, 52].

In addition to the listed advantages, the use of site-specific recombinases and integrases for targeted transgene insertion into an animal genome has a regulatory significance in the case of transgenic animals intended for practical use, due to the significant simplification of the characterization of the transformation event (the site of transgene integration into the recipient genome).

APPLICATION OF TARGETED GENOME EDITING TECHNOLOGIES IN ANIMAL TRANSGENESIS

The emergence of targeted genome editing technologies using site-specific nucleases has resulted in significant advances in the field of animal transgenesis that enable much more efficient transgene integration into a specific site of the recipient genome compared to the

sole use of sequences for homologous recombination flanking the transgene [53]. Below, we discuss the molecular mechanisms underlying the targeted genome editing technologies that seems to be the most promising for generating economically important animals that secrete recombinant proteins into milk.

Targeted transgene integration using site-specific nucleases is based on a significant increase in the site-specific efficiency of transgene integration into the recipient genome during the repair of double- or single-strand DNA breaks [54]. Targeted genome editing technologies significantly increase the efficiency in transgene integration into a pre-determined site of the genome, which, in some cases, eliminates the use of selective markers and, most importantly, enables highly efficient targeted transgene integration directly into the genome of a zygote, followed by the generation of transgenic animals [55–57].

There are several classes of artificial nucleases that are used for targeted genome editing and the production of transgenic animals: zinc finger nuclease (ZFN) [58], transcription activator-like effector nuclease (TALEN) [59], artificial meganucleases [60], and hybrid artificial nucleases (e.g., mega-TAL [61], etc). However, the emergence of a targeted genome editing technology based on the CRISPR/Cas9 system was a revolutionary breakthrough in this field, due to the simplicity of its practical implementation in combination with high efficiency compared to TALEN and ZFN [53].

ZFN was the first nuclease designed for use in genetic engineering for targeted genome editing. The nuclease contains DNA-binding domains of the zinc finger protein (ZFP) that provides highly specific binding to the target DNA sequence, as well as the catalytic domain of FokI restriction endonuclease that introduces a double-strand break into the binding site. Each zinc finger recognizes a certain triplet of nucleotides. Three to six zinc fingers are used to construct the DNA-binding domain of ZFN. Their combination can be used to generate ZFN for almost any DNA sequence [62]. The structure and application of ZFN are described in detail in [63].

Later, a simpler, compared to ZFN, code of transcription activator-like effector (TALE) was deciphered [64, 65]. TALE proteins of pathogenic plant bacteria of the genus *Xanthomonas* contain a DNA-binding domain consisting of a series of monomers. Each monomer binds to one nucleotide in the target nucleotide sequence. Monomers are tandem repeats of 33–35 amino acid residues, except for the last "half-repeat" that consists of 20 amino acid residues. The amino acid residues located at positions 12 and 13 of the monomer are highly variable and responsible for recognizing a specific nucleotide: Asn-Ile, Asn-Gly, Asn-Asn, and His-Asp bind to the nucleotides A, T, G, and C, respectively. Like ZFN, artificial TALEN nuclease is a chimera of the TALE DNA-binding domain consisting of 20-30 monomers and the FokI nuclease catalytic domain [66], which introduces a double-strand break into the immediate vicinity of the target DNA sequence recognized by the variable amino acid residues of TALEN monomers.

In the CRISPR/Cas9 system, the target is recognized as a consequence of the complementary interaction between CRISPR RNA (crRNA) and the target DNA site. In this case, a complex of trans-activating crRNA (tracrRNA), crRNA, and Cas9 nuclease is assembled and then a double-strand break is introduced into a RNA/DNA duplex by Cas9 nuclease [67]. Therefore, the specificity and targeted action of a nuclease in the CRISPR/Cas9 system require only the synthesis of RNA that is complementary to the target genomic DNA. In contrast, ZFN and TALEN-based technologies often require a complex and labor-intensive protein design. To date, a number of modifications and analogues of the CRISPR/Cas9 system have been developed, e.g., CRISPR/Cpf1 and CRISPR/C2c2 [68–72] with improved properties for editing the genome and solving certain target goals.

It should be noted that the artificial nucleases ZFN and TALEN do not possess absolute specificity. To a larger extent, this problem relates to the CRISPR/Cas9 system. The problems of DNA cleavage by artificial nucleases in non-targeted genomic sites can be solved in various ways that allow for increasing the specificity of the changes introduced into the genome and reducing the probability of unprogrammed genetic changes. However, the problem of nonspecific modifications in the recipient genome is not so critical upon generation of transgenic animals as compared to targeted genome editing technologies in the field of clinical applications, since accidental changes that occurr in non-targeted genome sites can be excluded during breeding.

In eukaryotic cells, double-strand breaks introduced by site-specific nucleases can be repaired through several mechanisms; in particular by homologous-directed repair (HDR), where a repair template is the sister or homologous chromatid as well as the donor DNA with 200–800 bp homology arms [73], which enables DNA integration between the homology arms into the site of the genomic DNA break [74]. In addition, DNA repair can be achieved by means of non-homologous end-joining (NHEJ), where non-homologous or low-homologous (2–5 nucleotides) ends are ligated, which may lead to deletions or insertions of several nucleotides in length [75]. Repair can also occur by means of microhomology-mediated end-joining (MMEJ), which requires 5- to 25-bp homologous DNA at or near the break and leads

to deletions, insertions, and translocations [76], as well as by means of single-strand annealing (SSA), which requires 30-bp or more homologous single-strand templates [77].

The key mechanism for the repair of breaks introduced by site-directed nucleases into a specific site of the genome is homologous recombination that enables integration of the transgene located between homology arms into a specific genomic site. This approach has been successfully implemented in animal transgenesis using double-strand templates containing a transgene flanked by 1- to 3-kb homology arms, with a repair efficiency of 0.5 to 20% [77–80]. Because the NHEJ mechanism is highly efficient in the repair of breaks introduced by artificial nucleases (up to 80%) [81], one of the ways to increase efficiency in homologous recombination and transgene insertion is by using NHEJ inhibitors [82, 83] that, however, have a mutagenic effect and increase the likelihood of transgene insertion into a non-targeted genomic locus [80]. Efficiency in homologous recombination can be increased by elongation of homology arms and by selection of optimal concentrations of components of the CRISPR/Cas9 system for genome modification microinjected into a zygote [78], as well as by using mutant Cas9 nuclease (nCas9, nickase) introducing distant single-strand DNA breaks into the plus and minus chains of a target genomic locus [84].

At the same time, alternative technologies have been developed which ensure targeted integration of extended (up to 10–15 kb) DNA fragments into a predetermined genomic site without using the HDR mechanism. For example, one of such technologies exploits NHEJ-based repair of breaks by ligating the complementary overlapping single-strand DNA ends of the genomic target site and the repair template comprising a transgene, which are generated by a ZFN nuclease pair upon cleavage of the targeted sequences of the genome and repair template [85, 86]. Insertion of extended DNA fragments into a pre-determined genomic site of the double-strand breaks introduced by TALEN or Cas9 nucleases can also occur via the MMEJ mechanism, when the homologous recombination template includes short sequences homologous to the DNA fragments adjacent to the nuclease cleavage site [87, 88].

Therefore, the rapid development of targeted genome editing technologies has allowed researchers to avoid a number of the drawbacks inherent to classical transgenesis: e.g., random transgene integration into the genome and uncontrolled variability in the number of transgene copies. The CRISPR/Cas9 technology enables the generation of transgenic animals with transgene integration into a specified genomic site, which, together with the use of homologous recombination, determines the controlled number of transgene copies. In particular, one of the most promising approaches to the generation of animals producing recombinant proteins in milk is the CRISPR/Cas9-targeted integration of the transgene into the genes that encode milk proteins in such a way that transgene expression is controlled by the endogenous regulatory sequences of the recipient gene. Application of these technologies will simplify and standardize the technologies for generating transgenic animals for the production of recombinant proteins. This will make the transgenesis process more efficient and reduce costs in the generation of economically important transgenic animals. Genome editing technologies will allow researchers to generate transgenic animals with one transgene copy integrated into a specific genomic site, which will enable a reliable comparison of the influence of certain genetic elements present in a construct for transgenesis on recombinant protein production in milk, which cannot be done using classical transgenesis due to the integration of an uncontrolled number of transgene copies into different genomic loci in different lines of transgenic animals.

CONCLUSION

The development of targeted genome editing technologies has opened new prospects for the generation of transgenic animals at a whole new level. The standardization of the generation of transgenic animals with specified and stable target traits is becoming possible thanks to the use of knowledge on the molecular genetic mechanisms of regulation of gene expression and genome functioning, as well as the available technologies of genetic engineering. That is fully applicable to the production of recombinant proteins in milk for the manufacturing of pharmaceuticals, biologically active additives, etc.

Taking into account the set of technologies generated to date, which are still under active development, the optimal direction of studies in the field of recombinant protein production in the milk of economically important animals points to the creation of animal lines (depending on the need in a target protein – rabbits, sheep, goats, and cows) whose genome is modified by the insertion of sequences for asymmetric directed recombination of the expression cassette into a milk protein-encoding gene (e.g., the β-casein gene). The promoter, and other regulatory sequences, of this gene will provide a high level of transgene expression. This insertion can be achieved with high efficiency through a microinjection into the oocytes of a genetic construct carrying an expression cassette, together with the corresponding recombinant integrase or its mRNA. These animal lines can be created with previously inaccessible efficiency by means of genome editing technologies us-

ing the CRISPR/Cas9 system or its analogues, thanks to the simplicity of implementation and design of this system. At the same time, the technologies of synthetic biology allow one to use mini-genes with artificial introns as a transgene, but not full-length gene copies, to facilitate efficient expression of the transgene and production of the target protein, thus simplifying the design and creation of genetic constructs for transgenesis.

Prospects for the development of such a direction in the production of recombinant proteins, primarily for medical needs, are supported by the two marketed drugs that are based on recombinant proteins obtained from the milk of transgenic animals. It should be noted that there is the possibility of producing significant quantities of recombinant proteins at costs substantially lower than those required for production in cellular systems. The use of modern technologies significantly simplifies compliance with regulatory requirements for describing the transformation event. At the same time, the requirements to the biological safety of recombinant protein production in milk will require a revision of the standards for the welfare of farm animals and veterinary control to exclude the presence of zoonotic and anthropozoonotic infectious agents, as well as controlled parameters of the manufactured drugs. ●

This work was supported by a grant from the Russian Science Foundation (project No. 16-14-00150).

REFERENCES

1. Wang Y., Zhao S., Bai L., Fan J., Liu E. // BioMed Res. Internat. 2013. V. 2013. P. 580463.
2. The Global Technology Revolution 2020, In-Depth Analyses. Bio/Nano/Materials/Information Trends, Drivers, Barriers, and Social Implications. RAND Corp., 2006. P. 145.
3. Maksimenko O.G., Deykin A.V., Khodarovich Yu.M., Georgiev P.G. // Acta Naturae. 2013. V. 5. № 1. P. 33–46.
4. Smith K. // Reprod. Nutr. Dev. 2001. V. 41. P. 465–485.
5. Niemann H., Kues A.W. // Anim. Reprod .Sci. 2000. V. 60–61. P. 277–293.
6. Levy J.H., Weisinger A., Ziomek C.A., Echelard Y. // Semin. Thromb. Hemost. 2001. V. 27. P. 405–416.
7. Coulibaly S., Besenfelder U., Miller I., Zinovieva N., Lassnig C., Kotler T., Kotler T., Jameson J.L., Gemeiner M., Müller M., et al. // Mol. Reprod. Dev. 2002. V. 63. P. 3003008.
8. Amiri Yekta A., Dalman A., Eftekhari-Yazdi P., Sanati M.H., Shahverdi A.H., Fakheri R., Vazirinasab H., Daneshzadeh M.T., Vojgani M., Zomorodipour A., Fatemi N., et al. // Transgenic Res. 2013. V. 22. P. 131–142.
9. Mikus T., Malý P., Poplstein M., Landa V., Trefil P., Lidický J. // Folia Biol. (Praha). 2001. V. 47. P. 187–195.
10. Carver A., Wright G., Cottom D., Cooper J., Dalrymple M., Temperley S., Udell M., Reeves D., Percy J., Scott A. // Cytotechnology. 1992. V. 9. P. 77–84.
11. Wright G., Carver A., Cottom D., Reeves D., Scott A., Simons P., Wilmut I., Garner I., Colman A. // Nat. Biotechnol. 1991. V. 9. P. 830–834.
12. Archibald A.L., McClenaghan M., Hornsey V., Simons J.P., Clark A.J. // Proc. Natl. Acad. Sci. USA. 1990. V. 87. P. 5178–5182.
13. Baldassarre H., Hockley D.K., Doré M., Brochu E., Hakier B., Zhao X., Bordignon V. // Transgenic Res. 2008. V. 17. P. 73–84.
14. Baldassarre H., Hockley D.K., Olaniyan B., Brochu E., Zhao X., Mustafa A., Bordignon V. // Transgenic Res. 2008. V. 17. P. 863–872.
15. Huang Y.-J., Huang Y., Baldassarre H., Wang B., Lazaris A., Leduc M., Bilodeau A.S., Bellemare A., Côté M., Herskovits P., et al. // Proc. Natl. Acad. Sci. USA. 2007. V. 104. P. 13603–13608.
16. Nuijens J.H., van Berkel P.H., Geerts M.E., Hartevelt P.P., de Boer H.A., van Veen H.A., Pieper F.R. // J. Biol. Chem. 1997. V. 272. P. 8802–8807.
17. Platenburg G.J., Kootwijk E.P., Kooiman P.M., Woloshuk S.L., Nuijens J.H., Krimpenfort P.J., Pieper F.R., de Boer H.A., Strijker R. // Transgenic Res. 1994. V. 3. P. 99–108.
18. Wang J., Yang P., Tang B., Sun X., Zhang R., Guo C., Gong G., Liu Y., Li R., Zhang L., et al. // J. Dairy Sci. 2008. V. 91. P. 4466–4476.
19. Li H., Liu Q., Cui K., Liu J., Ren Y., Shi D. // Transgenic Res. 2013. V. 22. P. 169–178.
20. Buchman A.R., Berg P. // Mol. Cell. Biol. 1988. V. 8. P. 4395–4405.
21. Bourdon V., Harvey A., Lonsdale D.M. // EMBO Rep. 2001. V. 2. P. 394–398.
22. Kang Y.K., Lee C.S., Chung A.S., Lee K.K. // Mol. Cells. 1998. V. 8. P. 259–265.
23. Liu K., Sandgren E.P., Palmiter R.D., Stein A. // Proc. Natl. Acad. Sci. USA. 1995. V. 92. P. 7724–7728.
24. Huang M.T., Gorman C.M. // Nuc. Acids Res. 1990. V. 18. P. 937–947.
25. Palmiter R.D., Sandgren E.P., Avarbock M.R., Allen D.D., Brinster R.L. // Proc. Natl. Acad. Sci. USA. 1991. V. 88. P. 478–482.
26. Choi T., Huang M., Gorman C., Jaenisch R. // Mol. Cell. Biol. 1991. V. 11. P. 3070–3074.
27. Barash I., Nathan M., Kari R., Ilan N., Shani M., Hurwitz D.R. // Nucl. Acids Res. 1996. V. 24. P. 602–610.
28. Tikhonov M.V., Maksimenko O.G., Georgiev P.G., Korobko I.V. // Mol Biol (Mosk). 2017. V. 51. P. 671–676.
29. Eszterhas S.K., Bouhassira E.E., Martin D.I., Fiering S. // Mol. Cell. Biol. 2002. V. 22. P. 469–479.
30. Emery D.W., Yannaki E., Tubb J, Nishino T., Li Q., Stamatoyannopoulos G. // Blood. 2002. V. 100. P. 2012–2019.
31. Guglielmi L., Le Bert M., Truffinet V., Cogné M., Denizot Y. // Biochim. Biophys. Res. Commun. 2003. V. 307. P. 466–471.
32. Truffinet V., Guglielmi L., Cogné M., Denizot Y. // Immunol. Lett. 2005. V. 96. P. 303–304.
33. Kong Q., Hai T., Ma J., Huang T., Jiang D., Xie B., Wu M., Wang J., Song Y., Wang Y., et al. // PLoS One. 2014. V. 9. P. e107945.
34. Eilertsen K.J., Power R.A., Harkins L.L., Misica P. // Anim. Reprod. Sci. 2007. V. 98. P. 129–146.
35. Campbell K.H., Fisher P., Chen W.C., Choi I., Kelly R.D., Lee J.H., Xhu J. // Theriogenology. 2007. V. 68. Suppl 1. P. S214–231.

36. Dinnyes A., Tian X.C., Yang X. // Reprod. Domest. Anim. 2008. V. 43. Suppl 2. P. 302–309.
37. Edmunds T., van Patten S.M., Pollock J., Hanson E., Bernasconi R., Higgins E., Manavalan P., Ziomek C., Meade H., McPherson J.M., et al. // Blood. 1998. V. 91. P. 4561–4571.
38. Yang P., Wang J., Gong G., Sun X., Zhang R., Du Z., Liu Y., Li R., Ding F., Tang B., et al. // PLoS One. 2008. V. 3. P. e3453.
39. Baldassarre H., Wang B., Kafidi N., Gauthier M., Neveu N., Lapointe J., Sneek L., Leduc M., Duguay F., Zhou J.F., et al. // Theriogenology. 2003. V. 59. P. 831–839.
40. Tasic B., Hippenmeyer S., Wang C., Gamboa M., Zong H., Chen-Tsai Y., Luo L. // Proc. Natl. Acad. Sci. USA. 2011. V. 108. P. 7902–7907.
41. Yu H., Wang X., Zhu L., He Z., Liu G., Xu X., Chen J., Cheng G. // Gene. 2013. V. 515. P. 367–371.
42. Wirth D., Gama-Norton L., Riemer P., Sandhu U., Schucht R., Hauser H. // Curr. Opin. Biotechnol. 2007. V. 18. P. 411–419.
43. Bockamp E., Maringer M., Spangenberg C., Fees S., Fraser S., Eshkind L., Oesch F., Zabel B. // Physiol. Genomics. 2002. V. 11. P. 115–132.
44. Bode J., Schlake T., Iber M., Schübeler D., Seibler J., Snezhkov E., Nikolaev L. // Biol. Chem. 2000. V. 381. P. 801–813.
45. Liu X., Wang Y., Guo W., Chang B., Liu J., Guo Z., Quan F., Zhang Y. // Nat. Commun. 2013. V. 4. P. 2565.
46. Jeong Y.H., Kim Y.J., Kim E.Y., Kim S.E., Kim J., Park M.J., Lee H.G., Park S.P., Kang M.J. // Zygote. 2016. V. 24. P. 442–456.
47. Lee S.M., Kim J.W., Jeong Y.H., Kim S.E., Kim Y.J., Moon S.J., Lee J.H., Kim K.J., Kim M.K., Kang M.J. // Asian-Australas J. Anim. Sci. 2014. V. 27. P. 1644–1651.
48. Robinson C., Kolb A.F. // Exp. Cell. Res. 2009. V. 315. P. 508–522.
49. Kumar S., Clarke A.R., Hooper M.L., Horne D.S., Law A.J., Leaver J., Springbett A., Stevenson E., Simons J.P. // Proc. Natl. Acad. Sci. USA. 1994. V. 91. P. 6138–6142.
50. Cosenza G., Pauciullo A., Colimoro L., Mancusi A., Rando A., Di Berardino D., Ramunno L. // Anim. Genet. 2007. V. 38. P. 655–658.
51. Soriano P. // Nat. Genet. 1999. V. 21. P. 70–71.
52. DeKelver R.C., Choi V.M., Moehle E.A., Paschon D.E., Hockemeyer D., Meijsing S.H., SancakY., Cui X., Steine E.J., Miller J.C., et al. // Genome Res. 2010. V. 20. P. 1133–1142.
53. Kasparek P., Krausova M., Haneckova R., Kriz V., Zbodakova O., Korinek V., Sedlacek R. // FEBS Lett. 2014. V. 588. P. 3982–3988.
54. Richardson C., Moynahan M.E., Jasin M. // Genes Dev. 1998. V. 12. P. 3831–3842.
55. Remy S., Tesson L., Menoret S., Usal C., De Cian A., Thepenier V., Thinard R., Baron D., Charpentier M., Renaud J.B., et al. // Genome Res. 2014. V. 24. P. 1371–1383.
56. Ménoret S., Fontanière S., Jantz D., Tesson L., Thinard R., Rémy S., Usal C., Ouisse L.H., Fraichard A., Anegon I. // FASEB J. 2013. V. 27. P. 703–711.
57. Porteus M.H., Carroll D. // Nat. Biotechnol. 2005. V. 23. P. 967–973.
58. Bogdanove A.J., Voytas D.F. // Science. 2011. V. 333. P. 1843–1846.
59. Silva G., Poirot L., Galetto R., Smith J., Montoya G., Duchateau P., Pâques F. // Curr. Gene Ther. 2011. V. 11. P. 11–27.
60. Boissel S., Jarjour J., Astrakhan A., Adey A., Gouble A., Duchateau P., Shendure J., Stoddard B.L., Certo M.T., et al. // Nucl. Acids Res. 2014. V. 42. P. 2591–2601.
61. Segal D.J., Beerli R.R., Blancafort P., Dreier B., Effertz K., Huber A., Koksch B., Lund C.V., Magnenat L., Valente D., et al. // Biochemistry. 2003. V. 42. P. 2137–2148.
62. Urnov F.D., Rebar E.J., Holmes M.C., Zhang H.S., Gregory P.D. // Nat. Rev. Genet. 2010. V. 11. P. 636–646.
63. Boch J., Scholze H., Schornack S., Landgraf A., Hahn S., Kay S., Lahaye T., Nickstadt A., Bonas U. // Science. 2009. V. 326. P. 1509–1512.
64. Moscou M.J., Bogdanove A.J. // Science. 2009. V. 326. P. 1501.
65. Christian M., Cermak T., Doyle E.L., Schmidt C., Zhang F., Hummel A., Bogdanove A.J., Voytas D.F. // Genetics. 2010. V. 186. P. 757–761.
66. Gaj T., Gersbach C.A., Barbas C.F. 3rd. // Trends Biotechnol. 2013. V. 31. P. 397–405.
67. Nemudryi A.A., Valetdinova K.R., Medvedev S.P., Zakian S.M. // Acta Naturae. 2014. V. 6. P. 19–40.
68. Ruan J., Xu J., Chen-Tsai R.Y., Li K. // Transgenic Res. 2017. V. 26. P. 715–726.
69. Stella S., Alcón P., Montoya G. // Nat. Struct. Mol. Biol. 2017. V. 24. P. 882–892.
70. Murugan K., Babu K., Sundaresan R., Rajan R., Sashital D.G. // Mol. Cell. 2017. V. 68. P. 15–25.
71. Mitsunobu H., Teramoto J., Nishida K., Kondo A. // Trends Biotechnol. 2017. V. 35. P. 983–996.
72. Chira S., Gulei D., Hajitou A., Zimta A.A., Cordelier P., Berindan-Neagoe I. // Mol. Ther. Nucl. Acids. 2017. V. 7. P. 211–222.
73. Urnov F.D., Miller J.C., Lee Y.L., Beausejour C.M., Rock J.M., Augustus S., Jamieson A.C., Porteus M.H., Gregory P.D., Holmes M.C. // Nature. 2005. V. 435. P. 646–651.
74. Moynahan M.E., Jasin M. // Nat. Rev. Mol. Cell. Biol. 2010. V. 11. P. 196–207.
75. Lieber M.R. // Annu. Rev. Biochem. 2010. V. 79. P. 181–211.
76. McVey M., Lee S.E. // Trends Genet. 2008. V. 24. P. 529–538.
77. Sugawara N., Ira G., Haber J.E. // Mol. Cell. Biol. 2000. V. 20. P. 5300–5309.
78. Wang B., Li K., Wang A., Reiser M., Saunders T., Lockey R.F., Wang J.W. // Biotechniques. 2015. V. 59. P. 201–208.
79. Wang H., Yang H., Shivalila C.S., Dawlaty M.M., Cheng A.W., Zhang F., Jaenisch R. // Cell. 2013. V. 153. P. 910–918.
80. Yang H., Wang H., Shivalila C.S., Cheng A.W., Shi L., Jaenisch L. // Cell. 2013. V. 154. P. 1370–1379.
81. Frit P., Barboule N., Yuan Y., Gomez D., Calsou P. // DNA Repair (Amst.). 2014. V. 17. P. 81–97.
82. Maruyama T., Dougan S.K., Truttmann M.C., Bilate A.M., Ingram J.R., Ploegh H.L. // Nat. Biotechnol. 2015. V. 33. P. 538–542.
83. Chu V.T., Weber T., Wefers B., Wurst W., Sander S., Rajewsky K., Kühn R. // Nat. Biotechnol. 2015. V. 33. P. 543–548.
84. Li K., Wang G., Andersen T., Zhou P., Pu W.T. // PLoS One. 2014. V. 9. P. e105779.
85. Maresca M., Lin V.G., Guo N., Yang Y. // Genome Res. 2013. V. 23. P. 539–546.
86. Cristea S., Freyvert Y., Santiago Y., Holmes M.C., Urnov F.D., Gregory P.D., Cost G.J. // Biotechnol. Bioeng. 2013. V. 110. P. 871–880.
87. Nakade S., Tsubota T., Sakane Y., Kume S., Sakamoto N., Obara M., Daimon T., Sezutsu H., Yamamoto T., Sakuma T., et al. // Nat. Commun. 2014. V. 5. P. 5560.
88. Sakuma T., Nakade S., Sakane Y., Suzuki K.T., Yamamoto T. // Nat. Protoc. 2016. V. 11. P. 118–133.

Three-Dimensional Structure of Cytochrome *c* Nitrite Reductase As Determined by Cryo-Electron Microscopy

T. N. Baymukhametov[1], Y. M. Chesnokov[1], E. B. Pichkur[1], K. M. Boyko[1,2], T. V. Tikhonova[2], A. G. Myasnikov[3,4,5], A. L. Vasiliev[1,6], A. V. Lipkin[1], V. O. Popov[1,2*], M. V. Kovalchuk[1,6]

[1]National Research Center «Kurchatov Institute», Akademika Kurchatova Sqr., 1, Moscow, 123182, Russia

[2]Bach Institute of Biochemistry, Research Center of Biotechnology of the Russian Academy of Sciences, Leninsky Ave., 33, bldg. 2, Moscow, 119071, Russia

[3]Petersburg Nuclear Physics Institute named by B.P. Konstantinov of NRC «Kurchatov Institute», 188300, Leningradskaya Oblast, Gatchina, mkr. Orlova roshcha, 1, Russia

[4]Centre for Integrative Biology, Department of Integrated Structural Biology, Institute of Genetics and of Molecular and Cellular Biology, 67404, 1 rue Laurent Fries, Illkirch, France

[5]University of California San Francisco Mission Bay, Genentech Hall, San Francisco, CA, 94158-2517, USA

[6]Shubnikov Institute of Crystallography of Federal Scientific Research Centre «Crystallography and Photonics»
Russian Academy of Sciences, Leninsky Ave., 59, Moscow, 119333, Russia

*E-mail: vpopov@inbi.ras.ru

Received February 05, 2018; in final form June 02, 2018

ABSTRACT **The structure of cytochrome *c* nitrite reductase from the bacterium *Thioalkalivibrio nitratireducens* was determined by cryo-electron microscopy (cryo-EM) at a 2.56 Å resolution. Possible structural heterogeneity of the enzyme was assessed. The backbone and side-chain orientations in the cryo-EM-based model are, in general, similar to those in the high-resolution X-ray diffraction structure of this enzyme.**

KEYWORDS **single particle analysis, high-resolution cryo-electron microscopy, structural biology, cytochrome *c* nitrite reductase.**

ABBREVIATIONS **TvNiR – cytochrome *c* nitrite reductase from *Thioalkalivibrio nitratireducens*, cryo-EM – cryo-electron microscopy, CMOS – complementary metal-oxide semiconductor, CTF – contrast transfer function, FSC – Fourier shell correlation.**

INTRODUCTION

With the recent advances in cryo-electron microscopy (cryo-EM) associated with improvements in spatial resolution and a decrease in the lower limit of the molecular weight accessible through this technique, the method has begun to rival X-ray crystallography [1, 2]. Owing to the unique opportunity of extracting structural information on heterogeneous objects in a nearly native state and a rather simple sample preparation [3], cryo-EM has become a powerful tool in modern structural biology [4, 5]. Cryo-EM is currently the only method capable of addressing such challenges as the structure determination of difficult-to-crystallize membrane proteins and searching for different states of molecular complexes, the method being complementary to classical X-ray crystallography [6].

In this work, the three-dimensional structure of cytochrome *c* nitrite reductase from the bacterium *Thioalkalivibrio nitratireducens* (TvNiR) [7] was studied for the first time by single-particle analysis [8] – a cryo-EM method for protein structure determination. This enzyme catalyzes the reduction of nitrite to ammonia without the release of reaction intermediates from the active site [7]. In solution and in the crystalline state, the enzyme exists as a stable hexamer that possess a bipyramidal shape with a characteristic height of ~150 Å and a base of ~120 Å [9]. The hexamer boasts D3 symmetry and a molecular weight of ~360 kDa, due to

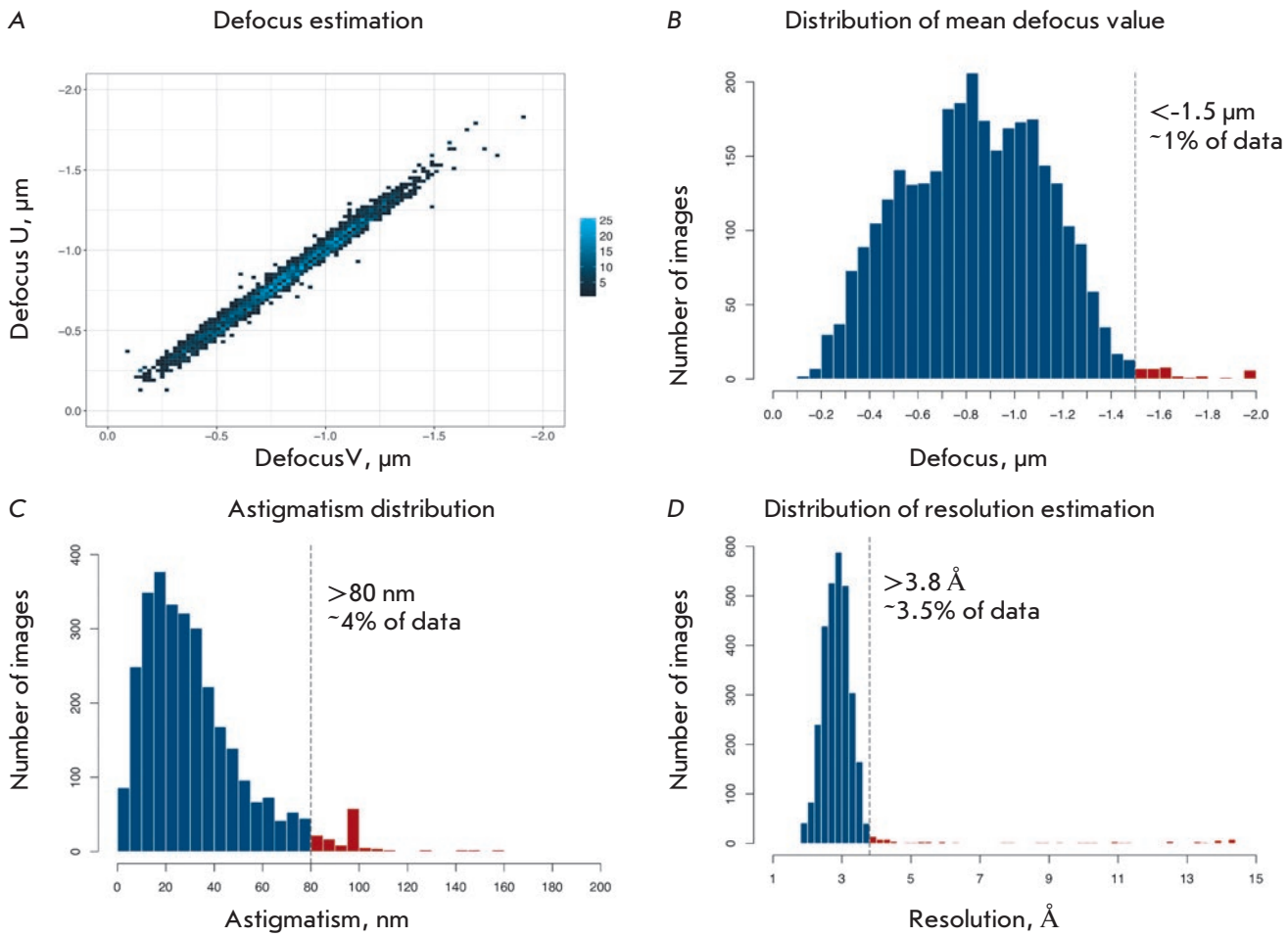

Fig. 1. Principal characteristics of the initial data based on CTF parameters estimated with the Gctf program. *A* – the defocus distribution along two orthogonal axes; the color corresponds to the density of values at a specified coordinate. *B–D* – the distributions of the average defocus, astigmatism, and resolution assessment, respectively, along with the threshold values. The data with parameters in the ranges indicated in red were excluded from further processing

which TvNiR is a very convenient object for cryo-EM. The goal of this work was to determine the structure of TvNiR by cryo-EM and compare it with the high-resolution X-ray structure determined earlier [9–11].

EXPERIMENTAL

Protein isolation and purification

Native TvNiR was isolated and purified in two steps, according to a procedure described earlier [7]. Anion-exchange chromatography was performed on a 35-mL column prepacked with DEAE Sepharose Fast Flow at 4°C using a BioLogic LP system (BioRad, USA). The column was pre-equilibrated with 25 mM potassium phosphate buffer, pH 7.0. After loading of the extract and washing of the column with the same buffer, the protein was eluted with a linear gradient of 0–1.0 M NaCl. Gel filtration chromatography was performed on an AKTA FPLC system (Amersham Biosciences, USA) equipped with a SuperdexTM200 10/300 column equilibrated with 50 mM potassium phosphate buffer, pH 7.0, supplemented with 0.15 M NaCl. For further structural studies, the protein was concentrated to 10 mg/mL.

Cryo-EM sample preparation

In order to determine the optimal protein concentration in solution, concentrations in a range of 0.1 to 6.0 mg/mL were tested. The protein solutions were applied to Lacey Carbon 300 mesh copper grids (Ted Pella, USA). The experimental data were collected using Quantifoil R1.2/1.3 300 mesh grids (Quantifoil, Germany) coated with a carbon support film containing regular arrays of 1.2-μm circular holes spaced by 2.5 μm. The grids were glow-discharged for 30 s using a PELCO easyGlow system designed for hydrophilization

Summary of data collection parameters, cryo-EM map reconstruction, and structure refinement statistics for TvNiR

Data collection	
Accelerating voltage, kV	300
Magnification	75000x
Pixel size, Å	0.86
Exposure time, s	1.5
Number of image stacks	3055
Total dose per stack, $e^-/Å^2$	~100
Number of images per stack	30
Defocus range, μm	[-1.5; -0.5]
Defocus step size, μm	0.1
Cryo-EM map reconstruction	
Final number of particle images	33891
Symmetry group	D_3
$FSC_{0.5}$ (with masking / without masking)	2.86 / 3.19
$FSC_{0.143}$ (with masking / without masking)	2.56 / 2.82
Resolution (average), Å	2.56
Structure refinement	
$FSC_{average}$	0.8679
R_f (weighted, overall), %	28.70
Average B-factor, $Å^2$	80.08
Rmsd bond lengths, $Å^2$	0.018
Rmsd bond angles, deg	1.989
MolProbity score, %	2.55
All-atom clashscore, %	13.31
Good rotamers, %	91.68
Ramachandran outliers, %	0.19
EMDB code	EMD-0020

(Ted Pella, USA) at a chamber pressure of 0.26 mbar and a current of 25 mA. A sample (3 μL, 6 mg/mL) was applied to the grids, and the grids were plunge-frozen in liquid ethane using a Vitrobot Mark IV vitrification device (Thermo Fisher Scientific, USA); the following parameters were set: blot force, 6; drain time, 1 s; temperature of the climate chamber, 4 °C; and humidity, 98 ± 2%.

Cryo-electron microscopy

The grids were transferred at liquid nitrogen temperature to a Titan Krios cryo-electron microscope (Thermo Fisher Scientific, USA) equipped with a Schottky-type field emission electron gun (FEI XFEG, the Netherlands), a spherical aberration corrector (CEOS GmbH, Germany), and a CMOS-based Falcon II direct electron detector (Thermo Fisher Scientific, USA). A total of 3,055 image stacks were recorded in an automatic mode using the EPU package (version 1.9.1.16REL) (Thermo Fisher Scientific, USA) with a total exposure time of 1.5 s. The microscope was operated at an accelerating voltage of 300 kV and 75000×magnification

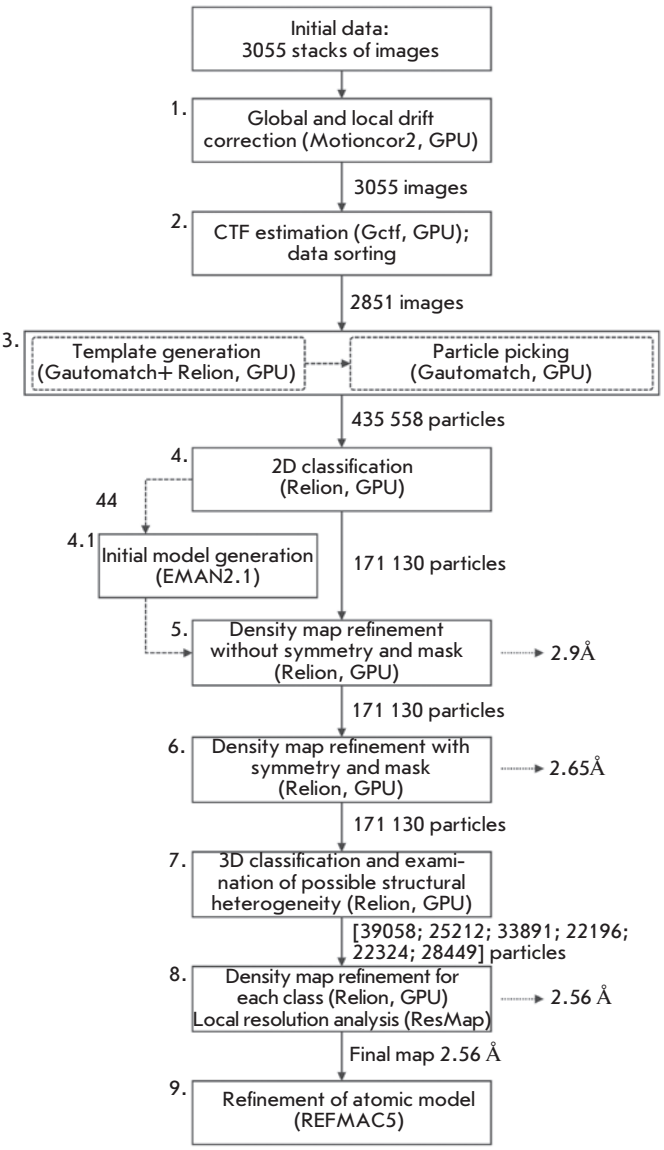

Fig. 2. Main data processing steps

corresponding to a pixel size of 0.86 Å at the specimen level, with objective lens defocused between −1.5 μm and −0.5 μm, with a step of 0.1 μm, using a total dose of ~100$e^-/Å^2$ evenly distributed across the image stack. The main data collection parameters are summarized in the *Table*. The principal data characteristics are shown in *Fig. 1A–D*.

RESULTS

Cryo-EM map reconstruction

The images were processed in several consecutive steps, presented in *Fig. 2*, using the computing resources of the Federal Collective Usage Center Complex for Simulation and Data Processing for Mega-Science

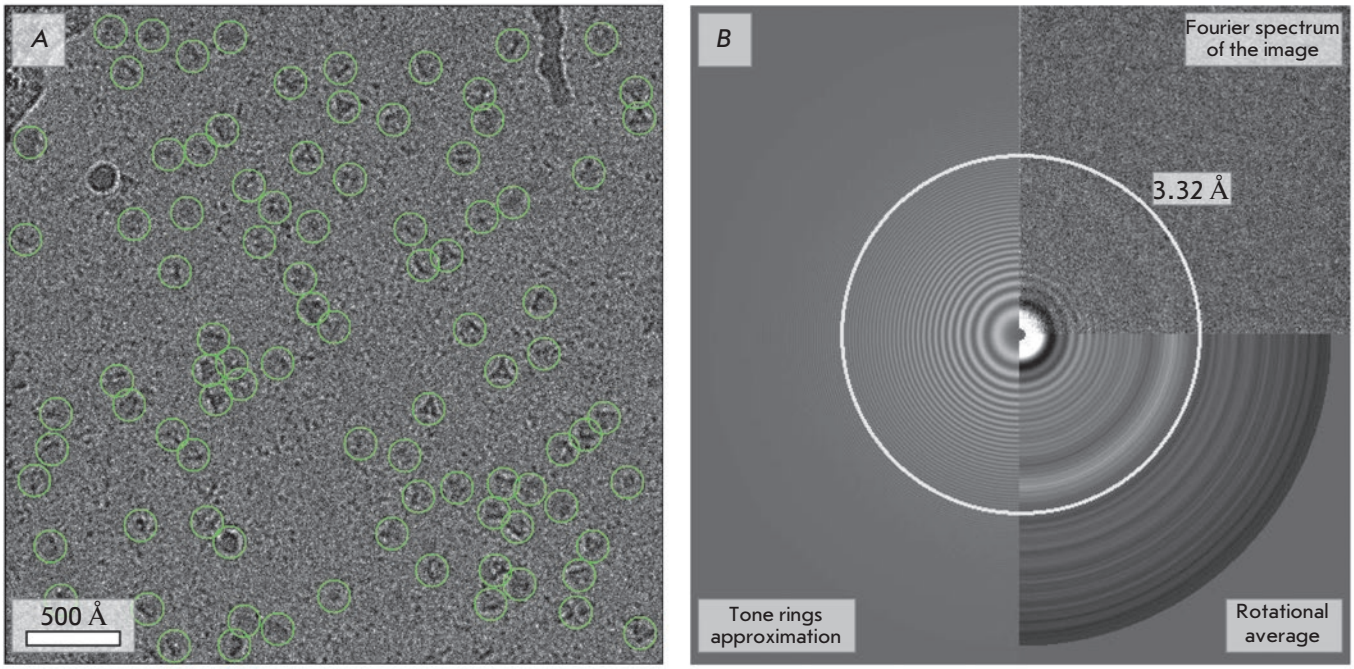

Fig. 3. Preliminary data processing after correction for drift and estimation of the CTF parameters. *A* – an image with projections of the particles picked with Gautomatch; *B* – the Fourier spectrum of this image is shown in the upper-right section of the panel and the rotational average of the power spectrum is in the lower-right section of the panel; Thon ring fitting is presented in the left section. The circle, the radius of which in direct space corresponds to the assessment of the maximum resolution (3.32 Å), is highlighted

Facilities at the National Research Centre Kurchatov Institute, equipped with Nvidia Tesla K80 graphics accelerators. The following image processing packages were employed: Motioncor2 (version 1.0.5) [12], Gctf (version 1.18) [13], Gautomatch (version 0.56) (K. Zhang, MRC Laboratory of Molecular Biology, Cambridge, UK, http://www.mrc-lmb.cam.ac.uk/kzhang/Gautomatch), and Relion (version 2.1) [14]. All these packages were optimized for computations on graphics processors.

In the first step (*Fig. 2*), 3,055 initial image stacks were individually corrected for beam-induced motion using Motioncor2. The following two averaged and corrected image sets were obtained: (1) images filtered depending on the electron dose exposed to the sample (Dose Weighting) [15], which were used for classification and refinement processes; and (2) non-filtered images that were used to estimate contrast transfer function (CTF) parameters. In the second step (*Fig. 2*), the CTF parameters were estimated with the Gctf program. For each image, the information limit (resolution assessment), defocus, and astigmatism were estimated based on Thon ring fitting. The distribution's tail points below the thresholds shown in *Fig. 1B–D* were excluded from further processing.

Therefore, 2,851 selected images with defocus, astigmatism, and resolution parameters not higher than −1.5 μm (in magnitude), 80 nm, and 3.8 Å, respectively, were used in all subsequent steps. A typical image after correction for drift is shown in *Fig. 3*.

In the third step (*Fig. 2*), particles were picked with Gautomatch. Initially, the procedure was applied for a subset of images recorded with a high degree of defocus. The 2D Gaussian function with a half-width corresponding to the characteristic size of an object was used as a template. The resulting set of particles was subjected to 2D classification in Relion. The classes containing projections of the object were utilized as templates to pick particles from the total data set. The resulting set contained 435,558 coordinates of possible particle positions.

The fourth step (*Fig. 2*) involved two sequential rounds of classification. In the first round, the particle images were divided into 40 classes. Then, the images that were combined into classes not containing projections of the object or those depicting artifacts, such as ice crystals, surface contamination, and carbon edges, were excluded from the data set. In the second round, the remaining images were clustered into 50 classes, followed by the exclusion of the particles belonging to

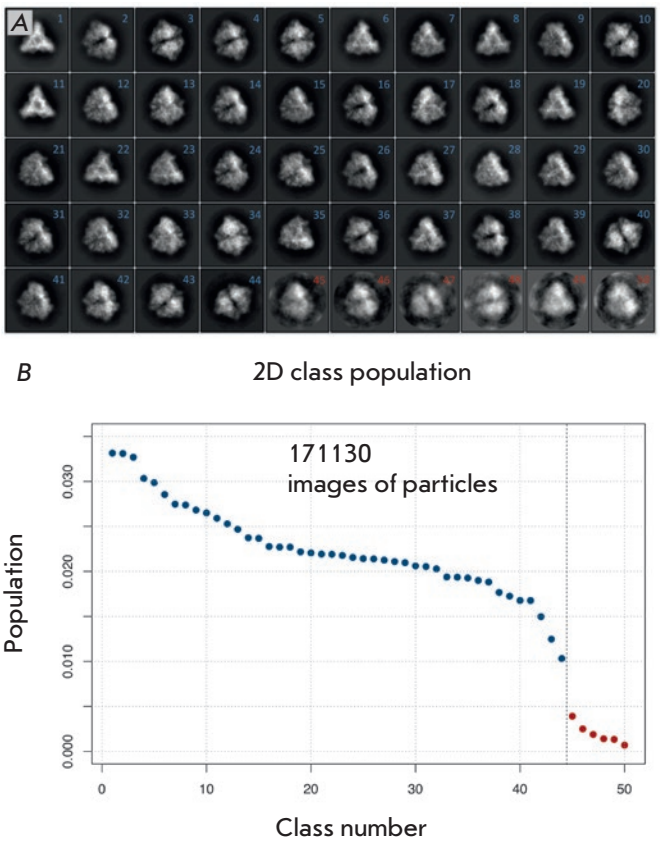

Fig. 4. Fourth data processing step. *A* – images merged in each class after the second classification round. Particle images belonging to classes 1 to 44 (numbered in blue) were used for further analysis and density map construction. Particle images belonging to classes 45 to 50 (numbered in red), which led to overtraining of reconstruction algorithms, were excluded from further data processing; *B* – class population. The colors of the points correspond to the colors of the numbers in panel *A*

classes in which the boundaries of the object were not well-defined (*Fig. 4 A, B*).

After classification, 171,130 particle images containing structural information on the object were selected. A low-resolution initial model was built with the EMAN2 image processing package [16] by the Monte-Carlo method, taking into account the known symmetry of the object based on 44 projections obtained by averaging images present in the most populated classes, after the second classification round (*Fig. 4B*).

In the fifth step (*Fig. 2*), the low-resolution model was refined by reassigning the Euler angles and fitting projections of the object to the cryo-EM map in each sequential iteration of the EM algorithm implemented in Relion [17–19]. The refinement was carried out using the 3D auto-refine procedure without resorting to *a-priori* data on the symmetry of the object after postprocessing and applying the binary mask that defined the boundary conditions for the calculation of cross-correlation coefficients between two independently refined maps [20]. The resolution of the final map was 2.9 Å, as determined by the FSC = 0.143 criterion [21].

The symmetry-imposed refinement in the sixth step (*Fig. 2*) resulted in resolution improvement to 2.65 Å. In the seventh step, the same particle set (*Fig. 2*) was subjected to 3D classification [22, 23] into six classes (*Fig. 5*) without angular or translational searches, using the same mask according to a procedure described in [24]. In the eighth step (*Fig. 2*), the maps were repeatedly refined for each class. This approach allowed us to select a data subset composed of 33,891 particle images (median defocus was −0.86 μm, with the values varying from −1.48 to −0.18 μm, as estimated with Gctf), which corresponded to the third 3D class and yielded a map with the best resolution of 2.56 Å (*Fig. 5*). In order to increase the resolution, the steps 6–8 (*Fig. 2*) were carried out with imposition of D_3 symmetry and using a binary mask (*Fig. 6A*) that was created by applying 5-pixel isotropic extension, smoothing the boundaries by 5 pixels, and using an isosurface threshold of 0.02.

Structure refinement with REFMAC5

The crystal structure of TvNiR at the best resolution of 1.4 Å (RCSB ID code is 3FO3) served as a starting model for the refinement. Solvent molecules, except for those corresponding to experimental density peaks, were removed from the dimer located in the asymmetric unit of the crystal. The TvNiR hexamer used for the refinement was generated by application of the appropriate symmetry operations. The refinement was performed with REFMAC5 [25] implemented in the CCP-EM suite [26].

A map of the third 3D class (*Fig. 5*), which had the best resolution, was used as the experimental cryo-EM map. To prevent the model from overfitting, the following approach was employed [27]. The images, from which the entire map was produced, were randomly divided into two subsets, and these subsets were used for the calculation of two independent 'half maps' and cross-validation. The high resolution of the experimental data allowed us to perform the refinement with no restraints, except for restraints on deviations of the bond lengths from the average value (jelly-body refinement [25]). To more correctly estimate steric constraints, hydrogen atoms were included in the refinement in fixed positions. After 30 refinement cycles, the fit of the refined model to the experimental density was visually inspected with Coot [28]. The influence of map sharpening/blurring on the refinement was assessed

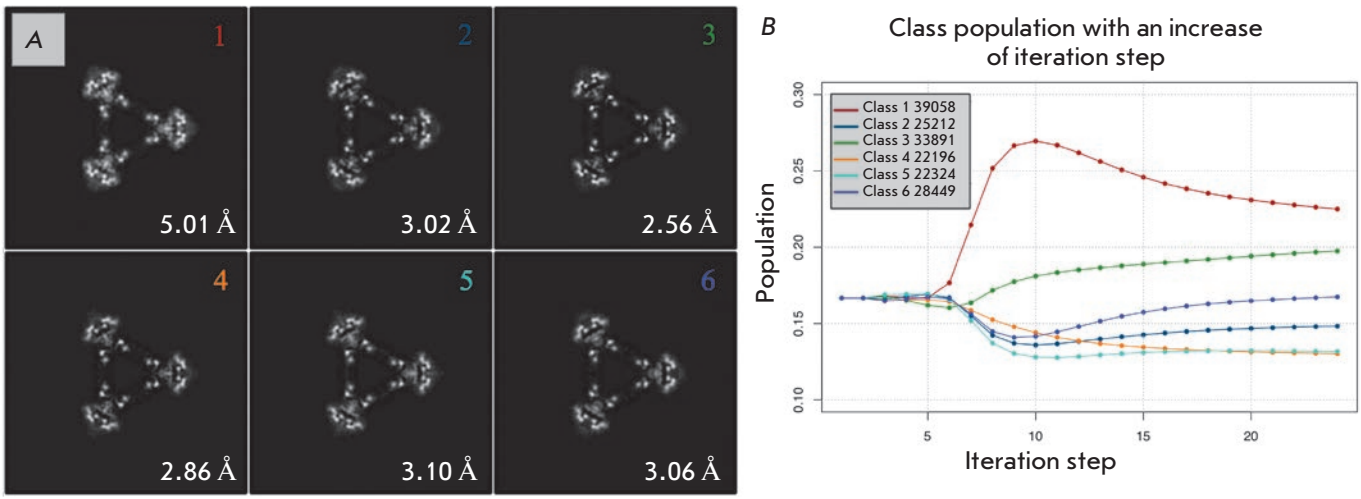

Fig. 5. Results of 3D classification. *A* – central sections of the classes. Images from 1 to 44 (blue) were used for further analysis and density map reconstruction. Images from 45 to 50 (red) were excluded from further data processing, *B* – changes in the class populations depending on the step of iteration. Dots are colored in accordance with a numbering color on the *A* panel

by performing a series of refinements with different degrees of blurring, from −150 to +150. The appropriate parameters for further refinement were selected based on the best R_f and FSC, which corresponded to a blur parameter of −80. In addition to the visual inspection, the quality of the refined model was validated with Molprobity [29]. The refined model was compared with the crystal structure of the protein using PDBeFOLD [30]. The Ramachandran plot analysis showed that the residues Gly285 and His361 of all subunits were in disallowed regions; however, these residues in all subunits had a well-defined electron density.

DISCUSSION

The 3D classification revealed no significant structural heterogeneity in the sample at the resolution level achieved, but it made it possible to select a subset of particles containing information on high spatial frequencies and providing maximum resolution for the final cryo-EM map (*Fig. 6 B,C*).

The distribution of projections for the angle classification, which was used in the refinement of the map without imposition of symmetry and the map for the third 3D class, is shown in *Fig. 6D*. It can be seen that the object has no preferred orientations in the amorphous ice layer. The assessment of the average resolution by the FSC = 0.143 and FSC = 0.5 criteria based on the results of postprocessing is shown in *Fig. 7*.

High symmetry of the object significantly simplifies the cryo-EM reconstruction, thereby compensating for a small number of projections with a rather high in-

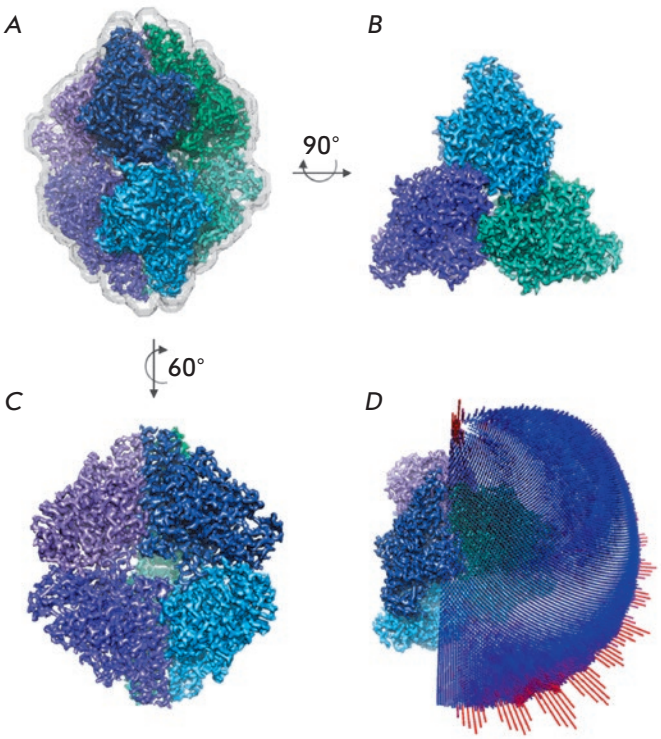

Fig. 6. Final density map with the best resolution of 2.56 Å. *A* – the mask used for reconstruction and resolution assessment is shown by a gray semi-transparent isosurface; *B*–*C* – density maps in different projections, individual subunits of the protein hexamer are highlighted in colors; *D* – distribution of projections for the angle classification used

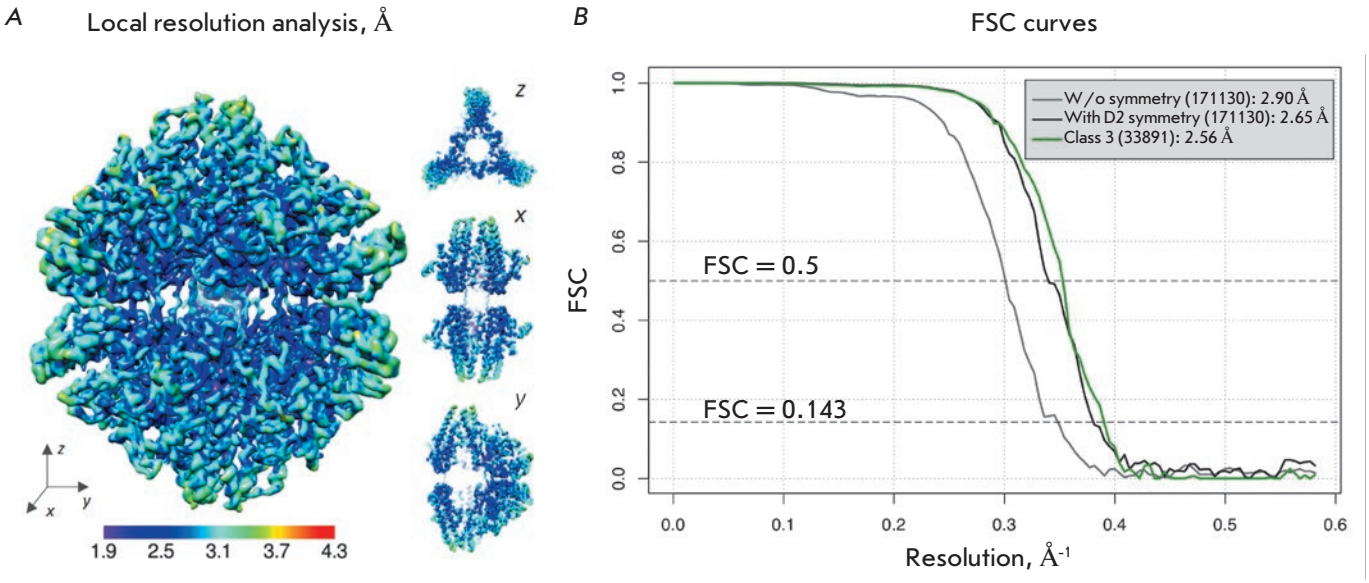

Fig. 7. Resolution assessment. *A* – local resolution for the density map of the third 3D class analyzed with MonoRes [31]; *B* – Fourier shell correlation (FSC) curves for the density maps without imposition of symmetry (gray curve), with symmetry constraints for the complete set of particle images (black curve), and for a particle set belonging to the third class (green curve)

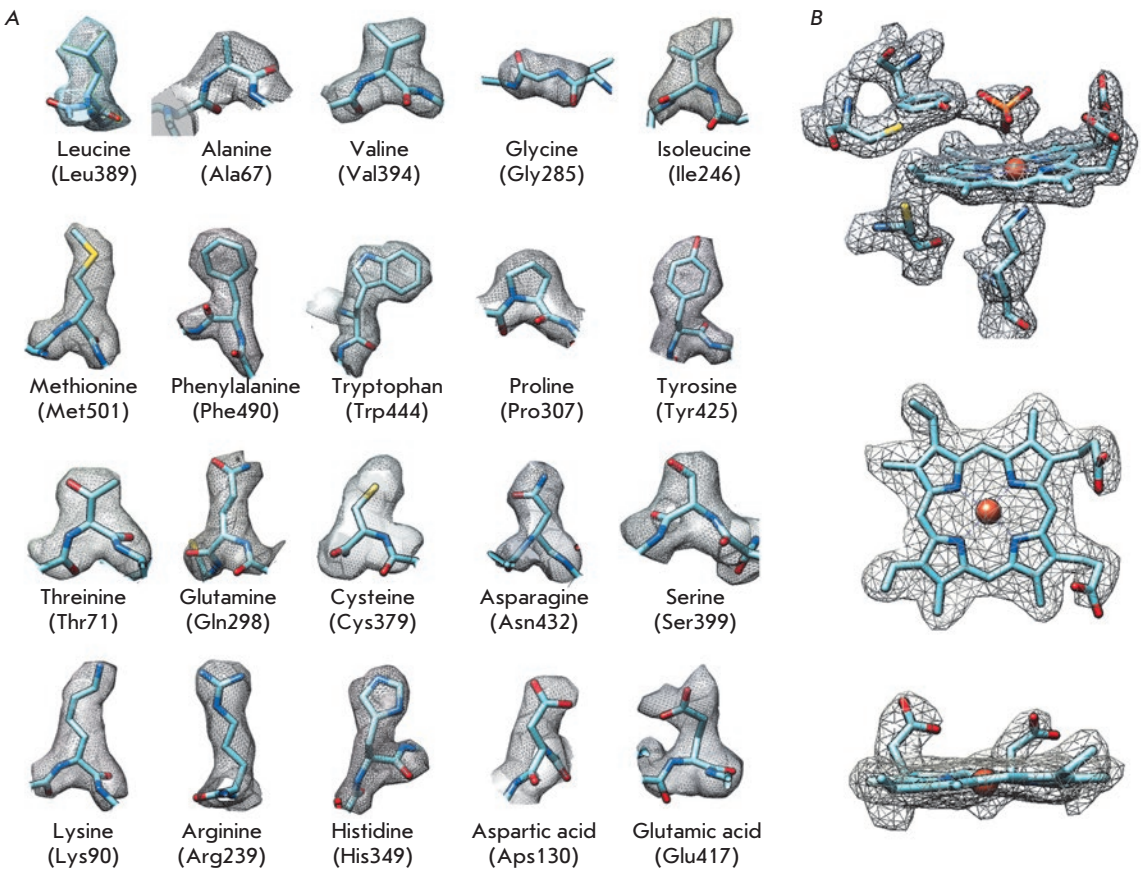

Fig. 8. Quality of the experimental density for the third 3D class. *A* – for the side chains of selected residues of the refined model; *B* – for the active-site heme and its environment

formation limit for this experiment and a low signal-to-noise ratio due to the low molecular weight of the object. The results of the refinement in Relion 2.1 after 3D classification clearly show the influence of the data quality on the final resolution. When applying symmetry of the object, the structural model was constructed using a total of 34,000 particle images from the 3D class that had the highest resolution of 2.56 Å (*Fig. 5*).

The fitting of the enzyme X-ray structure (RCSB ID code 3FO3) to the experimental 2.56 Å resolution cryo-EM map and the subsequent refinement yielded a final structure with a Molprobity score of 2.55 and the following parameters: $R_f = 28.70$, $FSC_{average} = 0.8679$ (*Table*). The high-quality map allowed us not only to trace the polypeptide chain, but also to identify the side chains of residues *(Fig. 8A*), including the unique covalent bond between the active-site tyrosine and cysteine (*Fig. 8B*) and the side chains of residues Arg52, Arg316, and Lys456 on the surface of the enzyme molecule, which were invisible in the crystal structure. The density observed in the active site of the enzyme was identified as phosphate based on the composition of the buffer used for crystallization (*Fig. 8B*). The binding of inorganic anions is characteristic of the active site of TvNiR, which is well-known from X-ray crystallography [9, 10].

The superposition of the refined cryo-EM structure on the initial crystal structure shows that their backbone structures are, in general, similar. The side-chain orientations are also similar, except for some residues on the surface of the enzyme, e.g., Asp40, Arg51, Glu337, Glu341, *etc.*, which may be attributed to their relatively high flexibility. The RMSD of the C_α atoms of these structures are not larger than 0.36 Å. Therefore, the cryo-EM structure of TvNiR is in good agreement with the crystal structure of the enzyme determined earlier by X-ray crystallography. The cryo-EM map was deposited in the Electron Microscopy Data Bank (EMDB) under the accession code EMD-0020.

CONCLUSION

The structure of cytochrome *c* nitrite reductase from the bacterium *T. nitratireducens* was studied by cryo-EM single-particle analysis; a cryo-EM map with a 2.56 Å resolution was obtained, and the appropriate three-dimensional model was constructed. The optimal algorithm was found for data collection and processing in order to achieve high resolution. A comparison of the three-dimensional TvNiR structures determined by X-ray crystallography (1.40 Å) and cryo-EM (2.56 Å) revealed no significant differences. At the resolution level achieved by cryo-EM, TvNiR does not exhibit structural heterogeneity. ●

This work was carried out using the computing resources of the Federal Collective Usage Center "Complex for Simulation and Data Processing for Mega-Science Facilities" at the National Research Centre "Kurchatov Institute," http://ckp.nrcki.ru (financial support from the Ministry of Education and Science of the Russian Federation, the unique project identifier RFMEFI62117X0016) and the facilities of the Resource Center of Probe and Electron Microscopy at the Centre for Nano, Bio, Info, Cognitive, and Social Sciences and Technologies (NBICS Centre) of the National Research Centre "Kurchatov Institute" and was supported by the Russian Science Foundation (grant No. 18-41-06001 supporting the data collection and processing and grant No. 14-24-00172 supporting the protein isolation and purification) and the Government Task No. 01201351365 (cultivation of the producer strain).

REFERENCES

1. Callaway E. // Nature. 2015. V. 525. P. 172–174.
2. Merk A., Bartesaghi A., Banerjee S., Falconieri V., Rao P., Davis M.I., Pragani R., Boxer M.B., Earl L.A., Milne J.L.S., et al. // Cell. 2016. V. 165. № 7. P. 1698–1707.
3. Iancu C. V., Tivol W.F., Schooler J.B., Dias D.P., Henderson G.P., Murphy G.E., Wright E.R., Li Z., Yu Z., Briegel A., et al. // Nat. Protoc. 2007. V. 1. № 6. P. 2813–2819.
4. Cheng Y. // Cell. 2015. V. 161. № 3. P. 450–457.
5. Gelfand A. // Biomedical Computation Review. 2016. V.1 . P. 13-21.
6. Bai X., McMullan G., Scheres S.H.W. // Trends Biochem. Sci. 2015. V. 40. № 1. P. 49–57.
7. Tikhonova T.V., Slutsky A., Antipov A.N., Boyko K.M., Polyakov K.M., Sorokin D.Y., Zvyagilskaya R.A., Popov V.O. // Biochim. Biophys. Acta Proteins Proteomics. 2006. V. 1764. № 4. P. 715–723.
8. Frank J., Zhu J., Penczek P., Li Y., Srivastava S., Verschoor A., Radermacher M., Grassucci R., Lata R.K., Agrawal R.K. // Nature. 1995. V. 376. № 6539. P. 441–444.
9. Polyakov K.M., Boyko K.M., Tikhonova T.V., Slutsky A., Antipov A.N., Zvyagilskaya R.A., Popov A.N., Bourenkov G.P., Lamzin V.S., Popov V.O. // J. Mol. Biol. 2009. V. 389. № 5. P. 846–862.
10. Trofimov A.A., Polyakov K.M., Boyko K.M., Tikhonova T.V., Safonova T.N., Tikhonov A.V., Popov A.N., Popov V.O. // Acta Crystallogr. Sect. D Biol. Crystallogr. 2010. V. 66. № 10. P. 1043–1047.
11. Trofimov A.A., Polyakov K.M., Boíko K.M., Filimonenkov A.A., Dorovatovskiĭ P.V., Tikhonova T.V., Popov V.O., Koval'chuk M.V. // Crystallogr. Reports. 2010. V. 55. № 1. P. 61–67.
12. Zheng S., Palovcak E., Armache J.-P., Cheng Y., Agard D. // bioRxiv. 2016. P. 1–30.
13. Zhang K. // J. Struct. Biol. 2016. V. 193. № 1. P. 1–12.
14. Kimanius D., Forsberg B.O., Scheres S.H.W., Lindahl E. // Elife. 2016. V. 5.
15. Grant T., Grigorieff N. // Elife. 2015. V. 4. P. e06980.

16. Tang G., Peng L., Baldwin P.R., Mann D.S., Jiang W., Rees I., Ludtke S.J. // J. Struct. Biol. 2007. V. 157. № 1. P. 38–46.
17. Dempster A.P.A., Laird N.M.N., Rubin D.D.B. Maximum likelihood from incomplete data via the EM algorithm. // Journal of the royal statistical society. Series B (methodological). 1977. P. 1-38
18. Scheres S.H.W. // J. Struct. Biol. 2012. V. 180. № 3. P. 519–530.
19. Scheres S.H.W. // J. Mol. Biol. 2012. V. 415. № 2. P. 406–418.
20. Chen S., McMullan G., Faruqi A.R., Murshudov G.N., Short J.M., Scheres S.H.W., Henderson R. // Ultramicroscopy. 2013. V. 135. P. 24–35.
21. Rosenthal P.B., Henderson R. // J. Mol. Biol. 2003. V. 333. № 4. P. 721–745.
22. Scheres S.H.W. // Methods in Enzymology. 2016. V. 579. Academic Press. P. 125–157.
23. Ludtke S.J. // Methods in Enzymology. 2016. V. 579. Academic Press. P. 159–189.
24. Hirschi M., Herzik M.A., Wie J., Suo Y., Borschel W.F., Ren D., Lander G.C., Lee S.Y. // Nature. 2017. V. 550. № 7676. P. 411-414.
25. Murshudov G.N., Skubák P., Lebedev A.A., Pannu N.S., Steiner R.A., Nicholls R.A., Winn M.D., Long F., Vagin A.A. // Acta Crystallogr. Sect. D Biol. Crystallogr. 2011. V. 67. № 4. P. 355–367.
26. Wood C., Burnley T., Patwardhan A., Scheres S., Topf M., Roseman A., Winn M. // Acta Crystallogr. Sect. D Biol. Crystallogr. 2015. V. 71. P. 123–126.
27. Brown A., Long F., Nicholls R.A., Toots J., Emsley P., Murshudov G. // Acta Crystallogr. Sect. D Biol. Crystallogr. 2015. V. 71. P. 136–153.
28. Emsley P., Lohkamp B., Scott W.G., Cowtan K. // Acta Crystallogr. Sect. D Biol. Crystallogr. 2010. V. 66. № 4. P. 486–501.
29. Chen V.B., Arendall W.B., Headd J.J., Keedy D.A., Immormino R.M., Kapral G.J., Murray L.W., Richardson J.S., Richardson D.C. // Acta Crystallogr. Sect. D Biol. Crystallogr. 2010. V. 66. № 1. P. 12–21.
30. Krissinel E., Henrick K. // Acta Crystallogr. Sect. D. 2004. V. 60. № 12-1. P. 2256–2268.
31. Vilas J.L., Gómez-Blanco J., Conesa P., Melero R., Miguel de la Rosa-Trevín J., Otón J., Cuenca J., Marabini R., Carazo J.M., Vargas J., et al. // Structure. 2018. V. 26. № 2. P. 337–344. e4.

Lynx1 Prevents Long-Term Potentiation Blockade and Reduction of Neuromodulator Expression Caused by $A\beta_{1-42}$ and JNK Activation

M. L. Bychkov[1,2], N. A. Vasilyeva[1], M. A. Shulepko[1,2], P. M. Balaban[3], M. P. Kirpichnikov[1,2], E. N. Lyukmanova[1,2*]

[1]Lomonosov Moscow State University, Leninskie Gori 1, Moscow, 119234, Russia

[2]Shemyakin-Ovchinnikov Institute of Bioorganic Chemistry, Russian Academy of Sciences, Miklucho-Maklaya Str., 16/10, Moscow, 117997, Russia

[3]Institute of Higher Nervous Activity and Neurophysiology, Russian Academy of Sciences, Butlerova Str., 5A, Moscow, 117485, Russia

*E-mail: ekaterina-lyukmanova@yandex.ru.

Received March 18, 2018; in final form June 27, 2018

ABSTRACT **Nicotinic acetylcholine receptors (nAChRs) are ligand-gated ion channels. Many neurodegenerative diseases are accompanied by cognitive impairment associated with the dysfunction of nAChRs. The human membrane-tethered prototoxin Lynx1 modulates nAChR function in the brain areas responsible for learning and memory. In this study, we have demonstrated for the first time that the β-amyloid peptide $A\beta_{1-42}$ decreases *Lynx1* mRNA expression in rat primary cortical neurons, and that this decrease is associated with the activation of c-Jun N-terminal kinase (JNK). In addition, we have demonstrated that the *Lynx1* expression decrease, as well as the blockade of the long-term potentiation underlying learning and memory, caused by $A\beta_{1-42}$, may be prevented by incubation with a water-soluble Lynx1 analogue. Our findings suggest that the water-soluble Lynx1 analogue may be a promising agent for the improvement of cognitive deficits in neurodegenerative diseases.**

KEYWORDS **nicotinic acetylcholine receptor, cognitive impairment, Alzheimer disease, β-amyloid peptide, Ly6/uPAR.**

ABBREVIATIONS **ACSF – artificial cerebrospinal fluid, AD – Alzheimer disease, HFS – high-frequency stimulation, LTP – long-term potentiation, fEPSPs – field excitatory postsynaptic potentials, Aβ – β-amyloid peptide, nAChR – nicotinic acetylcholine receptor, siRNA – small interfering RNA, ws-Lynx1 – water-soluble Lynx1.**

INTRODUCTION

Many neurodegenerative diseases, such as Alzheimer's disease (AD), are characterized by impaired cognitive processes associated with the dysfunction of nicotinic acetylcholine receptors (nAChRs) [1]. In AD, oligomers of the β-amyloid peptide (Aβ) form plaques and the most toxic Aβ is $A\beta_{1-42}$ [1]. $A\beta_{1-42}$ in a 200 nM concentration inhibits α7-nAChR, the most common nicotinic cholinergic receptor in the brain; and the interaction between Aβ and the receptor leads to internalization of the latter in AD [1]. In addition, Aβ inhibits the long-term potentiation (LTP) [2] that is a generally established model for the plasticity processes underlying memory and learning [3].

Previously, we demonstrated that a water-soluble variant of the human protein Lynx1 (ws-Lynx1) [4], which modulates the α7-nAChR function in the brain [5], competes with $A\beta_{1-42}$ for binding to α7-nAChR [6]. Pre-incubation of mouse cortical neurons with ws-Lynx1 was shown to reduce the cytotoxic effect of $A\beta_{1-42}$ [6]. In addition, Western blot analysis revealed a reduced Lynx1 expression in the cortex of AD modeling transgenic mice (3×Tg-AD) compared to wild-type mice [6]. Based on these facts, we argue that Lynx1 plays an important role in AD, and that the accumulation of $A\beta_{1-42}$ down-regulates the expression of this neuromodulator in the brain and disturbs the $A\beta_{1-42}$/Lynx1 balance, causing α7-nAChR dysfunction. We studied the effect of $A\beta_{1-42}$ on *Lynx1* gene expression in rat primary cortical and hippocampal neurons and evaluated the effect of ws-Lynx1 and $A\beta_{1-42}$ on LTP in mouse hippocampal slices.

EXPERIMENTAL

A primary neuron culture was prepared from the cortex and hippocampus of newborn Wistar rats according to the previously described procedure [7]. On the 14th day, the neuron culture was supplemented with either $A\beta_{1-42}$ (1 or 5 μM, Biopeptide Co) oligomerized according to the previously described protocol [8], or 5 μM $A\beta_{42-1}$ (reverse peptide used as a negative control; Biopeptide Co), or 10 μM ws-Lynx1 (prepared according to [4]), or a mixture (5 μM $A\beta_{1-42}$ + 10 μM ws-Lynx1), or 2.5 μM SP600125 (Tocris), or a mixture (5 μM $A\beta_{1-42}$ + 2.5 μM SP600125) and incubated for an additional 24 h. For JNK knockdown, on the 10th day cortical neurons were transfected with *JNK1* and *JNK2* small interfering RNAs (siRNAs) or with the control siRNA (*Table 1*). After that, the neurons were incubated for 72 h, then they were supplemented with 5 μM $A\beta_{1-42}$ and incubated for another 24 h.

Then, the total mRNA was isolated using an ExtractRNA reagent (Evrogen). The mRNA was treated with DNase I (Thermo Fisher Scientific, USA), and cDNA was then synthesized using a MMLV RT kit (Evrogen). Real-time PCR was carried out using a 5x mixture of qPCRmix-HS SYBR + HighROX (Evrogen); the list of primers is given in *Table 2*. The data were analyzed using the LinReg 2017.0 software. The mRNA level was normalized to the β-actin values.

Transversal hippocampal slices from eight-month-old C57BL/6 mice were perfused with an artificial cerebrospinal fluid (ACSF) (124 mM NaCl, 3 mM KCl, 2.5 mM $CaCl_2$, 1.3 mM $MgCl_2$, 26 mM $NaHCO_3$, 1.27 mM NaH_2PO_4, and 10 mM *D*-glucose, pH 7.4), continuously saturated with carbogen (95% O_2 + 5% CO_2) at 34 °C for 1 h. Then, a portion of the slices was perfused with ACSF containing 200 nM $A\beta_{1-42}$ and the other was perfused with ACSF containing 200 nM $A\beta_{1-42}$ + 2 μM ws-Lynx1 for 1 h. Control slices were perfused with ACSF without $A\beta_{1-42}$ and ws-Lynx1. Field excitatory postsynaptic potentials (fEPSPs) were recorded using a SliceMaster system (Scientifica, UK) at 32°C. A recording electrode (1-3 MΩ) filled with ACSF was positioned within hippocampal CA1 stratum radiatum. Synaptic responses were evoked by paired-pulse stimulation of Schaffer collaterals in the CA3 stratum radiatum area by using a bipolar electrode. A 50-ms interpulse interval was used, unless stated otherwise. The simulations were repeated at 0.033 Hz. Stimulus intensity was adjusted to elicit 40 % of maximal fEPSP amplitude.

Table 1. The small interfering RNAs used in the study

Gene	Interfering RNA sequence
Control	UUCUCCGAACGUGUCACGUTT
	ACGUGACACGUUCGGAGAATT
JNK1	GGCAUGGGCUAUAAAGAAATT
	UUUCUUUGUAGCCCAUGCCTT
JNK2	GCCAGAGACUUAUUAUCAATT
	UUGAUAAUAAGUCUCUGGCTT

After 20 minutes of recording test responses, a high-frequency stimulation (HFS) protocol was used to induce LTP: 10 trains with a frequency of 100 Hz (five stimuli per train) with an intertrain interval of 200 ms, four sessions with an interval of 30 s. After LTP induction, fEPSPs were recorded for 1.5 h. The obtained data were recorded, filtered, and analyzed using the Spike2 software (Cambridge Electronic Design Limited, UK) and SigmaPlot 11.0 (Systat Software Inc., USA). The post-tetanic tangent of the fEPSP slope was normalized to the mean slope of all fEPSPs recorded 20 min before LTP induction.

The statistical analysis of the LTP data and the data on the effect of $A\beta_{1-42}$, ws-Lynx1, SP600125, and siRNA on gene expression in primary neurons was performed using the GraphPad Prism 6.0 (GraphPad Software Inc.) software. A value of $p < 0.05$ was considered statistically significant. All experiments were performed in accordance with the guidelines set forth by the European Communities Council Directive of November 24, 1986 (86/609/EEC) and were approved by the ethical committees of the Shemyakin-Ovchinnikov Institute and Institute of Higher Nervous Activity and Neurophysiology, Russian Academy of Sciences.

RESULTS AND DISCUSSION

$A\beta_{1-42}$–induced decrease in *Lynx1* expression in neurons is associated with JNK activation

To test the hypothesis of the effect of amyloid peptide on Lynx1 expression, we incubated primary neurons of the rat cortex and hippocampus with 1 μM of oli-

Table 2. Primers used in the study

Gene	Forward primer	Reverse primer	Length, bp
β-actin	TCATGTTTGAGACCTTCAACAC	GTCTTTGCGGATGTCCACG	250
Lynx1	ACCACTCGAACTTACTTCACC	ATCGTACACGGTCTCAAAGC	81
α7-nAChR	TGCACGTGTCCCTGCAAGGC	GTACACGGTGAGCGGCTGCG	112

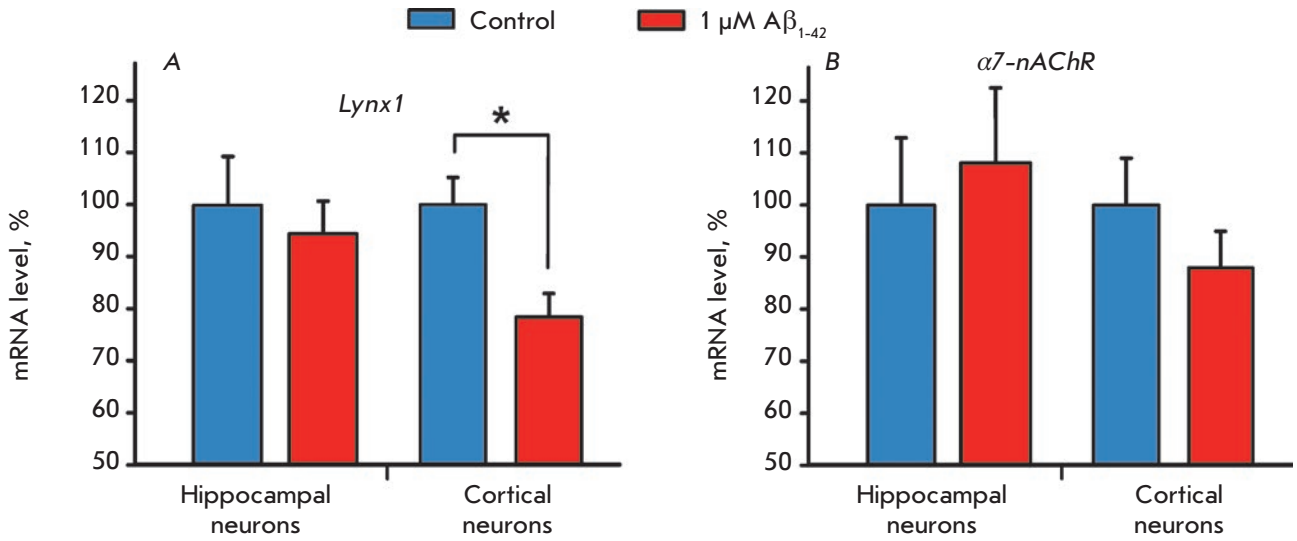

Fig. 1. Effect of $A\beta_{1-42}$ on *Lynx1* (A) and *α7-nAChR* (B) gene expression in primary cortical and hippocampal neurons. The data are presented as % of the control ± s.e.m. (n = 3). Data indicated by * ($p<0.05$) significantly differ from each other, based on a two-sided t-test

gomeric $A\beta_{1-42}$ and analyzed the *Lynx1* mRNA level (*Fig. 1A*). In hippocampal neurons, there was no significant decrease in neuromodulator expression, while a significant reduction in the *Lynx1* mRNA level (up to 78.4 ± 4.4% of the control level) was observed in cortical neurons. This is consistent with a previously observed decrease in Lynx1 expression in the cortex of AD modeling mice [6]. In contrast, $A\beta_{1-42}$ did not decrease the *α7-nAChR* mRNA level either in hippocampal or in cortical neurons (*Fig. 1B*). An increase in the $A\beta_{1-42}$ concentration to 5 μM led to a further decrease in *Lynx1* gene expression in cortical neurons (up to 65.8 ± 4.9% of the control level, *Fig. 2A*).

Nicotine-induced activation of α7-nAChR can regulate gene transcription through CREB phosphorylation and the activation of MAP/ERK signaling pathways, which is accompanied by an increase in the expression level of the early response c-Fos transcription factor [9]. On the other hand, binding of oligomeric $A\beta_{1-42}$ to α7-nAChR leads to the activation of c-Jun N-terminal kinase (JNK) [10], which plays a key role in the regulation of gene expression and other vital processes, including processing of the β-amyloid peptide precursor and formation of neurofibrillary tangles in AD [10]. In turn, JNK activation may lead to the inhibition of CREB transcription factor phosphorylation and, therefore, to a decrease in the expression level of the c-Fos transcription factor [11].

To elucidate whether the decreased *Lynx1* expression level in cortical neurons incubated with oligomeric $A\beta_{1-42}$ was associated with JNK activation, we incubated cortical neurons with $A\beta_{1-42}$ and SP600125, a selective inhibitor of JNK1, JNK2, and JNK3 which is considered now as one of the potential drugs for AD treatment [10]. Indeed, co-incubation of neurons with $A\beta_{1-42}$ and SP600125 prevented the decrease in *Lynx1* expression, indicating a possible association of this decrease with JNK activation (*Fig. 2B*). To confirm the role of JNK in the regulation of *Lynx1* transcription, we used knockdown of the *JNK1* and *JNK2* genes with small interfering RNAs. As expected, incubation of neurons with blocked *JNK1* and *JNK2* expression in the presence of $A\beta_{1-42}$ led to a recovery of the *Lynx1* mRNA expression level (*Fig. 2B*). In this case, transfection of the neuronal culture with control siRNA that did not inhibit gene transcription had no effect on the decrease in *Lynx1* mRNA expression caused by $A\beta_{1-42}$ (data not shown). Knockdown of *JNK1* and *JNK2* in the absence of $A\beta_{1-42}$ did not cause significant changes in the *Lynx1* expression level (*Fig. 2B*), which confirms the association of the amyloid peptide, JNK activation, and decreased neuromodulator transcription.

An analysis of the human *LYNX1* gene promoter in the human genome browser (chr8: 143841246 – chr8: 143879640) and the mouse *Lynx1* gene promoter (chr15: 74573409 – chr15: 74603409) revealed two potential binding sites for the AP-1 transcriptional complex formed by the c-Jun and c-Fos transcription factors (*Fig. 2C*). $A\beta_{1-42}$-induced activation of JNK is simultaneously accompanied by c-Jun activation [10] and c-Fos down-regulation [11]. For that reason, a possible imbalance between c-Jun and c-Fos can cause a disruption in the AP-1 transcriptional complex formation and lead to the decrease in *Lynx1* gene transcription. In accordance with this suggestion, incubation of cortical neurons together with ws-Lynx1 and $A\beta_{1-42}$ was

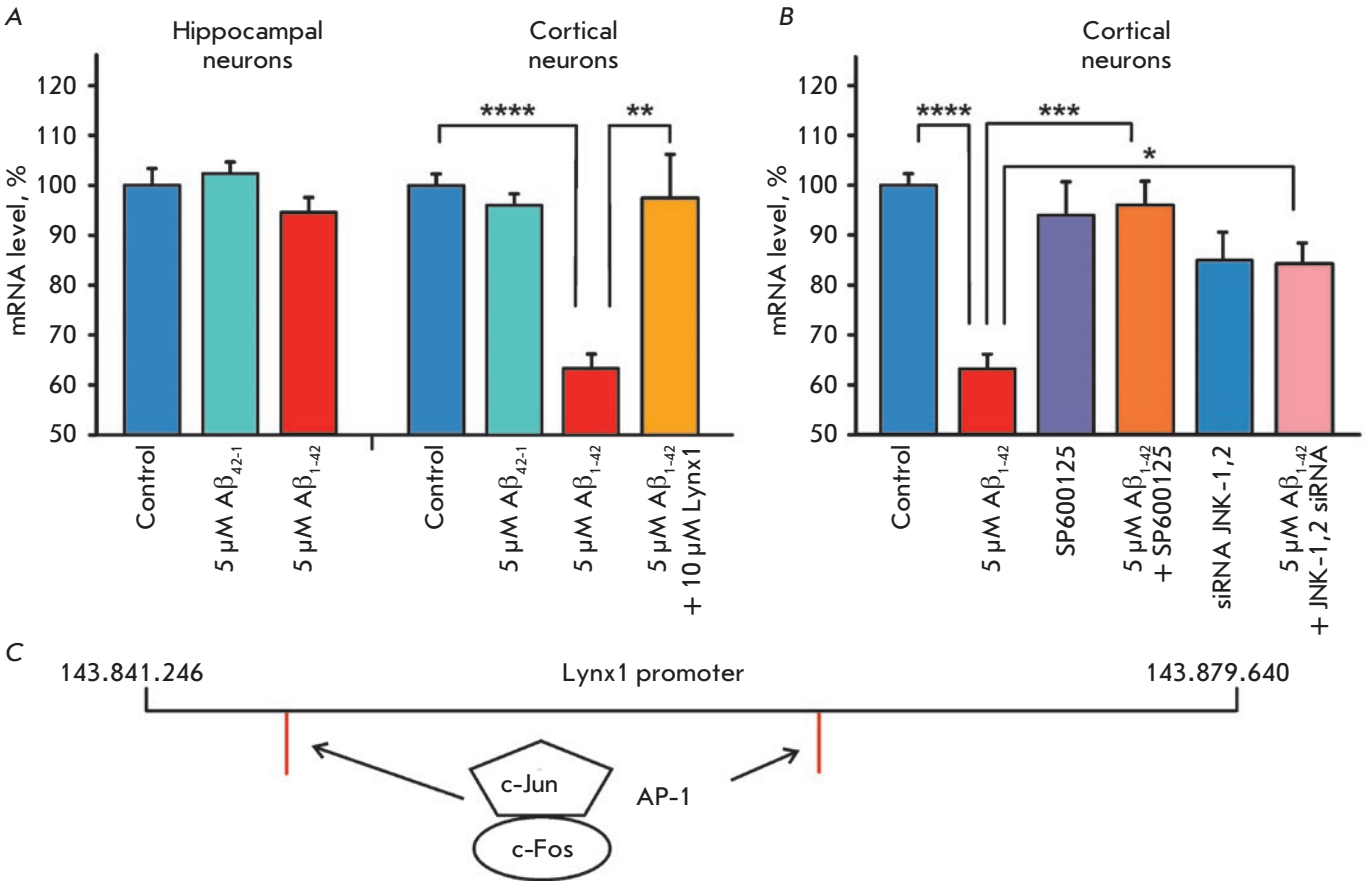

Fig.2. Ws-Lynx1 and JNK inhibition cancels the decrease in *Lynx1* expression in a primary culture of cortical neurons treated with $A\beta_{1-42}$. (*A*) Effect of $A\beta_{1-42}$, $A\beta_{42-1}$, and ws-Lynx1 on *Lynx1* expression. (*B*) Effect of $A\beta_{1-42}$, JNK inhibition by SP600125, and knockdown of the *JNK1* and *JNK2* genes on *Lynx1* expression. The data are presented as % of the control ± s.e.m. ($n = 4$). Data indicated by * ($p < 0.05$), ** ($p < 0.01$), and **** ($p < 0.0001$) mean a statistically significant difference between groups according to the one-sided ANOVA test, followed by the Tukey's/hoc test. (*C*) Schematic structure of the *Lynx1* gene. Red lines denote the c-Jun and c-Fos binding sites.

accompanied by recovery of the *Lynx1* mRNA level (*Fig. 2B*). Apparently, ws-Lynx1 competes with $A\beta_{1-42}$ for binding to α7-nAChR [6] and activates α7-nAChR in a nicotine-like manner, which leads to the c-Fos upregulation [9] and recovery of *Lynx1* transcription.

Ws-Lynx1 prevents $A\beta_{1-42}$–induced LTP blockade

Using SP600125, it was previously demonstrated that the LTP blockade observed during the incubation of hippocampal slices with oligomeric $A\beta_{1-42}$ was associated with JNK activation [12]. To study the effect of Lynx1 on the recovery of the synaptic plasticity impaired by the interaction between oligomeric $A\beta_{1-42}$ and α7-nAChR, as well as JNK activation, we investigated the influence of 200 nM $A\beta_{1-42}$ on LTP in the surviving mouse's hippocampal slices in the presence and absence of 2 μM ws-Lynx1. Pre-perfusion of the slices in a solution containing $A\beta_{1-42}$ for 1 h led to a significant decrease in the post-tetanic fEPSP, noticeable in the first minutes after LTP induction. In this case, the fEPSP slope averaged over the first 10 minutes of recording decreased almost 1.5-fold compared to the control fEPSP slope (*Fig. 3B*). A significant decrease in the fEPSP slope caused by $A\beta_{1-42}$ to the baseline fEPSP values was observed during the entire period after LTP induction.

However, incubation of hippocampal slices in a medium containing both $A\beta_{1-42}$ and ws-Lynx1 restored the LTP level almost to the control values (*Fig. 3*). The mean fEPSP slope upon simultaneous application of $A\beta_{1-42}$ and ws-Lynx1 was significantly higher than that of the fEPSP observed during incubation with $A\beta_{1-42}$ alone and was not statistically different from the mean fEPSP slope in the control throughout the recording time after HFS (*Fig. 3B*). Therefore, ws-Lynx1 prevents the inhibitory effect of $A\beta_{1-42}$ and facilitates the complete recovery of LTP.

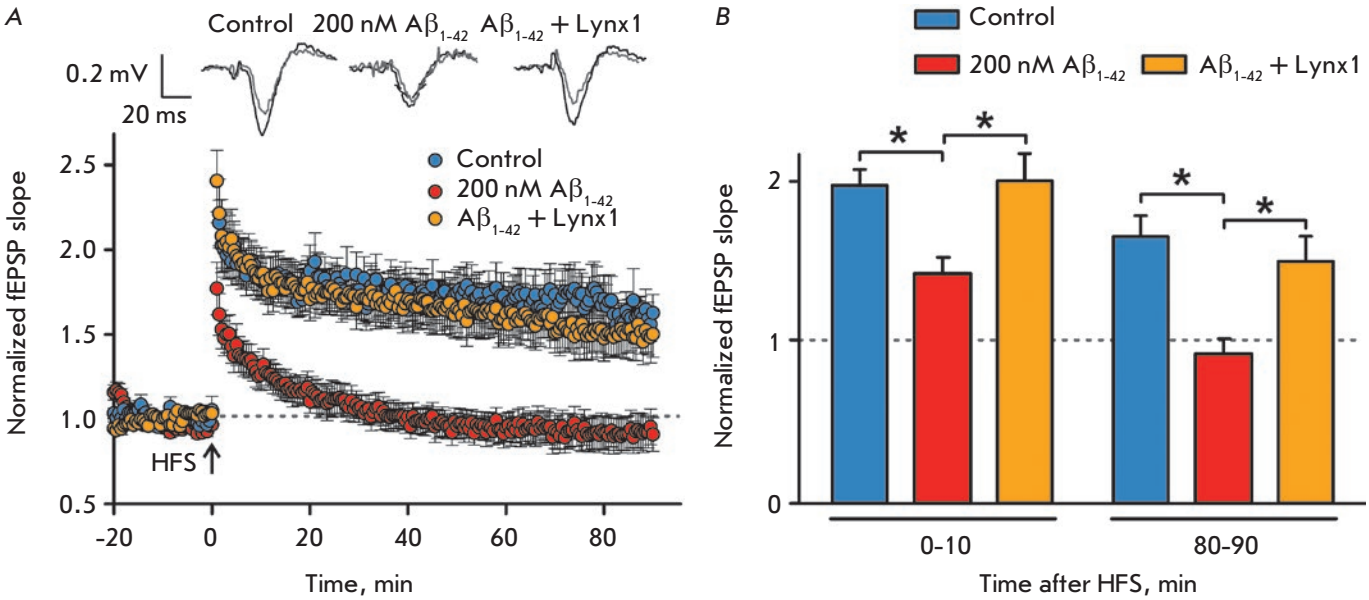

Fig. 3. Ws-Lynx1 prevents $A\beta_{1-42}$-induced LTP blockade in hippocampal slices. (*A*) Time course of changes in the fEPSP slope recorded in control hippocampal slices perfused with ACSF without $A\beta_{1-42}$ ($n = 8$), ACSF containing 200 nM $A\beta_{1-42}$ ($n = 6$), and ACSF containing 200 nM $A\beta_{1-42}$ + 2 μM ws-Lynx1 ($n = 5$). (*B*) fEPSPs slopes averaged during 0–10 min and 80–90 min after HFS. * ($p < 0.05$) means a statistically significant difference between groups according to the one-way ANOVA test, followed by the Tukey's/hoc test

CONCLUSION

Hereby, the presence of oligomeric $A\beta_{1-42}$ in the neuronal environment leads to a significant decrease in the expression of the Lynx1 neuromodulator that regulates α7-nAChR functioning in the brain. We have demonstrated for the first time that this decrease is associated with JNK activation and can be prevented by incubation with the water-soluble Lynx1 analogue. In addition, ws-Lynx1 is capable of correcting $A\beta_{1-42}$–induced impairments of hippocampal synaptic plasticity, which underlies memory impairment and other cognitive dysfunctions in AD. ●

This work was supported by the Russian Foundation for Basic Research (No. 16-34-01302; N.A.V., development of a system for registering currents in brain slices) and Russian Science Foundation (No. 16-14-00102; E.N.L., M.A.Sh., N.A.V., effects of $A\beta_{1-42}$, SP600125, siRNA, and ws-Lynx1 on LTP and gene expression).

REFERENCES

1. Buckingham S.D., Jones A.K., Brown L.A., Sattelle D.B. // Pharmacol. Rev. 2009. V. 61. P. 39–61.
2. Walsh D.M., Klyubin I., Fadeeva J.V., Cullen W.K., Anwyl R., Wolfe M.S., Rowan M.J., Selkoe D.J. // Nature. 2002. V. 416. P. 535–539.
3. Lynch M.A. // Physiol. Rev. 2004. V. 84. P. 87–136.
4. Lyukmanova E.N., Shenkarev Z.O., Shulepko M.A., Mineev K.S., D'Hoedt D., Kasheverov I.E., Filkin S.Y., Krivolapova A.P., Janickova H., Dolezal V., Dolgikh D.A., et al. // J. Biol. Chem. 2011. V. 286. P. 10618–10627.
5. Miwa J.M., Ibanez-Tallon I., Crabtree G.W., Sánchez R., Sali A., Role L.W., Heintz N. // Neuron. 1999. V. 23. P. 105–114.
6. Thomsen M.S., Arvaniti M., Jensen M.M., Shulepko M.A., Dolgikh D.A., Pinborg L.H., Härtig W., Lyukmanova E.N., Mikkelsen J.D. // Neurobiol. Aging. 2016. V. 46. P. 13–21.
7. Suntsova M., Gogvadze E.V., Salozhin S., Gaifullin N., Eroshkin F., Dmitriev S.E., Martynova N., Kulikov K., Malakhova G., Tukhbatova G., et al. // Proc. Natl. Acad. Sci. USA. 2013. V. 110. P. 19472–19477.
8. Klein W.L. // Neurochem. Int. 2002. V. 41. P. 345–352.
9. Hu M., Liu Q.S., Chang K.T., Berg D.K. // Mol. Cell. Neurosci. 2002. V. 21. P. 616–625.
10. Yarza R., Vela S., Solas M., Ramirez M.J. // Front. Pharmacol. 2016. V. 6 doi: 10.3389/fphar.2015.00321.
11. Yenki P., Khodagholi F., Shaerzadeh F. // J. Mol. Neurosci. 2013. V. 49. P. 262–269.
12. Wang Q., Walsh D.M., Rowan M.J., Selkoe D.J., Anwyl R. // J. Neurosci. 2004. V. 24. P. 3370–3378.

Biochemical and Functional Changes in the Eye As a Manifestation of Systemic Degeneration of the Nervous System in Parkinsonism

A. R. Kim[1*], T. A. Pavlenko[2], L. A. Katargina[2], N. B. Chesnokova[2], M. V. Ugrumov[1,3]
[1]Koltzov Institute of Developmental Biology of Russian Academy of Sciences, Vavilov Str., 26, Moscow, 119334, Russia
[2]Helmholtz Moscow Research Institute of Eye Diseases of Ministry of Health of the Russian Federation, Sadovaya-Chernogryazskaya Str., 14/19, Moscow, 105062, Russia
[3]National Research University Higher School of Economics, Myasnitskaya Str., 20, Moscow, 101000, Russia
*E-mail: alexandrrkim@gmail.com
Received March 23, 2018; in final form June 07, 2018

ABSTRACT **Parkinson's disease (PD) is a systemic neurodegenerative condition caused by the death of dopaminergic neurons of the nigrostriatal system of the brain. This disease is diagnosed after most neurons have already been lost, which explains the low efficiency of treatment. Hope for increasing treatment efficiency rests in the development of new strategies for early diagnosis of PD based on a search for peripheral markers that appear as early changes in non-motor functions. Since impairment of the visual function is one of the manifestations of PD, the purpose of our work was to identify biochemical and physiological changes in a mouse's eye and eyelid in models of preclinical (presymptomatic) and clinical (symptomatic) stages of PD. We found that the norepinephrine, dopamine, and serotonin levels in the mouse eye reduced not only in the model of the early clinical stage, but also in the model of preclinical stage, an indication that pathological changes in the monoaminergic systems of the brain had affected the eye even before the motor disorders emerged. Moreover, in both models of PD, mice had increased intraocular pressure, indicating the development of both metabolic and functional impairments, which can be used as diagnostic markers. Unlike in the eye, the serotonin level in the eyelid was increased in mice at both parkinsonism stages and in presymptomatic mice to a much higher extent than in symptomatic ones. Given that serotonin is involved in the regulation of lacrimal glands of the eyelid, an increase in its level in parkinsonian mice should alter the composition of tear fluid, which could serve as a diagnostic marker of early stage of PD. Thus, the changes in the metabolism of monoamines in the eye and eyelid observed in mice at the early stage of parkinsonism are accompanied by changes in the function of these structures and, therefore, can be used as diagnostic markers of the early stage of PD.**

KEYWORDS **Parkinson's disease, neurodegeneration, non-motor symptoms, experimental models.**

ABBREVIATIONS **5-HTP – 5-hydroxytryptophan, DHBA – 3,4-dihydroxybenzylamine HPLC-ED – high-performance liquid chromatography with electrochemical detection, IOP – intraocular pressure, *L*-DOPA – *L*-3,4-dihydroxyphenylalanine, MPTP – 1-methyl-4-phenyl-1,2,3,6-tetrahydropyridine, PD – Parkinson's disease.**

INTRODUCTION

Parkinson's disease (PD) is a widespread neurodegenerative disorder caused by the degeneration of the nigrostriatal system of the brain, the key element in the regulation of the motor function. Today, PD is diagnosed based on the presence of motor symptoms in the form of tremor or akinetic rigid syndrome, which appear only many years after the onset of the pathological process, when most nigrostriatal dopaminergic neurons have already been lost. The high degree of degradation of the nigrostriatal system and exhaustion of the compensatory reserves of the brain by the time of the diagnosis are the reason why conventional substitution therapy with dopamine agonists proves to be ineffective [1]. Therefore, there is a pressing need for developing early (preclinical) diagnosis of PD long be-

fore the appearance of motor symptoms, as this could make it possible to use neuroprotective therapy to slow down or even stop neurodegeneration [1].

The existing approach to the development of early diagnosis of PD is based on the idea that the disease is systemic; its non-motor symptoms caused by the impaired function of both brain regions beyond the nigrostriatal system and the peripheral nervous system appear long before the motor disorders [1, 2]. It is assumed that complex preclinical diagnosis of PD can be developed on the basis of early changes in non-motor functions and the corresponding changes in body fluids (cerebrospinal fluid and blood) [1].

Impairment of visual analyzer functions and auxiliary eye structures is one of the systemic manifestations of PD. For instance, at the clinical stage patients develop hallucinations, impaired eye and eyelid movement, and reduced amount and altered composition of tear fluid [3–5]. In addition, the dry eye symptom, blepharitis (bilateral recurrent inflammation of the part of the eyelid where the eyelashes grow), changes in eye accommodation (pupillary response to light), impaired secretion and outflow of intraocular fluid, reduced visual acuity, scotoma formation (areas in the field of vision where vision is either completely degenerated or partially diminished), and thinning of the retina layers, in particular, due to the reduction in the number of nerve fibers, are often observed in PD patients [5–7].

Impairments of neurotransmission and the metabolism of monoamines (primarily catecholamines) play a significant role in pathological changes in the visual system in PD, as they alter the monoamine content in eye tissues and intraocular fluid [8–12]. These changes are quite typical, since monoamines are involved in the transmission of visual information in the retina and affect the retinal and choroidal vascular tone [13–15]. In addition, catecholamines in the anterior part of the eye regulate the accommodation rate [16, 17] and the level of intraocular pressure (IOP) by controlling the secretion and outflow of intraocular fluid [18, 19]. In addition to the eyes, eyelids also undergo changes in PD, since they contain numerous glands (glands of Krause and Wolfring, meibomian glands, etc.), with their secretory product being a component of the fluid. The conjunctiva covering the inner surface of eyelids and the glands within it are sympathetically innervated [20, 21]. This innervation is impaired in PD [2], which may be the cause behind blepharitis and the changes in the composition of tear fluid.

It can be assumed that at least some of the abovementioned changes in the eye and eyelids diagnosed at the clinical stage of PD, i.e. after the onset of motor function disorders, are typical of patients at the preclinical stage, prior to motor impairments. This would allow to use these changes as diagnostic markers of the preclinical stage of the disease. This assumption can be verified only by using an experimental model of PD, since it is not yet possible to identify preclinical stage patients. Moreover, both the models of preclinical and clinical stages of PD need to be used to make sure that the model correctly reproduces at least the biochemical and physiological changes in the eye and eyelids observed in patients.

The aim of the current study is to identify early biochemical and physiological changes in the eye in the experimental model of PD. To achieve this, we measured IOP and evaluated the content of monoamines and metabolites in the eye and eyelid tissues in a neurotoxic mice model of the preclinical and early clinical stages of PD.

EXPERIMENTAL

A total of 98 male C57BL/6 mice aged 2–2.5 months (weight, 22–26 g) purchased from the Pushchino animal facility were used in the study. The animals were kept under standard conditions (22 ± 1°C, light from 8.00 a.m. to 8.00 p.m.) with free access to food and water. The model of the preclinical stage of PD was reproduced by two subcutaneous injections of 1-methyl-4-phenyl-1,2,3,6-tetrahydropyridine (MPTP) (Sigma, USA) at a single dose of 8 mg/kg. The model of early clinical stage was reproduced by four subcutaneous injections of MPTP at a single dose of 10 mg/kg. The interval between the injections was 2 h in both cases [22]. Animals in the control groups were given injections of 0.9% NaCl using the same scheme.

Prior to MPTP administration, the mice were assessed using a PhenoMaster animal behavior analysis system (TSE Systems, Germany) according to the total distance they traveled during the open-field test. The motor behavior of the animals was evaluated again two weeks after administration of MPTP or NaCl.

Two weeks after MPTP administration, IOP was measured 3 times in the animals using an automatic Tonovet veterinary tonometer (Icare, Finland) and the mean value was calculated. After the IOP measurements, material for a biochemical analysis was collected: the animals were decapitated, and the upper and lower eyelids were isolated. Eye specimens were then prepared by removing the lens and the vitreous body. The eye and eyelid specimens were weighed, frozen in liquid nitrogen, and stored at -70°C for further biochemical analysis.

The dorsal striatum was isolated from the mouse brain according to the previously described procedure used to assess the degree of dopamine decline in the nigrostriatal system of experimental animals [22]. Striatum samples were weighed, frozen in liquid nitrogen, and stored at -70°C for further biochemical analysis.

The content of biogenic amines and their metabolites (norepinephrine, dopamine, serotonin, *L*-dihydroxyphenylalanine (*L*-DOPA), and 5-hydroxytryptophan (5-HTP)) was measured using high-performance liquid chromatography with electrochemical detection (HPLC-ED). The samples were homogenized using a Labsonic M ultrasonic homogenizer (Sartorius, France) in 200 μl of 0.1 N $HClO_4$ (Sigma, USA) containing 3,4-dihydroxybenzylamine (DHBA, Sigma) as an internal standard at a concentration of 25 pmol/ml and then centrifuged at 2,000 g for 20 min.

HPLC separation was performed on a reversed-phase ReproSil-Pur column, ODS-3, 4 × 100 mm with pore diameter of 3 μm (Dr. Majsch GMBH, Germany) at a temperature of 30°C and a flow rate of 1.2 ml/min maintained by an LC-20ADsp liquid chromatograph (Shimadzu, Japan). The mobile phase consisted of 0.1 M citrate-phosphate buffer, 0.3 mM sodium octanesulfonate, 0.1 mM EDTA, and 9% acetonitrile (all reagents purchased from Sigma); pH 2.5. Decade II electrochemical detector (Antec Leyden, Netherlands) was equipped with a glassy carbon working electrode (+0.85 V) and an Ag/AgCl reference electrode. The peaks of biogenic amines and metabolites were identified according to their retention times in the standard solution. The content of the substances was evaluated by the internal standard method using the ratio between the peak areas in the standard solution and in the test sample using the LabSolutions software (Shimadzu, Japan).

Statistical analysis of the results was carried out using Student's t-test and the Statistica software package. $p \le 0.05$ was considered to be statistically significant.

RESULTS

Dopamine concentration in the mice striatum was decreased compared to the control values: down to 43.3% in the preclinical PD model and 20.1% in the model of the early clinical stage of PD (*Table*).

Meanwhile, the analysis of motor activity showed no differences in the total distance in the open-field test prior to MPTP or NaCl administration between the control and both study groups (*Table*). However, a 48.2% decrease in the total distance was observed in the model of the early clinical stage of PD compared to the control after MPTP administration (*Table*).

When modeling the preclinical stage of PD, the norepinephrine, dopamine, and serotonin levels in the eye decreased by an average of 37%, 29% and 26%, respectively, compared to the control. Furthermore, the *L*-DOPA level tended to go down ($p \le 0.12$) (*Fig. 1*). These changes were even more pronounced in the model of the early clinical stage of PD: the norepinephrine, dopamine, serotonin, and *L*-DOPA levels in the eye were reduced by 44%, 34%, 36%, and 40%, respectively, as compared to the control. Meanwhile, *L*-DOPA concentration in the eye was significantly lower in the mouse model of the early clinical stage of PD compared to that in the preclinical stage model (*Fig. 1*). In addition to the described biochemical changes, a small but statistically significant increase in IOP was revealed in mouse models of both stages of PD (*Fig. 2*).

An increased serotonin level was observed in mice eyelids in the models of both preclinical and early clinical stages of PD, with the level varying among the stages. A 3-fold increase in the serotonin level was observed at the preclinical stage, while an increase of approximately 56% was noted at the clinical stage (*Fig. 3*). However, the levels of dopamine and the precursor of serotonin, 5-HTP, in eyelids in both models of PD stages did not differ from the control values (*Fig. 3*).

Dopamine level in the striatum and the total distance in open-field test in the models of preclinical and early clinical stages of PD

Group		Dopamine level in the striatum	Total distance (open-field test)	
			prior to administration of MPTP/NaCl	after administration of MPTP/NaCl
		% of the control value		
Control (0.9% NaCl)		100 ± 2.0	100 ± 7.0	95.4 ± 8.8
PD model	at the preclinical stage (2×8 mg/kg MPTP)	43.3 ± 2.4*	101 ± 5.6	92.3 ± 6.8
	at the early clinical stage (4×10 mg/kg MPTP)	20.1 ± 2.5*	98 ± 6.1	51.8 ± 6.3*

* $p \le 0.05$ compared to the control.

DISCUSSION

Characterization of the experimental model of Parkinson's desease

An important feature of PD is that it has an estimated threshold of neurodegeneration at which motor symptoms occur, meaning the disease proceeds from the preclinical to the clinical stage. This threshold is equal to the death of 50–60% of the cell bodies of dopaminergic nigrostriatal neurons, 70–80% of their axons in the striatum, and loss of 70–80% of dopamine in the striatum in comparison to the control [1]. Since the death of axons of dopaminergic neurons in the striatum precedes the loss of the cell bodies of these neurons in the substantial nigra [1], the following key character-

istics of the experimental model of PD can be distinguished at different stages:

1. The preclinical stage is characterized by the absence of changes in the total distance in the open-field test, and a less than 70% decrease in the dopamine level in the striatum.

2. The early clinical stage is characterized by a decrease in the total distance in the open-field test and a more than 80% decrease in the dopamine level in the striatum.

We previously demonstrated a 56% reduction in the dopamine level in the striatum in a model of advanced preclinical stage of PD using two injections of MPTP at a single dose of 12 mg/kg; in the early clinical stage model of PD (four injections of MPTP at the same single dose), the dopamine level decreased by 75% compared with the control [22]. The MPTP doses used in this study for PD modeling in mice purchased from the Pushchino animal facility are slightly different from those we described earlier for animals from the Stolbovaya facility [22]. It is known that mice of the same line but obtained from different facilities may differ in sensitivity to MPTP [23]. Therefore, we additionally evaluated the aforementioned key characteristics of the model used in the study to make sure that it fully complied with the model described previously.

In the models of preclinical and clinical stages of PD, the dopamine level in the murine striatum was decreased by 57% and 80%, respectively (*Table*), in comparison to the control group; this finding almost completely coincides with the previously obtained data [22]. A 48% reduction in the total distance in the open-field test as compared to the control (*Table*) was found for the model of clinical stage of PD, which is similar to the motor dysfunctions observed in the previous study [22]. In addition, changes in motor activity for the animal model of preclinical stage of PD were noted neither in the present nor in the previous study (*Table*) [22].

Thus, the doses and schemes for MPTP administration used in this study completely reproduce the previously described mouse models of preclinical and early clinical stages of PD.

Changes in the metabolism of monoamines in eye tissues and physiological manifestations

The reduced content of monoamines (norepinephrine, dopamine and serotonin) detected in mouse eyes in the PD models of both early clinical and preclinical stages indicates that the systemic pathological processes developing in PD [2] spread to the eye and appear already at an early stage of PD, before motor symptoms emerge. These results are in good agreement with the published data stating that the dopamine level decreases in the retina of mice with MPTP-induced parkinsonism [24]. It

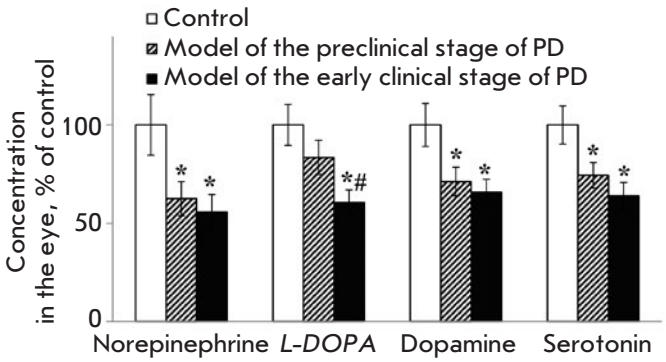

Fig. 1. Norepinephrine, *L*-DOPA, dopamine and serotonin concentrations in the mouse eye in the preclinical and clinical models of PD. * $p \leq 0.05$ in comparison to the control mice; # $p \leq 0.05$ in comparison to the preclinical model

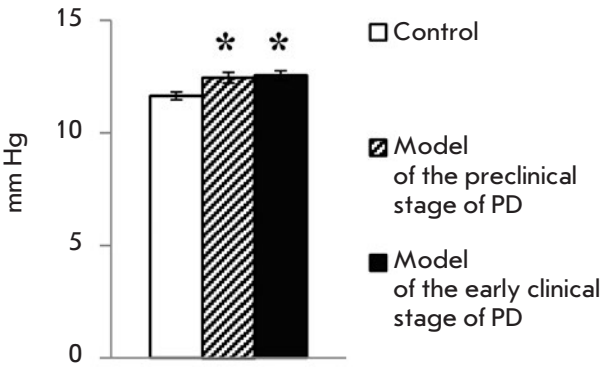

Fig. 2. Inctraocular pressure in the preclinical and clinical mouse models of PD. * $p \leq 0.05$ in comparison to the control mice

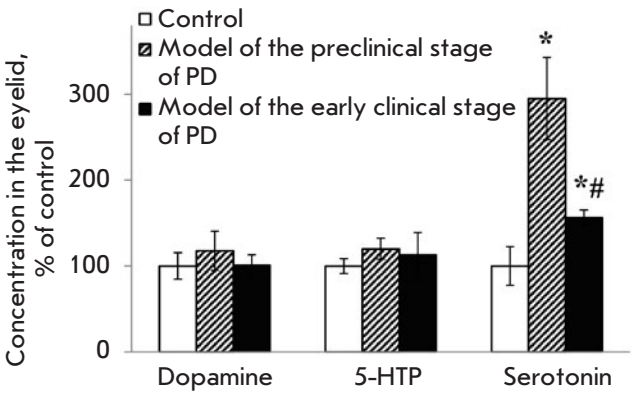

Fig. 3. Dopamine, 5-HTP and serotonin concentrations in the mouse eyelid in the preclinical and clinical models of PD. * $p \leq 0.05$ in comparison to the control mice; # $p \leq 0.05$ in comparison to the preclinical model

is interesting that no changes in the plasma level of norepinephrine as compared to the control were detected in the mouse models of both PD stages, unlike the situation with the norepinephrine level in the eyes [25]. This indicates that the decrease in the norepinephrine level in the eye in the PD model is region-specific.

Unlike the monoamine level, the *L*-DOPA concentration was reduced only at the clinical stage of PD. The absence of changes in the *L*-DOPA concentration at the preclinical stage of PD indicates that early pathological changes in the eye do not affect the metabolism of the key precursor of catecholamines.

Special attention should be given to the correlation between the decrease in dopamine levels in the striatum as a result of degradation of dopaminergic axons and in mouse eyes at the preclinical and clinical stages of PD, which indirectly confirms the systemic nature of PD pathogenesis. Dopamine level in these animals decreases not only in the striatum, but also in the substantia nigra, the area where the cell bodies of dopaminergic neurons are localized. However, neuronal degeneration in this brain area occurs in mice only at the clinical stage of PD [1, 22].

From a physiological point of view, it is of great interest that both stages of PD in mice are characterized by a slight but statistically significant increase in IOP ($p \leq 0.015$), indicating that functional disorders in the eye emerge prior to the occurrence of motor dysfunctions. It is quite likely that an increase in IOP may result from a reduced catecholamine level in eye tissues. Indeed, the IOP value depends on the rate of intraocular fluid secretion and outflow. Dopamine is involved in the regulation of these processes, as it interacts with the DA2 and DA3 receptors expressed in postganglionic sympathetic nerve endings and reduces the secretion of intraocular fluid, while the interaction between dopamine and the DA1 receptors localized in the ciliary body increases the secretion of intraocular fluid [19]. It is very likely that elevated intraocular pressure could be one of the earliest signs of PD in humans, and it's rather tempting to use this as a marker for early diagnosis. This possibility is indirectly confirmed by the increased incidence of glaucoma with elevated intraocular pressure in patients with PD compared to the age control [7].

It is yet impossible to understand whether the increase in IOP found in mouse models of PD is characteristic of patients, since this indicator in patients was assessed only at the advanced clinical stage after prolonged treatment with dopamine agonists [26]. In fact, in contrast to mice, the IOP level was reduced in patients. The final answer to the question of whether and how IOP is altered in PD patients can be obtained only after assessing this parameter in treatment-naïve patients at the early clinical stage of PD.

Changes in the metabolism of monoamines in eyelid tissues

The significant increase in serotonin level observed in the eyelid confirms its reportedly important role in the development of neuroinflammation in PD [27, 28]. There are two possible explanations for this increase. First, the synthesis of serotonin (mast cells being its source in the eyelid) [29] can increase under the influence of substance P, a neuroinflammation factor whose content rises in the central nervous system in PD [30, 31]. Second, the elevated serotonin level in the eyelid can be rooted in its impaired metabolism; for example, resulting from a reduced activity of N-acetyltransferase, the rate-limiting enzyme for the conversion of serotonin to melatonin. Indeed, a decrease in the activity of this enzyme is considered to be a risk factor for the development of PD [32].

Serotonin is involved in the regulation of the microcirculation of tear fluid and secretory activity of the lacrimal glands localized in the eye conjunctiva [33–36]. Therefore, a significant increase in the serotonin level in mouse eyelids can alter tear composition and cause pathological disturbances in its microcirculation [36], which can lead to the development of the dry eye symptom characteristic of PD [37, 38]. Hence, special attention should be given to an evaluation of tear fluid composition for the development of a preclinical diagnosis of PD. So far, only data on the increase in the TNF-α level in the tear fluid of PD patients are available [39]. Taking into account the important role played by serotonin in the regulation of tear fluid composition on the one hand and the significant difference in the serotonin level in mice eyelid between the models of preclinical and clinical stage of PD on the other hand, one can expect a significant variation in tear fluid composition in patients at preclinical and clinical stages. If this assumption is confirmed after the analysis of the tear fluid of mice in models of preclinical and clinical stages of PD, the changes in tear fluid composition at the preclinical stage could be considered as potential diagnostic markers of the early stage of PD.

Thus, neurotoxic modeling of the preclinical and clinical stages of PD in mice has revealed changes in the monoamine metabolism in the eye and eyelid. These changes are accompanied by an alteration of the functions of these structures and can be used as diagnostic markers of early PD, before the appearance of motor symptoms. ●

This work received financial support from the Program of the Presidium of the Russian Academy of Sciences № 41 "Basic Research for Biomedical Technologies" (project № 0108-2018-0014).

REFERENCES
1. Ugrumov M.V. // Korsakov Neurology and Psychiatry Journal. 2015. V. 11. P. 4-14.
2. Goldstein D.S. // Compr. Physiol. 2013. V. 3. P. 1569–1610.
3. Armstrong R.A. // J. Parkinsons Dis. 2015. V. 5. P. 715–726.
4. Archibald N.K., Clarke M.P., Mosimann U.P., Burn D.J. // Mov. Disord. 2011. V. 26. P. 2387–2395.
5. Nowacka B., Lubinski W., Honczarenko K., Potemkowski A., Safranow K. // Med. Sci. Monit. 2014. V. 20. P. 2243–2249.
6. Litvinenko I.V., Boiko A.V., Kulikov A.N., Dynin P.S., Trufanov A.G., Maltzev D.S., Yurin A.A. // Annals of Clinical and Experimental Neurology. 2016. V. 10. P. 11-16.
7. Chesnokova N.B., Pavlenko T.A., Ugrumov M.V. // Korsakov Neurology and Psychiatry Journal. 2017. V. 117. P. 124-131.
8. Nakahara T., Mori A., Kurauchi Y., Sakamoto K., Ishii K. // J. Pharmacol. Sci. 2013. V. 123. P. 79–84.
9. Dong F., An J.H., Ren Y.P., Yan D.S., Zhou X.T., Lü F., Hu D.N., Chen J.F., Qu J. // Zhonghua Yan Ke Za Zhi. 2007. V. 43. P. 1110–1113.
10. Ding C., Walcott B., Keyser K.T. // Invest. Ophthalmol. Vis. Sci. 2003. V. 44. P. 1513–1520.
11. Qi J.H., Li B.H. // Zhongguo Yao Li Xue Bao. 1992. V. 13. P. 153–156.
12. Hiromatsu S., Araie M., Fujimori K. // Jpn. J. Ophthalmol. 1994. V. 38. P. 123–128.
13. Firsov M.L., Astakhova L.A. // Neurosci. Behav. Physiol. 2016. V. 46. P. 138–145.
14. Lopatina E.V., Penniyaynen V.A., Tsyrline V.A. // Bull. Exp. Biol. Med. 2012. V. 153. P. 48–50.
15. Smith C.P., Sharma S., Steinle J.J. // Exp. Eye Res. 2007. V. 84. P. 75–81.
16. Okuda T., Tokutomi N., Tokutomi Y., Murai Y., Negi A., Nishi K. // Curr. Eye Res. 2001. V. 23. P. 455–462.
17. Wiederholt M., Schäfer R., Wagner U., Lepple-Wienhues A. // Ger. J. Ophthalmol. 1996. V. 5. P. 146–153.
18. Reitsamer H.A., Bogner B., Tockner B., Kiel J.W. // Invest. Ophthalmol. Vis. Sci. 2009. V. 50. P. 2301–2307.
19. Pescosolido N., Parisi F., Russo P., Buomprisco G., Nebbioso M. // Biomed. Res. Int. 2013. № 193048.
20. Dartt D.A., McCarthy D.M., Mercer H.J., Kessler T.L., Chung E.H., Zieske J.D. // Curr. Eye Res. 1995. V. 14. P. 993–1000.
21. Diebold Y., Ríos J.D., Hodges R.R., Rawe I., Dartt D.A. // Invest. Ophthalmol. Vis. Sci. 2001. V. 42. P. 2270–2282.
22. Ugrumov M.V., Khaindrava V.G., Kozina E.A., Kucheryanu V.G., Bocharov E.V., Kryzhanovsky G.N., Kudrin V.S., Narkevich V.B., Klodt P.M., Rayevsky K.S., Pronina T.S. // Neuroscience. 2011. V. 181. P. 175–188.
23. Jackson-Lewis V., Przedborski S. // Nat. Protoc. 2007. V. 2. P. 141–151.
24. Hamilton W.R., Trickler W.J., Robinson B.L., Paule M.G., Ali S.F. // Neurosci. Lett. 2012. V. 515. P. 107–110.
25. Kim A.R., Ugrumov M.V. // Proceedings of the Russian Academy of Sciences. 2015. V. 464. P. 494.
26. Nucci C., Martucci A., Cesareo M., Garaci F., Morrone L.A., Russo R., Corasaniti M.T., Bagetta G., Mancino R. // Prog. Brain Res. 2015. V. 221. P. 49–65.
27. Politis M., Niccolini F. // Behav. Brain Res. 2015. V. 277. P. 136–145.
28. Kempuraj D., Thangavel R., Selvakumar G., Zaheer S., Ahmed M., Raikwar S., Zahoor H., Saeed D., Natteru P., Iyer S., Zaheer A. // Front. Cell. Neurosci. 2017. V. 11. P. 216.
29. Conti P., Shaik-Dasthagirisaheb Y.B. // Neurotox. Res. 2015. V. 28. P. 147–153.
30. Thornton E., Vink R. // PLoS One. 2012. V. 7. № e34138.
31. Coleman J.W., Huang Q., Stanworth D.R. // Peptides. 1986. V. 7. P. 171–175.
32. Singh M., Khanna V.K., Shukla R., Parmar D. // Dis. Markers. 2010. V. 28. P. 87–93.
33. Turner H.C., Alvares L.J., Candia O.A., Bernstein A.M. // Curr. Eye Res. 2003. V. 27. P. 205–215.
34. Kirch W., Hornereber M., Tamm E.R. // Anat. Embryol. 1996. V. 193. P. 365–375.
35. Diebold Y., Rios J.D., Hodges R.R., Rawe I., Dartt D.A. // Invest. Ophthalmol. Vis. Sci. 2001. V. 42. P. 2270–2282.
36. Coman O.A., Savu O.R., Ghita I., Paunescu H., Coman L., Fulga I. // Oftalmologia. 2007. V. 51. P. 126–133.
37. Kwon O.Y., Kim S.H., Kim J.H., Kim M.H., Ko M.K. // J. Korean Med. Sci. 1994. V. 9. P. 239–242.
38. Chhadva P., Lee T., Sarantopoulos C., Hackam A., McClellan A., Felix E., Levitt R., Galor A. // Ophthalmology. 2015. V. 122. P. 1675–1680.
39. Çomoğlu S.S., Güven H., Acar M., Öztürk G., Koçer B. // Neurosci. Lett. 2013. V. 553. P. 63–67.

Whole-Genome Sequencing of Russian *Neisseria Gonorrhoeae* Isolates Related to ST 1407 Genogroup

A. A. Kubanov[1], A. V. Runina[1], A. V. Chestkov[1], A. V. Kudryavtseva[2], Y. A. Pekov[3], I. O. Korvigo[3], D. G. Deryabin[1*]

[1]State Research Centre of Dermatovenerology and Cosmetology, Korolenko Str., 3/6, Moscow, 107076, Russia

[2]Engelhardt Institute of Molecular Biology, Russian Academy of Sciences, Vavilova Str., 32, Moscow, 119991, Russia

[3]Ksivalue Data Analysis Studio, Leninsky Ave., 30A, Moscow, 117628, Russia

*E-mail: dgderyabin@yandex.ru

Received November 23, 2017; in final form June 27, 2018

ABSTRACT **The whole-genome sequencing data of three *N. gonorrhoeae* strains isolated in the Russian Federation in 2015 are presented. According to the NG-MAST protocol, these strains are related to the globally spread ST 1407 genogroup. The analysis of their resistomes showed the absence of *ermA/B/C/F* genes and the presence of wild-type alleles of *rpsE*, *rrs*, *rrl*, *rplD*, *rplV*, *macAB*, and *mefA* genes, and these patterns explain the susceptibility of the sequenced strains to aminocyclitols (spectinomycin) and macrolides (azithromycin). Conjugative resistance determinants (*blaTEM*, *tetM*) were absent in the genomes, and the *penC/pilQ*, *parE*, and *norM* alleles were shown to be wild-type, whereas single or multiple nucleotide substitutions were identified in the genes encoding targets for β-lactams (*ponA*, *penA*), tetracyclines (*rpsJ*), and fluoroquinolones (*gyrA*, *parC*). The additional mutations were found in *porB* gene and the promoter of *mtrR* gene, which nonspecifically reduced the susceptibility to antimicrobials due to the membrane permeability decrease and efflux pump overexpression. The diversity of mutations observed in the analyzed genomes prompted a revision of the phylogenetic relationships between the strains by comparing more than 790 groups of housekeeping genes. A high homology between the *N. gonorrhoeae* ST 1407 and *N. gonorrhoeae* ST 12556 genomes was confirmed; the latter had probably diverged from a common ancestor as a result of single mutation events. On the other hand, *N. gonorrhoeae* ST 12450 was an example of phenotypic convergence which appeared in the emergence of new drug resistance determinants that partially coincide with those of the ST 1407 genogroup.**

KEYWORDS *Neisseria gonorrhoeae*, **whole genome sequencing, genetic determinants of antimicrobial drug resistance, phylogenetic analysis.**

ABBREVIATIONS **MIC – minimal inhibitory concentration, MLST – multilocus sequence typing, NG-MAST – *Neisseria gonorrhoeae* multi-antigen sequence typing, PBP – penicillin-binding protein, QRDR – quinolone resistance-determining regions, ST – sequence type.**

INTRODUCTION

Gonorrhoea remains one of the four most widely spread sexually transmitted diseases. In 2012, its incidence among reproductive-age individuals reported by the WHO was 78.3 million new cases [1]. A total of 27,056 cases of gonococcal infection in 2015 in Russia, corresponding to 18.5 cases per 100,000, were reported [2]. Whereas in Russia these figures annually decrease by 10–20%, incidence of the infection worldwide continues to increase steadily.

The increase in gonorrhoea incidence is due to the appearance and spread of epidemic high-risk clones of *Neisseria gonorrhoeae* which possess multiple antibiotic resistance, including resistance to third-generation cephalosporins, the drugs of choice for treatment of the infection [3]. Currently, the genetic variant referred to ST 1407 [5] in accordance with the NG-MAST (*Neisseria gonorrhoeae* Multi-Antigen Sequence Typing) protocol [4] has gained much significance. By 2010, this sequence type had been reported in 20 out of 21 states of the European Union, accounting for over 10% of isolates in 13 EU states (including Austria, Belgium, Italy, the Netherlands, Portugal, Romania, Slovenia, Spain, and the UK) [6]. Genetic analysis revealed multiple antibiotic resistance determinants in *N. gonorrhoeae* ST 1407 [7], and that explains the increasing ineffectiveness of gonococcal infection therapy [3, 5].

The epidemic significance of ST 1407 is additionally determined by the existence of phylogenetically related molecular types of *N. gonorrhoeae* that are 99%

amino acid identical to *porB* or *tbpB* genes used for NG-MAST typing and are, therefore, considered to belong to the ST 1407 genogroup. Considering this, the percentage of *N. gonorrhoeae* isolates in the EU states is as high as 23% [6], while one of the representatives of this genogroup, ST 4378, is the predominant sequence type in Taiwan [8].

Cases of gonococcal infection caused by *N. gonorrhoeae* ST 1407 are sporadic in Russia, being reported in cities with intensive touristic (Moscow) or economic (Kaluga and Murmansk) migration from the EU states [9]. Earlier, we reported few potential representatives of the genogroup ST 1407 detected in Russia for the first time [10]. This study aimed to perform an in-depth genome characterization of these isolates using whole-genome sequencing, which has recently become a high-demanded tool for analyzing the molecular mechanisms of antibiotic resistance and phylogeny of pathogenic microorganisms.

MATERIALS AND METHODS

N. gonorrhoeae strains

Three *N. gonorrhoeae* strains as objects of the study were isolated from patients with a diagnosis of gonococcal infection of the lower genitourinary tract (ICD-10 diagnosis code A54.0) in 2015 and were deposited in a specialized collection of the State Research Center of Dermatovenereology and Cosmetology (Ministry of Health of the Russian Federation) with the identification codes 20/15/004, 41/15/003, and 19/15/005.

The *N. gonorrhoeae* strain 20/15/004 was isolated from a 41-year -old male patient in Kaluga; NG-MAST type referred to the epidemically high-risk genogroup ST 1407 (*porB* allele 908 and *tbpB* allele 110 according to the NG-MAST database nomenclature) [4]. *N. gonorrhoeae* strain 41/15/003 was obtained from a 19-year-old male patient in Tomsk and characterized as a novel sequence type ST 12556 carrying a previously unknown combination of six *tbpB* alleles and *porB* allele 971; the latter exhibited 99.97% homology with ST 1407. *N. gonorrhoeae* strain 19/15/005 was isolated from a 31-year-old female patient in Omsk and was also characterized as being a novel ST 12450 NG-MAST type with the combination of *porB* allele 931 and the previously unknown *tbpB* allele 2097 and with a 99.74% homology and with six other alleles of this gene described earlier. An analysis of these strains within sample consisting of 124 *N. gonorrhoeae* cultures conducted by comparing the fusion sequences of the *porB* and *tbpB* genes using the MEGA 6 (Molecular Evolutionary Genetics Analysis version 6.0) software [11] demonstrated that they belong to one genogroup of ST 1407 [10].

Table 1. Parameters of susceptibility of the analyzed *N. gonorrhoeae* strains to antimicrobials and their interpretation according to the Methodology Guidelines MUK 4.2.1890–04*

Antimicrobial (zones of susceptibility – S, moderate susceptibility – MS, and resistance – R; μg/ml)	MIC, μg/ml		
	20/15/004	41/15/003	19/15/005
Benzylpenicillin (S ⩽ 0.06; MS = 0.12–1; R ⩾ 2)	0.5 (MS)	2 (R)	1 (MS)
Ceftriaxone (S ⩽ 0.25; MS ⩾ 0.25)	0.015 (S)	0.03 (S)	0.015 (S)
Tetracycline (S ⩽ 0.25; MS = 0.5–1; R ⩾ 2)	2 (R)	4 (R)	2 (R)
Spectinomycin (S ⩽ 32; MS = 64; R ⩾ 128)	32 (S)	32 (S)	16 (S)
Azithromycin** (S ⩽ 0.25; MS = 0.5; R ⩾ 1)	0.25 (S)	0.5 (MS)	0.25 (S)
Ciprofloxacin (S ⩽ 0.06; MS = 0.12–0.5; R ⩾ 1)	16 (R)	8 (R)	16 (R)

*Methodology Guidelines MUK 4.2.1890–04. Determining Microorganism Susceptibility to Antibacterial Medications: Recommended Practices. Moscow: Federal Center of State Sanitary and Epidemiological Surveillance, Ministry of Health of the Russian Federation, 2004. P. 91.
**As the Methodology Guidelines MUK 4.2.1890–04 contains no criteria for azithromycin susceptibility, the evaluation was carried out using the criteria of the European Committee for Antimicrobial Susceptibility Testing (www.eucast.org)

An analysis of the susceptibility of the studied strains to six antimicrobials previously or currently recommended for the treatment of gonococcal infection showed either resistance or moderate susceptibility of the strains to benzylpenicillin, tetracycline, and ciprofloxacin. *N. gonorrhoeae* 41/15/003 was additionally characterized by moderate susceptibility to azithromycin (*Table 1*).

Sequencing of the *N. gonorrhoeae* genome

The genomic DNA was isolated from *N. gonorrhoeae* 1-colony cultures on chocolate agar supplemented with 1% ISOVitalex additive (Becton Dickinson, USA) incubated during 18–24 h using a PROBA-NK kit (DN-Technology, Russia). A library of random DNA fragments 400–700 bp long was prepared using the standard GS Rapid Library protocol. The libraries were amplified in emulsion PCR using GS Junior emPCR kit. Whole-genome sequencing was carried out by the 454

pyrosequencing technology on a GS Junior system (Roche, Switzerland). Each genome was sequenced using CS Junior Titanium Sequencing Kit in an individual sequencing run. The mean coverage of genomes was ≥ 20.

Bioinformatic analysis methods

FastQC and Trimmomatic was used for the quality control and trimming. Remaining reads were assembled using Spades. Assembled *N. gonorrhoeae* genomes were annotated using Prokka [12], employing the Swiss-Prot (high-priority species-level references) and UniProt-KB (genus-level references) datasets of amino acid sequences. Prior to annotation, the UniProt-KB dataset was clustered using CD-HIT [13], with 90% identity of protein length and amino acid sequences. Ribosomal RNA genes were annotated using Barrnap (https://github.com/tseemann/barrnap). Aragorn was used to annotate tRNAs. IslandViewer 4 [14] was used to detect genomic islands.

The search for the genetic determinants of antibiotic resistance in *N. gonorrhoeae* was performed by RGI analysis in the Comprehensive Antibiotic Resistance Database (CARD) [15].

The NGMASTER software was employed for NG-MAST sequence typing of *N. gonorrhoeae* [16]; multilocus MLST sequence typing was performed using the SRST2 software [17]. Orthologous protein groups belonging to the genus *Neisseria* were inferred by OrthoFinder [18] from annotated protein sequences of the analyzed isolates and 24 previously sequenced *N. gonorrhoeae* strains, as well as NCBI reference annotations of *N. meningitidis*, *N. lactamica* and *N. elongata*. Each of the 790 selected orthologous groups was subjected to multiple sequence alignment using MAFFT [19] with 2,000 refinement iterations. Each alignment was masked using Gblocks. Masked and concatenated alignments were used to infer a maximum likelihood phylogenetic tree of *N. gonorrhoeae* in RAxML [20] with 500 bootstrap replicates. The FigTree graphical viewer was used to visualize the tree with projected support values (http://tree.bio.ed.ac.uk/software/figtree/).

In order to characterize the overall evolution of the coding sequences and the sequences associated with the formation of antimicrobial resistance, we formed two sets of concatenated multiple sequence alignments of the corresponding orthogroups and calculated the *p*-distance within each set. Matching between the cells of two resulting matrices was estimated using the Spearman's rank correlation coefficient.

Table 2. Overall characteristics of the genomes of the analyzed *N. gonorrhoeae* strains

Characteristics	Strains		
	20/15/004	41/15/003	19/15/005
Genome size, bp	2271213	2236575	2223815
G+C content, %	52.6	52.5	52.7
Number of protein-coding genes	2448	2297	2293
Number of protein-coding genes with known function	1332	1266	1281
Number of the 16S-23S-5S rRNA genes	4	4	4
Number of tRNA genes	49	49	47
Number of tmRNA genes	1	1	1
Number of "genomic islands" along the bacterial chromosome	12	22	17
Plasmid size, bp	4556	5233	5266
Plasmid coverage depth to chromosome coverage depth	18.4	12.3	33.6

RESULTS AND DISCUSSION

Overall characterization of the *N. gonorrhoeae* genomes

The assembly of the genome sequences of the studied *N. gonorrhoeae* strains revealed a circular chromosome 2,223,815 to 2,271,213 bp long with G+C content of 52.5–52.7% in each genome (*Table 2*).

The total number of identified open reading frames was 2,448 (*N. gonorrhoeae* 20/15/004), 2,297 (*N. gonorrhoeae* 41/15/003), and 2,293 (*N. gonorrhoeae* 19/15/005). Among the genes, 1,332 (54.4%), 1,266 (55.1%), and 1,281 (55.9%) open reading frames were annotated as protein-coding genes with the known function, respectively.

Each of the analyzed genomes was found to contain 49 (*N. gonorrhoeae* 20/15/004 and *N. gonorrhoeae* 41/15/003) or 47 (*N. gonorrhoeae* 19/15/005) tRNA genes, one tmRNA gene, and four copies of 16S-23S-5S rRNA operon.

Cryptic plasmids varying in length from 4,556 (*N. gonorrhoeae* 20/15/004) to 5,266 bp (*N. gonorrhoeae* 19/15/005), carrying the relaxosome gene *MobC* (typical of conjugative plasmids), genes of the cryptic plasmid proteins A, B, and C, and five open reading frames with unknown functions were identified for each strain. The rate of mean plasmid coverage to the mean chromosome coverage in 20/15/004 and 41/15/003 strains yielded 18.4 and 12.3, respectively, versus 33.6 in 19/15/005 strain, thus characterizing the revealed plasmids to be present in multiple copies (> 10 copies per cell).

In general, the first stage of bioinformatic analysis revealed the analyzed genomes to be similar to those of

Table 3. Genetic determinants of antimicrobial resistance in *N. gonorrhoeae*

Genes (proteins)	Resistance to antimicrobials	Genes and nucleotide polymorphisms (amino acid substitutions)		
		20/15/004	41/15/003	19/15/005
Enzymes responsible for inactivation of antibiotics or modification of their targets				
blaTEM (β-lactamase)	β-lactams	-	-	-
ermA/B/C/F (rRNA methylases)	macrolides	-	-	-
Proteins targeting antibiotics				
ponA (PBP_1)	β-lactams	L421P	L421P	L421P
penA (PBP_2)	β-lactams	I312M V316T F504L N512Y G545S	I312M V316T F504L N512Y G545S	F504L P551S
tetM	tetracyclines	-	-	-
rpsJ (S10)	tetracyclines	V57M	V57M	V57M
rpsE (S5)	spectinomycin	wt	wt	wt
rrs (16S RNA)	spectinomycin	wt	wt	wt
rrl (23S RNA)	macrolides	wt	wt	wt
rplD (L4)	macrolides	wt	wt	wt
rplV (L22)	macrolides	wt	wt	wt
gyrA	fluoroquinolones	S91F D95G	S91F D95G	S91F D95G
parC	fluoroquinolones	S87R E91A	S87R E91A	wt
parE	fluoroquinolones	wt	wt	wt
Transport proteins delivering antibiotics into the cell				
penB /porB (PorB1b)	β-lactams tetracyclines	G120K A121N	G120K A121N	G120D
penC/pilQ	β-lactams	wt	wt	wt
Enzymatic antibiotic efflux systems				
mtrCDE	β-lactams tetracyclines macrolides	wt	wt	wt
mtrRpro		A35del	A35del	wt
macAB	macrolides	wt	wt	wt
macABpro		wt	wt	wt
mefA	macrolides	wt	wt	wt
norM	fluoroquinolones	wt	wt	wt
norMpro		wt	wt	wt

Note: "-" – the gene was not found; "wt" – wild-type sequence.

the reference FA1090 (GenBank: AE004969) and some other previously sequenced *N. gonorrhoeae* strains [21], including those of the ST 1407 genogroup [22]. A degree of quantitative variations between the compared genomes could be caused by the high genome plasticity conventionally attributed to the presence of prophages, transposons, and the insertion sequence elements IS110 and IS1016 [23], which were revealed within genomic islands in all three *N. gonorrhoeae* strains in a substantially high amount (*Table 2*).

The sequences of the *de novo* assembled genomes were deposited into the GenBank NCBI database with IDs NTCT00000000 (*N. gonorrhoeae* 20/15/004), NTCS00000000 (*N. gonorrhoeae* 41/15/003), and NTCU00000000 (*N. gonorrhoeae* 19/15/005).

Genetic determinants of antimicrobial resistance in *N. gonorrhoeae*

The next step in the bioinformatic analysis involved finding and studying four groups of genes encoding 1) the enzymes responsible for the inactivation of antibiotics or the modification of their targets, 2) the protein targets with mutations reducing their affinity for the respective antimicrobials, 3) the transport proteins delivering antibiotics into bacterial cell, and 4) the antibiotic efflux systems (*Table 3*).

Resistance determinants for β-lactams (penicillins and cephalosporins)

In the analyzed *N. gonorrhoeae* sequences, the results didn't reveal both *blaTEM-1* or *blaTEM-135* genes encoding the β-lactamase enzyme, which hydrolyzes the lactam ring in the penicillin molecule and other antimicrobials with a similar structure [24].

On the other hand, the sequences of chromosomal genes encoding penicillin binding proteins (PBPs) were found to carry a number of nucleotide substitutions that significantly reduce susceptibility to β-lactams. Thus, all three strains carried the mutation L421P in *ponA* gene encoding PBP_1, resulting in reduced affinity to penicillins compared to the wild-type protein [25]. Even greater changes were detected in the *N. gonorrhoeae* 20/15/004 and *N. gonorrhoeae* 41/15/003 *penA* gene sequences (encoding PBP_2), reflecting the concept of mosaic-like structure formed due to a genetic recombination with synanthropic commensals, such as *N. cinerea* and *N. perflava* [26]. More amino acid substitutions, namely F504L, N512Y, and G545S, were found in the C-terminal region of PBP_2, and they significantly reduced the binding rate between the peptidyl transferase center and the antimicrobial molecule imparing functionally important conformational changes [27]. Moreover, two other amino acid substitutions, I312M and V316T, are considered to be associated with the formation of cephalosporin resistance, especially in combination with the G545S substitution [28]. On behalf of this, two amino acid substitutions, F504L and P551S, which reduce the level of acylation of PBP_2, as much as other known mutations in the C-terminal region of this protein characterizing the *penA* allele in *N. gonorrhoeae* 19/15/005 [29].

The *penB* gene encoding the outer membrane porin PorB1b and currently denoted as *porB*, is also involved in the emergence of resistance to β-lactams in *N. gonorrhoeae*. The amino acid substitutions G120K and A121N in this protein reducing membrane permeability for hydrophilic antibiotics [30] were detected in *N. gonorrhoeae* 20/15/004 and *N. gonorrhoeae* 41/15/003, whereas the *N. gonorrhoeae* 19/15/005 strain carried a single G120D substitution.

The *pilQ* gene (previously known as *penC*) is another studied gene attributed to the resistance to β-lactams and other hydrophilic antibiotics in *N. gonorrhoeae*. The additional pores formed in the outer membrane by the product of this gene enable antibiotic diffusion into the periplasmic space of the bacterial cell. Mutation in the triplet 666(Gly) or complete deletion of *pilQ* gene can increase the level of antibiotic resistance in *N. gonorrhoeae*, especially when accompanied with the resistance determinants in the *penA* and *penB* genes [31]. However, this gene was wild-type in the analyzed genomes.

To finalize the analysis of the resistance determinants to β-lactams in *N. gonorrhoeae*, we must point out the three tangled genes present in all the analyzed strains. These genes lie within the multiple transferable resistance (Mtr) locus controlled by the MtrR repressor and encode the MtrC-MtrD-MtrE efflux pump system. The analysis of the *mtrR* promoter region revealed deletion A35del, which ensured elimination of this repression, together with an increase in antibiotic resistance [32]. This mutation was found in the *N. gonorrhoeae* strain 20/15/004 (ST 1407) and in the structurally related *N. gonorrhoeae* strain 41/15/003 (ST 12556) with a similar structure of *porB* gene. This is in accordance with the hypothesis that gonococci of the 1407 NG-MAST genogroup possess the above discussed mechanism of antibiotic resistance [5].

Tetracycline resistance determinants

A point mutation causing the amino acid substitution V57M in ribosomal protein S10 of the 30S ribosomal subunit was found in the chromosomal *rpsJ* gene in all three analyzed genomes. This substitution disrupts binding of the antimicrobial to ribosome and allows one to concider this as the mechanism underlying the resistance to tetracyclines in *N. gonorrhoeae* [33].

On the other hand, the genomes of the three analyzed strains were found to carry no Dutch or American variants of *tetM* gene [34]; the protein products of the variants interfere with the elongation factors EF-G and EF-Tu and make the ribosome inaccessible for interaction with the antimicrobial.

In turn, the nonspecific mechanisms of resistance to tetracyclines (identically to β-lactams) in the analyzed strains involved mutations in PorB1b protein and MtrC-MtrD-MtrE efflux system, which is an effective supplement to the specific resistance mechanism caused by a mutation in *rpsJ* gene [33].

Spectinomycin resistance determinants

The nucleotide sequence in *rrs* gene matched the sequence of a wild-type gene with cytosine at position 1186 (corresponding to position 1192 in *Escherichia coli*); this is the key nucleotide in the binding site for the interaction of aminocyclitols with helix 34 of 16S RNA [35].

Another analyzed chromosomal determinant was *rpsE* gene, which encodes the ribosomal protein S5 of 30S ribosomal subunit; mutations in this protein can cause spectinomycin resistance, although *rrs* gene remains to be wild-type. However, searching for the possible amino acid substitutions T24P [36] and K28E, as well as for deletion of codon 27 (Val) [37], confirmed the wild-type allele of *rpsE* gene.

Macrolide resistance determinants

Neither of the analyzed genomes contained *ermA/B/C/F* gene cluster, which codes rRNA methylases modifying the macrolide binding sites of the 23S rRNA molecule.

The results of the search for A2059G and C2611T mutations in *rrl* gene, which disrupt the interaction between macrolide antibiotics and their target (the peptidyl transferase center) in domain V of 23rRNA [38], indicate that all three strains were wild-type.

The products of the *rplD* and *rplV* genes (ribosomal proteins L4 and L22) that bind to domain I of 23S rRNA and likewise have multiple binding sites for the other domains of 23S rRNA, were also wild-type. Mutations in the L4 and L22 proteins alter the conformation of domains II, III, and V; this may affect the susceptibility of microorganisms to macrolides [39].

The analysis of *N. gonorrhoeae* resistance to macrolides revealed that all the three genomes possess functional alleles of the *macA* and *macB* genes encoding the MacA–MacB complex, which specifically recognizes and removes the antimicrobial from the periplasm of bacterial cells [40]. However, an analysis of position -10 of promoters of these genes characterized them as wild-type without efflux pump overexpression. The *mefA* gene encoding another transport protein responsible for macrolide resistance [41] was also wild-type in the studied genomes.

Fluoroquinolone resistance determinants

The search for chromosomal mutations defining fluoroquinolone resistance in *N. gonorrhoeae* included the analysis of quinolone resistance-determining regions (QRDRs) in the *gyrA*, *parC*, and *parE* genes encoding DNA gyrase subunit A, as well as the topoisomerase IV subunits C and E, the fluoroquinolone targets.

In the all three strains, *gyrA* gene was found to contain single-nucleotide polymorphisms TCC → TTC and GAC → GGC causing the S91F and D95G amino acid substitutions associated with fluoroquinolone resistance in *N. gonorrhoeae* [42].

The *parC* gene in *N. gonorrhoeae* 20/15/004 and *N. gonorrhoeae* 41/15/003 possessed wild-type triplets (86(D) and 88(S)), indicating a double mutation with S87R and E91A amino acid substitutions. This mutation, together with the changes in DNA gyrase, significantly modified the structure of the so-called quinolone-binding pocket [43], making impossible the interaction between the antimicrobial and the target. The analysis of all four amino acid substitutions demonstrated the presence of the wild-type *parC* gene in the genome of *N. gonorrhoeae* 19/15/005. Wild-type *parE* gene was present in all the analyzed *N. gonorrhoeae* trains.

Characterization of the nonspecific mechanism of fluoroquinolone resistance in *N. gonorrhoeae* revealed that each of the studied genomes contained one functional copy of the *norM* gene encoding the membrane transporter that removes cationic antimicrobials from the bacterial cell [44]. Also, the promoter region at position -35 was wild-type, suggesting no additional efflux pump overexpression.

Molecular typing and phylogenetic analysis of *N. gonorrhoeae*

The variation of antibiotic resistance determinants in the studied genomes of *N. gonorrhoeae* strains required a revision of their phylogenetic relationship. In this regard, we used a combination of NG-MAST and multilocus sequence typing (MLST) results to plot a dendrogram comparing the entire set of housekeeping genes.

The findings of the sequenced genomes analysis using the NGMASTER software [16] revealed a complete coincidence with the initial data referring the analyzed strains to the genogroups ST 1407, ST 12556, and ST 12450 (*Table 4*).

Furthermore, the SRST2 analysis [17] of the nucleotide sequences of conserved *abcZ*, *adk*, *aroE*, *fumC*, *gdh*, *pdhC*, and *pgm* genes [45] revealed *N. gonorrhoeae* strains 20/15/004 and 41/15/003 to refer to the MLST type 1901, which relates to the epidemic high-risk ST 1407 according to the NG-MAST sequence typing data [5]. On the other hand, four of seven alleles of N. gonorrhoeae 19/15/005 characterized this strain as the MLST type 6721. This has never been mentioned in publications concerning antimicrobial resistance, and the phylogenetic relation with ST 1407 has never been described.

Table 4. Results of molecular mapping of *N. gonorrhoeae*

Genes and the encoded molecular types (NG-MAST and MLST)	Sequence types and numbers of alleles of *N. gonorrhoeae* strains		
	20/15/004	41/15/003	19/15/005
NG-MAST	**1407**	**12556**	**12450**
porB	908	971	931
tbpB	110	6	2097
MLST	**1901**	**1901**	**6721**
abcZ	109	109	126
adk	39	39	39
aroE	170	170	67
fumC	111	111	111
gdh	148	148	146
pdhC	153	153	153
pgm	65	65	133

The phylogenetic relationship between the strains were evaluated by comparing the entire set of 790 orthologous groups of housekeeping genes in *Neisseriaceae* family members. We used additional data from the NCBI database on the genomes of the *N. meningitidis* and 24 *N. gonorrhoeae* strains, including the reference strain FA 19, five previously sequenced ST 1407 strains, and 18 strains of other NG-MAST types. *Figure* shows the phylogenetic tree designed by maximum likelihood estimation using the RAxML program [20] (the Gamma substitution model in combination with the BLOSUM62 scoring matrix). In order to assess the relation between the evolution of neutral coding sequences and the sequences involved in the formation of antibiotic resistance, we compared this phylogenetic tree to the dendrogram plotted for the orthologous groups associated with antimicrobial resistance.

The resulting data show an extremely high genotype likelihood between the strains 20/15/004 (ST 1407) and 41/15/003 (ST 12556), according to the set of housekeeping genes combined to a single cluster with the other previously sequenced representatives of the genogroups ST 1407, ST 6146, and ST 3520. Hence, the results of the study confirmed the hypothesis of a close phylogenetic relation between the analyzed strains. The first strain emerged in the population of *N. gonorrhoeae* in Russia after putative international migration, while the other one has diverged from their common ancestor as a result of single mutation events. On the other hand, the third analyzed strain, 19/15/005 (ST 12450), was substantially distant from the ST 1407 genogroup on the phylogenetic tree of housekeeping genes and exhibited no close genotypic relation to any of the formed genogroups. Therefore, there was a prominent discordance between the primary molecular typing data and the results of whole-genome sequencing of this strain, indicating that antibiotic-resistant strains in the current Russian *N. gonorrhoeae* population are polyphyletic.

Comparison of the concatenated multiple alignments of neutral coding sequences and sequences associated with the formation of antimicrobial resistance revealed a statistically significant ($p < 0.001$) positive correlation (the Pearson's correlation coefficient = 0.44). In particular, this correlation was demonstrated for representatives of genogroup ST 1407 (including 20/15/004 and 41/15/003 strains), except for ST 3520. The latter sequence type was also an isolate characterized by a mosaic structure of *penA* gene [46] but with probably its own independently developed mechanisms of antimicrobial resistance. The analysis of *N. gonorrhoeae* 19/15/005 (ST 12450) has confirmed the relatively independent phylogenetic position of this strain.

CONCLUSIONS

Whole-genome sequencing of three *N. gonorrhoeae* strains isolated in Russia in 2015 was performed [10]. According to the NG-MAST results, these strains possess multiple antimicrobial resistance and preliminarily were referred to the epidemic high-risk genogroup ST 1407, spread currently worldwide [6, 8].

The analysis of the genomes revealed that they essentially pertain to the reference *N. gonorrhoeae* strain FA1090 [21] and previously sequenced representatives of the ST 1407 genogroup [22]. The revealed absence of *ermA/B/C/F* genes and presence of wild-type alleles of the *rpsE*, *rrs*, *rrl*, *rplD*, *rplV*, *macAB*, and *mefA* genes explain the susceptibility of the studied strains to certain groups of antimicrobials, as mutations in these genes are associated with the emergence of resistance to aminocyclitols (spectinomycin) and macrolides (azithromycin). However, the conjugative resistance determinants (*blaTEM, tetM*) were absent in the genomes and the *penC/pilQ*, *parE,* and *norM* alleles were shown to be wild-type, whereas single or multiple nucleotide substitutions were identified in the genes encoding targets for β-lactams (*ponA, penA*), tetracyclines (*rpsJ*), and fluoroquinolones (*gyrA, parC*). The additional mutations were found in *porB* gene and the promoter of *mtrR* gene and, therefore, they nonspecifically reduced the susceptibility to antimicrobials due to membrane permeability decreasing and efflux pump overexpression. Hence, the findings in the results of the whole-genome sequencing coincide with the preliminary results of the phenotypic analysis. The analysis of genetic resistance determinants allowed us to predict susceptibility or resistance to certain antimicrobial groups, but no MIC values could be inferred from these data. In particular, although the genotypes of the *N. gonorrhoeae* strains 20/15/004 (ST 1407) and 41/15/003 (ST12556) are similar, the increased resistance of the latter from 2 up to 4-fold to penicillin, ceftriaxone, tetracycline, and azithromycin remains unexplained. Otherwise, the different mutation spectra of the genes involved in emergence of antimicrobial resistance in *N. gonorrhoeae* 20/15/004 (ST 1407) and 19/15/005 (ST 12450) resulted in similar parameters of antimicrobial resistance. This indicates the importance of the search for additional mechanisms of antimicrobial resistance in *N. gonorrhoeae* and developing computer algorithms to ensure sufficient consistency between the results of genotypic and phenotypic analyses [47].

Another important result of this study was the revision of the phylogenetic association of the analyzed clinical isolates, compared to initially formulated findings acording to the NG-MAST data. This study has confirmed a high homology between the *N. gonorrhoeae* 20/15/004 (ST 1407) and *N. gonorrhoeae* 41/15/003

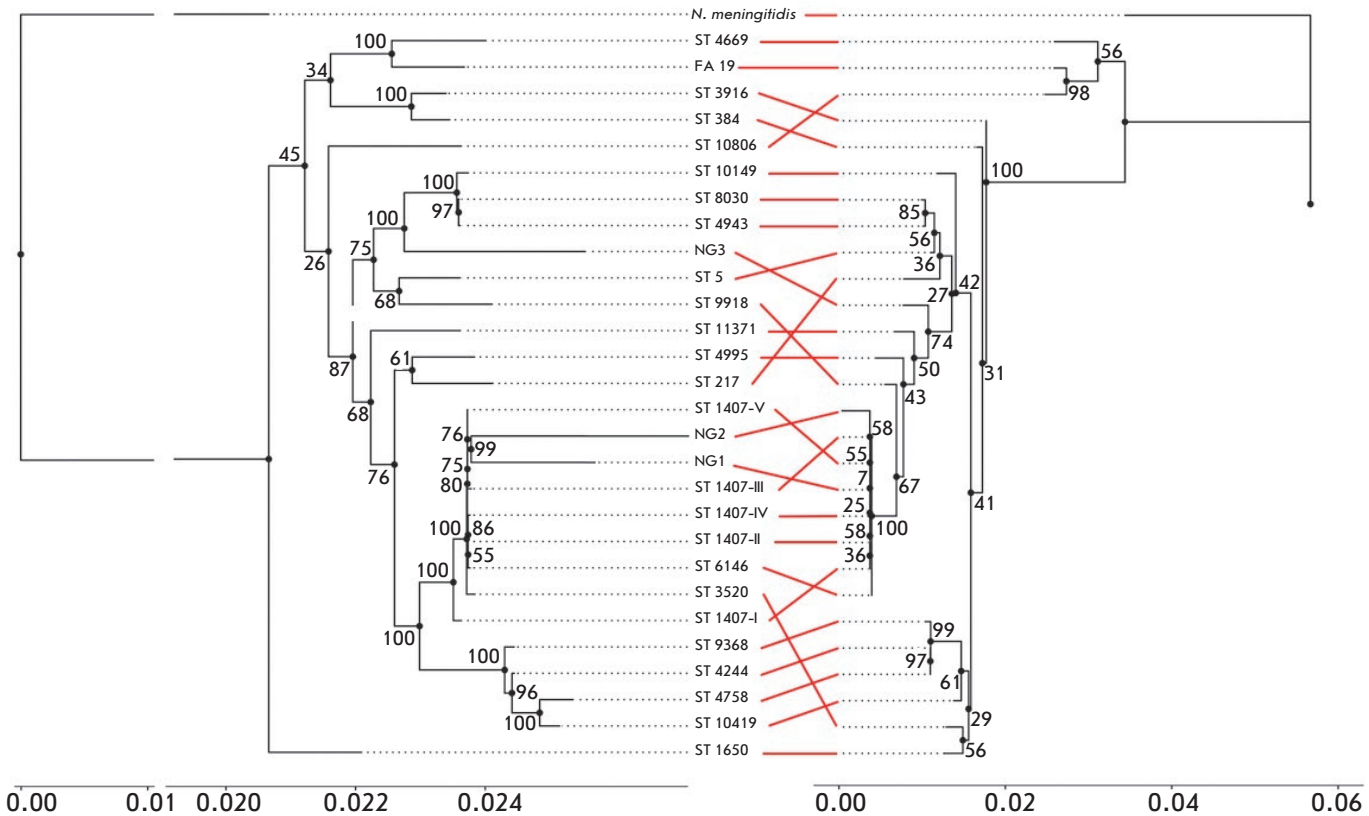

Phylogenic mapping of the analyzed isolates (NG1 = 20/15/004; NG2 = 41/15/003; NG3 = 19/15/005) referring to the other *N. gonorrhoeae* strains studied previously. Phylogenic mapping was performed by comparing the housekeeping genes (left-hand side) and orthologous groups related to the emergence of antimicrobial resistance (right-hand side). The correspondence of genome numbering in the NCBI database: ST 1407-I = SRR3349203; ST 1407-II = SRR3349826; ST 1407-III = SRR3357181; ST 1407-IV = SRR3357194; ST 1407-V = PMC3486552; ST 5 = SRR3349550; ST 217 = SRR3349568; ST 384 = SRR3350138; ST 1650 = SRR3343502; ST 3520 = SRR3357021; ST 3916 = SRR3343568; ST 4244 = SRR3350168; ST 4669 = SRR1661263; ST 4758 = SRR3343553; ST 4943 = SRR3349831; ST 4995 = SRR3349564; ST 6146 = SRR3349969; ST 8030 = SRR3349209; ST 9368 = SRR2736298; ST 9918 = SRR3349572; ST 10149 = SRR3349522; ST 10419 = SRR3343607; ST 10806 = SRR3349206; ST 11371 = SRR3349525.
The length of the branches of the phylogenetic tree (X axis) corresponds to the number of expected amino acid substitutions per position. The values at branch nodes represent the level of branch support. Red lines connect the homonymous branches

(ST 12556) genomes; the latter probably diverged in Russia from a representative of the internationally spread ST 1407 clone. On the other hand, *N. gonorrhoeae* strain 19/15/005 (ST 12450) was an example of phenotypic and genotypic convergence with independent formation of antimicrobial resistance by its own, although partially similar, mechanisms. This result indicates the antibiotic resistant strains in the population of *N. gonorrhoeae* in Russia as being polyphyletic, and this give reasons for further research in order to identify and consider an expanded list of epidemic high-risk genotypes. ●

REFERENCES

1. Newman L., Rowley J., Vander Hoorn S., Wijesooriya N.S., Unemo M., Low N., Stevens G., Gottlieb S., Kiarie J., Temmerman M. // PLoS One. 2015. V. 10. e0143304.
2. Kubanova A.A., Kubanov A.A., Melekhina L.E., Bogdanova E.V. // Vestnik dermatologii i venerologii. 2016. № 3. P. 12–28.
3. Ohnishi M., Golparian D., Shimuta K., Saika T., Hoshina S., Iwasaku K., Nakayama S., Kitawaki J., Unemo M. // Anti-

microb. Agents Chemother. 2011. V. 55. № 7. P. 3538–3545.
4. European centre for disease prevention and control. Molecular typing of *Neisseria gonorrhoeae* – results from a pilot study 2010–2011. 2012. Stockholm. ECDC.
5. Unemo M., Golparian D., Stary A., Eigentler A. // Euro Surveill. 2011. V. 16. № 43. Pii. 19998.
6. Chisholm S.A., Unemo M., Quaye N., Johansson E., Cole M.J., Ison C.A., van de Laar M.J. // Euro Surveill. 2013. V. 18. № 3. Pii. 20358.
7. Unemo M. // BMC Infect. Dis. 2015. V. 15. P. 364.
8. Chen C.C., Yen M.Y., Wong W.W., Li L.H., Huang Y.L., Chen K.W., Li S.Y. // J. Antimicrob. Chemother. 2013. V. 68. № 7. P. 1567–1571.
9. Vorobyev D.V., Solomka V.S., Plakhova X.I., Deryabin D.G., Kubanov A.A // Journal of Microbiology, Epidemiology and Immunobiology. 2016. № 4. P. 42–50.
10. Kubanov A., Vorobyev D., Chestkov A., Leinsoo A., Shaskolskiy B., Dementieva E., Solomka V., Plakhova X., Gryadunov D., Deryabin D. // BMC Infect. Dis. 2016. V. 16. P. 389.
11. Tamura K., Stecher G., Peterson D., Filipski A., Kumar S. // Mol. Biol. Evol. 2013. V. 30. № 12. P. 2725–2729.
12. Seemann T. // Bioinformatics. 2014. V. 30. № 14. P. 2068–2069.
13. Fu L., Niu B., Zhu Z., Wu S., Li W. // Bioinformatics. 2012. V. 28. № 23. P. 3150–3152.
14. Bertelli C., Laird M.R., Williams K.P., Lau B.Y., Hoad G., Winsor G.L., Brinkman F.S. // Nucl. Acids Res. 2017. V. 45. W30–W35.
15. McArthur A.G., Waglechner N., Nizam F., Yan A., Azad M.A., Baylay A.J., Bhullar K., Canova M.J., De Pascale G., Ejim L., et al. // Antimicrob. Agents Chemother. 2013. V. 57. № 7. P. 3348–3357.
16. Kwong J.C., Gonçalves da Silva A., Dyet K., Williamson D.A., Stinear T.P., Howden B.P., Seemann T. // Microb. Genom. 2016. V. 2. № 8. e000076.
17. Inouye M., Dashnow H., Raven L.A., Schultz M.B., Pope B.J., Tomita T., Zobel J., Holt K.E. // Genome Med. 2014. V. 6. № 11. P. 90.
18. Emms D.M., Kelly S. // Genome Biol. 2015. V. 16. № 1. P. 157.
19. Katoh K., Standley D.M. // Mol. Biol. Evol. 2013. V. 30. № 4. P. 772–780.
20. Stamatakis A. // Bioinformatics. 2014. V. 30. № 9. P. 1312–1313.
21. Abrams A.J., Trees D.L., Nicholas R.A. // Genome Announc. 2015. V. 3. № 5. e01052–15.
22. Anselmo A., Ciammaruconi A., Carannante A., Neri A., Fazio C., Fortunato A., Palozzi A.M., Vacca P., Fillo S., Lista F., et al. // Genome Announc. 2015. V. 3. № 4. e00903–15.
23. Bodoev I.N., Ilina E.N. // Molecular Genetics, Microbiology and Virology. 2015. V. 33. № 3. P. 22–27.
24. Muhammad I., Golparian D., Dillon J.A., Johansson A., Ohnishi M., Sethi S., Chen S.C., Nakayama S., Sundqvist M., Bala M., et al. // BMC Infect. Dis. 2014. V. 14. P. 454.
25. Ropp P.A., Hu M., Olesky M., Nicholas R.A. // Antimicrob. Agents Chemother. 2002. V. 46. № 3. P. 769–777.
26. Ameyama S., Onodera S., Takahata M., Minami S., Maki N., Endo K., Goto H., Suzuki H., Oishi Y. // Antimicrob. Agents Chemother. 2002. V. 46. № 12. P. 3744–3749.
27. Takahata S., Senju N., Osaki Y., Yoshida T., Ida T. // Antimicrob. Agents Chemother. 2006. V. 50. № 11. P. 3638–3645.
28. Tomberg J., Unemo M., Davies C., Nicholas R.A. // Biochemistry. 2010. V. 49. № 37. P. 8062–8070.
29. Powell A.J., Tomberg J., Deacon A.M., Nicholas R.A., Davies C. // J. Biol. Chem. 2009. V. 284. № 2. P. 1202–1212.
30. Olesky M., Zhao S., Rosenberg R.L., Nicholas R.A. // J. Bacteriol. 2006. V. 188. № 7. P. 2300–2308.
31. Helm R.A., Barnhart M.M., Seifert H.S. // J. Bacteriol. 2007. V. 189. № 8. P. 3198–3207.
32. Veal W.L., Nicholas R.A., Shafer W.M. // J. Bacteriol. 2002. V. 184. № 20. P. 5619–5624.
33. Hu M., Nandi S., Davies C., Nicholas R.A. // Antimicrob. Agents Chemother. 2005. V. 49. № 10. P. 4327–4334.
34. Turner A., Gough K.R., Leeming J.P. // Sex Transm. Infect. 1999. V. 75. № 1. P. 60–66.
35. Galimand M., Gerbaud G., Courvalin P. // Antimicrob. Agents Chemother. 2000. V. 44. № 5. P. 1365–1366.
36. Ilina E.N., Malakhova M.V., Bodoev I.N., Oparina N.Y., Filimonova A.V., Govorun V.M. // Front. Microbiol. 2013. V. 4. P. 186.
37. Unemo M., Golparian D., Skogen V., Olsen A.O., Moi H., Syversen G., Hjelmevoll S.O. // Antimicrob. Agents Chemother. 2013. V. 57. № 2. P. 1057–1061.
38. Jacobsson S., Golparian D., Cole M., Spiteri G., Martin I., Bergheim T., Borrego M.J., Crowley B., Crucitti T., van Dam A.P., et al. // J. Antimicrob. Chemother. 2016. V. 71. № 11. P. 3109–3116.
39. Gregory S.T., Dahlberg A.E. // J. Mol. Biol. 1999. V. 289. № 4. P. 827–834.
40. Rouquette-Loughlin C.E., Balthazar J.T., Shafer W.M. // J. Antimicrob. Chemother. 2005. V. 56. № 5. P. 856–860.
41. Cousin S.J., Whittington W.L., Roberts M.C. // Antimicrob. Agents Chemother. 2003. V. 47. № 12. P. 3877–3880.
42. Shultz T.R., Tapsall J.W., White P.A. // Antimicrob. Agents Chemother. 2001. V. 45. № 3. P. 734–738.
43. Su X., Lind I. // Antimicrob Agents Chemother. 2001. V. 45. № 1. P. 117–123.
44. Rouquette-Loughlin C., Dunham S.A., Kuhn M., Balthazar J.T., Shafer W.M. // J. Bacteriol. 2003. V. 185. № 3. P. 1101–1106.
45. Jolley K.A., Maiden M.C. // Future Microbiol. 2014. V. 9. № 5. P. 623–630.
46. Ison C.A., Town K., Obi C., Chisholm S., Hughes G., Livermore D.M., Lowndes C.M.; GRASP collaborative group. // Lancet Infect. Dis. 2013. V. 13. № 9. P. 762–768.
47. Eyre D.W., De Silva D., Cole K., Peters J., Cole M.J., Grad Y.H., Demczuk W., Martin I., Mulvey M.R., Crook D.W., et al. // J. Antimicrob. Chemother. 2017. V. 72. № 7. P. 1937–1947.

Antibacterial Effect of Thiosulfinates on Multiresistant Strains of Bacteria Isolated from Patients with Cystic Fibrosis

V. V. Kulikova[1], M. Yu. Chernukha[2], E. A. Morozova[1], S. V. Revtovich[1], A. N. Rodionov[1], V. S. Koval[1], L. R. Avetisyan[2], D. G. Kuliastova[2], I. A. Shaginyan[2], T. V. Demidkina[1*]

[1]Engelhardt Institute of Molecular Biology of the Russian Academy of Sciences, Vavilova Str., 32, Moscow, 119991, Russia

[2]N.F.Gamaleya National Research Centre of Epidemiology and Microbiology, Ministry of Health of Russian Federation, Gamaleya, Str., 18, Moscow, 123098, Russia

[*]E-mail: tvd@eimb.ru, tvdemidkina@yandex.ru

Received October 11, 2017; in final form June 26, 2018

ABSTRACT **The multiresistance of *A. ruhlandii* 155B, *B. cenocepacia* 122, and *P. aeruginosa* 48B strains isolated from patients with cystic fibrosis was established. The antibacterial effect of allicin, dimethyl thiosulfinate, and dipropyl thiosulfinate on multidrug-resistant strains was shown. Thiosulfinates can have both bacteriostatic and bactericidal effects depending on the microorganism and the concentration. The studied thiosulfinates may be candidates for the development of alternative antibiotic drugs to treat infections caused by multidrug-resistant pathogens.**

KEYWORDS **allicin, antibacterial activity, cystic fibrosis, methionine γ-lyase, thiosulfinates.**

ABBREVIATIONS **MGL – methionine γ-lyase, MIC – minimum inhibitory concentration, MBC – minimum bactericidal concentration.**

INTRODUCTION

The emergence of novel approaches to the development of effective antibacterial drugs is of utmost relevance because of the wide spread of antibiotic-resistant strains of bacteria. Multidrug-resistant microorganisms cause nosocomial infections, which can be the origin of complications in weakened patients. The chronic pulmonary infection caused by the association of such pathogens as *Pseudomonas aeruginosa*, *Staphylococcus aureus*, *Burkholderia cepacia complex*, etc. in patients with cystic fibrosis [1] is a serious problem associated with the formation of multi-resistant strains of microorganisms as a result of prolonged antibiotic therapy, which renders further antibiotic therapy ineffective.

Thiosulfinates are found in plants of the genus *Allium* and have an antimicrobial effect [2]. The antibacterial effect of allicin, the main thiosulfinate contained in garlic, is due to the combination of a reduced cellular glutathione level and inactivation of key metabolic enzymes as a result of the modification of their thiol groups [3, 4]. Since allicin, which oxidizes the thiol groups of enzymes and proteins, has many targets within the cell, it, alongside with other thiosulfinates, is unlikely to cause resistance [5].

Alliinase [EC 4.4.1.4] of the plants of the genus *Allium* catalyzes the decomposition of sulfoxides of the S-substituted analogues of *L*-cysteine to give rise to thiosulfinates. We have shown that thiosulfinates can be obtained using methionine γ-lyase (MGL, [EC 4.4.1.11]) (*Scheme*). Thiosulfinates formed by the cleavage of S-allyl-*L*-cysteine, S-methyl-*L*-cysteine, and S-ethyl-*L*-cysteine sulfoxides catalyzed by both wild-type MGL and its more efficient mutant form, C115H, inhibit the growth of Gram-positive and Gram-negative bacteria [6], including *P. aeruginosa* isolated from murine intestine [7].

The aim of the current work was to study the antibacterial effect of thiosulfinates obtained by β-elimination of three S-substituted *L*-cysteine sulfoxides (*Scheme*) catalyzed by C115H MGL on multidrug-resistant strains of the Gram-negative bacteria *Achromobacter ruhlandii* 155B, *B. cenocepacia* 122, and *P. aeruginosa* 48B isolated from patients with cystic fibrosis.

EXPERIMENTAL

Isolation of the enzyme, determination of its activity, synthesis of S-substituted *L*-cysteine sulfoxides, and production of thiosulfinates were carried out as previously described [6]. The concentrations of thiosulfinates were determined according to [8].

The antibacterial activity of thiosulfinates was determined by the two-fold serial dilution and agar diffusion method.

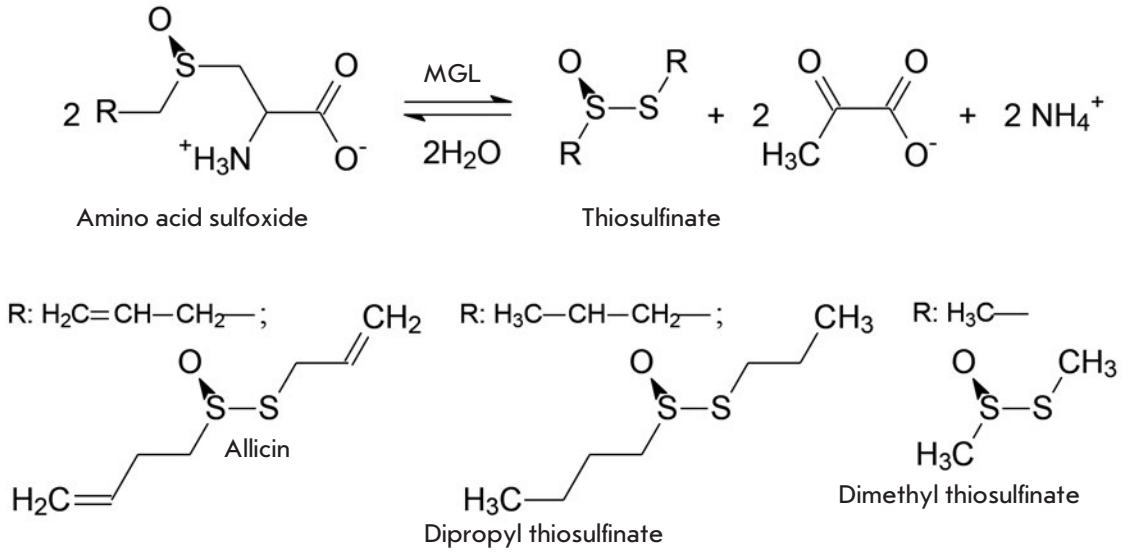

Scheme 1. β-elimination reaction of S-substituted *L*-cysteine sulfoxides

When determining the antibacterial activity of thiosulfinates by the method of two-fold serial dilutions [9], we used the Mueller-Hinton broth. Strains were cultivated at 10^5 CFU/ml and supplemented with agents at concentrations ranging from 1 to 0.0039 mg/ml, followed by inoculation into a dense growth medium (medium no. 1 for *P. aeruginosa* 48B and blood agar for *A. ruhlandii* 155B and *B. cenocepacia* 122).

The antibacterial activity of the agents on the solid growth medium was determined at a concentration varied from 2 to 0.05 mg/ml by inoculating diluted strains (10^4 to 10^7 CFU/ml) into Mueller-Hinton agar using the disc diffusion method and by directly applying the test samples at a volume of 10 μl.

Strain resistance to standard antibiotics prescribed to treat cystic fibrosis was determined by the serial dilution method according to the clinical recommendations on the threshold MIC values for each antibiotic [10].

The antibacterial efficacy of the thiosulphinates and antibiotics was compared using the disc diffusion method; strains were inoculated from the diluted cultures (10^6 CFU/ml) into Mueller-Hinton agar.

The duration of incubation on the solid growth medium was 24–48 h for all the experiments.

Strains *A. ruhlandii* 155B, *B. cenocepacia* 122, and *P. aeruginosa* 48B isolated from patients with cystic fibrosis and stored in the culture collection of the Laboratory of Molecular Epidemiology of Nosocomial Infections at the N.F.Gamaleya National Research Centre of Epidemiology and Microbiology (Ministry of Health of the Russian Federation) were used in this study.

RESULTS AND DISCUSSION

The antibacterial activities of allicin, dimethyl, and dipropyl thiosulfinate against the *A. ruhlandii* 155B, *B. cenocepacia* 122, and *P. aeruginosa* 48B strains isolated from patients with cystic fibrosis were determined (*Table 1*). The differences in the nature and degree of the antimicrobial effect of the thiosulfinates were revealed.

Allicin and dimethyl thiosulfinate turned out to exhibit the strongest effect against *B. cenocepacia* 122 and *P. aeruginosa* 48B, while dipropyl thiosulfinate was less active.

Table 1. The MIC and MBC values for thiosulfinates

Bacterial strain	Thiosulfinate	MIC	MBC
		mg/ml	
A. ruhlandii 155B	Allicin	0.50	1
	Dimethyl thiosulfinate	2.00*	–
	Dipropyl thiosulfinate	2.00*	–
B. cenocepacia 122	Allicin	0.03	≥ 0.03**
	Dimethyl thiosulfinate	0.03	≥ 0.03**
	Dipropyl thiosulfinate	0.25	0.5
P. aeruginosa 48B	Allicin	0.06	1
	Dimethyl thiosulfinate	0.06	–
	Dipropyl thiosulfinate	0.50	–

Note. "–" – no bactericidal effect.
*The data were obtained in the experiment on determining antibacterial activity on a solid growth medium using the disc diffusion method.
**But not exceeding 0.06.

Table 2. Antibacterial efficacy of thiosulfinates at different cell concentrations

Bacterial strain	Thiosulfinate	Diameter of inhibition zones (mm) at cell concentration, CFU/ml							
		10^4	10^5	10^6	10^7	10^4	10^5	10^6	10^7
		and thiosulfinate concentration*, mg/ml							
		2				0.4			
A. ruhlandii 155B	Allicin	30	30	30	30	0	0	0	0
	Dimethyl thiosulfinate	30	30	30	30	0	0	0	0
	Dipropyl thiosulfinate	30	30	30	30	0	0	0	0
B. cenocepacia 122	Allicin	25	25	25	25	0	0	0	0
	Dimethyl thiosulfinate	25	25	25	25	0	0	0	0
	Dipropyl thiosulfinate	20	20	20	20	0	0	0	0
P. aeruginosa 48B	Allicin	10	0	0	0	0	0	0	0
	Dimethyl thiosulfinate	15	15	15	15	10	-	-	-
	Dipropyl thiosulfinate	15	15	0	0	0	0	0	0

*Thiosulfinate concentrations of 0.2, 0.1, and 0.05 mg/ml are not presented in the table, since no antibacterial effect was noted at these concentrations.

Table 3. Resistance (+) of bacterial strains to antibiotics

Strain	Aztreonam	Amikacin	Gentamicin	Doxycycline	Imipenem	Colistin	Levofloxacin	Norfloxacin	Ofloxacin	Tobramycin	Chloramphenicol	Cefepime	Cefotaxime	Ceftazidime	Ceftriaxone	Cefuroxime	Ciprofloxacin
A. ruhlandii 155B	+		+	+	+	+	+	+	+	+	+	+	+	+	+	+	+
B. cenocepacia 122		+	+							+		+		+			+
P. aeruginosa 48B			+				+		+	+	+		+	+	+		+

The MIC and MBC values for the effect of the thiosulfinates on *B. cenocepacia* were either equal or similar, thus indicating that these two compounds exhibit a bactericidal effect. The MIC value for allicin lies in the range obtained for the activity of commercial allicin against several strains of the *B. cepacia* complex (0.008–0.062 mg/ml) [11].

Thiosulfinates exhibit a bacteriostatic effect on *P. aeruginosa* 48B, since the MBC value in the studied range of thiosulfinate concentrations was determined only for allicin (1 mg/ml). The MIC and MBC values for the activity of allicin against *P. aeruginosa* 48B correspond to the MIC (0.064–0.512 mg/ml) and MBC (0.128–1.024 mg/ml) values for the activity of allicin against the three clinical strains of *P. aeruginosa* [12].

The antibacterial effect of thiosulfinates on *A. ruhlandii* 155B was the least significant. The MIC values obtained in the experiment for determining antibacterial activity on a solid growth medium using the disc diffusion method (*Table 2*) were 2 mg/ml for dimethyl and dipropyl thiosulfinates, which exceeded the maximum concentration used in the serial dilution experiments. Allicin was the most effective thiosulfinate against *A. ruhlandii* 155B: it showed bactericidal action at a concentration of 1 mg/ml.

Changes in the antibacterial efficacy of thiosulfinates were determined depending on the concentration of bacterial cells. The experiment was carried out using the disc diffusion method (*Table 2*) and by applying samples on a solid nutrient medium. The results obtained through both methods coincided.

Thiosulfinates at a concentration of 2 mg/ml effectively inhibited the growth of *A. ruhlandii* 155B and *B. cenocepacia* 122 at a cell concentration ≤ 10^7 CFU/ml. The antibacterial effect of thiosulfinates against *P. aeruginosa* 48B was quite low. Allicin at maximum concentration only slightly suppressed the growth of *P. aeruginosa* 48B even at minimal cell concentration. Interestingly, it was only dimethyl thiosulfinate that, among all thiosulfinates, suppressed the growth of *P. aeruginosa* at a concentration of 0.4 mg/ml (*Table 2*). The results obtained for allicin and dimethyl thiosul-

Table 4. Antibacterial efficacy of thiosulfinates and antibiotics at a cell concentration of 10^6 CFU/ml

Concentration, μg/disc	Thiosulfinate	Inhibition zone diameter, mm		
		A. ruhlandii 155B	*B. cenocepacia* 122	*P. aeruginosa* 48B
20	Allicin	25	20	0
20	Dimethyl thiosulfinate	16	30	30
20	Dipropyl thiosulfinate	30	5	0
5	Imipenem	0	30	30
10	Tobramycin	0	0	0
10	Ciprofloxacin	0	0	0

finate are consistent with the data for *P. aeruginosa* from murine intestinal [7].

The absence of inhibition zones in the experiment on the solid growth medium with allicin and dimethyl thiosulfinate at low concentrations is probably due to the slow diffusion of substances into Muller-Hinton agar. Thus, the serial dilution method is the optimal technique for determining the antibacterial activity of the studied thiosulfinates.

The resistance of the *A. ruhlandii* 155B, *B. cenocepacia* 122, and *P. aeruginosa* 48B strains was evaluated using the 17 antibiotics most commonly prescribed to patients with cystic fibrosis (*Table 3*). The *A. ruhlandii* 155B strain showed resistance to 16 antibiotics, while the *B. cenocepacia* 122 and *P. aeruginosa* 48B strains were resistant to six and nine antibiotics, respectively. The obtained data confirmed that these strains develop resistance after prolonged antibiotic therapy. It is noteworthy that none of the antibiotics tested in this study had an antibacterial effect against all three bacterial strains.

We compared the efficacy of the antibacterial action of the thiosulfinates and broad-spectrum antibiotics belonging to the three different groups most commonly prescribed to patients with cystic fibrosis: imipenem belonging to the group of carbapenems, tobramycin belonging to the group of aminoglycosides, and ciprofloxacin belonging to the group of fluoroquinolones (*Table 4*). Identically to the case of two-fold serial dilutions, determination of antibacterial activity by the method of disc diffusion on a dense growth medium demonstrated that three strains were resistant to tobramycin and ciprofloxacin at standard concentrations of 10 μg/disc. The diameters of inhibition zones for *B. cenocepacia* 122 and *P. aeruginosa* 48B were similar to those for dimethyl thiosulfinate and slightly higher than the inhibition zone of allicin for *B. cenocepacia* 122. Allicin and dimethyl thiosulfinate inhibit the growth of *A. ruhlandii* 155B, while this strain is resistant to imipenem.

The obtained data open up possibilities for the development of agents for the antibacterial therapy of chronic pulmonary infections in patients with cystic fibrosis. ●

The authors would like to thank the staff of the N.F.Gamaleya National Research Centre of Epidemiology and Microbiology for the opportunity to conduct experiments on determining the antibacterial activity of drugs on clinical isolates.
The study was supported by the Russian Science Foundation (grant No. 15-14-00009).

REFERENCES

1. Shaginyan I.A., Kapranov N.I., Chernukha M.Yu., Alekseeva G.V., Semykin S.Yu., Avetisyan L.R., Kashirskaya N.Yu., Pivkina N.V., Danilina G.A., Batov A.B., Busuek G.P. // Journal of microbiology, epidemiology and immunobiology (Russian). 2009. № 5. P. 15-20.
2. Cavallito C.J., Bailey J.H. // J. Am. Chem. Soc. 1944. V. 66. P. 1950–1951.
3. Rabinkov A., Miron T., Konstantinovski L., Wilchek M., Mirelman D., Weiner L. // Biochim. Biophys. Acta. 1998. V. 1379. P. 233–244.
4. Muller A., Eller J., Albrecht F., Prochnow P., Kuhlmann K., Bandow J.E., Slusarenko A.J., Leichert L.I.O. // J. Biol. Chem. 2016. V. 291. P. 11477–11490.
5. Ankri S., Mirelman D. // Microb. Infect. 1999. V. 2. P. 125–129.
6. Morozova E.A., Kulikova V.V., Rodionov A.N., Revtovich S.V., Anufrieva N.V., Demidkina T.V. // Biochimie. 2016. V. 128–129. P. 92–98.
7. Kulikova V.V., Anufrieva N.V., Revtovich S.V., Chernov A.S., Telegin G.B., Morozova E.A., Demidkina T.V. // IUBMB Life. 2016. V. 68. P. 830–835.
8. Miron T., Rabinkov A., Mirelman D., Weiner L., Wilchek M. // Anal. Biochem. 1998. V. 265. P. 317–325.
9. Mironov A.N., Bunatyan N.D. et al. Guidelines for preclinical trials of drugs. Part one. M.: Grif and K, 2012. 944 p.
10. Methodological guidelines 4.2.1890-04 Determination of the sensitivity of microorganisms to antimicrobial drugs (version 2015-02).
11. Wallock-Richards D., Doherty C.J., Doherty L., Clarke D.J., Place M., Govan J.R.W., Campopiano D.J. // PLoS One. 2014. V. 9. № 12. e112726.
12. Reiter J., Levina N., van der Linden M., Gruhlke M., Martin C., Slusarenko A.J. // Molecules. 2017. V. 22. P. 1711.

Antidepressant Effect of an Orally Administered Dipeptide Mimetic of the Brain-Derived Neurotrophic Factor

P. Y. Povarnina*, T. L. Garibova, T. A. Gudasheva, S. B. Seredenin
Federal State Budgetary Institution "Research Zakusov institute of pharmacology", Baltic Str., 8, Moscow, 125315, Russia
*E-mail: povarnina@gmail.com
Received July 05, 2017; in final form June 06, 2018

ABSTRACT **Involvement of BDNF in the regulation of neuroplasticity and neurogenesis in the hippocampus, impairment of which underlies the pathophysiology of depression, makes this endogenous protein a promising object for the development of new-generation antidepressants with a neurophysiologically based mechanism of action. A low-molecular-weight BDNF mimetic, GSB-106 (a substituted dimeric dipeptide, *bis*-(N-monosuccinyl-*L*-seryl-*L*-lysine) hexamethylenediamide), was designed and synthesized at the Zakusov Institute of Pharmacology. GSB-106 was found to activate BDNF-specific TrkB receptors and their main post-receptor signaling pathways MAPK/ERK and PI3K/AKT. GSB-106 exhibited pronounced antidepressant activity in a rodent test battery at a dose of 0.1 to 1.0 mg/kg administered intraperitoneally. Because oral administration is preferable in the treatment of depression, which is associated with a prolonged duration and outpatient character of pharmacotherapy, we examined the antidepressant properties of GSB-106 administered orally as a pharmaceutical substance (PS) and in tablet dosage form (TDF). In the study, we used the Porsolt forced swim test in rats; a conventional antidepressant, Amitriptyline, was used as a reference drug. The antidepressant activity of GSB-106 was found to retain upon oral administration and to manifest at doses of 0.5–5.0 mg/kg for PS and 0.01–5.0 mg/kg for TDF. The effective dose of TDF was 50-fold lower than that of PS, and the efficacy of tableted GSB-106 exceeded that of Amitriptyline, the "gold standard" in antidepression care. Therefore, GSB-106, both as a substance and as a tablet dosage form, exhibits antidepressant activity when administered orally, which makes it a promising antidepressant agent, the first in the class of BDNF mimetics.**
KEYWORDS **dimeric dipeptide BDNF mimetic, GSB-106, depression, oral dosage form.**
ABBREVIATIONS **BDNF – brain-derived neurotrophic factor, PS – pharmaceutical substance, DF – dosage form.**

INTRODUCTION

Experimental and clinical data indicate a central role for the brain-derived neurotrophic factor (BDNF) in the pathogenesis of depression [1]. The antidepressant activity was observed in experiments with intracerebral administration of BDNF [2–4]. The BDNF level is reduced in the blood plasma of patients with depression; after treatment with antidepressants, the BDNF level returns to normal values [5]. In addition, a decreased BDNF level was detected in the hippocampus of patients with depression and in suicide victims [6, 7]. The pathogenetic role of BDNF in depression has been demonstrated to be associated with the regulation of neuroplasticity and neurogenesis in the hippocampus [8], impairment of which is considered to be the leading etiopathogenetic factor of the disease [9].

Obviously, BDNF is an important object in the development of antidepressants with a pathophysiology-based mechanism of action.

The physiological effects of BDNF, including the regulation of neurogenesis and maintenance of neuroplasticity, are mediated by TrkB receptors, with MAPK/ERK and PI3K/AKT being the main pathways of their signal transduction [10, 11]. We have developed low-molecular-weight compounds that mimic the beta-turns of some BDNF loops and experimentally proved that they selectively activate post-receptor cascades [12, 13]. In this case, BDNF mimetics selectively activating either PI3K/AKT or MAPK/ERK were found not to exhibit antidepressant activity, which indicates that both post-receptor signaling pathways are essential for this activity.

It should be noted that the clinical use of native BDNF is limited due to its unsatisfactory pharmacokinetic properties.

In this regard, the dipeptide GSB-106, a mimetic of the BDNF loop 4 beta-turn (*bis*-(N-monosuccinyl-*L*-seryl-*L*-lysine) hexamethylenediamide), was se-

lected as a promising antidepressant at the Zakusov Institute of Pharmacology. Western blot analysis revealed that GSB-106 activates BDNF-specific TrkB receptors and their post-receptor signaling pathways MAPK/ERK and PI3K/AKT [12, 16]. GSB-106 exhibited pronounced antidepressant activity in a rodent test battery at a dose of 0.1 to 1.0 mg/kg administered intraperitoneally [15, 17]. Probably, the mechanisms of GSB-106 antidepressant action, like those of the full-length protein, are associated with neurogenesis and synaptogenesis. The effect of GSB-106 on neurogenesis was previously demonstrated in a mouse predator stress model [18].

Obviously, the oral dosage form is preferable in depression, which is associated with a prolonged duration and outpatient character of pharmacotherapy. Therefore, we studied the antidepressant properties of GSB-106 administered orally both as a pharmaceutical substance (PS) and in tablet dosage form (TDF).

EXPERIMENTAL

Medicinal products

GSB-106 PS was synthesized at the Department of Pharmaceutical Chemistry of the Zakusov Institute of Pharmacology as described earlier [15]. GSB-106 TDF for oral use was developed and produced at the Experimental and Technological Department of the Zakusov Institute of Pharmacology and contained 1% of GSB-106 PS and 99% of a filler consisting of lactose, microcrystalline cellulose, polyethylene glycol-polyvinyl alcohol copolymer, and magnesium stearate.

Amitriptyline in an injectable dosage form was produced at the Moscow Endocrine Plant (Russia).

Animals

Experiments were performed on 188 white outbred male rats weighing 240–270 g received from the Stolbovaya Branch of the Scientific Center of Biomedical Technologies of the Federal Medical Biological Agency. The animals were kept at the vivarium with a natural light cycle and free access to standard pellet feed and water in accordance with Sanitary Regulations 2.2.1.3218-14 Sanitary and epidemiological requirements for organization, equipment, and maintenance of experimental biological clinics (vivaria) of August 29, 2014, No. 51. The study was organized and implemented in accordance with Order of the Ministry of Health of Russia No. 199 of April 1, 2016 On Approval of the Rules for Good Laboratory Practice. The experiments were approved by the Biomedical Ethics Commission of the Zakusov Institute of Pharmacology (Protocol No. 2 of February 20, 2017).

Investigation of antidepressant activity

The antidepressant activity of GSB-106 in rats was determined in the Porsolt forced swim test [19, 20]. The setup for assessing antidepressant activity consisted of six cylindrical vessels, each 20 cm in diameter and 60 cm in height, separated by opaque walls. The vessels were filled with 40 cm of water at a temperature of 22°C. First, each animal was placed in a vessel with water for 15 min, after which the animal was left to dry and then returned to its home cage. After 24 h, the animals were placed in water for 5 min to assess the time of a characteristic immobile posture (no active struggle behavior). The behavior of the animals was recorded with a video camera. Video recordings of the experiments were processed in semi-automatic mode using the RealTimer software (Open Science, Russia).

Experimental design

GSB-106 PS was dissolved in distilled water and administered to rats daily for 14 days at doses of 0.1, 0.5, 1, 5, and 10 mg/kg orally in a volume of 1 mL/kg. Control animals received distilled water in the same regimen. GSB-106 TDF was suspended in a 1% starch solution and administered to rats daily for 14 days at doses of 0.001, 0.01, 0.05, 0.1, and 5.0 mg/kg orally in a volume of 1 mL/kg. The control animals received a placebo in the same regimen, which was a suspension of the TDF filler in a 1% starch solution. The classical tricyclic antidepressant Amitriptyline was used as a reference drug; it was diluted in distilled water and administered orally to rats at a dose of 5.0 mg/kg [21] in a volume of 1.0 mL/kg for 14 days. The control animals were administered distilled water in the same regimen. Twenty-four hours after the last administration of the preparations, the rats were put into cylinders with water to foster a depressive-like state; after another 24 hours, testing was performed.

Statistical analysis

Intergroup differences were assessed using the Student's *t*-test and the Mann-Whitney U test (the Bonferroni adjustment was used if more than two groups were compared). Differences were considered statistically significant at $p \leq 0.05$. The data were presented as means and standard errors of the means.

RESULTS

Antidepressant activity of orally administered GSB-106 PS

In the Porslot forced swim test, the control rats receiving distilled water, after a period of activity, adopted a characteristic immobility posture (no active struggle behavior) and retained it with small interruptions until

Table 1. Antidepressant-like effects of orally administered GSB-106 in a Porsolt forced swim test in rats

Antidepressant effect of GSB-106 PS				
Group	n	Dose, mg/kg	Immobility, s	Decrease in the immobility time, as a fraction of control
Control (water)	8		177.9 ± 9.3	
Amitriptyline	8	5.0	134.5 ± 10.1*#	0.77
GSB-106	8	0.1	184.8 ± 16.6	
	8	0.5	116.9 ± 21.6#	0.67
Control (water)	18		199.2 ± 10.0	
GSB-106	18	1.0	163.2 ± 7.9#	0.83
Control (water)	10		216.3 ±13.8	
GSB-106	10	5.0	137.1 ± 12.3*#	0.63
Control (water)	10		190.8 ± 9.8	
GSB-106	10	10.0	202.2 ± 14.9	
Antidepressant effect of GSB-106 TDF				
Group	n	Dose, mg/kg	Immobility, s	Decrease in the immobility time, as a fraction of control
Control (placebo)	10		245.7 ± 13.4	
GSB-106	10	0.001	192.5 ± 13.2	
GSB-106	10	0.01	155.2 ± 20.3**	0.63
GSB-106	10	0.05	134.9 ± 18.8***	0.56
GSB-106	10	0.1	165.4 ± 15.1**	0.67
Control (placebo)	10		201.2 ± 12.1	
GSB-106	10	1.0	159.9 ± 23.6#	0.77
GSB-106	10	5.0	92.8 ± 17.2***	0.45

Note. *n* is the number of animals in a group. Data are presented as means and standard errors of the means. * – $p \le 0.05$; ** – $p < 0.01$; *** – $p < 0.001$ compared to the control group (Mann-Whitney U test); # – $p \le 0.05$ compared to the control group (Student's *t* test).

the end of the experiment. The immobility time in the control animals in different experiments ranged from 178 to 216 s, on average. GSB-106 PS at doses of 0.5, 1.0, and 5.0 mg/kg statistically significantly ($p \le 0.05$) reduced the immobility time compared to that in the controls (*Table*), 1.5-, 1.2-, and 1.6-fold, respectively, which was an indication of the presence of antidepressant activity. At doses of 0.1 and 10 mg/kg, GSB-106 had no antidepressant activity, which was an indication of the effect's dependence on the dose. In this case, the effect of GSB-106 PS at a dose of 0.5 mg/kg was comparable to that of Amitriptyline at a dose of 5.0 mg/kg (per os) (*Table*).

Therefore, GSB-106 PS was found to trigger antidepressant activity upon oral administration at a dose of 0.5–5 mg/kg.

Antidepressant activity of orally administered GSB-106 TDF

The immobility time in the control rats receiving placebo was 246 and 201 s in two experiments. In the Porsolt forced swim test, orally administered GSB-106 TDF at a dose of 0.01, 0.05, 0.1, and 5.0 mg/kg statistically significantly ($p < 0.01$) reduced the immobility time in rats compared to that in the controls 1.6-, 1.8-, 1.5-, and 2.2-fold, respectively (*Table*). The effect of GSB-106 TDF was dose-dependent and was absent at a dose of 0.001 mg/kg.

DISCUSSION

The study revealed that the antidepressant activity of dipeptide BDNF mimetic GSB-106, which had been earlier detected upon intraperitoneal administration at doses of 0.1–1.0 mg/kg, was retained upon oral administration and was exhibited at doses of 0.5–5.0 mg/kg for PS and 0.01–5.0 mg/kg for TDF of GSB-106. GSB-106 TDF was active at 50-fold lower doses than GSB-106 PS, and the efficacy of GSB-106 TDF exceeded that of Amitriptyline, the gold standard in antidepression care.

It is important that the activity of orally administered GSB-106 is comparable to that of intraperitoneal administration. This stability of GSB-106 in biological media is associated with the absence of bond targets

for proteases, aminopeptidases, and carboxypeptidases (due to its dipeptide nature) and protected N- and C-termini, respectively. This confirms the prospects and advantages of substituted dipeptides as oral medication compared to oligopeptides that easily degrade in the gastrointestinal tract and do not penetrate the gastrointestinal barrier. Therapeutic oligopeptides affecting the central nervous system are used mainly in intranasal forms, and oligopeptides exhibiting peripheral effects are used in injectable forms. However, dipeptide drugs, such as the nootropic agent Noopept (N-phenylacetyl-*L*-prolylglycine ethyl ester), the antipsychotic drug Dilept (N-caproyl-*L*-prolyl-*L*-tyrosine methyl ester), and the anxiolytic agent GB-115 (N-phenylhexanoyl-glycyl-*L*-tryptophan amide) have been demonstrated to retain their activity upon oral administration [22, 23]. As found earlier [24, 25], there are specific transport systems for the transfer of dipeptides through the enteral mucosa of the gastrointestinal tract (PEPT-1) and through the blood-brain barrier (PEPT-2).

Therefore, the GSB-106 dipeptide and its tablet dosage form possess antidepressant activity, which makes GSB-106 an original antidepressant drug, the first in its class.

CONCLUSION

The dimeric dipeptide BDNF mimetic GSB-106 exhibits its antidepressant activity when administered orally. The developed dosage form of GSB-106 is superior to the pharmaceutical substance both in doses and in antidepressant effect.

The study results demonstrate the reasonability of developing a dipeptide GSB-106-based drug that, based on its dipeptide structure and BDNF-ergic mechanism of action, may be classified as first in its class. ●

This work was supported by a grant from the Presidium of the RAS "Investigation of the role of synaptogenesis and neurogenesis in the mechanism of antidepressant activity of the brain-derived neurotrophic factor using its dipeptide mimetics that are the first in the class of potential antidepressants" and a grant from the Russian Science Foundation (No. 18-15-00381).

REFERENCES

1. Castrén E., Kojima M. // Neurobiol. Dis. 2017. V. 97. Pt B. P. 119–126.
2. Shirayama Y., Chen A.C., Nakagawa S., Russell D.S., Duman R.S. // J. Neurosci. 2002. V. 22. № 8. P. 3251–3261.
3. Hoshaw B.A., Malberg J.E., Lucki I. // Brain Res. 2005. V. 1037. № 1–2. P. 204–208.
4. Hu Y., Russek S.J. // J. Neurochem. 2008. V. 105. № 1. P. 1–17.
5. Polyakova M., Stuke K., Schuemberg K., Mueller K., Schoenknecht P., Schroeter M.L. // J. Affect. Disord. 2015. V. 174. P. 432–440.
6. Karege F., Vaudan G., Schwald M., Perroud N., La Harpe R. // Mol. Brain Res. 2005. V. 136. № 1–2. P. 29–37.
7. Thompson R.M., Weickert C.S., Wyatt E., Webster M.J. // J. Psychiatry Neurosci. 2011. V. 36. № 3. P. 195–203.
8. Autry A.E., Monteggia L.M. // Pharmacol. Rev. 2012. V. 64. № 2. P. 238–258.
9. Wainwright S.R., Galea L.A. // Neural Plast. 2013. V. 2013. P. 805497.
10. Jiang C., Salton R. // Transl. Neurosci. 2013. V. 4. № 1. P. 46–58.
11. Islam O., Loo T.X., Heese K. // Curr. Neurovasc. Res. 2009. V. 6. № 1. P. 42–53.
12. Gudasheva T.A., Povarnina P., Logvinov I.O., Antipova T.A., Seredenin S.B. // Drug Des. Dev. Ther. 2016. V. 10. P. 3545–3553.
13. Gudasheva T.A., Tarasiuk A.V., Sazonova N.M., Povarnina P.Y., Antipova T.A., Seredenin S.B. // Dokl. Biochem. Biophys. 2017. V. 476. № 1. P. 291–295.
14. Seredenin S.B., Gudasheva T.A. Patent No. 2410392. RU. 2011
15. Gudasheva T.A., Tarasyuk A.V., Pomogaybo S.V., Logvinov I.O., Povarnina P., Antipova T.A., Seredenin S.B. // Bioorg Khim. 2012. V. 38 (3). P. 280–290.
16. Gudasheva T.A., Logvinov I.O., Antipova T.A., Seredenin S.B. // Dokl Biochem Biophys. 2013. V. 451 (5). P. 577–580.
17. Seredenin S.B., Voronina T.A., Gudasheva T.A., Garibova T.L., Molodavkin G.M., Litvinova S.A., Elizarova E.A., Poseva V.I. // Acta naturae. 2013. V. 5. № 4 (19). P. 105–109.
18. Gudasheva T.A., Povarnina P., Seredenin S.B. // Bull Exp Biol Med. 2016. V. 162 (10). P. 448–451.
19. Porsolt R.D., Anton G., Blavet N., Jalfre M. // Eur. J. Pharmacol. 1978. V. 47. № 4. P. 379–391.
20. Buccafusco J.J. Methods of Behavior Analysis in Neuroscience, 2nd edition. Boca Raton (FL): CRC Press/Taylor & Francis, 2009. 360 p.
21. Takamori K., Yoshida S., Okuyama S. // Pharmacology. 2001. V. 63. № 3. P. 147–53.
22. Gudasheva T.A. // Russ. Chem. Bull. Internat. Ed. 2015. V. 64. № 9. P. 2012–2021.
23. Zherdev V.P., Boyko S.S., Shevchenko R.V., Gudasheva T.A. // J Pharmacokinet Pharmacodyn. 2017. № 1. P. 3–10.
24. Sala-Rabanal M., Loo D.D., Hirayama B.A., Turk E., Wright E.M. // J. Physiol. 2006. V. 574. Pt 1. P. 149–166.
25. Ganapathy M.E., Prasad P.D., Mackenzie B., Ganapathy V., Leibach F.H. // Biochim. Biophys. Acta. 1997. V. 1324. № 2. P. 296–308.

A Novel Approach to Anticancer Therapy: Molecular Modules Based on the Barnase:Barstar Pair for Targeted Delivery of HSP70 to Tumor Cells

A. M. Sapozhnikov*, A. V. Klinkova, O. A. Shustova, M. V. Grechikhina, M. S. Kilyachus, O. A. Stremovskiy, E. I. Kovalenko, S. M. Deyev

Shemyakin – Ovchinnikov Institute of Bioorganic Chemistry RAS, Miklukho-Maklaya Str., 16/10, Moscow, 117997, Russia

*E-mail: amsap@ibch.ru

Received June 20, 2018; in final form August 25, 2018

ABSTRACT **One important distinction between many tumor cell types and normal cells consists in the translocation of a number of intracellular proteins, in particular the 70 kDa heat shock protein (HSP70), to the surface of the plasma membrane. It has been demonstrated that such surface localization of HSP70 on tumor cells is recognized by cytotoxic effectors of the immune system, which increases their cytolytic activity. The mechanisms behind this interaction are not fully clear; however, the phenomenon of surface localization of HSP70 on cancer cells can be used to develop new approaches to antitumor immunotherapy. At the same time, it is known that the presence of HSP70 on a cell's surface is not a universal feature of cancer cells. Many types of tumor tissues do not express membrane-associated HSP70, which limits the clinical potential of these approaches. In this context, targeted delivery of exogenous HSP70 to the surface of cancer cells with the aim of attracting and activating the cytotoxic effectors of the immune system can be considered a promising means of antitumor immunotherapy. Molecular constructs containing recombinant mini-antibodies specific to tumor-associated antigens (in particular, antibodies specific to HER2/neu-antigen and other markers highly expressed on the surface of a wide range of cancer cells) can be used to target the delivery of HSP70 to tumor tissues. In order to assess the feasibility and effectiveness of this approach, recombinant constructs containing a mini-antibody specific to the HER2/neu-antigen in the first module and HSP70 molecule or a fragment of this protein in the second module were developed in this study. Strong selective interaction between the modules was ensured by a cohesive unit formed by the barnase:barstar pair, a heterodimer characterized by an unusually high constant of association. During testing of the developed constructs in *in vitro* models the constructs exhibited targeted binding to tumor cells expressing the HER2/neu antigen and the agents had a significant stimulating effect on the cytotoxic activity of NK cells against the respective cancer cells.**

KEYWORDS **cancer immunotherapy, NK cells, 70 kDa heat shock protein, targeted delivery, HER2/neu antigen, mini-antibody, barnase:barstar.**

ABBREVIATIONS **HSP70 – 70 kDa heat shock protein, Hsp70 – inducible form of human HSP70, Hsp70/16 – 16 kDa C-terminal fragment of Hsp70, 4D5 scFv – anti-HER2/neu mini-antibody.**

INTRODUCTION

The search for novel approaches to cancer immunotherapy remains relevant, although a large number of studies have focused on this problem [1–3]. One of the reasons why malignant neoplasms emerge and develop in the organism is that the surface of tumor cells is devoid of antigens that can activate the cytotoxic effectors of the immune surveillance system which are responsible for the elimination of transformed cells. In this context, targeted modification of a tumor cell's surface with molecular structures that are recognized by natural killer cells and, thus, induce a cytolytic response is one of the promising approaches to antitumor immunotherapy. It has recently been demonstrated that heat shock proteins (HSPs) with a molecular weight of 70 kDa (HSP70) are among such structures.

The family of heat shock proteins includes a wide range of highly conserved intracellular proteins which are characterized by both heterogeneous physicochemical properties and a variety of functions. HSPs are expressed in all cell types; various damaging agents can increase their expression level manifold. An elevated

intracellular level of HSPs is the universal protective response of cells, which is associated with the unique ability of these proteins to prevent stress-induced aggregation of intracellular proteins and their denaturation, as well as to ensure repair of partially damaged proteins or their proper elimination if irreversible damage occurs. The listed functions and involvement in the folding of newly synthesized polypeptides and transport of intracellular proteins are referred to as the so-called "chaperon" properties of the constitutive pool of HSPs, which is expressed in cells under normal physiological conditions in the absence of stress [4, 5]. However, localization of HSPs is not confined to the intracellular space. In a large series of studies, these proteins were found on the cell surface. In particular, surface HSPs were detected on the plasma membrane in normal [6, 7] and tumor cells [8–14], virus-infected lymphocytes [15], and apoptotic T cells [16–18]. It was demonstrated that HSPs with various molecular weights are expressed on the cell surface, but that surface localization is most typical of 70 kDa HSPs (HSP70). The phenomenon of unusual surface expression of HSPs was described not only for *in vitro* cultured cells, but also for the cells of different patient-derived tissues [12, 14].

The functions of HSPs exposed on the cell surface remain virtually unstudied. At the same time, a hypothesis has been suggested that these cell surface proteins are immunologically important, as their emergence on the plasma membrane can be a signal for the immune system to activate cytotoxic effectors and ensure the elimination of infected, transformed, and damaged cells [19]. Indeed, it is well known today that different subpopulations of T cells and NK cells are capable of recognizing highly conserved determinants of various HSPs. In particular, recognition of the membrane-resident HSP70 and Grp75 by γδ-T cells is MHC-nonrestricted [20]; recognition of Hsp70 (the inducible form of HSP70) by NK cells is also MHC-nonrestricted [21, 22]. Surface-resident HSPs of tumor cells attract NK cells: their count can increase up to 500-fold in tumors expressing these proteins on their surface [23]. Data in the literature is indicative of *in vitro* MHC class I-restricted recognition of Hsp70 by human NK cells on the surface of human K562 erythroleukemia cells and human sarcoma cells exposed to heat shock [24]. It was also demonstrated that surface HSP70 proteins cause a strong humoral and cell-mediated adaptive immunity response. According to a number of studies, HSP70 can be attributed to tumor-associated antigens recognized by various types of T cells, such as $CD4^-$ $CD8^-$ [25], αβ- and γδ-lymphocytes [26, 27], and natural killer (NK) cells [10, 11, 21]. The recognition of both the constitutive and inducible forms of HSP70 by MHC-restricted and nonrestricted immune cells indicates that surface HSP70 proteins play a crucial role in antitumor immune responses. Based on this fact, a model of immune surveillance was suggested where these cells ensure the first line of defense against infectious agents carrying HSPs on their surface, protect against virus-infected or transformed cells, and against damaged autologous cells. The lymphocyte pool recognizing conserved HSPs is probably induced during ontogenesis as the skin and intestinal microflora develop. The periodic reactivation of these lymphocytes can be caused by common viral and bacterial infections, as well as various stressful stimuli [19].

Application of HSP70 in antitumor therapy attracted the attention of researchers exploring various approaches to this problem [28–32]. However, most of these approaches are based on the ability of HSP70 to form strong complexes with tumor-specific peptides, rather than on direct recognition of membrane-associated HSP70 by cytotoxic effectors of the immune system. This is possibly related to the fact that *in vivo* expression of these proteins on cancer cells is observed not in all types of tumor tissues. This circumstance serves as the basis for the assumption that induction of HSP70 translocation onto the surface of tumor cells or targeted delivery of these molecules into malignant neoplasms to attract and activate cytotoxic immune effectors of the immune system is a new, promising direction in antitumor immunotherapy [33].

It has been recently found by a number of researchers and in our preliminary studies that both full-length HSP70 molecules and synthetic analogues of some HSP70 fragments exhibit an activating effect on natural killer cells. In particular, addition of synthetic HSP70 fragments to a human NK cell culture significantly stimulated the production of IFN-γ by natural killer cells, identically to how this took place in the experiments with recombinant HSP70 [34, 35]. Therefore, HSP70 molecules and fragments of this protein can be regarded as promising structures to be used in bioengineering approaches to the fabrication of molecular constructs for targeted modification of the surface of tumor cells in order to potentiate the antitumor cytotoxic immune response. Targeted delivery of such "cytolytic markers" can be performed by incorporating recombinant mini-antibodies against tumor-specific antigens into the recombinant construct module being designed. In particular, antibodies specific to the HER2/neu antigen ($p185^{HER2}$) or to other cancer markers expressed on the surface of a wide range of malignant neoplasms can be used as such mini-antibodies.

This study was aimed at developing a method for targeted HER-2/neu-specific delivery of HSP70 or its fragment to the surface of tumor cells using a two-module construct, with the barnase:barstar pair em-

ployed as a cohesive linker for protein modules. In this construct, the function of the first module carrying a high-specificity anticancer antibody and barnase consists in targeted binding to the surface of cancer cells. In its turn, barnase exposed on tumor cells due to this interaction acts as a site of selective binding between the second module consisting of barstar and HSP70 (or its fragment) and the target cells. In the approach being designed, the selective interaction between the first and the second modules is ensured by an unusually high constant of barstar binding to barnase. This protein heterodimer forms a complex with $K_d \sim 10^{-14}$ M, which is comparable only to that of the streptavidin–biotin system ($K_d \sim 10^{-15}$ M). In our previous studies, we have proved that the barnase:barstar complex shows a high potential as an agent for the targeted delivery of various drugs to tumor cells [36–39].

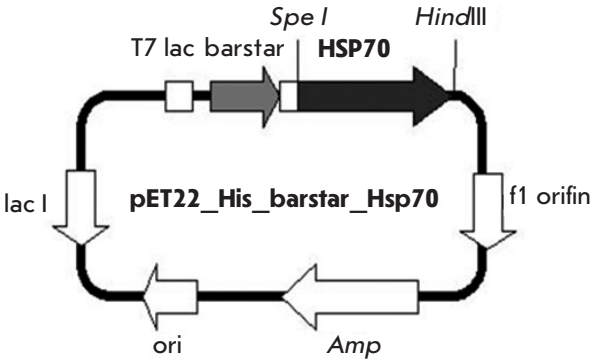

Fig. 1. Scheme of the plasmid pET22_His_barstar_Hsp70 encoding the second module of the molecular construct carrying the Hsp70 effector protein. T7lac is the early promoter of bacteriophage T7 RNA polymerase; *HSP70* is the gene encoding Hsp70; *Amp* is the ampicillin resistance gene

EXPERIMENTAL

The principles of building two-module molecular constructs for the targeted delivery of HSP70 to tumor cells

In order to build a supramolecular complex containing the HSP70 protein and the targeting mini-antibody, the barnase:barstar module had to be used to bind HSP70 to one of its components, barstar. It is known from experimental data [10] that the C-terminal domain of HSP70 is responsible for the stimulation of the cytotoxic and proliferative activities of NK cells. Therefore, the C-terminus of HSP70 in the recombinant protein being constructed had to remain unbound and accessible for interaction with natural killer cells, while barstar had to be attached to the N-terminus via a flexible peptide linker ensuring unrestricted rotation of functional domains in the target recombinant protein. These theoretical considerations were taken into account when constructing a plasmid encoding the target recombinant protein His_6-barstar-HSP70, which consisted of the HSP70 protein (the inducible form of human HSP70 – Hsp70) linked to barstar with its N-terminus via the hinge peptide of human immunoglobulin IgG3 (ThrProLeuGlyAspThrThrHisThrSerGly) and carrying the hexahistidine tail at its N-terminus (*Fig. 1*). Similar procedures were conducted to build the second variant of the effector module that carried the 16 kDa C-terminal Hsp70 fragment (His_6-barstar-Hsp70/16), instead of the full-length Hsp70 molecule. The previously designed 4D5 scFv-dibarnase construct [36] was used in this study as the first (targeting) module carrying specific anti-HER2/neu mini-antibodies.

Cultures of tumor target cells

SKOV3 human ovarian adenocarcinoma cells and BT-474 human breast carcinoma cells overexpressing the HER-2/neu antigen were chosen as the target cells to be treated with the designed constructs. The cells were cultured in 6-well plates (Nunk, USA) and in 25 cm^2 cell culture flasks (Costar, USA) in a RPMI 1640 medium (Flow Laboratories, UK) supplemented with 10% fetal calf serum (FCS), 50 μg/ml of streptomycin (Sintez, Russia), and 50 μg/ml of penicillin (Biosintez, Russia) in 5% CO_2 at 37°C. The adherent cells attached to the culture flask substrate were removed from the substrate using a Versene solution. Human embryonic kidney cells (HEK 293) cultured under identical conditions were used as the control.

The expression level of the tumor-associated HER-2/neu antigen on the surface of the cultured cell lines was tested using fluorescence microscopy and the previously designed recombinant constructs for visualizing cancer cells expressing the HER-2/neu antigen (anti-HER2/neu mini-antibody-barstar•GFP-barnase) [36, 37]. It has been demonstrated that the cell culture samples being used are characterized by a sufficiently high level of expression of the HER-2/neu surface antigen (the data are not shown).

Treatment of the target cells with the designed constructs

Hsp70 and its fragment, Hsp70/16, were delivered to tumor cells as the components of barstar-Hsp70 and barstar-Hsp70/16 recombinant proteins. At the first stage of targeted delivery, anti-HER2/neu mini-antibody (4D5 scFv protein) within the first module of the designed supramolecular complex was bound to the respective tumor-specific antigen on the cell surface (20 μg/ml, 60 min). Next, the barstar-Hsp70 and barstar-Hsp70/16 recombinant proteins were also strongly

adsorbed onto the cell membrane (50 μg/ml, 60 min) due to the barnase:barstar interaction.

Assessment of the efficiency of the binding between the designed constructs and target cells

Flow cytofluorimetry was used to assess the efficiency of the targeted delivery of the heat shock protein to the surface of the target cells. The samples of the cells that had interacted with the first and second modules of the designed supramolecular complex were stained according to the conventional procedure [14] using BRM22 antibodies (Sigma, USA) specific to the C-terminus of HSP70 and anti-mouse IgG-FITC (Sigma, USA) as the second antibodies. The measurements were performed on a FACScan laser flow cytometer (Becton Dickinson, USA). At least 10,000 cells were analyzed for each sample. The statistical analysis was performed using the WinMDI software for processing the histograms recorded during the cytofluorimetric analysis.

Laser scanning confocal microscopy was used to visualize the targeted delivery of Hsp70 and its Hsp70/16 fragment to the surface of the tumor target cells. In these experiments, the target cells sequentially treated with the first and second modules of the designed constructs were stained with anti-HSP70 antibodies and second antibodies conjugated to AF488 fluorochrome (Molecular Probes, USA) using the conventional staining procedure. The cell precipitate obtained after centrifugation was placed onto a microscope slide; a specialized Mowioll gel-like polymerizable medium (Biomeda, USA) retaining cell morphology and preventing fluorochrome photobleaching was subsequently applied. The microscope slide was covered with a coverslip and left in the dark until the microscopic analysis. The photographs of the cells were taken on an ECLIPSE TE2000-E confocal microscope (Nikon, Japan).

Assessment of the effect of treating tumor cells with the designed constructs on the cytotoxic activity of NK cells against these target cells

NK cells isolated from human peripheral blood were used as cytotoxic effector cells in a series of *in vitro* experiments conducted to analyze the antitumor effect of the designed constructs. The magnetic separation technique using an NK cell isolation kit (MACS NK cell isolation kit II, Miltenyi Biotec, Germany) was employed to isolate NK cells from the mononuclear cell fraction obtained by density gradient sedimentation of peripheral blood from donors. The level of NK cell-mediated cytotoxicity was evaluated by CytoTox96 non-radioactive cytotoxicity assay (Promega, USA) based on a quantification of the lactate dehydrogenase (LDH) released from the target cells due to the action of natural killers on tumor cells. The experiments were conducted in accordance with the manufacturer's protocol. Each experimental point was recorded in three replicas. The ratio between NK cells and the target cells placed into the wells was 7:1. BT-474 cells added to the wells 4 h prior to the experiment and subsequently treated with the tested recombinant constructs were used as the targets. At each stage of this procedure, after the addition of the components of the supramolecular complex in the wells and subsequent incubation of the target cells for 30 min at 4°C, the cells were precipitated by centrifugation. Supernatant was then removed, and the wells were washed to remove unbound recombinant proteins.

RESULTS AND DISCUSSION

The cytofluorimetric analysis demonstrated that the designed constructs can efficiently deliver Hsp70 and Hsp70/16 to the surface of tumor target cells. Similar findings characterizing the binding of Hsp70 and Hsp70/16 to the cell surface were obtained in experiments with the BT-474 and SKOV3 cell lines. Hence, below we summarize the results of the interaction between the designed constructs and BT-474 cells. The components of the 4D5 scFv-dibarnase:barstar-Hsp70(Hsp70/16) supramolecular complex efficiently binded to the cell surface: 4D5 scFv-dibarnase binded to the $p185^{HER2}$ antigen, followed by interaction of barstar-Hsp70(Hsp70/16) with 4D5 scFv-dibarnase (*Fig. 2*). Furthermore, our findings indicate that the barstar-Hsp70 and barstar-Hsp70/16 proteins can independently interact with the cell membrane, leading to a shift in the histogram peaks of the respective control

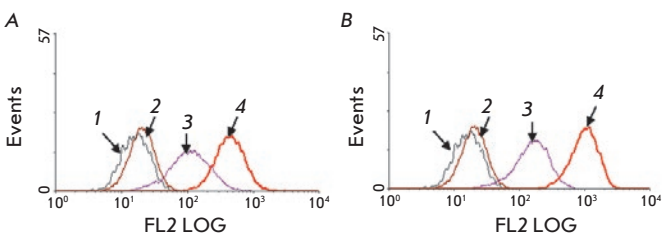

Fig. 2. Cytofluorimetric analysis of the binding of the 4D5 scFv-dibarnase:barstar-Hsp70 (*A*) and 4D5 scFv-dibarnase:barstar-Hsp70/16 (*B*) complexes to the surface of BT-474 tumor cells. The cells were incubated with the first and second modules, and the samples were stained with the first anti-HSP70 antibodies (BRM22) and second FITC-labeled antibodies. X axis – fluorescence intensity; Y axis – number of events. The histograms: *1* – autofluorescence control; *2* – 4D5 scFv-dibarnase control; *3* – barstar-Hsp70 (*A*) or barstar-Hsp70/16 (*B*) control; *4* – 4D5 scFv-dibarnase:barstar-Hsp70 (*A*) or 4D5 scFv-dibarnase:barstar-Hsp70/16 (*B*).

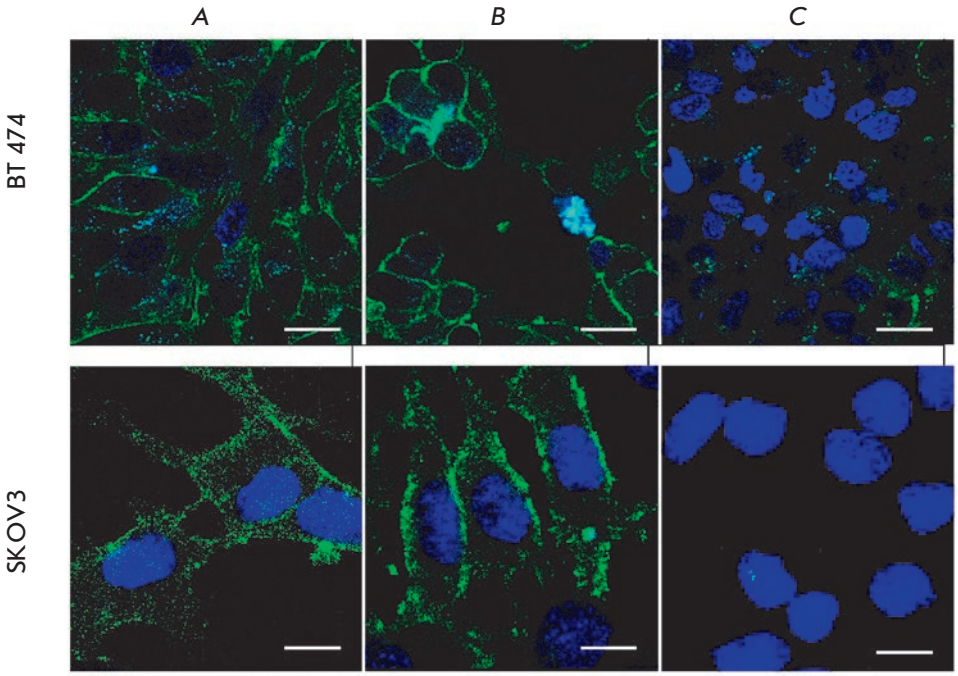

Fig. 3. Visualization of the interaction between the developed constructs and two types of tumor cells. Upper row: BT-474 cells were treated with 4D5 scFv-dibarnase:barstar-Hsp70 (*A*) or 4D5 scFv-dibarnase:barstar-Hsp70/16 (*B*). Bottom row: SKOV3 cells were treated with 4D5 scFv-dibarnase:barstar-Hsp70 (*A*) or 4D5 scFv-dibarnase:barstar-Hsp70/16 (*B*). The treated cell samples were stained with the first anti-Hsp70 antibodies (BRM22) and second Alexa Fluor 488-labeled antibodies. *C* – control cell samples stained only with the second antibodies. Cell nuclei were stained with DAPY. The images were recorded using an ECLIPSE TE2000-E laser confocal microscope (Nikon, Japan). Scale bars, 10 μm

samples towards higher fluorescence signals. According to the literature data, some types of tumor cells can adsorb exogenous HSP70 onto their surface [15, 16].

BT-474 cells expressed the $p185^{HER2}$ antigen targeted by the mini-antibody in the first module. HEK 293 human embryonic kidney cells were used as a control for nonspecific binding of 4D5 scFv-dibarnase to the cell surface. The cytofluorimetric analysis showed that nonspecific binding to the cell membrane was observed for neither the first (4D5 scFv-dibarnase) nor the second (barstar-Hsp70(Hsp70/16)) module (the data are not shown).

Hence, the results indicate that the barnase:barstar systems ensure highly specific and efficient delivery of constructs carrying Hsp70 or its C-terminal fragment to the surface of tumor cells expressing the HER2/neu marker.

The efficiency of using the designed constructs for a targeted delivery of Hsp70 and its fragment, Hsp70/16, to the surface of BT-474 and SKOV3 cells was visualized by laser confocal microscopy. The target cells sequentially treated with the first and second modules of the designed constructs were stained with anti-HSP70 antibodies and the second antibodies conjugated to AF488 fluorochrome using the conventional staining procedure. The level of fluorescent staining was analyzed on an ECLIPSE TE2000-E confocal microscope. The results confirmed that Hsp70 and Hsp70/16 were present on the surface of the treated target cells (*Fig. 3*).

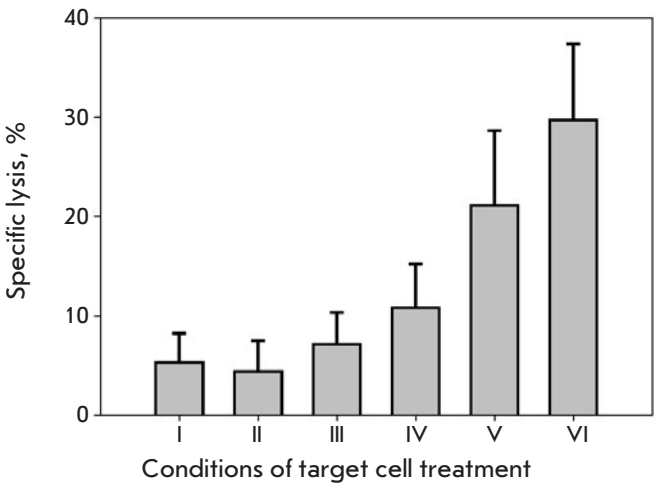

Fig. 4. *In vitro* analysis of the effect of treating tumor target cells (BT-474) with the developed agents on the cytolytic activity of NK cells. I – control (no treatment); II – target cells treated with 4D5 scFv-dibarnase; III – target cells treated with barstar-Hsp70/16; IV – target cells treated with barstar-Hsp70; V – target cells treated with 4D5 scFv-dibarnase:barstar-Hsp70/16; and VI – target cells treated with 4D5 scFv-dibarnase:barstar-Hsp70

The influence of the designed constructs on the activation of cytotoxic effectors of the immune system was studied in the *in vitro* model of interaction between NK cells and the target tumor cells. BT-474 cells were

used as the targets. Assessment of the interaction between effector cells and the target cells in this model demonstrated that targeted delivery of both the Hsp70 and Hsp70/16 molecules to the surface of tumor cells significantly enhances the antitumor cytolytic effect of NK cells. In our experiments, targeted delivery of the full-length Hsp70 molecule and its C-terminal fragment, Hsp70/16, to BT-474 cells enhanced the cytolytic effect of NK cells by more than five- and fourfold, respectively. Treatment of the target cells with individual components of the designed supramolecular complex (4D5 scFv-barnase acting as the "targeting" module and barstar-Hsp70 and barstar-Hsp70/16 acting as "effector" modules) did not significantly influence the cytolytic effect of NK cells. These findings are shown in *Fig. 4*.

CONCLUSIONS

We have demonstrated that the designed two-module molecular construct was efficient in a targeted delivery of molecules that activate the cytotoxic effectors of the immune system (heat shock protein Hsp70 and its C-terminal fragment) to tumor target cells. The approach proposed in this study can underlie the design of novel agents for antitumor immunotherapy. ●

This work was supported by the Russian Science Foundation (grant No. 14-24-00106, gene construction and recombinant protein production) and the Program of the Presidium of the Russian Academy of Sciences "Fundamental Research for Biomedical Technologies" (studying the cytotoxic activity of effector cells of the immune system).

REFERENCES

1. Shilova O.N., Shilov E.S., Lieber A., Deyev S.M. // J. Control Release. 2018. V. 286. P. 125–136. doi: 10.1016/j.jconrel.2018.07.030.
2. Deyev S.M., Lebedenko E.N., Petrovskaya L.E., Dolgikh D.A., Gabibov A.G., Kirpichnikov M.P. // Russian Chemical Reviews. 2015. V. 84. № 1. P. 1–26.
3. Polanovski O.L., Lebedenko E.N., Deyev S.M. // Biochemistry (Moscow). 2012. V. 77. № 3. P. 227–245.
4. Craig E.A., Weissman J.S., Horwich A.L. // Cell. 1994. V. 78. P. 365–372.
5. Hartl F.U. // Nature. 1996. V. 381. P. 571–580.
6. Erkeller-Yeksel F.M., Isenberg D.A., Dhillon V.B., Latchman D.S., Lydyard P.M. // J. Autoimmun. 1992. V. 5. P. 803–814.
7. Ishiyama T., Koike M., Akimoto Y., Fukuchi K., Watanabe K., Yoshida M., Wakabayashi Y., Tsuruoka N. // Clin. Exp. Immunol. 1996. V. 106. P. 351–356.
8. Ferrarini M., Heltai S., Zocchi M.R., Rugarli C. // Int. J. Cancer. 1992. V. 51. P. 613–619.
9. Altmeyer A., Maki R.G., Feldweg A.M., Heike M., Protopopov V.P., Masur S.K., Srivastava P.K. // Int. J. Cancer. 1996. V. 69. P. 340–349.
10. Multhoff G., Hightower L.E. // Cell Stress Chaperones. 1996. V. 1. P. 167–176.
11. Multhoff G., Botzler C., Jennen L., Schmidt J., Ellwart J., Issels R. // J. Immunol. 1997. V. 158. P. 4341–4350.
12. Rogias J., Wallen E.S., Loening S.A., Moseley P.L. // Adv. Exp. Med. Biol. 1998. V. 451. P. 225–229.
13. Sapozhnikov A.M., Ponomarev E.D., Tarasenko T.N., Telford W.G. // Cell Prolif. 1999. V. 32. P. 363–378.
14. Hantschel M., Pfister K., Jordan A., Scholz R., Andreesen R., Schmitz G., Schmetzer H., Hiddenman W., Multhoff G. // Cell Stress Chaperones. 2000. V. 5. P. 438–442.
15. Di Cesare S., Poccia F., Mastino A., Colizzi V. // Immunology. 1992. V. 76. P. 341–343.
16. Poccia F., Piselli P., Vendetti S., Bach S., Amendola A., Placido R., Colizzi V. // Immunology. 1996. V. 88. P. 6–12.
17. Sapozhnikov A.M., Gusarova G.A., Ponomarev E.D., Telford W.G. // Cell Proliferation. 2002. V. 35. P. 193–206.
18. Tőrők Z., Horváth I., Goloubinoff P., Kovács E., Glatz A., Balogh G., Vígh L. // Proc. Natl. Acad. Sci. USA. 1997. V. 94. P. 2192–2197.
19. Multhoff G., Botzler C., Issels R. // Biol. Chem. 1998. V. 379. P. 295–300.
20. Breloer M., Fleischer B., Bonin A. // J. Immunol. 1999. V. 162. P. 3141–3147.
21. Multhoff G., Botzler C., Wiesnet M., Eissner G., Issels. R. // Blood. 1995. V. 86. P. 1374–1382.
22. Ponomarev E.D., Tarasenko T.N., Sapozhnikov A.M. // Immunol. Lett. 2000. V. 74. V. 133–139.
23. Hightower L.E., Hendershot L.M. // Cell Stress Chaperones. 1997. V. 2. P. 1–11.
24. Multhoff G. // Int. J. Hyperthermia. 1997. V. 13. P. 39–48.
25. Tamura Y., Tsuboi N., Sato N., Kikuchi K. // J. Immunol. 1993. V. 151. P. 5516–5524.
26. Menoret A., Patry Y., Burg C., Le Pendu J. // J. Immunol. 1995. V. 155. P. 740–747.
27. Wei Y-g., Zhao X., Karuya Y., Fukata H., Teshigawara K., Uchida A. // Cancer Res. 1996. V. 56. P. 1104–1110.
28. Srivastava P.K., Amato R.J. // Vaccine. 2001. V. 19. P. 2590–2597.
29. Sashchenko L.P., Dukhanina E.A., Yashin D.V., Shatalov Y.V., Romanova E.A., Korobko E.V., Demin A.V., Lukyanova T.I., Kabanova O.D., Khaidukov S.V., Kiselev S.L., Gabibov A.G., Gnuchev N.V., Georgiev G.P. // J. Biol. Chem. 2004. V. 279. P. 2117–2124.
30. Shevtsov M.A., Komarova E.Y., Meshalkina D.A., Bychkova N.V., Aksenov N.D., Abkin S.V., Margulis B.A., Guzhova I.V. // Oncotarget. 2014. V. 5. P. 3101–3114.
31. Yuan J., Kashiwagi S., Reeves P., Nezivar J., Yang Y., Arrifin N.H., Nguyen M,. Jean-Mary G., Tong X., Uppal P.,, et al. // J. Hematol. and Oncol. 2014. V. 7. P. 15.
32. Yashin D.V., Ivanova O.K., Soshnikova N.V., Sheludchenkov A.A., Romanova E.A., Dukhanina E.A., Tonevitsky A.G., Gnuchev N.V., Gabibov A.G., Georgiev G.P., Sashchenko L.P. // J. Biol. Chem. 2015. V. 290. P. 21724–21731.
33. Guzhova I.V., Margulis B.A. // Hum. Vaccin. Immunother. 2016. V. 12. P. 2529–2535.
34. Kovalenko E.I., Vlaskin P.A., Kanevskii L.M., Strel'nikova Y.I., Sapozhnikov A.M. // Dokl. Biol. Sci. 2006. V. 406. P. 4–6.
35. Multhoff G., Pfister K., Gehrmann M., Hantschel M., Gross C., Hafner M., Hiddemann W. // Cell Stress Chaperones. 2001. V. 6. P. 337–344.

36. Deyev S.M., Waibel R., Lebedenko E.N., Schubiger A.P., Plückthun A. // Nature Biotechnology. 2003. V. 21. P. 1486–1492.
37. Shipunova V.O., Zelepukin I.V., Stremovskiy O.A., Nikitin M.P., Care A., Sunna A., Zvyagin A.V., Deyev S.M. // ACS Appl. Mater. Interfaces. 2018. V. 10. № 20. P. 17437–17447. doi: 10.1021/acsami.8b01627
38. Martsev S.P., Chumanevich A.A., Vlasov A.P., Dubnovitsky A.P., Tsybovsky Y.I., Kravchuk Z.I., Cozzi A., Arosio P., Deyev S.M. // Biochemistry. 2000. V. 39. № 27. P. 8047–8057.
39. Generalova A.N., Sizova S.V., Zdobnova T.A., Zarifullina M.M., Oleinikov V.A., Zubov V.P., Deyev S.M., Artemyev M.V., Baranov A.V. // Nanomedicine. 2011. V. 6. № 2. P. 195–209.

Expression and Intracellular Localization of Paraoxonase 2 in Different Types of Malignancies

M. I. Shakhparonov, N. V. Antipova, V. O. Shender, P. V. Shnaider, G. P. Arapidi, N. B. Pestov, M. S. Pavlyukov*

Shemyakin–Ovchinnikov Institute of Bioorganic Chemistry, Miklukho-Maklaya Str., 16/10, Moscow, 117997, Russia

*E-mail: marat.pav@mail.ru

Received December 07, 2017; in final form June 05, 2018

ABSTRACT **PON2 belongs to the paraoxonase protein family that consists of lactone hydrolyzing enzymes with different substrate specificities. Unlike other members of the family, PON2 exhibits substantial antioxidant activity, is localized predominantly inside the cell, and is ubiquitously expressed in all human tissues. Previously, it was proffered that defense against pathogens, such as *Pseudomonas aeruginosa*, is the main function of paraoxonases. However, recent findings have highlighted the important role played by PON2 in protection against oxidative stress, inhibition of apoptosis, and progression of various types of malignancies. In the current study, we performed a bioinformatic analysis of RNA and DNA sequencing data extracted from tumor samples taken from more than 10,000 patients with 31 different types of cancer and determined expression levels and mutations in the *PON2* gene. Next, we investigated the intracellular localization of PON2 in multiple cancer cell lines and identified the proteins interacting with PON2 using the LC-MS/MS technique. Our data indicate that a high PON2 expression level correlates with a worse prognosis for patients with multiple types of solid tumors and suggest that PON2, when localized on the nuclear envelope and endoplasmic reticulum, may protect cancer cells against unfavorable environmental conditions and chemotherapy.**

KEYWORDS **paraoxonase, cancer, apoptosis, glioblastoma, protein-protein interactions.**

ABBREVIATIONS **PON2 – paraoxonase 2, TCGA – The Cancer Genome Atlas.**

INTRODUCTION

The paraoxonase family comprises three enzymes: PON1, PON2, and PON3. A phylogenetic analysis of these proteins seemed to demonstrate that PON2 is the most ancient member of this family, which later gave rise to PON1 and PON3 during evolution [1]. All these enzymes exhibit a pronounced lactonase activity but differ in terms of substrate specificity. Furthermore, paraoxonases have different expression profiles. Hence, PON1 and PON3 are synthesized by the liver; in blood plasma, the proteins are associated with high-density lipoproteins. Unlike those, PON2 is ubiquitously expressed in all human tissues and is localized mostly within the cell. Interestingly, the main function of PON2 in some cell types is related to the antioxidant activity of this enzyme [2]. Thus, PON2 has been shown to significantly reduce the production of superoxide ions as it interacts with complex I and III of the electron transport chain on the inner mitochondrial membrane and also participates in peroxidation of lipids in the plasma membrane [3]. The antioxidant activity of PON2 is independent of the lactonase activity of this enzyme [4].

Detailed studies focused on the structure of PON2 have demonstrated that this protein weighs ~40 kDa, carries two glycosylation sites, a short intracellular domain (1–5 a.a.), a transmembrane domain consisting of a single α-helix (6–24 a.a), as well as a hydrophobic domain (67–81 a.a.) and a enzymatic domain (168–246 a.a.) residing on the outer side of the plasma membrane. Due to its transmembrane domain, PON2 is incorporated into the lipid bilayer during translation and is distributed between the endoplasmic reticulum, the perinuclear region, mitochondria, and the plasma membrane. However, data on the predominant localization of PON2 inside the cell is rather controversial [3, 5, 6, 7].

There has recently been a keen interest in paraoxonase 2, as this protein was found to be associated with malignancy progression. Over the past year, many laboratories have described the important role played by PON2 in tumor cells. Hence, they have demonstrated that PON2 contributes to the progression and metastasizing of pancreatic cancer by stimulating glucose uptake [8], accelerates the proliferation of and resist-

ance to oxidative stress in bladder cancer [9], protects glioblastoma cells against apoptosis [10], and reduces the sensitivity of oral cancer cells to radiation therapy [11]. However, the exact role played by PON2 in other cancer types is yet to be elucidated.

MATERIALS AND METHODS

Cell Culture

Cells were grown in air enriched with 5% (v/v) CO_2 at 37°C in Dulbecco's modified Eagle's medium (DMEM) supplemented with 10% (v/v) fetal bovine serum (FBS) and a 2mM L-glutamine and penicillin (100 units/ml) streptomycin (100μg/ml) mixture. The cells were transfected with the Lipofectamine LTX reagent (Thermo Fisher Scientific; USA) according to the manufacturer's protocol.

Immunofluorescence microscopy

The cells were washed 3 times with phosphate buffered saline (PBS) and fixed with 4% PFA in PBS for 15 min at room temperature. Next, the cells were washed 2 times with PBS and permeabilized with 0.2% Triton-X100 in PBS for 15 minutes. After permeabilization, the cells were blocked for 5 min with 1% BSA in PBST (0.1% Tween 20 in PBS). Next, they were incubated with primary antibodies against PON2 (1:200 dilution; HPA029193, Sigma) or against CRM1 (1:200 dilution; NB100-79802, Novus Biologicals) in PBST for 1 hour. Then, they were washed 5 times with PBST and incubated for an additional hour with secondary antibodies conjugated with Alexa Fluor 555 (dilution 1:500; A32732, Thermo Fisher Scientific) in PBST. Finally, the cells were washed 6 times with PBST to remove unbounded secondary antibodies and stained with DAPI (4',6-diamidino-2-phenylindole). After 10 min of incubation, the cells were analyzed under a fluorescent microscope.

Plasmid Construction

The DNA fragment encoding PON2 was amplified from the previously obtained one by the PCR technique using the primer pair BglII-PON2 (AAA AAG ATC TAT GGG GCG GCT GGT GGC TGT G) and PON2-SalI (AAA AGT CGA CAG TTC ACA ATA CAA GGC TCT GTG GTA) and cloned into the BglIII/SalI sites of the pTurboGFP-N or pTagRFP-C plasmid (Evrogen) to generate the pTurboGFP-N-PON2 and pTagRFP-C-PON2 plasmids, respectively. The DNA fragment encoding 1-27 a.a. of PON2 was amplified from the previously obtained one by the PCR technique using the primer pair BglII-PON2 and PON2_rev2 (TAT TGT CGA CAG TCG ATT TCT GAG TGC CA) and cloned into the BglIII/SalI sites of the pTurboGFP-N plasmid to generate the pTurboGFP-N-PON2-1 plasmid. The DNA fragment encoding 1-83 a.a. of PON2 was amplified from the previously obtained one by the PCR technique using the primer pair BglII-PON2 and PON2_rev3 (AAT TGT CGA CCC TCC AGG CTT ATC T) and cloned into the BglIII/SalI sites of the pTurboGFP-N plasmid to generate the pTurboGFP-N-PON2-2 plasmid. The DNA fragment encoding 1-168 a.a. of PON2 was amplified from the previously obtained one by the PCR technique using the primer pair BglII-PON2 and PON2_rev4 (ATT TGT CGA CAT GTC ATT CAC ACT TGG A) and cloned into the BglIII/SalI sites of the pTurboGFP-N plasmid to generate the pTurboGFP-N-PON2-3 plasmid. For overexpression of full length PON2 fused to Halo-tag, we amplified the Halo-tag sequence from the pFC20K HaloTag T7 SP6 Flexi plasmid (Promega) by the PCR technique using the primer pair SalI-Halo (AGG AGT CGA CTG AGG ATC TGT ACT TTC A) and Halo-NotI (GAG GGC GGC CGC TTA ACC GGA AAT CTC CAG AGT A) and cloned into the SalI/NotI sites of the pTurboGFP-N-PON2 plasmid. Thus, we had replaced the GFP coding sequence with the Halo-tag coding sequence. The resulting plasmid was named pTurboHALO-N-PON2. In all cases, the absence of unwanted mutations in the inserts and vector-insert boundaries was verified by sequencing.

Purification of PON2 interacting proteins

U87MG cells were grown on a T75 flask and transfected with the pTurboHALO-N-PON2 plasmid. Forty-eight hours after transfection, the cells were dissociated by a Trypsin-Versene solution and washed twice with ice-cold PBS. Next, the cells were lysed in mammalian cell lysis buffer (50 mM Tris-HCl, 150 mM NaCl, 1% Triton X100, 0.1% sodium deoxycholate, 1 mM PMSF, pH 7.5). Lysate was centrifuged for 15 min, 20,000 g at 4°C. After this, the PON2-interacting proteins were purified with Magne HaloTagBeads (Promega), according to the manufacturer's protocol.

Trypsin digestion

The proteins were eluted from magnetic beads through 30-min incubation with a buffer containing 8M Urea, 2M Thiourea, and 10 mM Tris (pH 8). Then, protein disulfide bonds were reduced with 5 mm DTT at RT for 30 min and, afterwards, alkylated with 10 mm iodoacetamide at room temperature for 20 min in the dark. Next, the samples were diluted (1:4) with 50 mM ammonium bicarbonate buffer and digested with trypsin (0.01 μg of trypsin per 1 μg of protein) for 14 hr at 37°C. After trypsin digestion, the reaction was stopped by addition of formic acid to a final concentration of 5%. The obtained tryptic fragments were desalted by Dis-

covery DSC-18 50 mg microcolumns (Sigma, USA), dried in vacuum, and re-dissolved in 3% ACN with a 0.1% FA solution prior to the LC-MS/MS analysis.

LC-MS/MS Analysis

The LC-MS/MS Analysis was performed on a TripleTOF 5600+ mass-spectrometer with a NanoSpray III ion source (ABSciex) coupled with a NanoLC Ultra 2D+ nano-HPLC system (Eksigent, USA). The HPLC system was configured in a trap-elute mode. For sample-loading buffer and buffer A, a mixture of 98.9% water, 1% methanol, and 0.1% formic acid (v/v) was used. Buffer B was 99.9% acetonitrile and 0.1% formic acid (v/v). The samples were loaded on a Chrom XP C18 trap 3 μm 120 Å 350 μm*0.5 mm column (Eksigent, USA) at a flow rate of 3 μl/min for 10 min and eluted through a 3C18-CL-120 separation column (3 μm, 120 Å, 75 μm*150 mm; Eksigent) at a flow rate of 300 nl/min. The gradient ranged from 5 to 40% of buffer B in 90 min, followed by 10 min at 95% buffer B and 20 min re-equilibration with 5% of buffer B. The information-dependent mass-spectrometer experiment included 1 survey MS1 scan, followed by 50-dependent MS2 scans. The MS1 acquisition parameters were as follows: mass range for the MS2 analysis was 300–1250 m/z, and signal accumulation time was 250 ms. Ions for the MS2 analysis were selected on the basis of intensity with a threshold of 200 cps and a charge state ranging from 2 to 5. The MS2 acquisition parameters were as follows: the resolution of quadrupole was set to UNIT (0.7 Da), the measurement mass range was 200–1800 m/z, and signal accumulation time was 50 ms for each parent ion. Collision-activated dissociation was performed with nitrogen gas with a collision energy ramping from 25 to 55 V within a signal accumulation time of 50 ms. Analyzed parent ions were sent to a dynamic exclusion list for 15 sec in order to generate an MS2 spectra at the chromatographic peak apex. A β-Galactosidase tryptic solution (20 fmol) was run with a 15-min gradient (5-25% of buffer B) every 2 samples and between sample sets to calibrate the mass-spectrometer and to control overall system performance, stability, and reproducibility.

LC-MS/MS Data Analysis

Raw LC-MS/MS data were converted to .mgf peak lists with ProteinPilot (version 4.5). For this procedure, we ran ProteinPilot in an identification mode with the following parameters: Cys alkylation by iodoacetamide, trypsin digestion, TripleTOF 5600 instrument, and thorough ID search with detected protein threshold 95.0% against UniProt human Protein knowledgebase (version 2013_03, with 150600 entries). For thorough protein identification, the generated peak lists were searched with the MASCOT (version 2.2.07) and the X! Tandem (CYCLONE, 2013.2.01) search engine against UniProt human Protein knowledgebase (version 2013_03), with a concatenated reverse-decoy dataset (with 301200 entries altogether). Precursor and fragment mass tolerance were set at 20 ppm and 0.04 Da, respectively. Database searching parameters included the following: tryptic digestion with 1 possible miss cleavage, static modifications for carbamidomethyl (C), and dynamic/flexible modifications for oxidation (M). For X! Tandem, we also selected parameters that allowed a quick check for protein N-terminal residue acetylation, peptide N-terminal glutamine ammonia loss, or peptide N-terminal glutamic acid water loss. Result files were submitted to the Scaffold 4 software (version 4.0.7) for validation and a meta analysis. We used the LFDR scoring algorithm with standard experiment-wide protein grouping. For the evaluation of peptide and protein hits, a false discovery rate of 5% was selected for both. False positive identifications were based on reverse database analysis.

RESULTS AND DISCUSSION

In order to identify the types of malignancies for which PON2 can play a potentially important oncogenic role, we compared the expression levels of this protein using the RNA sequencing data from the TCGA (The Cancer Genome Atlas) database. Having analyzed the data obtained for more than 10,000 patients with 31 types of malignancies, we found that the highest expression level of PON2 is observed in liver and brain cancer (grade 1–3 gliomas and grade 4 glioblastoma), while the lowest expression level of this protein is typical of leukemia (myeloid leukemia and B-cell lymphoma) (*Fig. 1A*). In order to understand whether the observed disturbance of PON2 expression is caused by mutations in the respective gene, we analyzed the genomic DNA sequencing data to reveal any possible amplifications or deletions of this gene in different tumor types. One can see from *Fig. 1B* that amplification of the *PON2* gene is typical of glioblastoma, while deletion of this gene is usually observed in leukemia. This result is in good agreement with our findings obtained by analyzing PON2 expression.

In order to assess the effect of PON2 on the proliferation and resistance of tumor cells to therapy, we analyzed how the expression level of this protein is associated with the survival of patients with different types of cancer. The data in *Fig. 2* convincingly demonstrate that a high PON2 level correlates with poor prognosis for patient survival in liver cancer, glioma, and glioblastoma, while the opposite is true for leukemia: an elevated level of paraoxonase 2 is a good prognostic indicator. These results are fully consistent with our

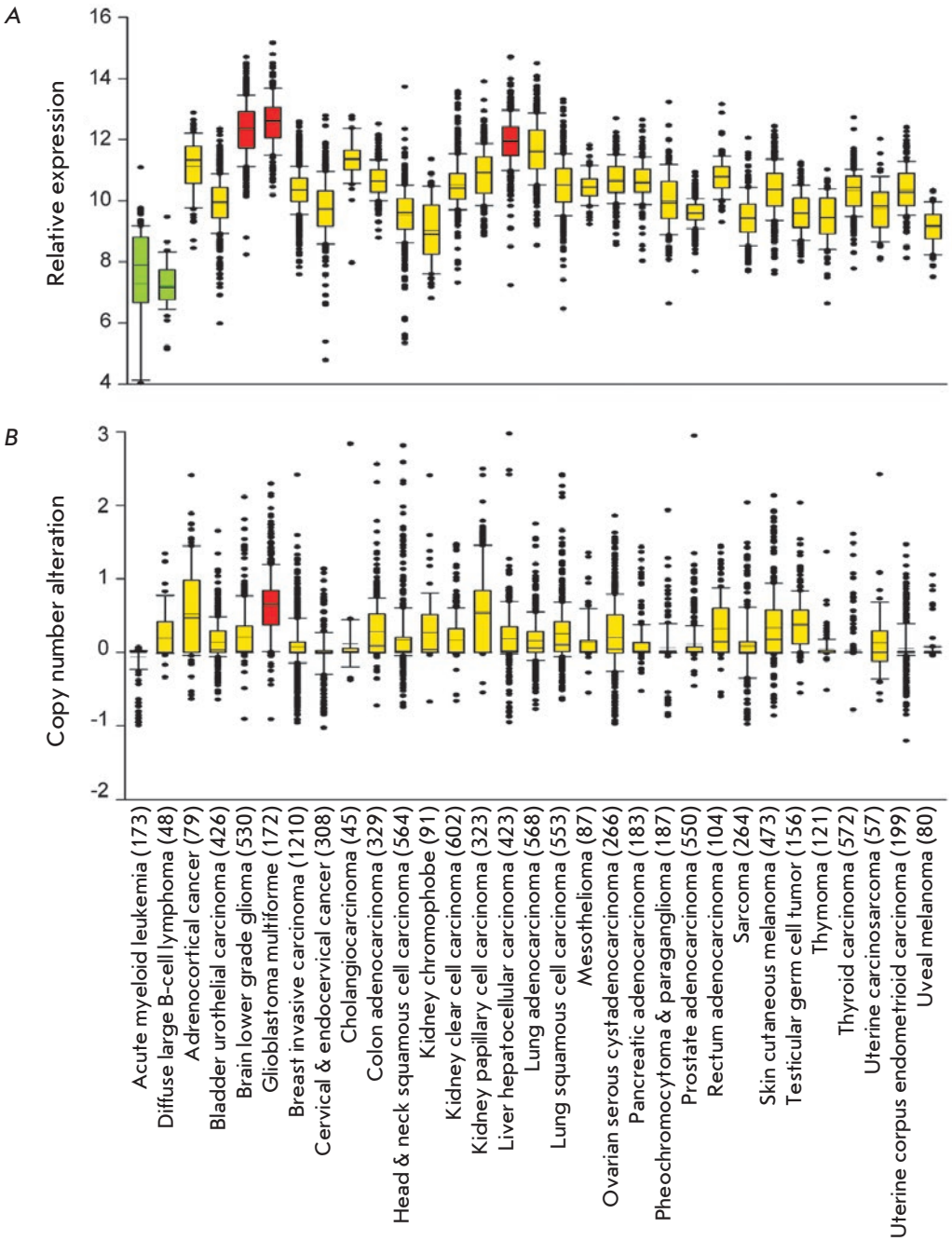

Fig. 1. Relative expression level (*A*) and copy number variation (*B*) of the *PON2* gene in tumors from patients with different types of cancer. Results were obtained by bioinformatic analysis of RNA and DNA sequencing data from the TCGA database. The number of patients for each cohort is indicated in brackets

findings on the expression level and mutations in the *PON2* gene.

The large necrotic zone emerging in the tumor center, its volume often being many times larger than the amount of viable tumor tissue, is a distinctive clinical feature of brain cancer [12]. Such a high level of cancer cell death is associated with an insufficient blood supply to glioblastoma and extremely limited space for growth. For this reason, glioblastoma cells are continuously exposed to the stress caused by the lack of nutrients and the toxic components released by neighboring dying cells. A similar situation is observed in the liver, since potentially harmful substances are delivered from blood to this organ. Hence, it is fair to assume that PON2 plays a crucial role in liver and brain cancer cells, as it helps them adapt to existence in an environment with a high concentration of toxic metabolic products and lack of nutrients. Therefore, selection of tumors with an increased PON2 expression level may take place as these tumors develop and one of the reasons is

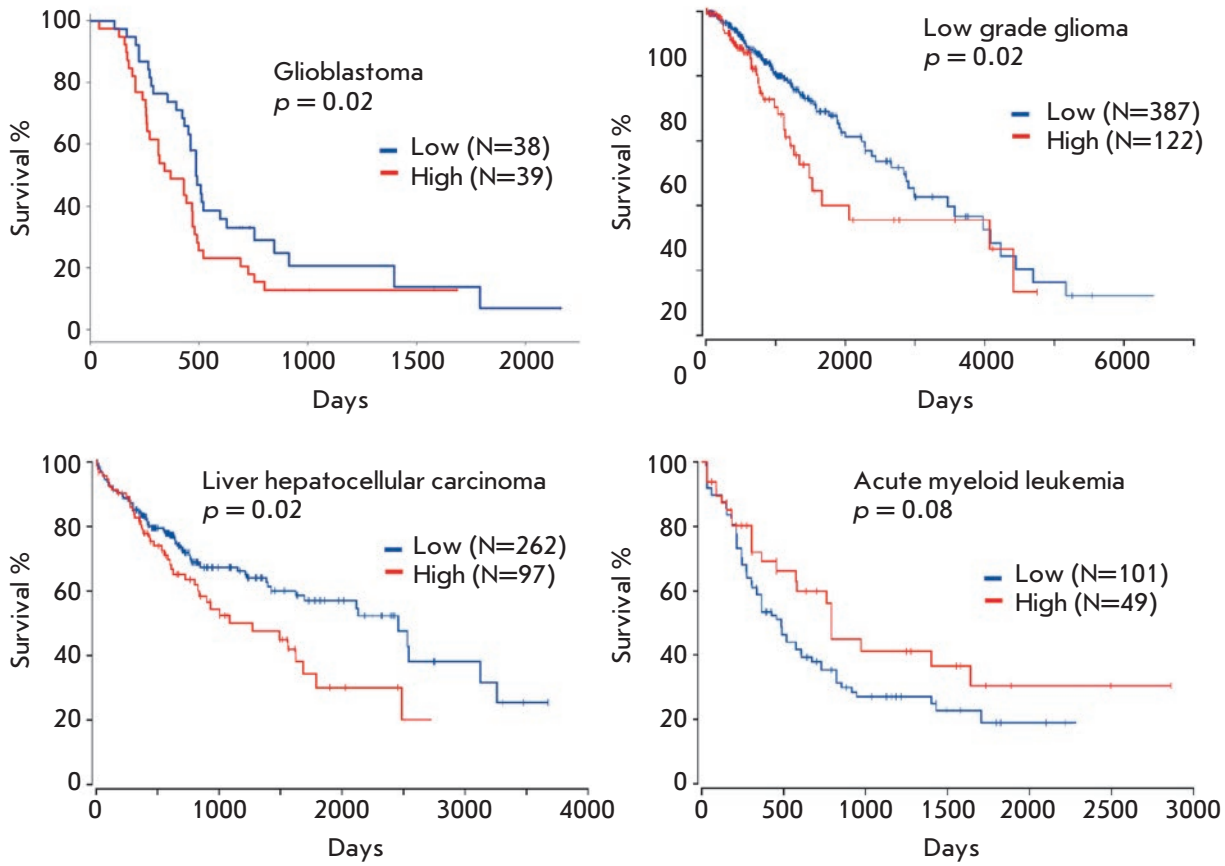

Fig. 2. The Kaplan–Meier survival curve for patients with glioblastoma, low grade glioma, liver hepatocellular carcinoma and acute myeloid leukemia divided into two groups based on the PON2 expression level. Results were obtained by bioinformatic analysis of the TCGA database. The number of patients in each group and the *p* value (log-rank test) are indicated

the amplification of the respective gene. Contrariwise, leukemia cells exist in a favorable environment that is rich in oxygen and nutrients and contains no potentially toxic substances. As a result, they do not require a high PON2 expression level; conversely, the reduced PON2 level seems to be responsible for the more aggressive phenotype of these tumor cells.

In order to glean more information about the functions of PON2 in tumor cells, we stained 6 cell lines (U87-MG – glioblastoma; MRC5-V2 – embryonic lung; SKOV3 – ovarian carcinoma; A549 – lung carcinoma; HepG2 – liver carcinoma; and HT1080 – fibrosarcoma) with antibodies specific to this protein. Our results demonstrated that staining with the highest intensity is observed in glioblastoma and liver carcinoma cells, which is consistent with the bioinformatic analysis data (*Fig. 3A*). In all the analyzed cell types, PON2 was localized in the perinuclear region. Since the quality of immunocytofluorescence staining did not allow us to accurately identify the localization of PON2 in cells, the next step was to study the localization of exogenously expressed paraoxonase 2. For this purpose, we cotransfected U87-MG cells with plasmids pTagRFP-C-PON2 (encodes the red fluorescent protein linked to the N-terminus of PON2) and pTurboGFP-N-PON2 (encodes the green fluorescent protein linked to the C-terminus of PON2) and stained the transfected cells with anti-PON2 antibodies. One can see in *Fig. 3B* that PON2 was predominantly localized around the nucleus, regardless of where the fluorescent protein was inserted.

In order to determine PON2 localization more accurately, we stained the transfected cells with antibodies specific to the CRM1 protein, a marker of the nuclear envelope. One can see in *Fig. 4A* that PON2 around the nucleus is completely colocalized with CRM1, suggesting that a significant portion of PON2 in the cell resides on the nuclear envelope.

Next, we attempted to identify the amino acid sequence of PON2 required to ensure localization of this protein on the nuclear envelope. With this in mind,

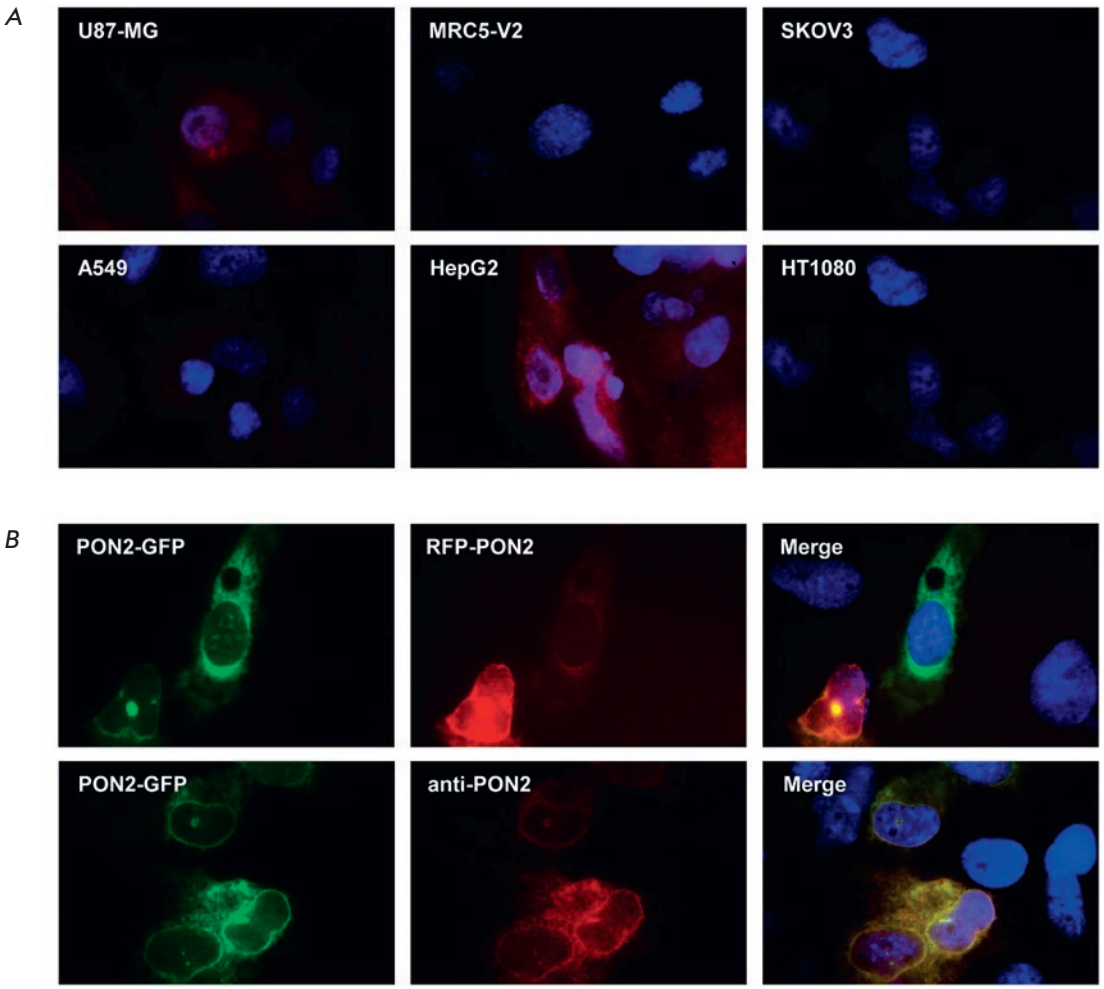

Fig. 3. *A* – Immunofluorescent staining of different cell lines with anti-PON2 antibodies. *B* – Fluorescence images of cells cotransfected with the pTagRFP-C-PON2 and pTurboGFP-N-PON2 plasmids (upper panel) and cells transfected with the pTurboGFP-N-PON2 plasmid and then stained with anti-PON2 antibodies (lower panel)

we created plasmids encoding three PON2 fragments (1–27 a.a.; 1–83 a.a.; and 1–168 a.a.) carrying the green fluorescent protein at their N-terminus. *Figure 4B* demonstrates that the first 27 amino acids of PON2 encoding the transmembrane segment of this protein are sufficient for ensuring localization of PON2 on the nuclear envelope.

Finally, we employed the LC-MS/MS method to identify the intracellular proteins interacting with PON2. We transfected the cells with a plasmid encoding either PON2 or the control protein, labeled with the Halo Tag at its C-terminus. Magnetic particles with Halo Tag ligand were used to isolate exogenous PON2 and the proteins interacting with it. Subsequent LC-MS/MS analysis allowed us to identify 286 proteins coprecipitating with PON2. Among those, 168 proteins were also detected in the control sample, while 119 proteins interacted exclusively with PON2, rather than with the control protein (*Table*). Among the proteins exhibiting a unique interaction with PON2, there were six localized on the nuclear envelope (CACYBP, TMPO, S100A6, RAN, UBXN4, and TOR1AIP1). It is important to mention that the highest number of peptides (not counting PON2) was identified for the CACYBP protein, which can be indicative of a high intensity of interaction between CACYBP and PON2.

CONCLUSIONS

A large body of studies describing the functions of PON2 in several types of malignancies has been published over the past year. In order to acquire more general information about the role played by this protein in various types of malignancies, we have, for the first time, analyzed the expression level and mutations in the *PON2* gene in 31 types of malignancies and investigated the association between the expression level of PON2 and patient survival. Our findings demonstrate that the highest level of PON2 expression is observed in solid tumors, in particular in brain tumor and liver cancer. Amplification of the *PON2* gene and correlation of its expression with unfavorable prognosis of survival are also typical of these tumors. Contrariwise, hema-

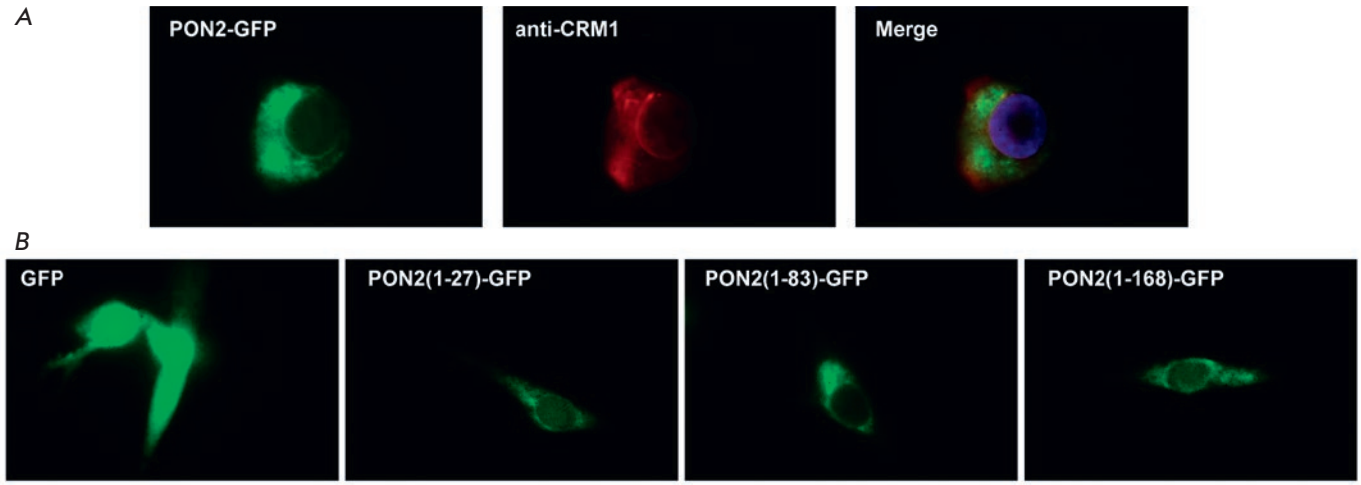

Fig. 4. *A* – Fluorescence images of cells transfected with the pTurboGFP-N-PON2 plasmid and then stained with anti-CRM1 antibodies. *B* – Fluorescence images of cells transfected with plasmids encoding different fragments of PON2 (1–27 a.a.; 1–83 a.a.; 1–168 a.a.) or GFP alone as a control

Table. List of the proteins coprecipitated with PON2

Gene	MW	N	Gene	MW	N	Gene	MW	N	Gene	MW	N
PON2	39	9	RPS20	13	2	RPS18	18	1	SNU13	14	1
CACYBP	26	7	RPS7	22	2	RPL12	18	1	HNRNPD	31	1
RPS10	19	6	RPL11	20	2	RPL14	23	1	FKBP3	25	1
RPS19	16	6	RPL30	13	2	ADD3	74	1	PTRF	43	1
HSPA1A	70	6	NARS	63	2	AIDA	35	1	DHX15	91	1
PARP1	113	6	DTD1	23	2	CTNNBL1	65	1	PSME3	30	1
RPS5	23	5	EIF2S2	38	2	FLJ51636	12	1	DEK	43	1
EIF3A	75	5	EIF3G	36	2	CCDC124	26	1	DR1	19	1
EIF5	49	5	EXOSC2	33	2	COL12A1	333	1	S100A11	12	1
MANF	21	5	FARSLA	58	2	CSTB	11	1	S100A6	10	1
NELFE	43	5	GTF2F2	28	2	DCD	11	1	SEC61G	8	1
AHNAK	629	5	HDGF	27	2	MCM4	97	1	PTD004	20	1
FLJ20643	32	5	CDC37	44	2	DNAJC17	35	1	SARNP	24	1
ERP29	29	4	HYPK	15	2	DNAH10	515	1	SRSF1	28	1
EIF3J	29	4	IMPDH2	56	2	EEF1B2	25	1	SRSF3	19	1
EIF4B	69	4	TIMM8B	9	2	GTF2F1	58	1	STK10	112	1
FEN1	43	4	PYM1	23	2	GAPDHS	45	1	STK24	23	1
METAP1	43	4	CWC27	54	2	RAN	24	1	SARS	59	1
RPL9	22	3	PABPC1	71	2	HNRNPUL1	96	1	SNRPF	10	1
ATP5O	23	3	PTBP1	57	2	HIST1H2AB	14	1	CWC15	27	1
DNAJB1	38	3	PAWR	37	2	HIST1H4A	11	1	STMN1	17	1
HNRNPA1	39	3	PDIA3	57	2	IGF2BP1	63	1	TOR1AIP1	66	1
KRT2	65	3	MAGOHB	17	2	ITIH3	100	1	TCEAL4	25	1
TMPO	75	3	PBDC1	26	2	LIMS1	38	1	TUBA1C	50	1
TIMM8A	11	3	SNRPB	25	2	ZFYVE28	96	1	PTPN1	50	1
PA2G4	45	3	TARS	83	2	MESDC2	26	1	YARS	59	1
FAM50A	40	3	NSUN2	86	2	METAP2	53	1	UBXN1	33	1
SKIV2L2	118	3	MRPS11	21	1	MAPRE1	30	1	UBXN4	57	1
TCEA1	34	3	RPS16	16	1	DNAJC19	12	1	HDLBP	141	1
RPS15	17	2	RPS17	16	1	NAA50	19	1			

Note. Gene name (Gene), molecular weight in kDa (MW), and the number of unique peptides identified by LC-MS/MS mass spectrometry (N) are indicated.

tologic malignancies are characterized by a low level of this protein, deletions of the respective gene, and correlation of the level of PON2 expression with a favorable prognosis. It is known that PON2 plays various functions in the cell, such as lactone cleavage, reduction of free radical production in mitochondria, and protection of membrane lipids against peroxidation. According to the data on the localization of this protein in the cell and on its interaction with other proteins, it is fair to assume that PON2 in tumor cells mainly protects the intracellular membranes against oxidation and, possibly, prevents free radicals from percolating through the nuclear envelope and damaging the genetic material contained in the cells. However, further research is needed for definitive confirmation of this hypothesis. ●

This work was supported by the Russian Science Foundation № 16-14-10335.

REFERENCES

1. Costa L.G., de Laat R., Dao K., Pellacani C., Cole T.B., Furlong C.E. // Neurotoxicology. 2014. V. 43. P. 3–9.
2. Ng C.J., Wadleigh D.J., Gangopadhyay A., Hama S., Grijalva V.R., Navab M., Fogelman A.M., Reddy S.T. // J. Biol. Chem. 2001. V. 276. P. 44444–44449.
3. Hagmann H., Kuczkowski A., Ruehl M., Lamkemeyer T., Brodesser S., Horke S., Dryer S., Schermer B., Benzing T., Brinkkoetter P.T. // FASEB J. 2014. V. 28. P. 1769–1779.
4. Altenhöfer S., Witte I., Teiber J.F., Wilgenbus P., Pautz A., Li H., Daiber A., Witan H., Clement A.M., Förstermann U., et al. // J. Biol. Chem. 2010. V. 285. P. 24398–24403.
5. Aviram M., Rosenblat M. // Free Radic. Biol. Med. 2004. V. 37. P. 1304–1316.
6. Horke S., Witte I., Wilgenbus P., Krüger M., Strand D., Förstermann U. // Circulation. 2007. V. 115. P. 2055–2064.
7. Rothem L., Hartman C., Dahan A., Lachter J., Eliakim R., Shamir R. // Free Radic. Biol. Med. 2007. V. 43. P. 730–739.
8. Nagarajan A., Dogra S.K., Sun L., Gandotra N., Ho T., Cai G., Cline G., Kumar P., Cowles R.A., Wajapeyee N. // Mol. Cell. 2017. V. 67. P. 685–701.
9. Bacchetti T., Sartini D., Pozzi V., Cacciamani T., Ferretti G., Emanuelli M. // Oncotarget. 2017. V. 8. P. 28785–28795.
10. Tseng J.H., Chen C.Y., Chen P.C., Hsiao S.H., Fan C.C., Liang Y.C., Chen C.P. // Oncotarget. 2017. V. 8. P. 14666–14679.
11. Krüger M., Amort J., Wilgenbus P., Helmstädter J.P., Grechowa I., Ebert J., Tenzer S., Moergel M., Witte I., Horke S. // Oncotarget. 2016. V. 7. P. 51082–51095.
12. Brat D.J., Castellano-Sanchez A.A., Hunter S.B., Pecot M., Cohen C., Hammond E.H., Devi S.N., Kaur B., van Meir E.G. // Cancer Res. 2004. V. 64. P. 920–927.

Influence of the Activation of NMDA Receptors on the Resting Membrane Potential of the Postsynaptic Cell at the Neuromuscular Junction

S. E. Proskurina[1*], K. A. Petrov[1,2,3], E. E. Nikolsky[1,2,3,4]

[1]Open Laboratory of Neuropharmacology, Kazan Federal University, Kremlyovskaya Str., 18, Kazan, 420008, Russia

[2]Laboratory of Biophysics of Synaptic Processes, Kazan Institute of Biochemistry and Biophysics, Russian Academy of Sciences, Lobachevsky Str., 2/31, Kazan, 420111, Russia

[3]A.E. Arbuzov Institute of Organic and Physical Chemistry, Russian Academy of Sciences, Arbuzov Str., 8, Kazan, 420029, Russia

[4]Department of Medical and Biological Physics, Kazan State Medical University, Butlerova Str., 49, Kazan, 420012, Russia

*E-mail: svetlana-proskurina@mail.ru

Received June 23, 2017; in final form, June 26, 2018

ABSTRACT **Impaired function or insufficient expression of glutamate N-methyl-D-aspartate (NMDA) receptors underlies a number of brain pathologies; these receptors are, therefore, regarded as a pharmacological target for many neuroactive drugs. It was shown that in the CNS, this type of glutamate receptors participate in the processes of neuronal excitation, synaptic plasticity [1, 2], and excitotoxicity in neurodegenerative diseases and are also involved in the pathogenesis of epilepsy and seizures. However, until recently, the presence and activity of NMDA receptors beyond the CNS had never been considered. This research shows that activation of NMDA receptors at the mammalian neuromuscular junction alters the resting membrane potential of the postsynaptic cell evoked by cation entry through the receptor-associated channel.**

KEYWORDS **Neuromuscular transmission, NMDA receptor, glutamate, glycine, electrophysiology.**

ABBREVIATIONS **NMDA – N-metyl-*D*-aspartate; ACh – acetylcholine; GABA – γ-aminobutyrilic acid; ATP – adenosine triphosphate; CNS – central nervous system; RMP – resting membrane potential; 5,7-DCKA – 5,7-dichlorokynurenic acid; AP5 – *DL*-2-amino-5-phosphonopenthatoic acid.**

INTRODUCTION

Neuromuscular synaptic transmission is indispensable for the process of human life, as it is the mechanism that transfers cerebral commands to activate muscle contractions. The neuromuscular junction (NMJ) is a synapse composed of the presynaptic motor nerve terminal, the synaptic cleft, and the postsynaptic region of muscle fiber. The NMJ is a chemical-type synapse in which transmission of basic signals is mediated by acetylcholine (ACh). However, it is worth mentioning that other neurotransmitters (glutamate, ATP, GABA) have been shown to exist in this presumably cholinergic synapse, whose putative role is fine-tuning of ACh release [3, 4, 5].

NMDA receptors (NMDAR) are ionotropic ligand-gated receptors associated with the cation-permeable channel [6]. Simultaneous presence of two co-agonists (glutamate and glycine) and removal of the magnesium block are required to activate them [7]. It has been shown that Mg^{2+} blockade can be voided by membrane depolarization under native conditions or by using a Mg^{2+}-free Ringer solution, in experiments.

We have previously shown the role played by these receptors in the modulation of ACh release [8] and regulation of acetylcholinesterase activity [9] at mammalian NMJ. Furthermore, postsynaptic localization of the NMDA receptor NR1-subunit has been demonstrated [10]. Such localization suggests that the agonists of these receptors may change membrane excitability (namely, the resting membrane potential) with the development of depolarization.

MATERIALS AND METHODS

Male Wistar rats (200–300 g body weight) were used for all the experiments. The experiments were carried out in compliance with the guidelines for using labora-

tory animals of the Kazan Federal University and Kazan Medical University (ethical approval by the Institutional Animal Care and Use Committee of the Kazan State Medical University N9-2013). The experimental protocol met the requirements of the European Communities Council Directive 86/609/EEC and was approved by the Ethics Committee of the Kazan Medical University. All possible efforts were made to minimize animal suffering and to reduce the number of animals used. The experiments were performed using isolated nerve–muscle preparations of the EDL (extensor digitorum longus) muscle excised from ether-anaesthetized rats. Isolated muscles with a nerve stump (10–15 mm long) were placed in a chamber and superfused (at a rate of 2–3 mL/min) with an oxygenated Ringer–Krebs rat solution with the following composition (mM): 120.0 NaCl, 5.0 KCl, 2.0 $CaCl_2$, 1.0 $MgCl_2$, 23.0 $NaHCO_3$, 1.0 NaH_2PO_4, and 11.0 glucose; or Mg^{2+}-free solution: 121.0 NaCl, 5.0 KCl, 2.0 $CaCl_2$, 0.0 $MgCl_2$, 23.0 $NaHCO_3$, 1.0 NaH_2PO_4, and 11.0 glucose. The pH was maintained at 7.2–7.4.

Changes in the membrane potential were recorded at the endplate region of the muscle fibers using the standard current clamp technique at 20–22 ˚C as described by Petrov et al. [11]. Glass microelectrodes (resistance, 10–15 MΩ) were filled with 3 M KCl.

Glutamate, glycine, AP5, and 5,7-DCKA were purchased from Sigma-Aldrich (USA); μ-conotoxin was purchased from Alamone Lab (Israel). The animals received the agents through a perfusion system.

The statistical significance of the results was assessed using the unpaired Student's t-test; the difference between two data sets was considered significant at $p < 0.05$; errors are shown as a standard deviation (SD).

RESULTS AND DISCUSSION

It was suggested that, in the presence of functionally active NMDA receptors on the postsynaptic membrane, opening of receptor-associated channels caused by the application of agonists results in the entry of cations, leading to membrane depolarization. The depolarization intensity would depend on the quantity of activated receptors and concentration of extracellular ions. However, it was demonstrated that, at the resting membrane potential (RMP), Mg^{2+} blocks the NMDAR channel but these ions could be dislodged by depolarization or, in the experiments, by usage of a magnesium-free solution [12, 13].

Application of glutamate (100 μM) and NMDAR co-agonist glycine (700 μM) in a Mg^{2+}-free solution reduced the resting membrane potential by 6.5% (74.2 ± 0.3 mV, $n = 140$ vs. 79.4 ± 0.2 mV in control, $n = 270$, $p < 0.05$, *Figure*). In order to elucidate whether this effect was due to the activation of NMDARs, we performed the experiments using APV (DL-2-amino-5-phosphonopenthatoic acid), a selective reversible NMDAR blocker. Addition of 500 μM APV had no effect on the RMP; subsequent application of glutamate and glycine in the presence of the blocker evoked a smaller depolarization amounting to only 1.5% (78.15 ± 0.39 mV vs. 79.37 ± 0.24 mV in the control; $n = 127$, $p < 0.05$).

The infeasibility of total blockade by APV can be explained by the fact that APV is a reversible blocker that competitively binds to the glutamate-binding site of NMDAR and its affinity is close to that of glutamate; therefore, the amino acid could displace the blocker. In order to completely eliminate the effect of amino acids, we additionally applied 5,7-dichlorokynurenic acid (5,7-DCKA), an NMDAR glycine binding site blocker, at a concentration of 100 μM. Neither addition of 5,7-DCKA nor simultaneous application of APV and 5,7-DCKA affected the resting membrane potential ($n = 79$), but the combined action of 5,7-DCKA and APV prevented the effect of amino acids on the resting membrane potential (78.8 ± 0.22 mV vs. 79.37 ± 0.24 mV in control; $n = 85$, *Figure*).

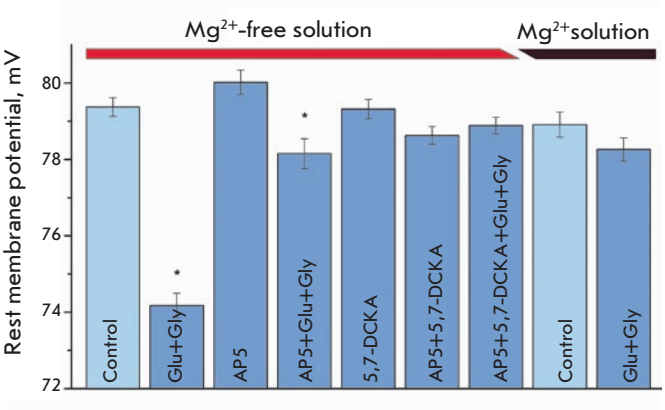

The effect of the activation of NMDA receptors on the resting membrane potential of a postsynaptic cell. The RMP value in the Mg^{2+}-free solution decreased after the application glutamate (100 μM) and glycine (700 μM). Addition of NMDA receptor blockers, APV (DL-2-amino-5-phosphonopenthatoic acid, 500 μM) or 5,7-dichlorokynurenic acid (5,7-DCKA; 100 μM), or simultaneous application of these agents had no effect on RMP. Addition of glutamate and glycine against a APV background slightly reduced RMP, but the effect was completely inhibited when two blockers, APV and 5,7-dichlorokynurenic acid, were applied. In the solution containing magnesium ions, application of glutamate and glycine had no effect on the RMP of postsynaptic cell. * – statistically significant difference vs. control ($p < 0.05$)

Magnesium blockade is an alternative physiological way to block NMDAR. If the observed effects on the membrane potential are caused by the activation of these receptors, the presence of magnesium in solution should prevent the development of depolarization after NMDAR agonists are applied. Indeed, amino acids had no effect on the membrane potential in the presence of Mg^{2+}. Hence, the membrane potential value in the Mg^{2+}-containing solution was 78.91 ± 0.32 mV and remained unchanged (78.26 ± 0.31 mV, $n = 105$, *Figure*) after glycine and glutamate addition. These results provide grounds to infer that a population of functional NMDARs is localized on the postsynaptic membrane; their activation causes statistically significant changes in the membrane potential. This depolarization, evoked by a cation current through the receptor channel, is blocked by a selective blocker of NMDAR glutamate and glycine binding sites: it is not observed when the magnesium block is preserved.

CONCLUSIONS

Hence, a functionally active population of NMDA receptors is present on the postsynaptic membrane of mammalian muscle fibers; their activation can change the excitability of muscle fiber and trigger a wide variety of intracellular reactions through the system of calcium-dependent secondary messengers, due to the relatively high permeability of the NMDA receptor channel to calcium ions. Given the variety of possible functions mediated by the NMDA receptor, further research into their role in the neuromuscular synapse seems to be an important and highly topical task. ●

REFERENCES

1. Waerhaug O., Ottersen O. P. // Anatomy and Embryology (Berlin). 1993. V. 188. № 5. P. 501–513.
2. Silinsky E.M., Redman R.S. // J. Physiol. 1996. V. 492 (Pt 3). P. 815–822.
3. Malomuzh A.I., Nurullin L.F., Nikolsky E.E. // Dokl. Biochem. Biophys. 2015. V. 463. P. 236–238. doi: 10.1134/S1607672915040092.
4. Berger U.V., Carter R.E., Coyle J.T. // Neuroscience. 1995. V. 64. № 4. P. 847–850.
5. Personius K.E., Slusher B.S., Udin S.B. // J. Neurosci. 2016. V. 36. № 34. P. 8783–8789
6. Fu W.M., Liou J.C., Lee Y.H., Liou H.C. // J. Physiol. 1995. V. 489 (Pt 3). P. 813–823.
7. Frahm S., Antolin-Fontes B., Görlich A., Zander J.F., Ahnert-Hilger G., Ibañez-Tallon I. // Elife. 2015. V. 4. P. 1–31.
8. Petrov K.A., Malomouzh A.I., Kovyazina I.V., Krejci E., Nikitashina A.D., Proskurina S.E., Zobov V.V., Nikolsky E.E. // Eur. J. Neurosci. 2013. V. 37. № 2. P. 181–189.
9. Pinard A., Lévesque S., Vallée J., Robitaille R. // Eur. J. Neurosci. 2003. V. 18. № 12. P. 3241–3250.
10. Malomouzh A.I., Mukhtarov M.R., Nikolsky E.E., Vyskocil F., Lieberman E.M., Urazaev A.K. // J. Neurochem. 2003. V. 85. № 1. P. 206–213.
11. Evans R.H., Francis A.A., Watkins J.C. // Experientia. 1977. V. 33. № 4. P. 489–491.
12. Malomouzh A.I., Nurullin L.F., Arkhipova S.S., Nikolsky E.E. // Muscle Nerve. 2011. V. 44. № 6. P. 987–989.
13. Lowe G. // J. Neurophysiol. 2003. V. 90. № 3. P. 1737–1746.

GENERAL RULES

Acta Naturae publishes experimental articles and reviews, as well as articles on topical issues, short reviews, and reports on the subjects of basic and applied life sciences and biotechnology.

The journal is published by the Park Media publishing house in both Russian and English.

The journal *Acta Naturae* is on the list of the leading periodicals of the Higher Attestation Commission of the Russian Ministry of Education and Science. The journal Acta Naturae is indexed in PubMed, Web of Science, Scopus and RCSI databases.

The editors of *Acta Naturae* ask of the authors that they follow certain guidelines listed below. Articles which fail to conform to these guidelines will be rejected without review. The editors will not consider articles whose results have already been published or are being considered by other publications.

The maximum length of a review, together with tables and references, cannot exceed 60,000 characters with spaces (approximately 30 pages, A4 format, 1.5 spacing, Times New Roman font, size 12) and cannot contain more than 16 figures.

Experimental articles should not exceed 30,000 symbols (approximately 15 pages in A4 format, including tables and references). They should contain no more than ten figures.

A short report must include the study's rationale, experimental material, and conclusions. A short report should not exceed 12,000 symbols (8 pages in A4 format including no more than 12 references). It should contain no more than four figures.

The manuscript and the accompanying documents should be sent to the Editorial Board in electronic form:
1) text in Word 2003 for Windows format;
2) the figures in TIFF format;
3) the text of the article and figures in one pdf file;
4) the article's title, the names and initials of the authors, the full name of the organizations, the abstract, keywords, abbreviations, figure captions, and Russian references should be translated to English;
5) the cover letter stating that the submitted manuscript has not been published elsewhere and is not under consideration for publication;
6) the license agreement (the agreement form can be downloaded from the website www.actanaturae.ru).

MANUSCRIPT FORMATTING

The manuscript should be formatted in the following manner:

- Article title. Bold font. The title should not be too long or too short and must be informative. The title should not exceed 100 characters. It should reflect the major result, the essence, and uniqueness of the work, names and initials of the authors.
- The corresponding author, who will also be working with the proofs, should be marked with a footnote *.
- Full name of the scientific organization and its departmental affiliation. If there are two or more scientific organizations involved, they should be linked by digital superscripts with the authors' names. Abstract. The structure of the abstract should be very clear and must reflect the following: it should introduce the reader to the main issue and describe the experimental approach, the possibility of practical use, and the possibility of further research in the field. The average length of an abstract is 20 lines (1,500 characters).
- Keywords (3 – 6). These should include the field of research, methods, experimental subject, and the specifics of the work. List of abbreviations.
- INTRODUCTION
- EXPERIMENTAL PROCEDURES
- RESULTS AND DISCUSSION
- CONCLUSION

  The organizations that funded the work should be listed at the end of this section with grant numbers in parenthesis.
- REFERENCES

  The in-text references should be in brackets, such as [1].

RECOMMENDATIONS ON THE TYPING AND FORMATTING OF THE TEXT

- We recommend the use of Microsoft Word 2003 for Windows text editing software.
- The Times New Roman font should be used. Standard font size is 12.
- The space between the lines is 1.5.
- Using more than one whole space between words is not recommended.
- We do not accept articles with automatic referencing; automatic word hyphenation; or automatic prohibition of hyphenation, listing, automatic indentation, etc.
- We recommend that tables be created using Word software options (Table → Insert Table) or MS Excel. Tables that were created manually (using lots of spaces without boxes) cannot be accepted.
- Initials and last names should always be separated by a whole space; for example, A. A. Ivanov.
- Throughout the text, all dates should appear in the "day.month.year" format, for example 02.05.1991, 26.12.1874, etc.
- There should be no periods after the title of the article, the authors' names, headings and subheadings, figure captions, units (s – second, g – gram, min – minute, h – hour, d – day, deg – degree).
- Periods should be used after footnotes (including those in tables), table comments, abstracts, and abbreviations (mon. – months, y. – years, m. temp. – melting temperature); however, they should not be used in subscripted indexes (T_m – melting temperature; $T_{p.t}$ – temperature of phase transition). One exception is mln – million, which should be used without a period.
- Decimal numbers should always contain a period and not a comma (0.25 and not 0,25).
- The hyphen ("-") is surrounded by two whole spaces, while the "minus," "interval," or "chemical bond" symbols do not require a space.
- The only symbol used for multiplication is "×"; the "×" symbol can only be used if it has a number to its

right. The "·" symbol is used for denoting complex compounds in chemical formulas and also noncovalent complexes (such as DNA·RNA, etc.).
- Formulas must use the letter of the Latin and Greek alphabets.
- Latin genera and species' names should be in italics, while the taxa of higher orders should be in regular font.
- Gene names (except for yeast genes) should be italicized, while names of proteins should be in regular font.
- Names of nucleotides (A, T, G, C, U), amino acids (Arg, Ile, Val, etc.), and phosphonucleotides (ATP, AMP, etc.) should be written with Latin letters in regular font.
- Numeration of bases in nucleic acids and amino acid residues should not be hyphenated (T34, Ala89).
- When choosing units of measurement, SI units are to be used.
- Molecular mass should be in Daltons (Da, KDa, MDa).
- The number of nucleotide pairs should be abbreviated (bp, kbp).
- The number of amino acids should be abbreviated to aa.
- Biochemical terms, such as the names of enzymes, should conform to IUPAC standards.
- The number of term and name abbreviations in the text should be kept to a minimum.
- Repeating the same data in the text, tables, and graphs is not allowed.

GUIDENESS FOR ILLUSTRATIONS

- Figures should be supplied in separate files. Only TIFF is accepted.
- Figures should have a resolution of no less than 300 dpi for color and half-tone images and no less than 500 dpi.
- Files should not have any additional layers.

REVIEW AND PREPARATION OF THE MANUSCRIPT FOR PRINT AND PUBLICATION

Articles are published on a first-come, first-served basis. The members of the editorial board have the right to recommend the expedited publishing of articles which are deemed to be a priority and have received good reviews.

Articles which have been received by the editorial board are assessed by the board members and then sent for external review, if needed. The choice of reviewers is up to the editorial board. The manuscript is sent on to reviewers who are experts in this field of research, and the editorial board makes its decisions based on the reviews of these experts. The article may be accepted as is, sent back for improvements, or rejected.

The editorial board can decide to reject an article if it does not conform to the guidelines set above.

The return of an article to the authors for improvement does not mean that the article has been accepted for publication. After the revised text has been received, a decision is made by the editorial board. The author must return the improved text, together with the responses to all comments. The date of acceptance is the day on which the final version of the article was received by the publisher.

A revised manuscript must be sent back to the publisher a week after the authors have received the comments; if not, the article is considered a resubmission.

E-mail is used at all the stages of communication between the author, editors, publishers, and reviewers, so it is of vital importance that the authors monitor the address that they list in the article and inform the publisher of any changes in due time.

After the layout for the relevant issue of the journal is ready, the publisher sends out PDF files to the authors for a final review.

Changes other than simple corrections in the text, figures, or tables are not allowed at the final review stage. If this is necessary, the issue is resolved by the editorial board.

FORMAT OF REFERENCES

The journal uses a numeric reference system, which means that references are denoted as numbers in the text (in brackets) which refer to the number in the reference list.

For books: the last name and initials of the author, full title of the book, location of publisher, publisher, year in which the work was published, and the volume or issue and the number of pages in the book.

For periodicals: the last name and initials of the author, title of the journal, year in which the work was published, volume, issue, first and last page of the article. Must specify the name of the first 10 authors. Ross M.T., Grafham D.V., Coffey A.J., Scherer S., McLay K., Muzny D., Platzer M., Howell G.R., Burrows C., Bird C.P., et al. // Nature. 2005. V. 434. № 7031. P. 325–337.

References to books which have Russian translations should be accompanied with references to the original material listing the required data.

References to doctoral thesis abstracts must include the last name and initials of the author, the title of the thesis, the location in which the work was performed, and the year of completion.

References to patents must include the last names and initials of the authors, the type of the patent document (the author's rights or patent), the patent number, the name of the country that issued the document, the international invention classification index, and the year of patent issue.

The list of references should be on a separate page. The tables should be on a separate page, and figure captions should also be on a separate page.

The following e-mail addresses can be used to contact the editorial staff: vera.knorre@gmail.com, actanaturae@gmail.com, tel.: (495) 727-38-60, (495) 930-87-07